Partial Oxidation Gas Turbine for Power and Hydrogen Co-Production from Coal-Derived Fuel in Industrial Applications

Final Report

DOE Award Number: DE-FC26-05NT42649

Recipient: Gas Technology Institute (GTI)
1700 S. Mount Prospect Rd.
Des Plaines, IL 60018

Principal Investigator: Joseph Rabovitser, GTI
847-768-0548
joseph.rabovitser@gastechnology.org

DOE Program Manager: Charles Alsup
National Energy Technology Laboratory
304-285-5432
Charles.Alsup@netl.doe.org

Reporting Period: October 01, 2005 - September 30, 2009

Date of Report: April, 2010

DISCLAIMER

Acknowledgements

Partial Oxidation Gas Turbine feasibility study is being supported by the United States Department of Energy National Energy and Technology Laboratory (DOE NETL), Gas Research Institute (GRI), and Utilization Development Company (UTD). Authors acknowledge the guidance and help of the DOE NETL Program Manager Mr. Richard Dennis, Project Managers Mr. Charles Alsup and Mr. Tom George, GRI's Program Manager, Dr. Maureen Droessler, and UTD Administrator, Mr. Greg Maxfield.

Authors: Gas Technology Institute - Joseph K. Rabovitser, John M. Pratapas,

Dmitri V. Boulanov

Siemens Energy – Dennis A. Horazak;

Oak Ridge National Laboratory – James R. Keiser;

Georgia Institute of Technology – Timothy C. Lieuwen;

Year of publication: 2010

Report title: Partial Oxidation Gas Turbine for Power and Hydrogen Co-Production from Coal-Derived Fuel in Industrial Applications

Abstract

The report presents a feasibility study of a new type of gas turbine. A partial oxidation gas turbine (POGT) shows potential for really high efficiency power generation and ultra low emissions. There are two main features that distinguish a POGT from a conventional gas turbine. These are associated with the design arrangement and the thermodynamic processes used in operation. A primary design difference of the POGT is utilization of a non-catalytic partial oxidation reactor (POR) in place of a conventional combustor. Another important distinction is that a much smaller compressor is required, one that typically supplies less than half of the air flow required in a conventional gas turbine. From an operational and thermodynamic point of view a key distinguishing feature is that the working fluid, fuel gas provided by the POR, has a much higher specific heat than lean combustion products and more energy per unit mass of fluid can be extracted by the POGT expander than in the conventional systems. The POGT exhaust stream contains unreacted fuel that can be combusted in different bottoming cycle or used as syngas for hydrogen or other chemicals production. POGT studies include feasibility design for conversion a conventional turbine to POGT duty, and system analyses of POGT-based units for production of power solely, and combined production of power and syngas/hydrogen for different applications. Retrofit design study was completed for three engines, SGT-800, SGT-400, and SGT-100, and includes: replacing the combustor with the POR, compressor downsizing for about 50% design flow rate, generator replacement with 60-90% power output increase, and overall unit integration, and extensive testing. POGT performances for four turbines with power output up to 350 MW in POGT mode were calculated. With a POGT as the topping cycle for power generation systems, the power output from the POGT could be increased up to 90% compared to conventional engine keeping hot section temperatures, pressures, and volumetric flows practically identical. In POGT mode, the turbine specific power (turbine net power per lb mass flow from expander exhaust) is twice the value of the conventional turbine. POGT-based IGCC plant conceptual design was developed and major components have been identified. Fuel-flexible fluid bed gasifier, and novel POGT unit are the key components of the 100 MW IGCC plant for co-producing electricity, hydrogen and/or syngas. Plant performances were calculated for bituminous coal and oxygen-blown versions. Various POGT-based, natural gas fueled systems for production of electricity only, co-production of electricity and hydrogen, and co-production of electricity and syngas for gas-to-liquid and chemical processes were developed and evaluated. Performance calculations for several versions of these systems were conducted. 64.6 % LHV efficiency for fuel to electricity in combined cycle was achieved. Such a high efficiency arise from using of syngas from POGT exhaust as a fuel that can provide required temperature level for superheated steam generation in HRSG, as well as combustion air preheating. Studies of POGT materials and combustion instabilities in POR were conducted and results reported. Preliminary market assessment was performed, and recommendations for POGT systems applications in oil industry were defined. POGT technology is ready to proceed to the engineering prototype stage, which is recommended.

1.0 EXECUTIVE SUMMARY

Introduction

There are two main features that distinguish a POGT from a conventional gas turbine: the design arrangement and the operational thermodynamics. One design specific is utilization of a non-catalytic POR in place of a conventional combustor. An important secondary design distinction is that a much smaller compressor is required, one that typically supplies less than half of the air flow required in a conventional gas turbine. From thermodynamic specifics, the turbine working fluid provided by the POR (a H_2-rich fuel gas) has higher specific heat than lean complete combustion products. This allows much higher energy per unit mass of fluid to be extracted by the POGT expander than in the conventional case. A POGT thus produces two products: power and secondary fuel that usually is a H_2-rich fuel gas.

GTI has been advancing the POGT concept since 1995. Siemens with GTI's participation has performed technical feasibility and cost analysis studies of the partial oxidation power cycle. GTI, Solar, Alturdyne and Tritek have designed, built and successfully tested a 200 kW POGT consisted of a non-catalytic POR integrated with the retrofitted 200 kW gas turbine. The experimental studies were completed for the 200 kW POGT solely, and for a CHP unit consisting of the POGT and a boiler with modified burner. The results are positive; a detailed report has been issued including recommendation for retrofit conversion of a conventional gas turbine to POGT duty.

Under the DOE project, the team has evaluated POGT applications for co-production of power and hydrogen/syngas, liquid fuels and chemicals from coal derived fuel or natural gas, conducted a feasibility design study to retrofit conventional gas turbines with power output 5 – 100 MWe to POGT operation, and conducted evaluation of materials for hot sections of POGT as well as combustion instabilities in the POR.

Project Objectives

- Develop a feasibility design for retrofitting a conventional gas turbine for partial oxidation duty in the industrial power plant;
- Produce a conceptual IGCC plant design (systems study) that integrates the retrofitted turbine design;
- Conduct a preliminary market study that projects demand for the IGCC plant for industrial applications.

Accomplishments

- Three candidate turbines f have been selected for feasibility design study of retrofit conversion to POGT: SGT-800, SGT-400 and SGT-100 from Siemens with power output in the range from 5 to 100 MW. In addition, POGT performance evaluation was performed for SGT6-6000G from Siemens with power output 350 MW in POGT mode;
- Retrofit design study is completed and detailed plans including schedule and budget have been developed for the SGT-800, SGT-400 and SGT-100 : replacing the combustor

with the POR, compressor downsizing for about 50% design flow rate, generator replacement with 60-90% power output increase, and overall unit integration;

- POGT performances for three selected turbines have been calculated. The more detailed calculations were performed for the SGT-800. Comprehensive calculations of the SGT-400 and SGT-100 in POGT mode were also completed. In addition, GT and POGT performances were calculated for SGT6-6000G. With a POGT as the topping cycle for power generation systems, the power output from the POGT could be increased up to 90% compared to conventional engine keeping hot section temperatures, pressures and volumetric flows practically identical;
- Validation testing of an existing Spartan T-350 industrial gas turbine converted to POGT mode was conducted. Calculated performance characteristics of POGT cycle were confirmed experimentally.
- An advanced POGT-based IGCC detailed scheme has been developed and major components have been identified. Fuel-flexible fluid bed gasifier with moderate product gas temperature, ~1800 ˚F, (~980 °C) and novel POGT unit are the key components of the 100 MW IGCC plant for co-producing electricity, hydrogen and/or syngas;
- Gasifier performance has been calculated for bituminous coal in both air-blown and oxygen-blown versions. The oxygen-blown gasifier and a cryogenic air separation unit (ASU) have been selected for the study. Two versions of gas cooling and cleaning systems have been considered, and the more advanced warm system has been selected;
- Performance calculations were conducted for several IGCC-POGT systems with different power/hydrogen or power/syngas ratios.
- Several POGT-based, natural gas fueled systems for production of electricity only, co-production of electricity and hydrogen, and co-production of electricity and syngas for gas-to-liquid and chemical processes were developed and evaluated. Performance calculations for several versions of these systems were conducted. 64.6 % LHV efficiency for fuel to electricity in combined cycle was achieved.
- Preliminary market assessment was performed, and recommendations for POGT systems applications in oil industry were defined;
- ORNL has completed one series testing for POGT hot section materials in a reducing atmosphere. Total of 25 samples from Siemens and Solar have been tested. Processing and analyses of the test data have been performed and reported;
- Study of combustion instabilities in POR has been completed by Georgia Tech, and final report has been submitted.

Approach

The project approach includes experimental, analytical, modeling and design studies of turbine performances and POGT-based systems, retrofit design study for conversion of a conventional turbine to a POGT, combustion instabilities study in POR, and experimental study of materials for hot sections of the turbines in reducing atmosphere. The following steps are being taken: selection of gas turbine candidates for retrofit to POGT duty; evaluation of the POGT performance for the retrofitted turbines and comparison with performances of conventional turbines; identification of the IGCC and power plant schemes for industrial applications; preparation of an Aspen-based model for POGT and IGCC plant studies; definition of specifications for retrofit design of the selected turbines to POGT; fulfillment of the feasibility retrofit design for the selected three turbines; development of a conceptual design of a IGCC-POGT plant and selection the major units; conducting performance analysis to form the basis for decision making to build POGT and new power plants offering a mix of multiple products (electricity, syngas and/or hydrogen, steam) for industrial high efficiency and low emissions operations.

Results

A procedure for POGT performance definition was developed and implemented for four Siemens gas turbines, SGT-100, SGT-400, SGT-800 and SGT6-6000G. For SGT-800, POGT performances were defined for both coal-derived fuel and natural gas. For SGT-100, SGT-400, and SGT6-6000G, POGT performances were identified for natural gas as a main fuel. The procedure for performance calculation was developed by GTI and Siemens, and is briefly described below for the SGT6-6000G.

Siemens has provided design-point data for these turbines, including mass flows, volumetric flows, pressures, and temperatures for the compressors, burners, and expanders. GTI has produced the Aspen-Plus models for SGT6-6000G, for operation in both conventional and POGT modes. Four models were actually generated. In the first step, GTI has calculated the performance for the engine in conventional mode with the goal to match as close as possible the major parameters, such as power output, turbine inlet temperature and pressure ratios for compressor and expander, and mass and volumetric flow rates. The results of calculations were sent to Siemens, and after approval of the matching parameters, GTI has conducted calculation of POGT mode for SGT6-6000G. Siemens has reviewed the results of the first Aspen run trials and sent comments and required steam flows to provide the needed blade path temperatures and cooling capacities. It is worth to notice that in POGT mode turbine net power could be increased by about 40 to 80%, and the POGT specific power (turbine net power per lb expander exhaust mass flow) is twice value of the conventional turbine.

POGT feasibility design was completed for conversion of three conventional gas turbines, SGT-100, SGT-400 and SGT-800 to POGT mode operation. Design approach and major specifications were defined from POGT performances calculated using the developed procedure.

The basic development approach for the POGT is to use existing SGT-engine components as much as possible, making whatever modifications are necessary to meet specified performance requirements. A heat transfer analysis supported by Aspen-Plus calculation is needed to

indentify the cooling steam flows to provide the required cooling capacity for the turbine expander. The design conditions for the compressor and expander for the POGT are within the capabilities of existing commercial technology, but some equipment is physically different from commercially available equipment. Therefore, a certain amount of development effort would be needed to produce a POGT.

Feasibility design for conversion of the three engines, SGT-100, SGT-400 and SGT-800 to POGT duty was completed and presented in the report.

The conversion of an existing Spartan T-350 industrial gas turbine to a POGT configuration was done as the most efficient approach for validation testing. Conversion consisted of developing and fabrication of Partial Oxidation Reactor (POR), interconnecting of POR with the Spartan engine, switching turbine shaft seal and turbine nozzle inlet cooling from air to steam and modification of engine control system. Compressor was left unchanged, although its capacity was much higher than required for POGT operation. Excessive compressed air was exhausted to atmosphere that led to excessive in-cycle power consumption.

Converted T-350 turbine was tested to determine effects of engine speed, turbine inlet temperature, back pressure and stoichiometric ratio on POGT parameters. Comparison of power output from POGT and conventional Spartan shows that POGT is capable of generating 300 kW at TIT below 1400F while the Spartan output was 200 kW at TIT=1600F.

An advanced IGCC-POGT plant with oxygen-blown fluidized bed gasifier was developed and detailed performance calculated. Using the prepared Aspen-Plus model, performance calculations of the IGCC key components, gasifier and POGT, have been completed. Syngas recirculation was used for the oxygen-blown fluid-bed gasifier to maintain the required gasifier performance. Gasifier performances for bituminous coal and oxygen-blown version have been calculated, and product gas and clean syngas compositions as well as all required parameters have been defined. Based on gas turbine standards for gaseous fuel contaminant levels, the impurity requirements have been also calculated to set the basis for the clean-up system evaluation. Two versions of the gas cooling and cleaning system have been considered, and the more advanced warm system has been selected for future evaluations.

ASPEN Plus calculations were conducted for hydrogen production using H2 separation membranes for the IGCC-POGT plant with oxygen-blown gasifier. POGT was based on Siemens SGT – 800 turbine. Four locations of the separation units were evaluated. The first is just at the gasifier exit where the syngas temperature is the highest. The second is in the syngas recycling stream where the gases are partially cleaned and cooled. The third location is after the cleaning and cooling system before POGT. In the fourth, the H2 Membrane Separator is located in the exhaust stream after POGT. Because of the low partial pressure of hydrogen, an additional H2 compressor is required to bring the hydrogen pressure to a level similar to other separation units. All four options are being evaluated in details, and hydrogen production rate and syngas composition and performance after the hydrogen separators were calculated.. Total plant thermal efficiency for the cases considered varies from 48 % HHV (without syngas production) to 63 % HHV (with syngas production).

Advanced natural gas–fired POGT cycles based on existing and prospective gas turbines were modeled using ASPEN Plus and demonstrated significant efficiency increase for electricity production solely.

Siemens gas turbines SGT6–6000G (conventional mode) and SGT–400 (POGT mode) integrated in a GT–POGT unit can provide 61.4 – 63.7% LHV efficiency for fuel to electricity in combined cycle. Such a high efficiency arise from using of syngas from POGT exhaust as a fuel can provide the required temperature level for superheated steam generation in HRSG, and for preheating of combustion air. Further efficiency increase, up to 64.6%, can be achieved by using nitrogen for cooling in POGT.

The selected turbines (SGT6–6000G and SGT–400) can be used to make similar cycles fueled by syngas produced from natural gas in a separate POR. In this case, total cycle efficiency will be at least at the level 61.4% for electricity only, but this cycle has a possibility to extract hydrogen from POR and supply the compressed hydrogen as required.

If high–pressure gas turbine will become available; it can be combined with existing turbines to produce a unit with at least 61.8% LHV efficiency in a combined cycle and 48% in a simple cycle. Using of oxygen deficient air as an oxidant in the high – pressure turbine running in POGT mode, can benefit significantly due to decreasing of in–cycle steam demand and provide additional increase in efficiency by 2-3 percentage points. A patent application for the described above GT-POGT cycles was filed.

A conventional gas turbine (Siemens SGT–800) converted to POGT technology was modeled using ASPEN Plus software and was fond capable to produce electricity and hydrogen from natural gas with thermal efficiency up to 71% of fuel HHV. A hydrogen selective membrane could be used for hydrogen separation from POR as well as from POGT exhaust.

Some advanced natural gas – fired POGT cycles for co-production of Liquid Fuels, Chemicals and Electric Power were developed and patented. Key advantages of these cycles compare to existing technologies (Steam Methane Reforming (SMR), Autothermal Reforming) include: (i) using waste heat for direct production of electric power; (ii) non-catalytic process; (iii) concentrated CO2 stream suitable for sequestration; (iv) higher overall thermal efficiency; (v) smaller foot print for the proposed POGT – based system vs. a conventional SMR.

Experimental testing of samples of 25 different base material/coating combinations was done by ORNL. Test data processing and analyses were conducted under the procedure used by ORNL for similar tests. Samples were exposed to a simulated POGT reducing atmosphere. The samples were selected and supplied by Siemens and Solar. Temperature and pressure in the test unit were selected, and set at 1700ºF (927ºC) and 350 psia (~24 atm). Test duration for one gas composition: 1000 hrs. Brief results are: (i) most coatings did not provide an improvement on the corrosion resistance; (ii) the alumina forming alloys generally showed smaller weight gains than the majority of chromia forming alloys.

Study of combustion instabilities in a POGT has been conducted by Georgia Tech. The main conclusion is “POGT systems are stable wherever DLN systems are unstable”.

Preliminary market assessment was performed, and recommendations for POGT systems applications in oil industry were defined.

Recommendations

The research performed contributes significantly into understanding of advanced turbine technologies suitable both for IGCC and natural gas – fired plants producing electricity solely, and for co-production of electricity and hydrogen, syngas, liquid fuels and chemicals. It was demonstrated that POGT technology can significantly improve performance of these plants.

According to the results obtained, POGT technology allows to increase thermal efficiency of co-production of power and hydrogen/syngas for IGCC plants to 48 – 63 % HHV; natural gas – fired plants to 61 – 71 % HHV, and for electricity production only up to 64.6%LHV with current turbine inlet temperature and pressure. Such a high efficiency values cannot be obtained by other available technologies. Besides, POGT technology can significantly improve other industrial processes such as hydrogen and liquid fuels production, and other chemical technologies involving syngas production and usage. Siemens' feasibility estimations demonstrate that development of commercial POGT unit can be done with existing technologies and components within a reasonable timeframe and cost. POGT should be considered for applications in which syngas/hydrogen and electric power are in high demand and which are expected to experience industrial expansion or replacement of existing equipment.

POGT technology is ready to proceed to the engineering prototype stage, which is recommended.

TABLE OF CONTENT

2.0 Introduction

A natural gas-fired gas turbine-generator operating in a "simple cycle" converts between 25 and 32 percent of the natural gas heating value to useable electricity. In a recuperated simple cycle, an air recuperator is installed to capture waste heat from the turbine's exhaust to preheat combustion air and boost efficiencies up to 40% Lower Heating Value (LHV). In large power plants, a "combined cycle" configuration is usually used, in which gas turbine cycle is combined with a steam turbine bottoming cycle. In the bottoming cycle, a "heat recovery steam generator"(HRSG) is installed to recover the heat from gas turbine exhaust and generate superheated steam for a steam turbine-generator. Combined cycle efficiency approaches 60% LHV.

The combined cycle plants can also be fueled by syngas produced through gasification of solid fuel (coal, petcoke, biomass, etc). In this case gas turbine (GT) unit is being integrated with syngas – production unit forming Integrated Gasification Combined-Cycle (IGCC) plant. The IGCC concept allows both enhancing efficiency and obtaining environmental benefits. Environmental benefits include extremely low SOx, NOx, and particulate emissions from burning coal-derived gases. Sulfur in coal, for example, is converted to hydrogen sulfide and can be captured by processes presently being used in the chemical industry. In some methods, the sulfur can be extracted in either a liquid or solid form that can be sold commercially. In an IGCC plant, the syngas produced is virtually free of fuel-bound nitrogen. NOx from the gas turbine is limited to thermal NOx. Burning low – caloric syngas allows for NOx emissions as low as 15 parts per million. Multi-contaminant control processes are being developed to reduce pollutants to parts-per-billion levels and will be effective in cleaning mercury and other trace metals, in addition to other impurities. Coal gasification may offer a further environmental advantage in addressing concerns over the atmospheric buildup of greenhouse gases, such as carbon dioxide. If oxygen is used in a coal gasifier instead of air, carbon dioxide is emitted as a concentrated gas stream in syngas at high pressure. In this form, it can be captured and sequestered more easily and at lower costs.

As mentioned above, the reported efficiency of modern natural gas –fired combined cycle power plants approaches 60% of natural gas LHV. Demonstrated efficiency of pilot IGCC plants is in the range from 36.5 % (Tampa Electric Polk power plant) [1] to 39.7% (Wabash River plant)[2] of fuel Higher Heating Value (HHV) that corresponds to 38 – 41% of fuel LHV. Further efficiency increase of GT – based systems is limited by various factors, such as limitation of turbine inlet temperature/pressure due to availability of materials and relatively high temperature of exhaust gases due to near – atmospheric pressure at the GT exhaust (apart from vacuum at the steam turbine exhaust) and others.

For system efficiency increase, the hot gases from GT exhaust could be used for preheating of combustion air and/or for additional power production through conventional Rankine steam cycle. But using of such waste heat – utilization methods also has its limitations.

Modern GT runs on relatively high pressure (about 300 psig). The compressed air is already preheated, so an only limited amount of waste turbine heat can be recuperated through

combustion air. The combination of air preheating and steam generation is not effective and usually is not used due to low grade steam produced and, as a result, low efficiency in the bottoming cycle.

The GT exhaust temperature (typically about 1000 °F) is relatively high, however, it not high enough for production of highly superheated steam (typically 1100 °F and higher) required for modern and prospective highly efficient steam turbines with reheat. This limitation is even more significant in the presence of combustion air preheating from the GT exhaust. In this case, due to both low efficiency and small portion of additional power generation, installation, and operation of steam turbine (ST) often becomes economically unattractive.

The limitations listed can be overcome by two methods. The first is creating new materials that can withstand higher pressures/temperatures. The second is by developing advanced gas turbine cycles that are more suitable for currently available materials and technologies and have potential for more efficient power generation. One example of such advanced gas turbine cycles is Partial Oxidation Gas Turbine (POGT) cycle.

Research and development (R&D) into the application of POGT concepts for power generation was first performed by the Institute of High Temperature (IVTAN) in the former Soviet Union in the late 1950s[3]. The result of this R&D was the demonstration of a working POGT. In one published application by IVTAN[4], residual fuel oil was partially combusted to produce high-pressure steam and a fuel gas, which was then cooled and cleaned to remove ash and sulfur compounds. The steam and purified fuel gas were then used for power generation. A 1970 patent was filed for a POGT by Jacques Ribesse of the JARIX company in Brussels, Belgium, followed by a technical paper in 1971[5], and a second paper describing further improvements in 1991[6]. The second paper described the gas turbine, air compressor, catalytic partial oxidation reactor (POR), and expansion turbine. Partial or total combustion of the combustible gas (leaving the POR) and passing through the expansion turbine was accomplished by injecting air into the turbine vanes. This simultaneously accomplished both the needed cooling and, through local combustion, an isothermal expansion[7].

In 1992, IVTAN published a paper describing an innovative combined cycle utilizing a POGT for the repowering of existing natural-gas-fired steam turbine power plants. The retrofit modifications were estimated to improve the fuel efficiencies to about 70-80% and reduce the NOx emissions by a factor of 10 or more[8]. Efficiencies are increased mainly because of (i) complete use of the thermal energy of the hot pressurized gasified product gas supplied by the POGT; (ii) reduced air flow requirements typically about 65% of that used for a conventional expansion turbine, (iii) much larger volumetric gas flow in the turbine, taking into account the lower density of the partial oxidation products, (iv) higher specific heat of the turbine working fluid, and (v) close to isothermal expansion, allowing a better utilization potential of the heat[3].

Hodrien and Fairbairn in 1993 evaluated the POGT in a report prepared for British Gas as a highly promising cycle with a potential efficiency above 60%[9]. Further study at the University of Liege (Belgium) in collaboration with other European partners, which included preliminary

analysis and testing, concluded that POGT has good potential for power generation applications and CHP applications as well[10].

GTI has been actively working on the POGT concept since 1995. With support from the US Department of Energy (DOE) and Gas Research Institute (GRI), GTI (formerly Institute of Gas Technology) teamed up with Siemens Westinghouse Power Corporation (SWPC) (formerly Westinghouse) to perform a system study of POGT applications[3]. The cycles studied included (i) a conventional natural-gas-fired gas turbine with a POGT utilized as a topping cycle, (ii) a combined cycle plant joining a POGT with a steam turbine, and (iii) a repowering system for coal-fired power plants using a POGT as a topping cycle. In a continuation of this work, Westinghouse performed technical feasibility studies and cost analyses of the partial oxidation (PO) power cycle and concluded that there was potential for significant plant heat rate and cost-of-electricity improvements[11].

In a recent development effort to demonstrate a POGT for on-site CHP generation, GTI with support from the California Energy Commission, GRI, and Utilization Technology Development (UTD), has teamed with Solar, Tritek, Alturdyne, and the Belcan Corporation to design, fabricate, and install at a 7-MWth pressurized non-catalytic POR at GTI. This POR replaces the combustor of the Solar's Spartan-350 conventional gas turbine modified to operate in a POGT mode. GTI together with Solar, Alturdyne, and Tritek developed a design approach for conversion of a conventional turbine to operate in POGT duty. The design was implemented for conversion of the Spartan-350 to a POGT unit that was installed and successfully tested at GTI's combustion laboratory.

2.1. Background and Overview

2.1.1. POGT Relationship to Conventional Gas Turbines

Combustion in a conventional turbine consists of mixing fuel and more than sufficient air to burn all of the fuel, igniting the mixture, and managing the combustion products to drive an expansion turbine for power generation. In POGT processes, the amount of air used is considerable less than what is required for complete combustion. Consequently, the products of partial oxidation still have appreciable unburned chemical energy in the reaction gases and those exhaust gases as a syngas are the secondary product of the POGT. The reactor which contains the partial oxidation process is called the POR. In a POGT, the POR replaces the combustor as the source of pressurized hot gas. An amount of air, which is less than needed for complete combustion, is first compressed in a conventional compressor then reacted with the fuel under pressure and the fuel is partially burned or oxidized. The resulting hot fuel gases (POGT working fluid) expand to ambient pressure in an expansion turbine of conventional design.

Like in a conventional gas turbine, the expansion turbine drives the compressor and the electrical generator. Also, the combustion products are too hot for the expansion turbine if a conventional fuel, natural gas, distillate oil, kerosene or jet fuel, and the correct amount of air for complete combustion were used. To remedy this situation, a significant amount of excess air is delivered by the compressor and dilutes and absorbs excess heat from what would be the too

hot gas products. This delivers hot pressurized gas to the expansion turbine at a temperature no hotter than the materials of the expansion turbine can be exposed to for reliable operation. In a conventional gas turbine, about three times the air needed for complete combustion is used in the combustor (300% theoretical air). The expansion turbine inlet temperature is within the limits of the turbine for long life, high efficiency, and reliable operation.

In a POGT, insufficient air, typically 35% to 45% of which is required for stoichiometric combustion, is used in the reactor/combustor where the partial oxidation/combustion reaction takes place. Steam, at an appropriate pressure, is also injected into the POR as part of the POR temperature control process. Again this delivers hot pressurized fuel gas to the expansion turbine at a temperature no hotter than the materials of the expansion turbine can reliably accept.

In the POR an unusual phenomenon occurs; the volume of the combustor exhaust gas is slightly more than double of which occurs if a conventional combustor were used on a conventional gas turbine, operating with excess air to control the exit gas temperature. In a POGT, at a stoichiometric ratio of 0.4 (40% of the air needed for complete combustion is used), with steam injection sufficient to limit the reaction products. For a typical microturbine operation (turbine inlet 1650 ℉ at a pressure of 3.95 atmospheres), the POR reaction generates 2.28 volumes (moles) of reaction products per volume (mole) of air compressed. This is contrasted with a conventional gas turbine where the combustor produces only 1.035 moles of combustion products per mole of air compressed. This increase in gas volume is basically the breakup of one volume of methane plus one-half a volume of oxygen into a combination of one volume of carbon monoxide and two volumes of hydrogen, for a total of three volumes. Some of the carbon monoxide or hydrogen appears as carbon dioxide or water vapor when the stoichiometric ratio is above 0.25. This is the minimum value that can be used without ensuring soot (fine carbon particles) in the reactor products.

The additional 0.035 moles in combustion in a conventional gas turbine are the consequence of the input (already compressed) fuel to the combustor.

This most unusual volumetric increase is real. It is the source of both the high efficiency and the need for approximately double the volumetric capacity of the expansion turbine process as compared with a conventional gas turbine. The lower compressor capacity per unit of expansion turbine capacity leads to higher POGT specific power (kW output per pound mass flow). This is an important cost advantage which is expected to be reflected in lower price to the user and more favorable energy system economics to the owner.

The POGT process is power generation at very high net fuel utilization efficiency, 68.5%, is based on the net fuel energy consumed. The fuel energy in the POGT exhaust can be used in a fuel – fired boiler or furnace, and as a feedstock for chemical syntheses as well. In one case study, net fuel utilization efficiency is the net power delivered divided by the net fuel energy consumed. The difference between the fuel input to the POGT and the combustible fuel gas delivered to whatever application the host has need for. It is to be noted the POGT receives some “free power” in the form of the fuel (compressed natural gas) entering the POGT being

already compressed. For the same conditions, but with the fuel entering the POGT at the same pressure as the ambient air, a power consuming compressor is required for fuel compression and the efficiency will be slightly reduced.

High efficiency can only be obtained when hydrocarbon fuel is partially combusted and the low energy content fuel in the POGT exhaust used in a second, serial, fuel utilizing application.

The POGT exhaust gas is of low to medium heating value content as only a part of the energy in the incoming fuel is used in the POR to supply heat to the POGT working fluid. The high efficiency of the POGT is real; however it only applies to a portion of the energy in the incoming hydrocarbon fuel convertible to heat in a partial oxidation reaction.

Generally, there are two efficient applications for the POGT. One is when the hydrocarbon fuel is used only for its heat value, as in a turbine, internal combustion engine, boiler, furnace, or process heater, etc. The other is when the hydrocarbon fuel is converted into syngas for use as a hydrogen source for a chemical application. In these two applications, power (such as electricity) can be generated at high efficiency when converting the fuel from a high energy content to a low energy content. It can then be used for heat or chemical purposes.

Produced fuel gas obtained with POR technology contains a significant amount of hydrogen. This hydrogen can potentially be extracted either before or after expansion in a turbine by hydrogen – selective membranes and used in various onsite applications. Other components in the gas include CO, CO_2, N_2, and steam. This clean gas at the pressure of the POGT exhaust is readily suited to provide supplemental energy via burnout combustion for a variety of applications. Applications include furnaces, boilers and heat engines, reciprocating engines or gas turbines which are capable of using such low heating value fuel at POGT discharge pressure. Potential applications under study include power and hydrogen/syngas co-production.

Major benefits projected with POGT technology compared with a fired cogeneration system are:

- Increase in overall thermal efficiency of over 30% for the portion of the fuel energy used in the power generation process
- Reduced cost for electrical power generated
- Reduced gaseous emissions of 50 to 70% for NOx and CO from the eventual burnout of the fuel gas that is the POGT exhaust
- Production of a hydrogen enriched secondary fuel in addition to electrical power

2.1.2. Engineering Embodiment of a POGT

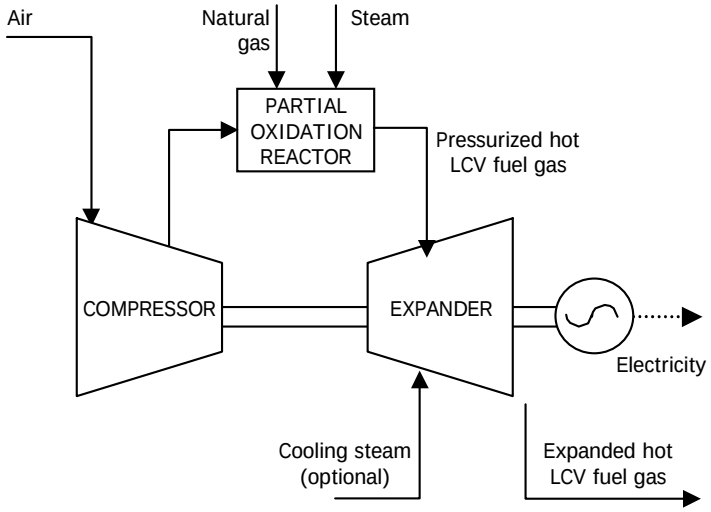

Figure 1. Conceptual Depiction of POGT.

The basic concept of the POGT unit is illustrated in Figure 1. The can combustor typically found in conventional turbine arrangements is replaced with a pressurized, non-catalytic, POR assembly. POR fuel (typically natural gas) and air combine and premix at substoichiometric (less air than needed for complete combustion of the fuel) concentrations in an injector unit. Steam is also injected into the POR in order to control the temperature of the hot reaction product gases to levels which the expansion turbine and the POR walls themselves can accommodate in a manner consistent with long life and durable operation. These mixed gases exit the injector into a reaction chamber and partially combust at elevated temperatures. The steam provides both dilution cooling of the POR exhaust gases and modifies the chemical species of the fuel gas produced from the POR. Potentially, hot pressurized water can also be used as a cooling agent for POR allowing to reduce steam consumption. The produced fuel gas exiting the POR are directed into an expansion turbine for conversion of energy in flowing hot, pressurized gas into shaft power for subsequent electric power generation. The reduced pressure turbine exhaust gas (hot and fuel rich) is used in onsite energy consuming operations to complete the POGT technology scheme. The end result is an increase of the efficiency of power generation compared to conventional CHP heat schemes employed in industry today.

2.1.3. Turbo machinery component consideration for POGT

The feature enabling POGT to be efficient in power generation from the process of converting a portion of the energy in the fuel from high BTU fuel to low BTU fuel is the accompanying volume increase, as mentioned above. This feature, however, has a challenging aspect. The turbine-air compressor pairs used in conventional gas turbines have been designed for a gas product to air molar ratio of 1.035 rather than a ratio of 2.28 in POGT systems. A consequence of this 2.2 relative increase in expander gas molar volume to air compressor molar volume suggests the existing gas turbines experience difficulty in conversion to POGT cycles. This is when the original air compressor and the expansion turbine are retained in their present 1:1 configuration. There are several ways to avoid an enlarged turbine size. One is to use two expansion turbines and two POR reactor/combustors per POGT air compressor. The other is to

use one POR, one compressor and one turbine. This can be used in modifying existing turbines for POGT use. In the following chapters, there is a detailed description of the conversion of the existing conventional gas turbine to POGT duty.

The report consists of seven chapters.

3.0 IGCC-POGT Conceptual Plant Study

3.1. Selecting IGCC Plant Scheme

Coal gasification technology for the IGCC-POGT plant was selected by evaluation and modeling of two alternative technologies – 1) high – temperature General Electric Energy (GEE) entrained bed gasifier and 2) moderate temperature GTI U-Gas fluidized bed gasifier with about 1800 ˚F outlet temperature. Comparison of the IGCC schemes shows the high temperature entrained flow gasifier schemes are focused on application in large utility plants with capacity much more than 100 MW and narrow range of used coal. The fluidized bed gasifier schemes could be effectively applied to up 100 MW IGCC plants that are currently considered the preferred size for industrial applications. Also fuel flexibility and variation in operating conditions is usually required in industrial application make the fluidized bed gasifier the most attractive candidate for the POGT-IGCC study in the project.

Separate study was done to select prospective gas turbine for retrofit conversion into POGT. Based on this study, Siemens SGT-800 was used in the further plant schemes as a power generation unit. It was agreed with Siemens that in order to size the plant, one has to keep volumetric flow rate, turbine inlet temperature and pressure ratio in POGT mode at the same level as for original conventional SGT-800 turbine.

Two IGCC- POGT plants were initially studied, one with an air-blown and another with oxygen-blown gasifier. Aspen-Plus models have been developed and calculations were conducted for both plants. Simplified schematics of these versions of the IGCC-POGT plants are presented in Figure 2 and Figure 3. Syngas recirculation was used for the oxygen-blown fluid-bed gasifier to maintain the required gasifier flow rate, and the portion of syngas recirculation for the oxygen-blown gasifier was varied to optimize the overall system performance.

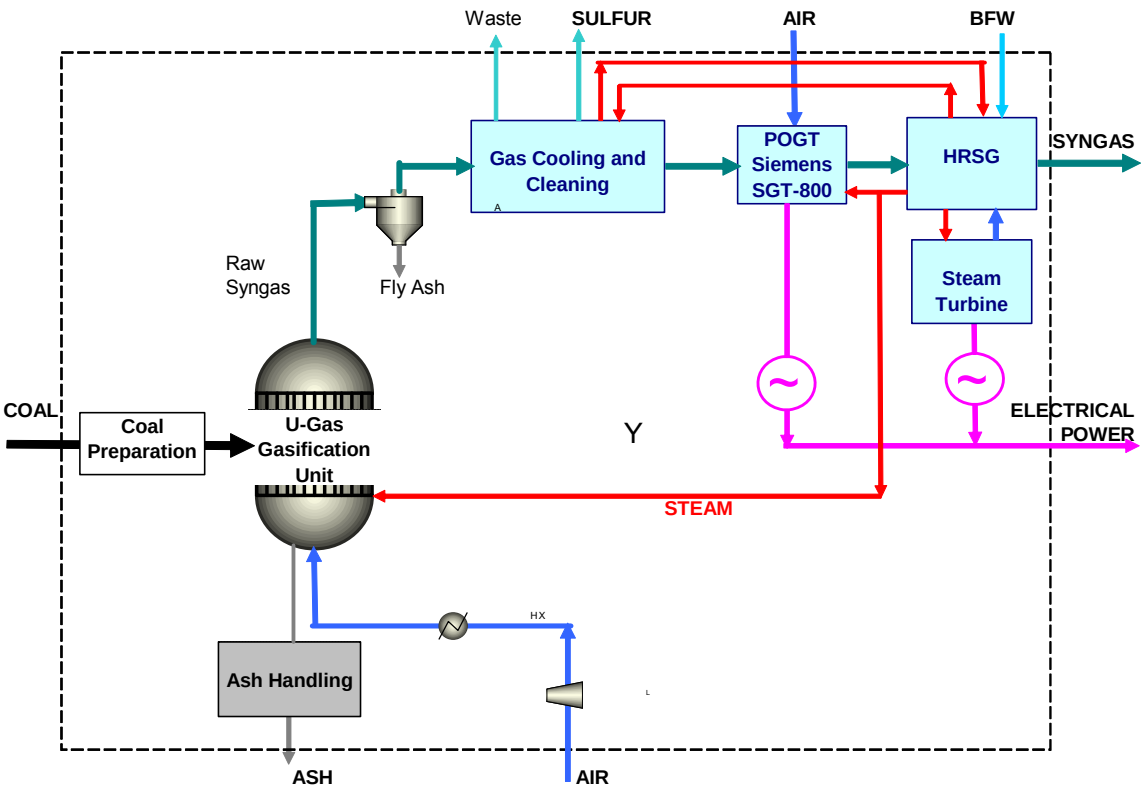

Figure 2. IGCC-POGT plant schematic with an air-blown gasifier.

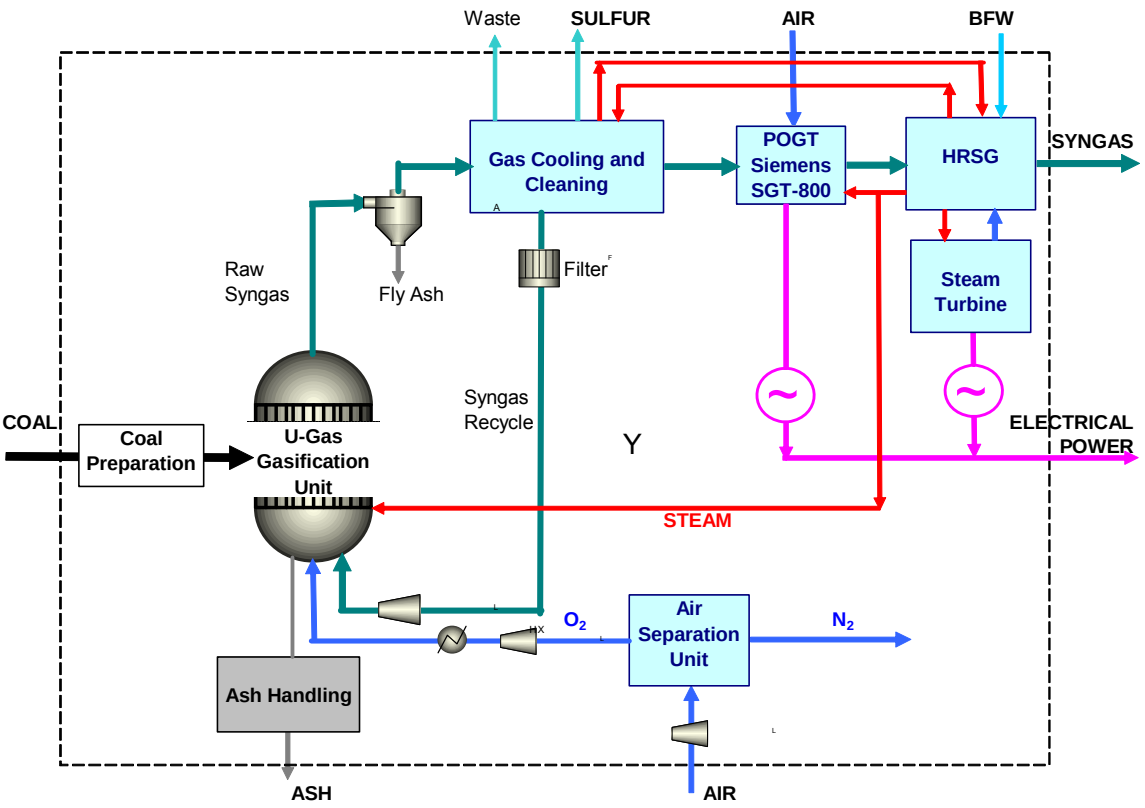

Figure 3. IGCC-POGT plant schematic with an oxygen-blown gasifier.

Gasifier performances for bituminous coal for both air-blown and oxygen-blown versions have been calculated, and product gas and clean syngas compositions as well as the required parameters have been defined. Based on gas turbine standards for gaseous fuel contaminant levels, the impurity requirements have been also calculated to set the basis for the clean-up system evaluation.

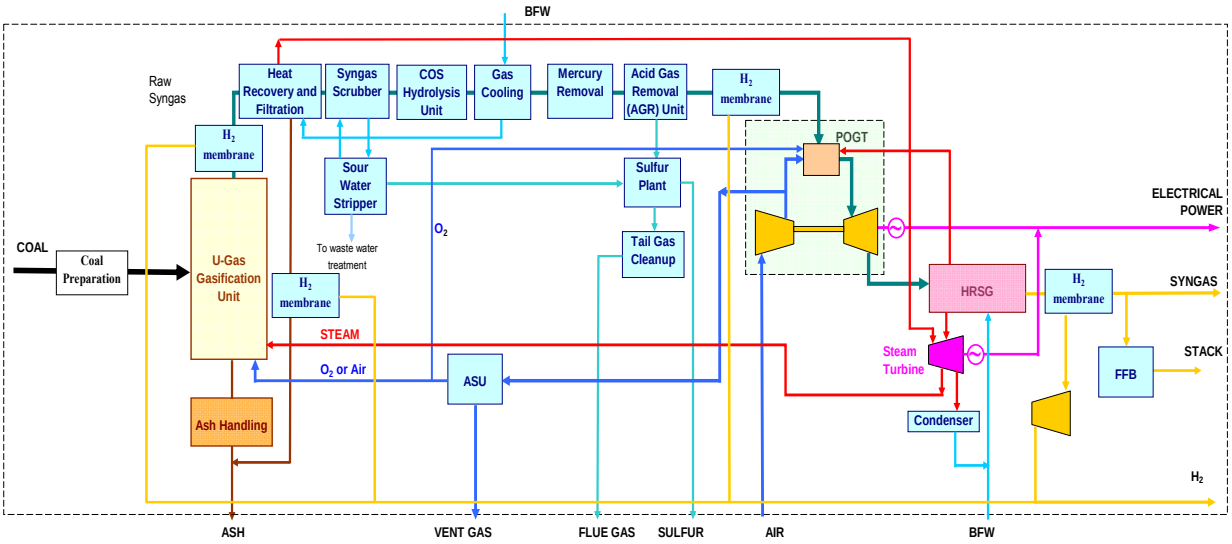

Figure 4. IGCC Plant Scheme using POGT for Co-Production of Power and Syngas/Hydrogen.

Based on the conducted study of two conceptual IGCC-POGT plants with air-blown and oxygen-blown gasifiers, the plant with an oxygen-blown gasifier has been selected for in depth conceptual IGCC-POGT plant evaluation. Schematics and equipment for the Air Separation Unit (ASU) have been reviewed, and based on Siemens recommendation, a cryogenic ASU has been selected for application in the IGCC-POGT plant.

Further analyses were based on the IGCC – POGT plant scheme shown in Figure 4. The plant consists of four major units: gasifier with coal, oxygen, and steam supplies; clean-up system; POGT for co-production of power and syngas; and hydrogen separation units for production of hydrogen with required purity and pressure.

Evaluation of the cold cleanup system has been conducted. A schematic of the system is shown in Figure 5.

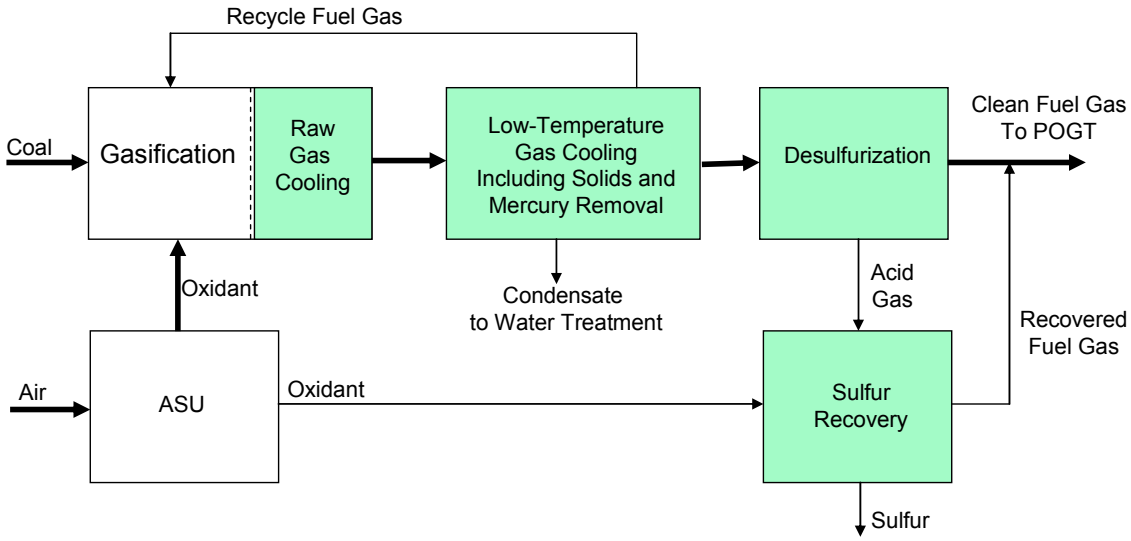

Figure 5. Cold Gas Cooling and Cleaning simplified schematic.

Siemens has estimated the performance and auxiliary requirements for the syngas cooling and cleaning portion of a POGT plant. These are based on the syngas inlet stream properties shown in Figure 6 below.

The assumptions included: cooling water temperature 70 °F (21 °C) with 20 °F (11 °C) of heating; HP steam at 1800 psig; syngas inlet to Cooling and Cleaning block around 1850 °F (1010 °C); and syngas exit from Cooling and Cleaning block around 600 °F (316 °C).

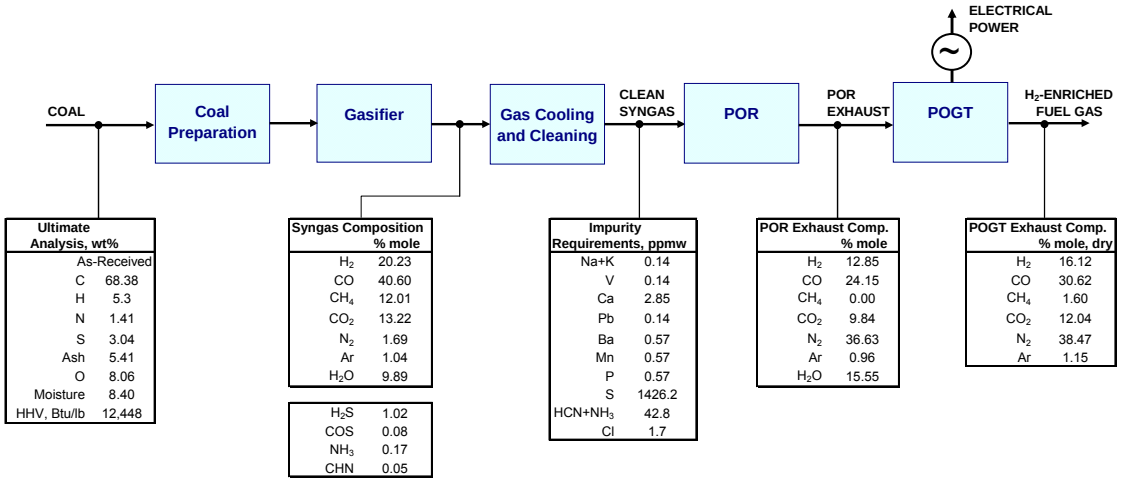

Figure 6. Compositions of coal, syngas, impurities, and turbine working fluid and product fuel gas for the IGCC-POGT plant with an oxygen-blown gasifier.

Further system analyses were dedicated to implementation of hydrogen-selective membranes into the process. The main advantage of membranes usage is the high quality of product hydrogen which eliminates the need in special hydrogen cleaning unit or, at least, significantly decreasing its size. On the other hand, significant amount of hydrogen will be left in the syngas after the membrane separators. However the hydrogen production is integrated with POGT system and this off-gas will be used for electricity production.

3.2. Selective Gas Membranes for Hydrogen Production

The grown number of researches dedicated to the development of membrane technologies of hydrogen separation and purification has been recently reviewed in [12]. The main findings from this review are outlined below.

In hydrogen production from fossil fuels, separation and purification is a critical technology. In order to obtain high purity hydrogen from syngas, separation of H_2 from other syngas constituents such as CO, CO_2, N_2 and CH_4 is necessary. Existing processes for hydrogen separation from the components listed include pressure swing adsorption (PSA) and membrane separation. According to experience of hydrogen separation in refineries [13], membrane systems are more economical than PSA.

Besides, if H_2 is selectively removed from the reaction system, thermodynamic equilibrium is shifted to the products side, leading to higher conversions of hydrocarbon feedstock into H_2. Enhanced performance of steam reforming with a real membrane catalytic system was firstly reported in [14], consistent with computer simulation studies. According to the calculation [15], membrane separation can result in the significant conversion improvement on the CH_4 steam-reforming in a lower temperature range of 935 -1115 ^{o}F (500– 600 °C).

A schematic of the membrane separation process is shown in Figure 7. The driving force for required separation is often pressure or concentration gradient across the membrane. An authoritative summary of basic concepts and definitions for membranes is available in an IUPAC (International Union of Pure and Applied Chemistry) report [16].

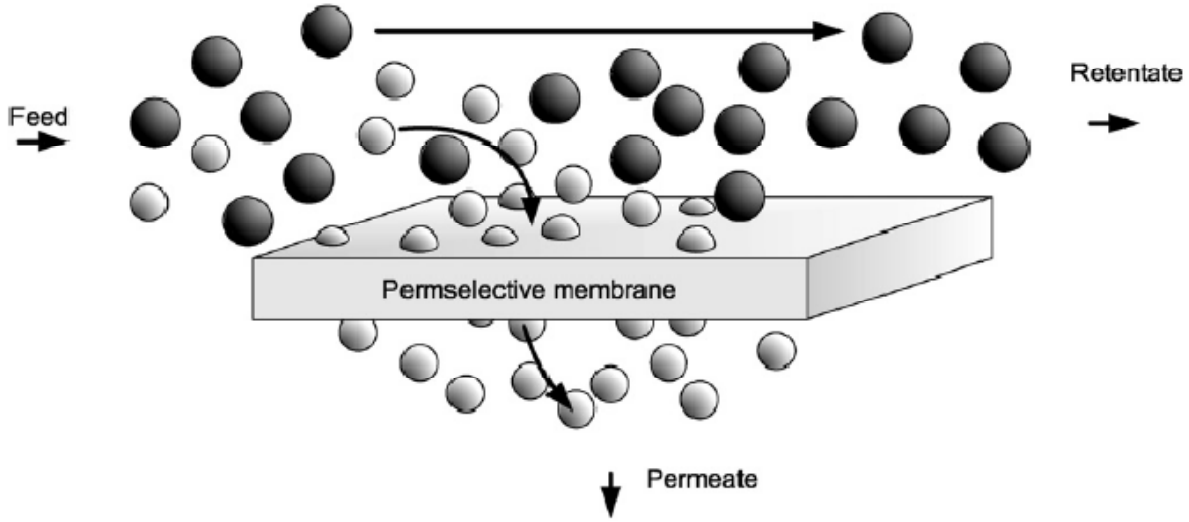

Figure 7. Simplified schematic of membrane separation process [12].

A membrane is a physical barrier allowing selective transport of mass species, widely used for separation and purification in many industries. Membranes can be classified into organic, inorganic, and hybrids of organic/inorganic systems. Performance characteristics of organic and inorganic membranes are compared in Table 1. Organic membranes can be further divided into polymeric and biological constituents, whilst inorganic ones to metallic (dense phase) and ceramic (porous and non-porous) membranes.

Membranes' performance is characterized by permeability and selectivity. Permeability indicates the capacity of a membrane for processing the permeate. High permeability means high flow of the component separated. Selectivity indicates membrane's ability to separate a desired component from the feed mixture. Industrial applications demand both high permeability and high selectivity.

Table 1. Comparison of polymeric and inorganic membranes [12].

Membrane	Advantages	Disadvantages	Current status
Inorganic	• Long term durability • High thermal stability • Chemical stability in wide pH • High structural integrity	• Brittle (Pd) • Expensive • Some have low hydrothermal stability	• Small scale applications • Surface modifications to improve hydrothermal stability
Polymeric	• Cheap • Mass production (larger scale) • Good quality control	• Structurally weak, not stable, temperature limited • Prone to denature & be contaminated (short life)	• Wide applications in aqueous phase, and some gas separations

Although polymeric membranes have been used for industrial hydrogen separation at low temperatures [17], they are not appropriate for hydrogen production from hot (above 200 °C)

syngas. Due to higher thermal stability, inorganic membranes are more suitable for hydrogen extraction from syngas.

Dense phase metallic membranes have attracted a great deal of attention largely because they are commercially available. These membranes exist in a variety of compositions and can be made into large-scale continuous films for membrane module assemblies. Pd-based alloys demonstrate high hydrogen selectivity, although permeability is low for most large-scale units.

Porous ceramic membranes are normally prepared by solid–gel or hydrothermal methods, and have high stability and durability in high temperature, harsh impurity and hydrothermal environments. In general, inorganic ceramic membranes possess lower H_2 selectivity but higher flux. In particular, microporous membranes show promise in the water gas shift reaction at higher temperatures.

So, as of today, inorganic membranes for hydrogen separation under conditions present in IGCC-POGT cycle are not commercially available and still under development. An economic study [18] for the water–gas shift reaction carried out in an IGCC system, by using microporous silica membranes, indicated more stable and more selective gas separation membranes are necessary in order to have favorable investment and operational costs. But, taking into account the efforts applied in this area, suitable membranes will be commercially available by time of maturity of IGCC-POGT technology itself.

3.3. Oxygen-blown IGCC – POGT plant for Hydrogen/Syngas/Electricity Co – Production

Three different locations of hydrogen membranes shown in Figure 8 and their combinations were tested by the ASPEN Plus modeling to determine the optimum membrane location for overall plant performance and the total energy production point of view.

Gasifier modeling details were discussed and agreed with DOE – model with temperature penalties for specific reactions was used.

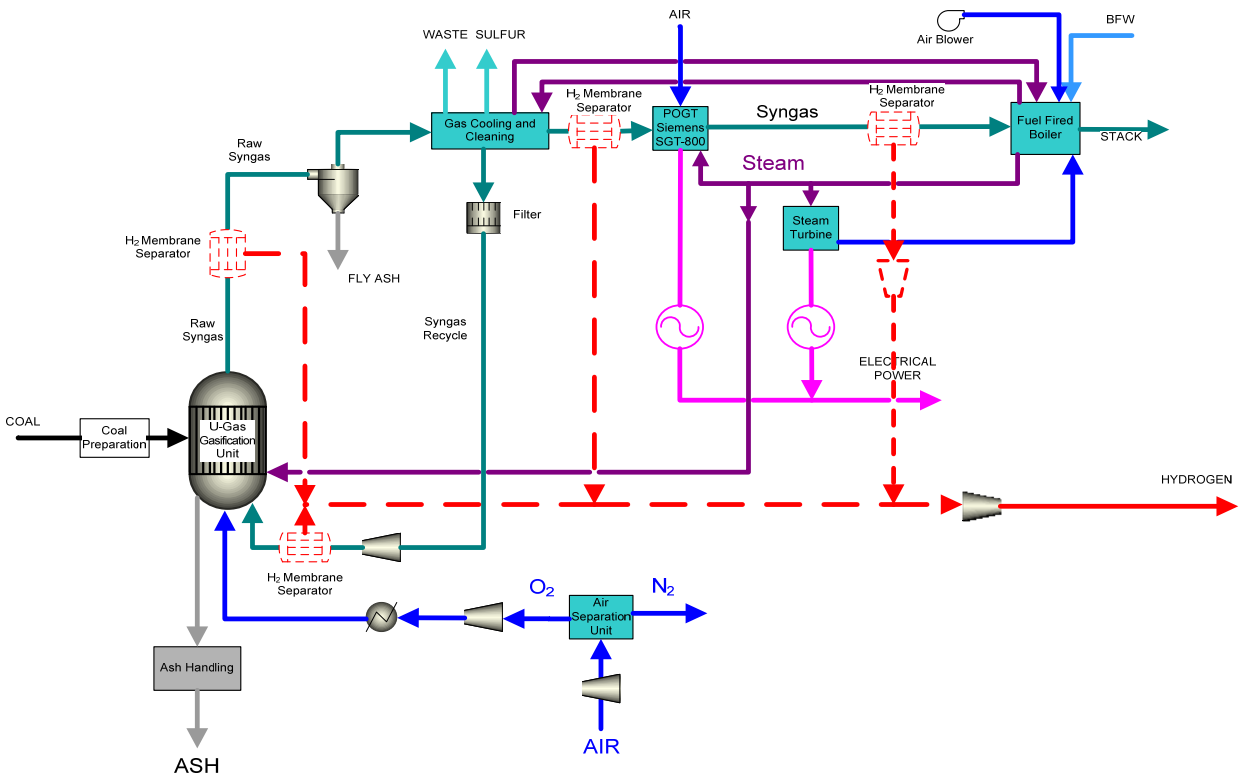

Figure 8. IGCC Plant Scheme using POGT for Co-Production of Power and Hydrogen by membrane separation.

The core U-gas process, was found [19], and allows turn-down ratio of at least 0.5 in air-blown mode. This indicates in the oxygen-blown mode, it is possible to decrease the syngas recycle rate from 0.44 to 0.33 which corresponds to 1.5 times decrease in the recycled syngas flowrate. Composition of cooled syngas at the gasifier outlet remains practically unchanged (Table 2) due to constant temperature and mixture composition.

Table 2. Syngas composition with different recirculation rates.

	R=0.44	R=0.33
H_2	20.23	20.23
CO	40.60	40.60
CH_4	12.01	12.01
CO_2	13.22	13.22
N_2	1.69	1.69
Ar	1.04	1.04
H_2O	9.89	9.89
H_2S	1.01	1.01
COS	0.08	0.08
NH_3	0.17	0.17
CHN	0.05	0.05

As mentioned above, Siemens SGT-800 was selected as a prospective gas turbine model to retrofit into POGT. The turbine was modeled using the ASPEN Plus software both in complete

combustion and POGT mode. Performance characteristics obtained by the ASPEN modeling and provided by Siemens are compared in Table 3.

Table 3. Performance characteristics of Siemens SGT-800 turbine.

	Siemens complete combustion	GTI ASPEN Plus, complete combustion	GTI ASPEN Plus, POGT
Compressor Exit Temperature, F	883.8	874.0	833.5
Expander Exit Temp., F	1001.0	1004.0	1078.7
TIT, F		2318.0	2286.5
Compressor Power, MW	61.1	61.1	28.0
Expander Power, MW	105.9	105.4	111.3
Nominal Net Power MWe	44.80	44.4	83.4

The overall plant thermal efficiency was calculated for the following H_2 membranes locations:

- At the gasifier outlet –1800 °F, 355 psi
- Clean syngas outlet – 600 °F, 285 psi
- Recycle syngas line – 650 °F 415 psi
- POGT exhaust – 1225 °F 14.7 psi

Outlet hydrogen pressure was assumed to be at 30 psi, the membrane in location 4 has a hydrogen compressor with an intercool. Hydrogen pressure ratio across the membranes was assumed to be at 0.5. The produced hydrogen was cooled down to 130 °F by water which is required for POGT steam production. Calculations results are presented in Table 4.

Table 4. Performance characteristics of IGCC-POGT cycles with H_2 selective membranes.

H_2 membranes locations		1+2+3	1+2+3, no SG	1+2+3 +4	1+2+3 +4, no SG	1+2+4	1+3+4	2+3+4
Chemical energy input (HHV)	MW	779.7	779.7	754.5	779.7	717.3	747.9	732.3
	% of fuel input	100%	100%	100%	100%	100%	100%	100%
Compressor work required, including GT, ASU and H_2 compressors	% of fuel input	6%	6%	7%	7%	7%	7%	7%
Turbine work produced	% of fuel input	13%	13%	14%	13%	15%	14%	15%
Net power produced in topping cycle	MWe	57.3	57.3	56.8	47.3	60.8	56.3	57.5
	% of fuel input	7%	7%	8%	6%	8%	8%	8%
Hydrogen energy produced	% of fuel input	19%	19%	25%	39%	22%	23%	20%
Syngas energy produced	% of fuel input	23%	0%	19%	0%	20%	20%	20%
Total heat produced	% of fuel input	31%	51%	28%	35%	28%	29%	31%

Hydrogen and syngas sensible heat	% of fuel input	2%	0%	3%	1%	3%	3%	3%
FFB exhaust sensible heat	% of fuel input	5%	10%	5%	6%	5%	5%	5%
Heat losses	% of fuel input	12%	12%	12%	12%	11%	11%	11%
Electricity production through bottoming steam cycle	MWe	100	165	89	115	85	92	95
	% of fuel input	13%	21%	12%	15%	12%	12%	13%
Total energy production	MW	485.5	374.3	479.6	465.2	446.3	467.9	447.1
	% of fuel input	62%	48%	64%	60%	62%	63%	61%

ASPEN Plus model schematics for the selected IGCC – POGT schemes are shown in Figures 9 and 10. Hydrogen membranes at the POGT exhaust in the scheme shown in Figure 9 are bypassed by switching splitter block MEM4-SPL, so only 3 membrane locations are active on this scheme compare to 4 locations in Figure 10..

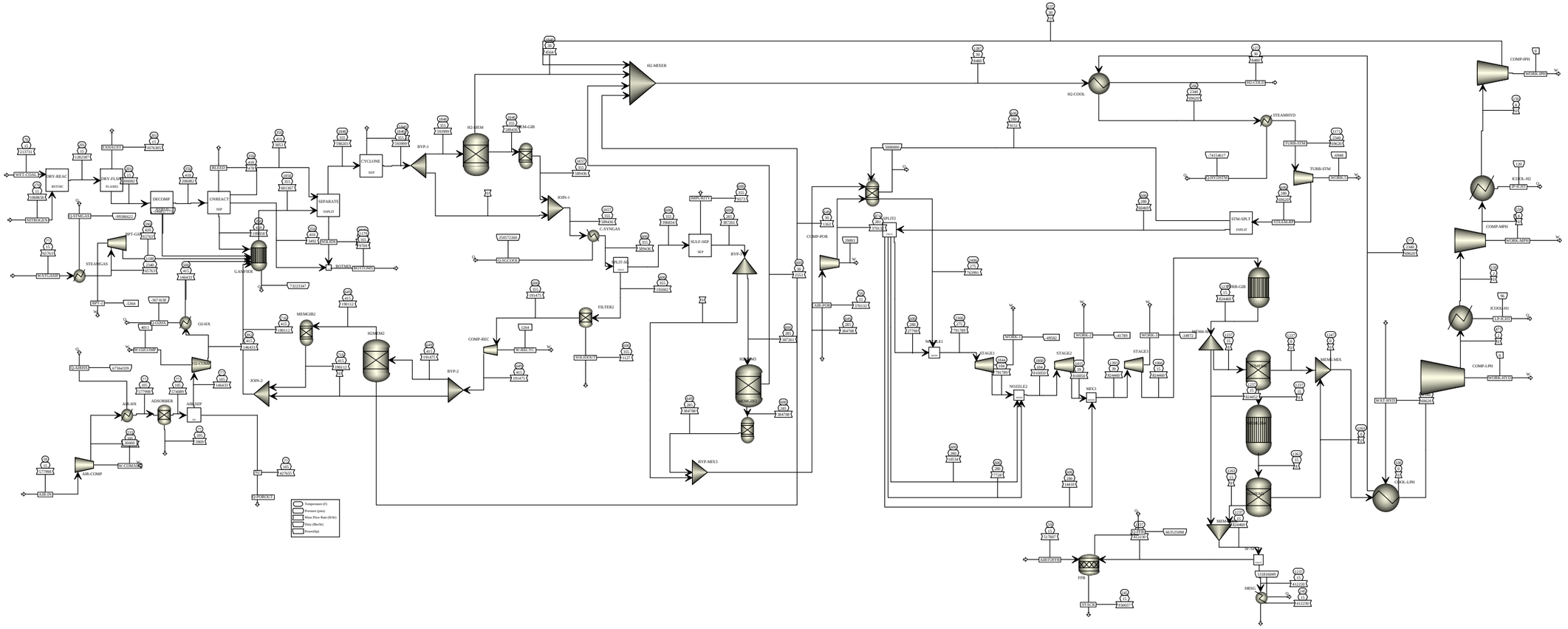

Figure 9. IGCC-POGT unit model schematic with H2 membranes located at the gasifier outlet, clean syngas outlet, and recycle syngas line.

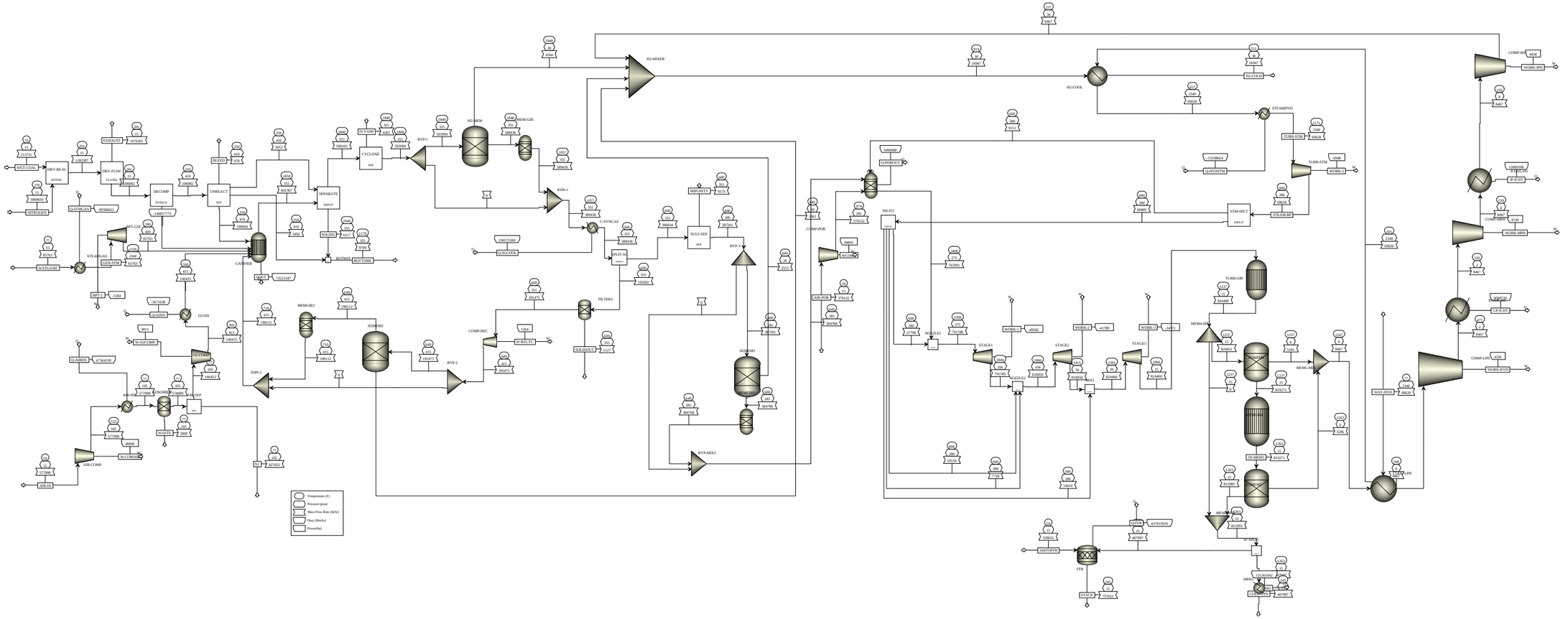

Figure 10. IGCC – POGT unit model schematic with H_2 membranes located at the gasifier outlet, clean syngas outlet, recycle syngas line, and POGT exhaust..

4.0 Experimental Study of 200kW POGT-Spartan

4.1. Technical approach for converting Spartan-350 to POGT configuration

A specifically designed POGT system would involve a modified air compressor, an expansion turbine, all based on the technology used to engineer and build current gas turbines. A POR, however, would be based on gas turbine combustor technology but would be of a more specific configuration. It is expected that a POGT would not be any more difficult to design and manufacture than a standard gas turbine. Depending on the extent to which existing turbo machinery components and gas turbine recuperator unit cells or industrial heat exchangers can be used, the development would be one of modest cost and duration.

In this project, the conversion of an existing Spartan T-350 industrial gas turbine to a POGT configuration was selected as the most efficient approach for validation testing. Solar loaned one of the Spartan T-350 gas turbine generator sets for conversion to a POGT configuration. A cut-away view of the engine is shown in Figure 11.

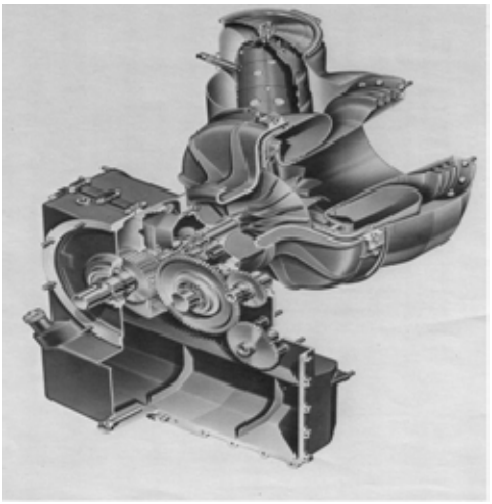

Figure 11. Cut-away view of Spartan T-350.

The general layout of the Spartan-350 engine/generator set converted to POGT (shown with steam injection) is provided in Figure 12.

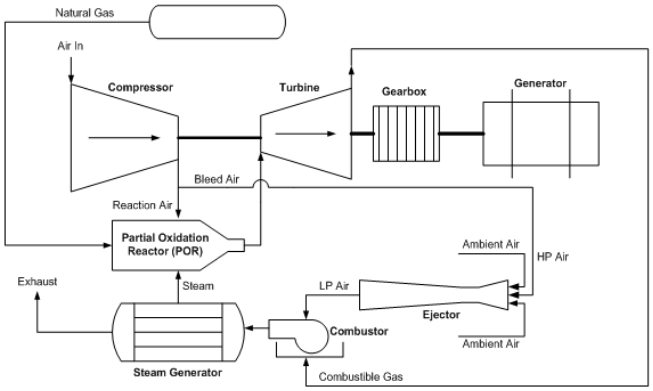

Figure 12. Spartan POGT Schematic.

The conversion required that modifications be made in three major areas:

- Engine
- Combustor
- Balance of plant (e.g., start-up and controls)

Mechanical modifications to the engine were required as the POR requires significantly different mass flow rates of the fuel and air for the same power output as a conventional Spartan-350. There were also constraints placed on the POR design by the mechanical design of the engine. These constraints limited the casing configuration when such parts as the air bleed ports were incorporated into the design. There are also secondary requirements involving replacement of the engine control system and the development of special light-off and shut-down procedures. The replacement of the combustor with a POR involved both the engine mechanical modifications and the design compromises of the POR subsystem.

4.1.1. Review of Conception Partial Oxidation Reactor Designs

An analysis of conventional combustors made it apparent that no true conversion of an existing gas turbine combustor to a POR was feasible; specifically for the Spartan T-350 a total combustor replacement would be needed. The replacement system would include a POR chamber, complete with a new pressure casing and new instrumentation for both control and performance evaluation.

Three different POR conceptual arrangements were evaluated. The concept finally selected for the POR detailed design and fabrication incorporated steam cooling provisions for the reaction chamber with angled injectors. The intent of the conceptual review was to determine the best type of design of a POR assembly to conduct experimental tests in a rig setting and for performance demonstration purposes in a Spartan T-350 engine converted to operate in POGT mode. One note to remember, the converted POGT Spartan engine incorporates an air bleed port, which would be omitted in a specifically designed POGT turbine engine. As a consequence overall efficiency projected from Spartan T-350 demonstration tests is not expected to match estimates compared to operation with a dedicated POGT designed system.

The first of two related Spartan POR conceptual designs, designated as POR1, is shown in Figure 13. The POR1 approach for fuel and air injection uses parallel straight air-fuel jets with

an internal shroud element to induce through entrainment local recirculation and vortices. POR1 also employs steam cooling. This provision utilizes a separate steam housing encapsulating the entire reaction chamber. Steam flow is directed into the annular volume between the steam housing and reaction chamber to control metal temperatures and for dilution cooling of the POR exhaust gases. A separate pressure case is located around the reaction chamber/steam housing to support the operation at the required turbine delivery pressures. The second conceptual design, POR2, is presented in Figure 14 and is comparable with POR1 but without steam cooling. POR2 method of fuel and air injection is the same and instead of steam housing, insulating material fills the interior volume between the reaction chamber and the pressure case.

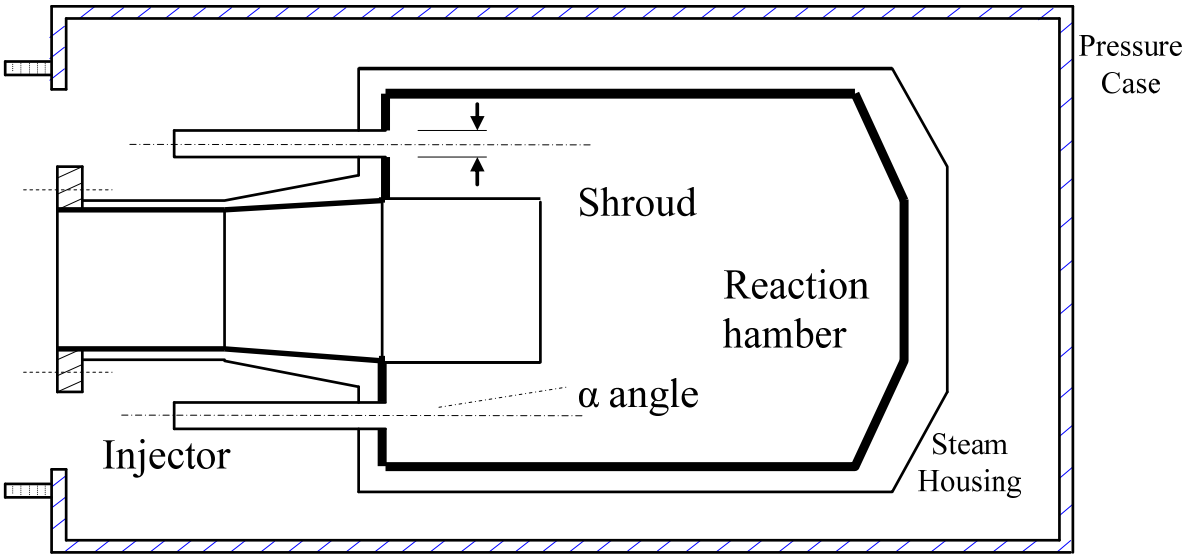

Figure 13. POR1 Schematic; Steam-Cooled, Internal Shroud, Parallel Injector Reaction Chamber Concept.

A third concept studied, POR3, was developed from the review of the two preceding concepts and is shown in Figure 15. In this case, injector ports were equally spaced and installed at an angle instead of a parallel configuration. Studies indicated angled ports improved the premixing of air and gaseous fuel and created internal jets that merge on the reactor centerline and formed a local vortex.

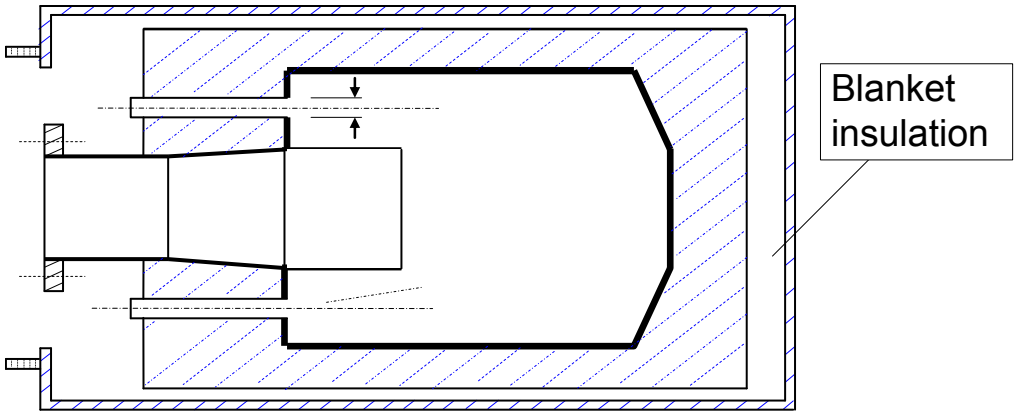

Figure 14. POR2 Schematic; Insulated (Un-cooled), Internal Shroud, Parallel Injector Reaction Chamber Concept.

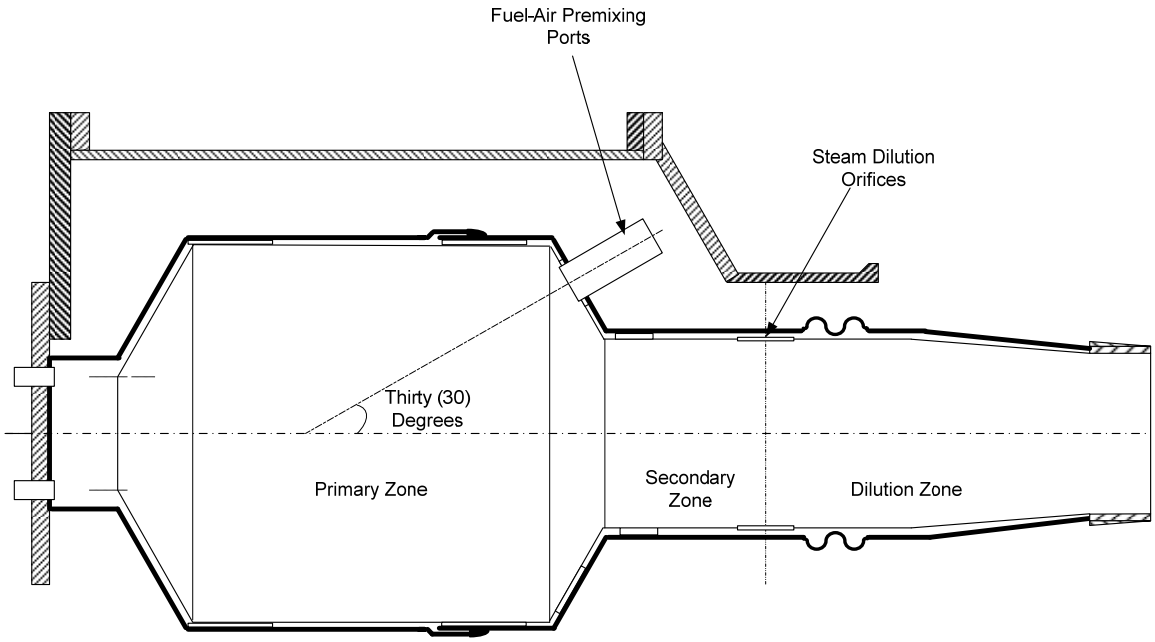

Figure 15. POR3 Schematic, Steam Cooled, Angled Injector, without Internal Shroud Reaction Chamber Concept.

The POR3 concept has no internal "hot parts" that usually not in favor of combustor designers. Because of process considerations to provide a strong recirculation pattern of hot gases to expedite and stabilize the reaction, the diameter of the primary reaction zone has to be relatively large. Large diameters reduce the jet cross-flow velocities and allow the jets of air and fuel to penetrate to the center of the reaction zone and create the necessary recirculation flow pattern. And because methane conversion reaction rates are generally slow (low OH radical concentrations due to low oxygen levels) the size of the POR has to be relatively larger than a conventional combustor. Of the three conceptual designs evaluated, POR3 was selected for final design and fabrication. This version consists of a larger diameter main reaction chamber and a smaller diameter dilution and mixing section. Additional reaction will take place in the dilution section between the steam used to reduce the reaction temperatures to turbine inlet temperature

(TIT) level and the carbon monoxide present in the gases leaving the main reaction section. This shift reaction will provide improved hydrogen exhaust concentrations.

All conceptual designs under consideration were developed and analyzed using standard engineering practices along with support of computational fluid dynamics (CFD) modeling using FLUENT simulation software. Simulation results characterized the effect of different design elements such as reaction chamber dimensions, number of injectors, injector diameter and injector installed angle. These CFD studies supported the rapid investigation, selection, and refinement of the final POR design. The results from CFD simulations compare predicted parameters in POR1, POR2, and POR3 reaction chambers. POR3 design provides more uniform temperatures in the reaction chamber and better mixing of the fuel/air stream out of the injector.

4.1.2. POR Design Approach

The design and size of the POR depends first and foremost on whether almost equilibrium or non-equilibrium operation is required. Because of the limited data available on performance and size relationships for non-equilibrium POR systems it is really difficult to produce a preliminary design. For equilibrium systems, the process is a little easier because combined theoretical and empirical correlations exist that tie global reaction rates to a volume needed to reach near equilibrium conditions. For this program, emphasis is being placed on the reaction rate controlled near the equilibrium systems that can produce syngas or hydrogen rich exhaust gases. Primarily the performance required, that is the overall efficiency of the POGT and the split between the electrical power produced and the chemical energy contained in the fuel gases that are both produced, determines the design of the POR. In addition, the need to minimize the gaseous pollutant emissions also affects the design process.

The design of the selected POR concept is such that the air and fuel will be premixed in external ports or nozzles and the reactor walls will be blanketed with steam to avoid any air leaking into the hot flammable fuel-rich product gases. The reactor design thus employs two annular passages surrounding the “can” reactor the inner passage is being filled with steam and the outer passage filled with air. The steam is pressurized to the point of supplying leaks into the steam passage.

The design of the premixing ports or nozzles is based on both theoretical and empirical models using data generated by both GTI and others. The designs are relatively simple in concept. The air nozzles or ports are simple tubes around 1-inch in diameter that have both a single point fuel injection tube and a tube with multiple radial holes fixed at the center of the air-tube terminating just inside the air-tube inlet. The single point fuel injection system is typically made from standard 0.125-inch tubing and is used for start purposes. A large curved section of the main tube in which the air and fuel is mixed allows the air to enter radially and accelerate into the main air-fuel mixing section. The acceleration of the flow from the larger to the smaller diameter enhances the air mixing process and eliminates or minimizes any abnormal velocity profiles or disturbances.

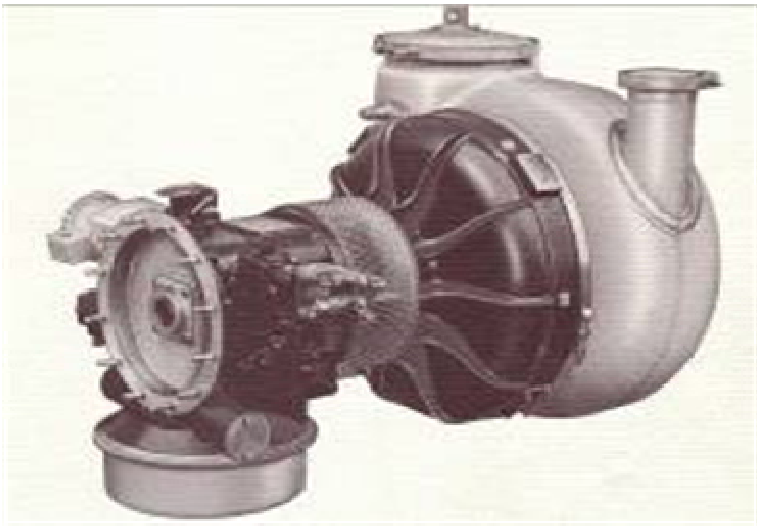

Figure 16. Spartan T-350 Engine Showing Can.

Using a rich, premixed fuel-air charge ensures the reactions will be reaction rate controlled. Thus the assumed reaction rate allows an estimate of the size of the POR to be made for a given reaction efficiency. The size of the POR has to increase as the desired level of efficiency is increased. Here the reactor efficiency is defined in terms of as the amount of methane actually reacted compared to the theoretical equilibrium predicted levels. The levels of methane remaining in the exhaust gases over and above the equilibrium levels are a measure of the system inefficiency. The reactor performance is strongly tied to the reactor size particularly when an equilibrium product mix is required. To achieve a high efficiency (typically 99.9%) the POR will be large, if the product mixture leaving the POR is to be near equilibrium. This large reaction volume requirement ties in with the POR aerodynamic requirements. Low cross velocities over the incoming air-fuel jets are required to allow them to penetrate to the centerline of the reaction chamber. This penetration is critical in creating the large recirculating flow to stabilize the reactions.

In the case of Spartan T-350, the POR replays conventional can-type combustor. Thus the POR needed must fit a can type geometry. However the POR has to be considerably larger in diameter than the combustor it replaces. These large (can) systems often make the production of the needed internal aerodynamic flows a more complicated task than for the more common smaller can systems which are usually associated with small gas turbines. The existing exhaust dimension where the original combustor mates to the turbine volute or transition duct is approximately 7-inches in diameter. The transition from the POR diameter to the 7-inch diameter exit creates velocity gradients that tend to hinder the desired flow recirculation(s) necessary to stabilize the reacting flow. Larger diameters can provide better recirculating flows but at some point the pressure drop of the POR could be increased to provide the required jet penetration.

4.1.3. POR Final Design

The POR, as noted earlier, is a novel piece of equipment for which there was little precedent to follow in guiding its design activity. Overall attention given to the POR design considered

features such as functionality, structural safety, ruggedness, flexibility, and its cost to construct. Careful analysis of operating requirements led to an initial POR mechanical design, which was based on engineered estimates, good practices and hand calculations.

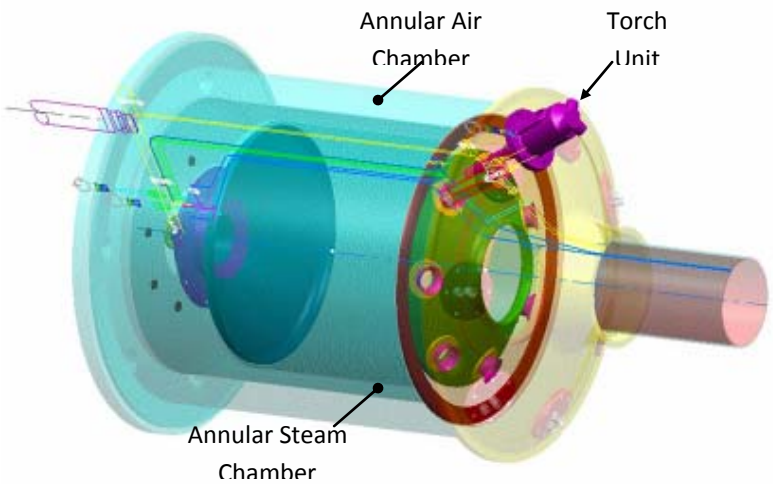

Figure 17. Solid Model of POR Final Design Assembly.

As the design progressed, the project team felt justified in the preparation and investment of conducting a finite element analysis and study of various design options and design sensitivities. With results from the finite element analysis, a final POR mechanical design was established; a solid model view of the entire POR assembly is shown in Figure 17**.**

Briefly, the POR mechanical design consists of a Pressure Case, a Steam Housing, a Heat Shield, and the essential Reaction Chamber. Other major components include: multiple fuel-air mixing ports commonly referred to as injectors, one torch unit (for start-up only), and a system of process stream manifolds with interconnection tubes. Process streams include compressed air, steam (dilution cooling and process services), and natural gas (start gas and main fuel services).

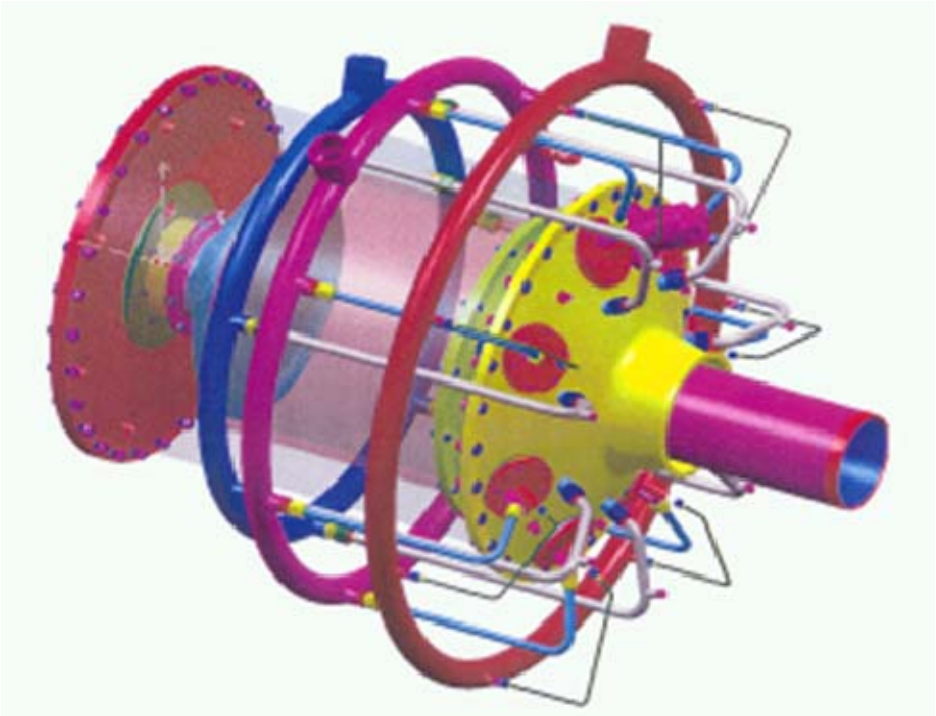

Figure 18. View of POR Annular Steam and Air Chambers.

For clarity, another solid model view of the POR design is given in Figure 18 without the manifolds and with the color faded on the Pressure Case components. Here the shape of the Reaction Chamber is distinguished as well as the annular Steam Housing surrounding the Reaction Chamber and the annular chamber containing compressed air for the injectors. On the rear dome, an auxiliary port is provided to vent a portion of the compressed air for fine tuning of the air flow entering the POR.

This cross-section also shows the position of the injectors (premixing ports) and how the air-fuel jet produced enters the POR proper. The POR as designed is considerably larger than the combustor that it replaces and the liner is approximately three times the diameter of the original combustor. This larger diameter with its corresponding long residence times is needed because the reaction rates under the fuel rich conditions of the POR are much lower than those found under fuel lean conditions.

The stability of the POR is also very important and the operation depends strongly on the internal aerodynamics of the reaction chamber. The angled premixing ports produce a series of jets that penetrate to the POR centerline where they merge. The bulk of the merged jet flow moves toward the POR dome on the centerline. When the resulting merged jet flow reaches the dome, the flow is forced to turn 180 degrees. This 180 degree change adds very little delta P and minimal impact on compressor power is estimated. Pressure drop across the POR is in the range from 2 to 4% of supply pressure, similar with conventional engines. No decrease in mean fluid velocity

entering the turbine is expected because of the POR outlet tube design. The resulting flow field is a confined vortex that recirculates hot reacted gases over and between the incoming air-fuel

jets. Sufficient mixing between the incoming jets and the recirculation of hot gases from within the POR ensures ignition of the jets and maintain a stable flame. The pressure drop in the POR is expected to be between 2% and 4%, which is the comparable to lean premixed low NOx combustors on current design conventional gas turbines. To ensure that the product gas composition can be accurately controlled, the air and fuel entering the POR has to be well premixed. To accomplish this, mixing an air-fuel premixing port was designed based on proven concepts. A cut-away solid model drawing of the port is shown in Figure 19.

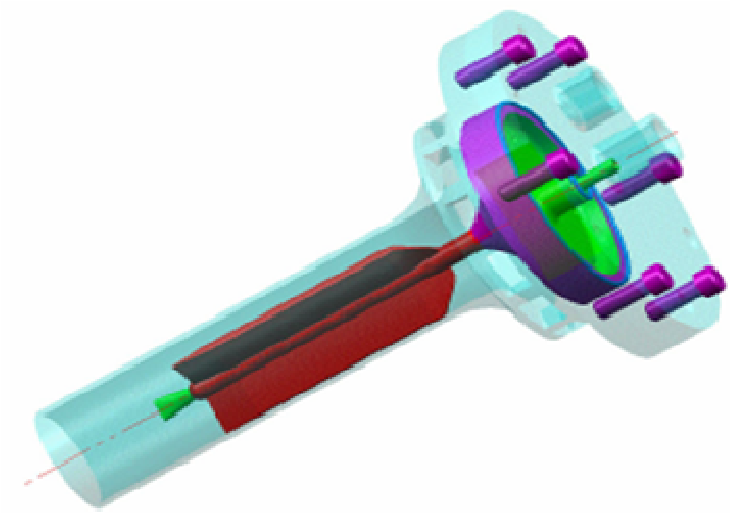

Figure 19. POR Injector.

The structures shown as pale blue in are the main assemblies of the port and its mounting system. The section in blue where the bolts are located is a cover-plate that fastens to the outer casing and covers the access holes for the ports. The section with a radius smaller than the cover plates that has slots cut into it is the air inlet. Air flow direction in this diagram of the premixing port is from right to left. Air enters through the slots and flows radially inward to the cylindrical or tubular piece and then moves from right to left through the vaned passages. The air is accelerated as it moves radially inward and in doing so it tends to mix and produce a "flatter" velocity profile than if the air had entered axially. This inlet air mixing also helps minimize any flow disturbances caused by structures external to the ports that might enter with the air flow. Located concentrically within the cylindrical section is the start fuel line and nozzle. This start fuel is injected into the air stream near the exit of the port to minimize mixing and thus aid light-off. The start fuel line is held in place with a three-vane "spider" type structure.

The division of the cylindrical section into three smaller mixing ducts by the start fuel line support vanes improves mixing of the main fuel and air by reducing the effective hydraulic diameter of the ducts. The main fuel is injected through a number of small holes in the back face of the air inlet section. Referring to Figure 18, the green section is a plenum distributing the main fuel to each of the injection holes. The opposite side of the circular wall (shown green) is the face of the air inlet section. After injection the natural gas jets and the air mix and by the time the gases leave the cylindrical section they are near perfectly mixed.

If desired, steam for reaction purposes can be injected with the air and fuel through the start fuel tube. This would occur after light-off and when the start fuel line connection valve has been closed. To accommodate the reaction steam, the air and fuel flows would be reduced but the equivalence ratios could be maintained at near constant levels to produce a high ratio of hydrogen to carbon monoxide in the exhaust gases. Under rich combustion conditions increasing stoichiometric ratio (SR) will increase temperatures and decrease hydrogen and carbon monoxide concentrations in the POR exhaust. Test operation data will be collected to quantify chemical composition of the syngas.

Maintaining the temperature of the POR liner below roughly 1700°F requires little cooling. However the cooling potential of the steam used as a "blanket" is sufficiently high that over-cooling can easily occur. The cooling concept employed involves a series of radiation shields with essentially non-flowing steam between them. The outer annular passage (with the casing as the outer wall) conveys the engine air around the POR and the heat shields to the bleed ports located in the casing dome. The steam filled passages prevent any undesired air leakage into the reaction chamber.

In the case of the Spartan, the TIT is lower than the POR reaction temperatures and thus as mentioned above the steam addition is required to reduce the gas temperature. Majority of the steam that fills the annular passages between the heat shields flows rearward and enters the POR dilution section through holes that are depicted as small rectangular structures attached to the POR liner. The injected steam jets mix with hot gases leaving the POR reaction chamber and moves into the turbine inlet collector or scroll piece. This cools the POR exhaust by dilution.

The POR does not include a diffusion flame for either start-up or continuous operation. Start fuel is partially premixed and the main fuel is fully mixed. Evaluation of soot formation is planned during tests with the POGT converted Spartan turbine. Several provisions in the POR design to suppress soot formation consist of intense flue gas recirculation patterns and process steam injection directed along the internal walls of the reaction chamber.

4.1.4. Detailed Design

Detailed design for this first-of-a-kind experimental POR assembly was engineered with technical assistance from Belcan Corporation's Advanced Engineering and Technology Division. Based on POR performance requirements, a comprehensive design analysis was conducted by Belcan evaluating structural integrity, system thermal stresses, and process flow capabilities. Structural, thermal and stress analyses were conducted using ANSYS which is a finite element modeling package for numerically solving a wide variety of mechanical problems such as static/dynamic structural analysis (both linear and non-linear), heat transfer, fluid problems, and more. Figure 20 below shows an ANSYS prediction of thermal gradients for the POR reaction chamber.

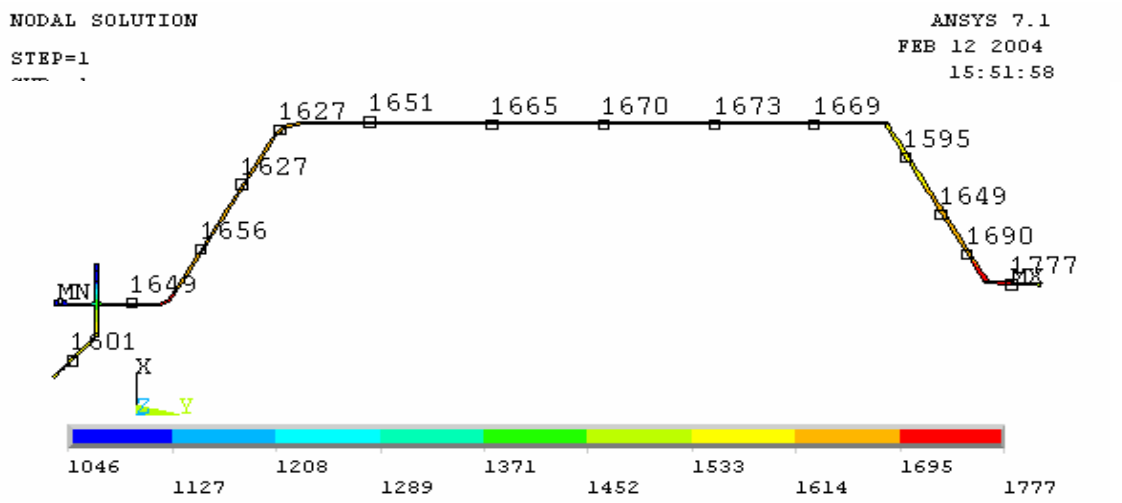

Figure 20. POR Reaction Chamber metal temperature predictions by ANSYS.

The final design became slightly more complex as a result of the interface required for the Injectors, Torch and Igniters with the Reaction Chamber, Steam Housing and Pressure case. This interface was a series of grommet/retainer sets, which provide the means for the barrel sections of the Injectors along with the Torch and Igniters to penetrate internal metal walls without restricting metal thermal growth and high mechanical stresses. The remainder of the design is relatively simple, consisting of plates and sheet metal. Final design analysis also incorporated an insulation jacket over the heat shield surrounding the Reaction Chamber to maintain chamber wall temperatures above 1660 °F lower limit as specified for POR operation. This resulting design provides an excellent platform with functionality to conduct both experimental and performance technology evaluations. The proof of concept testing of POR technology in a test cell setting and later performance testing, replaced a conventional can combustor on a prototype Spartan T-350 test engine which was converted for POGT operation.

Spartan T-350 turbine engine modifications required for POGT operation included the following:

- POR-Spartan Interconnect
- Bleed port addition
- Steam seal buffering
- Transition duct cooling (steam)
- Instrumentation and Controls

POR to Spartan Interconnect

The POR reactor mechanical design incorporated details to facilitate integration with the Spartan T-350 engine. During this development, it became clear a custom Hook-up assembly was required to mitigate concerns of over stress at the Spartan inlet scroll as well as at its outer casing Marmon flange connection due to the differential thermal expansion between the engine and the outlet tube of the POR Unit. This interconnection, referred to as the hook-up assembly, consisted of a bellows element with inlet and outlet sleeves placed between the POR outlet and

Spartan inlet scroll. With the bellows, mechanical stress to the turbine scroll and outer casing from thermal expansion of the hot POR outlet was eliminated. In addition, the bellows mechanically isolated the Spartan engine from POR operational disturbances if encountered.

Before fabrication of the hook-up assembly, alternative designs were first modeled to ensure proper mating with the Spartan engine. Figure 21 shows the as-built POR/Spartan hook-up assembly.

Figure 21. Hook-Up Assembly.

The hook-up unit expansion joint is a 6" diameter corrugated bellows constructed with multiply layers of Hastelloy-X material. The bellows inlet sleeve consists of an enlarged collar section on top to accept a machined distributor ring built into the POR outlet tube design. The bellow's outlet sleeve is equipped with machined distributor ring having 30, 0.156" diameter holes for even distribution of steam or inert gas for the prevention of air ingress at the joint. The bellows outlet distributor ring press fits into the Spartan scroll inlet collar. Flow of inert medium is independently supplied through a spare port on the engine casing previously used for igniter service. During POR operation, nitrogen was used at this location while at the POR outlet tube joint with the hook-up unit, which contained an identical ring design, used steam.

The POR to Spartan assembly sequence started with attachment of an extension pipe spool to the POR casing outlet flange. The POR assembly because of its size was secured in the test cell and supported by a spring system mounted from an independent structural framed table.

The extension pipe is bolted directly to the POR outlet flange and properly aligned to match with the ½" ports constructed in the hook-up assembly bellows inlet sleeve for steam injection as noted earlier. The other end of this extension spool is fabricated with a Marmon clamp fitting to accommodate connection with the Spartan outer engine casing flange. The hook-up assembly is then pressed into the Spartan inlet scroll collar and the steam connection with bellows outlet distributor ring at the engine inlet scroll is made.

The POGT engine is skid mounted and rolled into place underneath the axis of the POR outlet and then slowly raised. The bellows inlet sleeve slides up into the extension spool and engages

the POR outlet distributor ring. The engine placement is secured after a satisfactory fit of the engine casing Marmon clamp connection is achieved.

Final assembly of the steam injection ports were then built. The steam injection probe utilizes a bellow element to accommodate thermal growth between the internal Hook-up assembly and the Extension spool casing. At this juncture the POGT prototype engine is ready for pre start check out. An overall diagram showing the POR-Spartan interconnection is given in Figure 22.

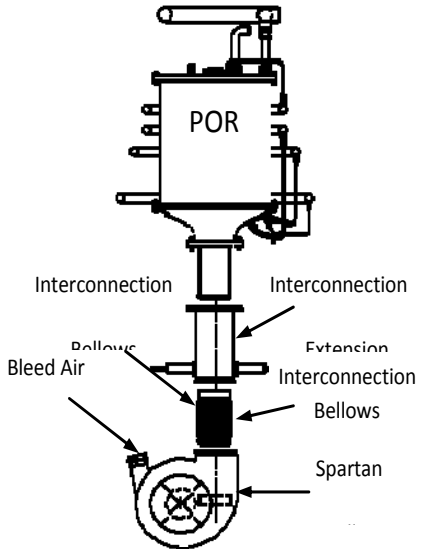

Figure 22. Schematic of POR to Spartan Connection.

POGT Spartan Bleed Air Modification

The particular engine selected for POGT conversion was originally a standby generator set for a telephone utility company. In order to perform as a POGT, the airflow entering the POR has to be considerably less than the flow that would have entered the standard combustor. To achieve this flow reduction, the simplest approach was adopted. This consisted of bleeding air from the compressor exit in a manner similar to that used by the Spartan bleed machines.

Some versions of the Spartan engine have a specifically designed bleed port mounted on the combustor scroll casing diametrically opposite the combustor location. This existing design approach has been adopted as the primary method of bleeding air. However, the difficulty of cutting the sheet metal casing and installing reinforcing sufficient to allow mounting of the bleed port limited the size of the bleed port for installation. The final design required that small bleed ports be located on the dome of the POR casing in addition to a four-inch conventionally mounted bleed port. The former was mounted in a ring around the edge of the dome plate and allowed the bleed air to flow over the POR reaction section for cooling purposes before it is vented.

A bleed port size of 4 inch was selected based on information from past applications of this engine. Figure 23 shows an early picture of the Spartan engine casing with the bleed port.

Figure 23. Spartan with new 4" Bleed Port.

The maximum bleed estimate of the Spartan is 2 to 3 pounds per second (pps) air at 54 psia. The flow rates quoted were for zero power output and were assumed to be the maximum flows allowable before compressor surge was encountered. In the POGT arrangement, there is unlikely to be any surge problems due to additional mass flow in the form of steam and extra natural gas, which is added in the POR and helps drive the turbine. This additional mass flow when combined with the much higher turbine volumetric flow and specific heat, allows the maximum power (200-kW) to be produced while bleeding about 2.9-pps of air from the compressor discharge.

It is estimated (from performance analyses) the desired bleed flow of 3.0-pps can be bled from the Spartan compressor (when operated as a POGT) with a small reduction in output power. This bleed flow provides a reasonable balance between the POR reaction temperature (2000 ºF) and the turbine inlet temperature (1575 ºF) while maintaining the power produced.

Steam Cooling

The Spartan employs a shaft seal located between the compressor and the turbine that prevents hot gases from contacting the shaft. To ensure that no hot gases reach the shaft, a small quantity of buffering air leaks past the seal and flows outward in a radial direction along the back-face of the radial turbine. This air flow enters the hot gas stream at the rim or inlet of the turbine. For POGT operation, this air stream has to be replaced with steam or other inert gas. The backpressure on the seal provided by the steam effectively prevents the air from leaking to the hot gas side of the seal and thus eliminates the problem of the creation of local hot spots on the turbine blades. Steam then entered the Spartan air buffering flow path through lines that penetrate from the outside casing and through the diffuser vanes to a space above the shaft seal plate rim (see Figure 24). A series of orifices drilled through the wall separating this space from the seal plate allowed the steam access to the seal plate rim. Cooling and process steam was raised in an external supplemental boiler.

In addition to this steam for seal buffering, the unmodified Spartan employs air cooling for the back of the turbine nozzle inlet section. Steam was also used to replace this air.

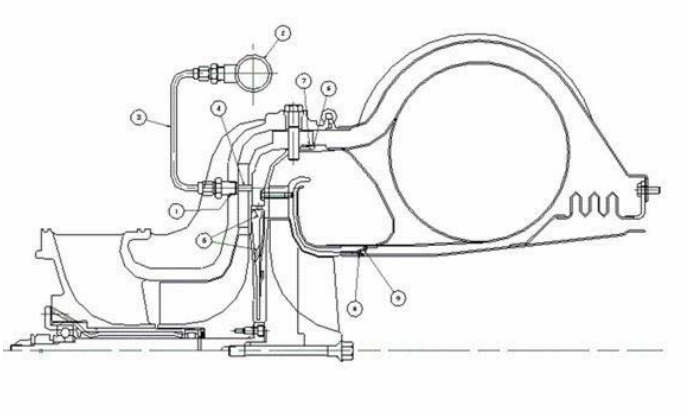

Figure 24. Spartan T-350 Showing Locations Where Steam is used for Sealing and Cooling.

POGT Engine Control and Management

A management and control system dedicated to safely start-up and monitor the Spartan turbine engine under POGT mode of operation was developed, implemented and demonstrated. The POGT Test Cell control platform consists of an Allen Bradley 1500 Micro Logic PLC and Siemens 353, stand alone process controllers. A personal computer National Instruments I/O interface system provided data acquisition and archiving function of test cell instrumentation. An overview diagram of the POGT test rig process streams and instrumentation is shown in Figure 25.

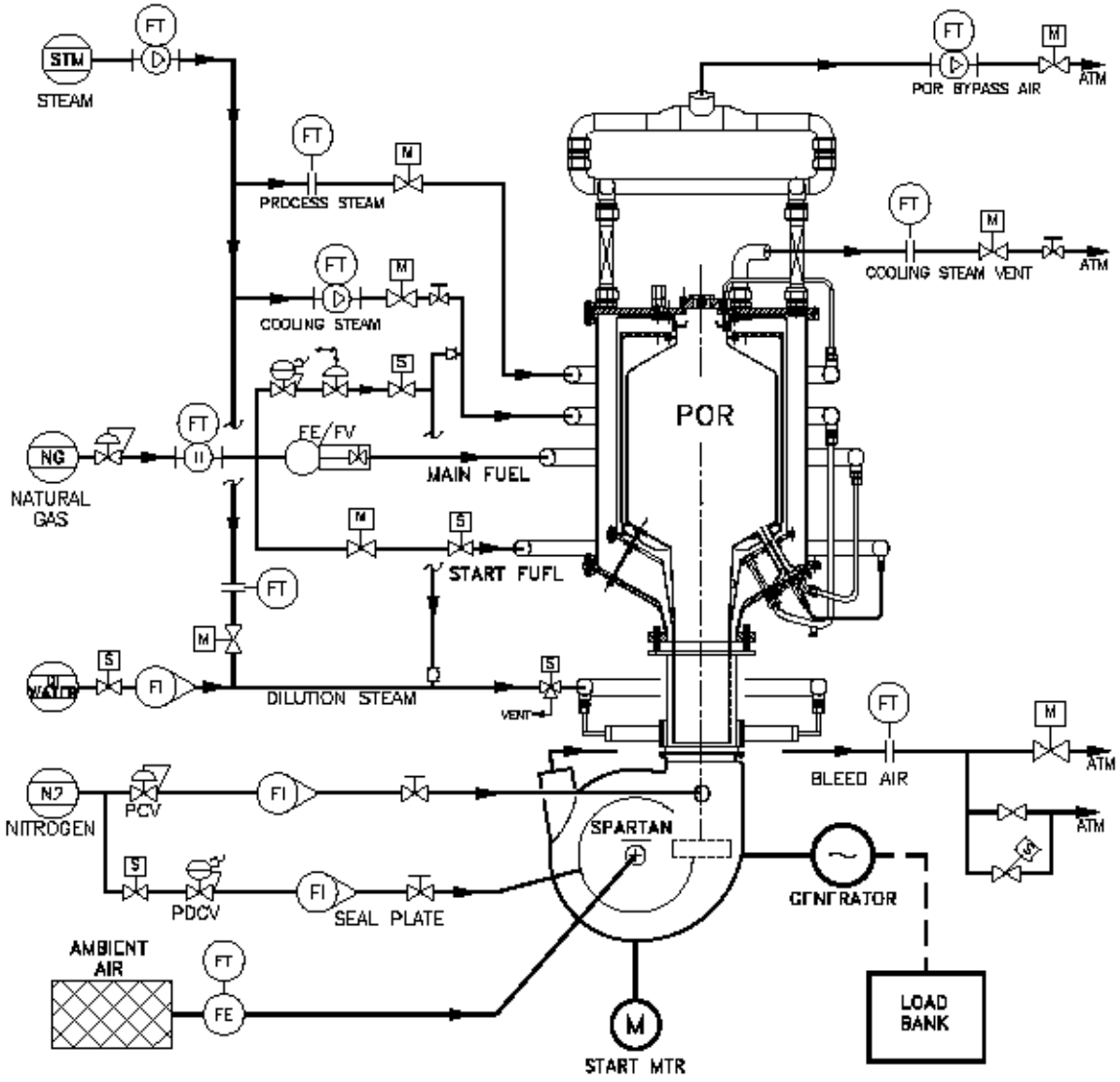

Figure 25. POGT Test Rig Process Diagram.

Steam flow is distributed between process, cooling, and dilution services. Natural gas flow is divided between start and main fuel streams. During testing, a small amount of fuel was also combined and mixed with cooling and dilution steam for process evaluation. Nitrogen was used as an inert medium for the seal plate and the buffer medium at the Spartan scroll inlet connection. Excess air generated from the compressor wheel was released and vented through the turbine new bleed air port as well at the POR, which had provisions to vent air from the reactors air jacket compartment. Hot de-ionized water was atomized and combined with dilution steam flow to provide additional control for cooling and for maintaining the temperature of the POR exhaust gases. The POR steam annular compartment also included a port from which steam was vented as a means to regulate the reaction chamber top metal skin temperature.

Initial control development efforts involved construction of empirical and theoretical models for evaluating the low load or low rpm conditions that the Spartan experiences during starting and acceleration. This analysis involved static algorithms for a given speed and TIT. For each speed, a reaction temperature was estimated and then for a given air bleed and steam injection rate, a TIT is determined and a fuel flow calculated. The reaction temperatures or TIT values are adjusted to produce a reasonable fuel schedule as a function of speed.

Control management and sequencing of the POGT Spartan engine control devices from start-up through stable load condition was developed and successfully demonstrated. POGT engine sequencing and safety logic functions were controlled in Allen-Bradley's 1500 series PLC; real-time control of fuel scheduling and engine speed was handled in a Siemens 353 process controller. In addition, speed regulation of the POGT engine utilized the generator set voltage regulator to modulate the resistive load of the test cell load bank in maintaining the engine speed at set point. Logic to implement basic engine sequencing was configured in the form of an event driven state machine. A simplified block diagram of this state machine is given in Figure 26 below.

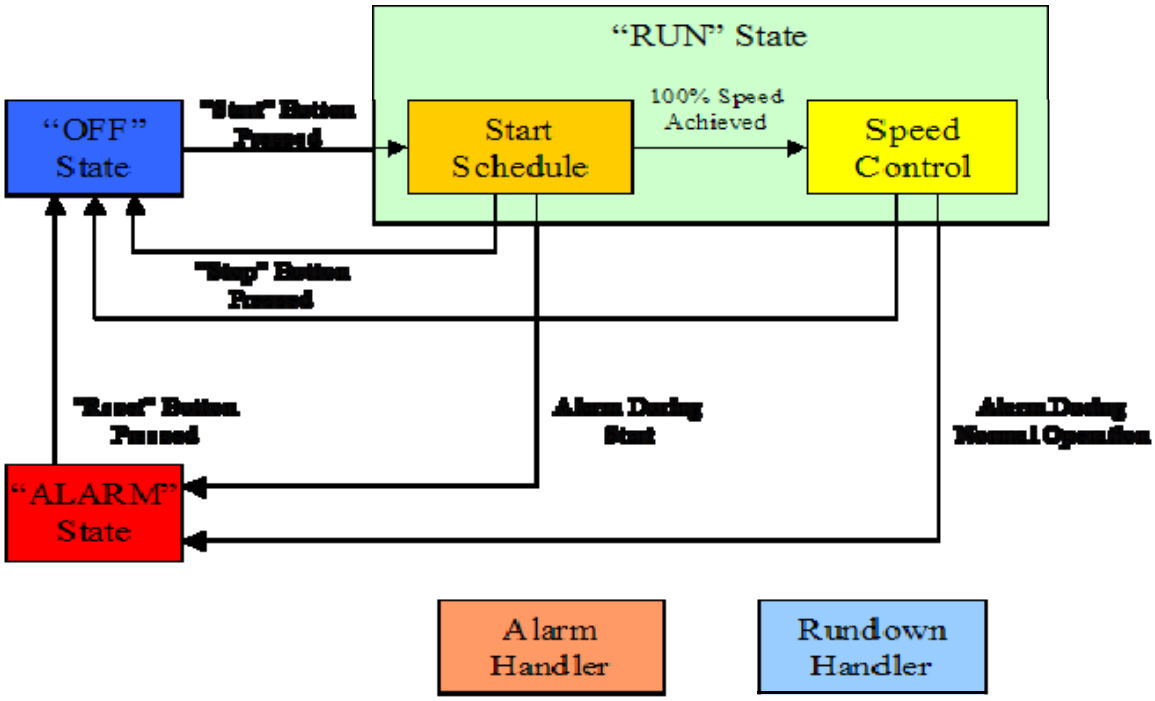

Figure 26. Simplified POGT State Machine Block Diagram.

There are three basic, exclusive, states in which the system can reside. These are the "Off" state, the "Run" state, and the "Alarm" state. Within the "Run" state, there are two sub-states. These are the "Start-Schedule" state and the "Speed-Control" state. In addition, there is the "Alarm Handler" and the "Rundown Handler." These handlers are not state driven, but instead operate and monitor continuously.

The Rundown Handler simply watches the state machine to detect when it leaves the "Run" state. When this occurs, it starts an internal 2 minute (+/- 10 sec) inhibit timer. While this timer is

active, the state machine is prevented from transitioning from the "Off" state to the "Run" state. This allows the rotor assembly time to decelerate and stop from a previous run before initiating a new start.

The "Alarm Handler" allows alarms to be enabled or disabled by events within the state machine. It continuously monitors all enabled alarms. In the event that an enabled alarm is triggered, the state machine is automatically transitioned to the "Alarm" state.

The following is a list of major alarms (i.e. shutdowns) monitored by the alarm handler:

- Emergency Stop (E-STOP)
- Locked Rotor (LR)
- Failure to Light (FL)
- Failure to Start / Over crank (OC)
- Low Oil Pressure (LOP)
- High Oil Temperature (HOT)
- High Exhaust Temperature (HET)
- Under-speed (US)
- Over-speed (OS)
- Backup Over-speed (BUOS)

Of these shutdown alarms, only Emergency Stop is enabled all the time. All other alarms are enabled and disabled by state machine signals.

4.1.5. POGT Operation Sequence

Upon energizing the power to the POGT main system panel, valves are automatically driven into a safe state. An operator triggers the engine "Ready" state via a pushbutton located on the main engine control panel. In this transition, the dilution steam flow control valve opens to establish a preset start-up flow. This flow is diverted to a vent via a three-way automated valve until called upon during engine acceleration. In addition, the engine's start motor 24 V dc capacitor bank charges.

After the capacitor bank charge time has elapsed, the operator starts the engine via another panel pushbutton. The POR torch igniter starts followed by opening of the dedicated torch gas and air solenoids. Control logic verifies torch temperature is acceptable before the main engine sequence starts.

With the POR torch on, the operator starts the engine by enabling the PLC sequence logic. This logic initiates a ramp algorithm in the Siemens controller driving the valve position for POGT fuel, bleed air, and steam flow valves. At start up, the engine start motor runs, simultaneously nitrogen flow is introduced to the seal plate for cooling and prevention of air in-leakage. Confirmation of engine rotation allows the Start fuel valve to open and initially regulates the POR chamber fuel schedule; shortly, as engine speed increases, the POR Main fuel valve opens and its ramp schedule begins. Engine acceleration reaches full speed in a period of about 40 to

50 seconds. Acceleration ramp schedules of the different POR bleed air and steam valves were tuned to automatically manage the engine start-up from ignition at fuel lean conditions to POGT mode (fuel rich) operation. At full speed, sequence control is disabled and engine regulatory control logic maintains the turbine RPM (revolutions per minute) at set point.

4.1.6. POGT Unit Testing

As described above, conventional Spartan T-350 was retrofitted to a POGT unit. The original Spartan compressor was used in the unit and because only about half of the compressor discharged air was used as a combustion air, the other half was vented to the atmosphere through a bleed port and POR bypass. In the POR, compressed air and process steam react with natural gas under substoichiometric conditions to produce hot syngas which as a working fluid expands in the turbine to generate power. The POGT was operated using a GTI engineered control and instrumentation system.

Test Plan

The POGT unit has been equipped with a comprehensive automatic and remote controls including control of the following parameters: engine speed; start-up and main fuel flows; total, combustion and bleed air flows; cooling, process and dilution steam flows; turbine inlet temperature (TIT) additional control through saturated water injection to the dilution steam, etc. Using this control system, required variations of the POGT parameters during the unit's operation could be set up.

For the POGT performance testing, the following variables and their ranges were selected:

- Engine speed which defines the unit load, 75—90%
- Combustion air to fuel ratio, stoichiometric ratio (SR), 0.3—0.7
- Turbine Inlet Temperature (TIT) 1300—1450◦F
- Flame temperature, 1950—2200◦F, and
- Back pressure (BP) at engine exhaust, 1—28 in. W.C. (Water Column)

A Test Matrix for the planned POGT performance testing is presented below in Table 5.

Table 5. Test Plan for POGT Performance Evaluation

		TEST MATRIX				
Test Series	**Test #**	**Speed, %**	**SR**	**Flame T, F**	**TIT, F**	**BP, inWC**
1-Speed	1	***85***	0.6	2050	1350	1
	2	***75***	0.6	2050	1350	1
	3	***90***	0.6	2050	1350	1
2-SR	4	85	***0.7***	2050	1350	1
	5	85	***0.5***	2050	1350	1
	6	85	***0.3***	2050	1350	1
3-TIT	7	85	0,5	2050	***1300***	1
	8	85	0.5	2050	***1380***	1
	9	85	0.5	2050	***1450***	1
4-BP	10	85	0,5	2050	1350	***10***
	11	85	0.5	2050	1350	***16***
	12	85	0.5	2050	1350	***28***

Four series of tests were planned. In each of the test series, one of the major parameters, (speed, SR, TIT, and BP) was considered as a main variable. The flame temperature is not considered an independent variable and was held almost constant at the given test. The effect of major variables on the major POGT output parameters were analyzed.

The POGT was operated using the GTI-engineered control and instrumentation system described above. Several test trials were conducted to develop the startup procedure and the sequence of the operation. The POGT startup approach is to provide transition from lean to rich combustion during the acceleration of the engine while keeping overall startup time about 40 sec (similar to conventional gas turbine of this size) and avoiding over- temping for TIT and EGT (Exhaust Gas Temperature).

In Figure 27 below, the POGT parameters during startup are presented. The curves were plotted from the recorded data during POGT-Boiler testing on 03-14-08. Transition from lean to rich condition occurs on the 25 – 30th seconds after "push-button" where the flame temperature and TIT reached the maximum and gradually went to lower readings. Fuel flow and the calculated equilibrium ratio have a delay due to the long response time (about 1 min) for natural gas meter. And the engine speed, air flows and temperature approached the stable readings at the 40th sec according the low inertia transmitters.

The startup procedure and control sequence of operation were used for all following POGT performance testing.

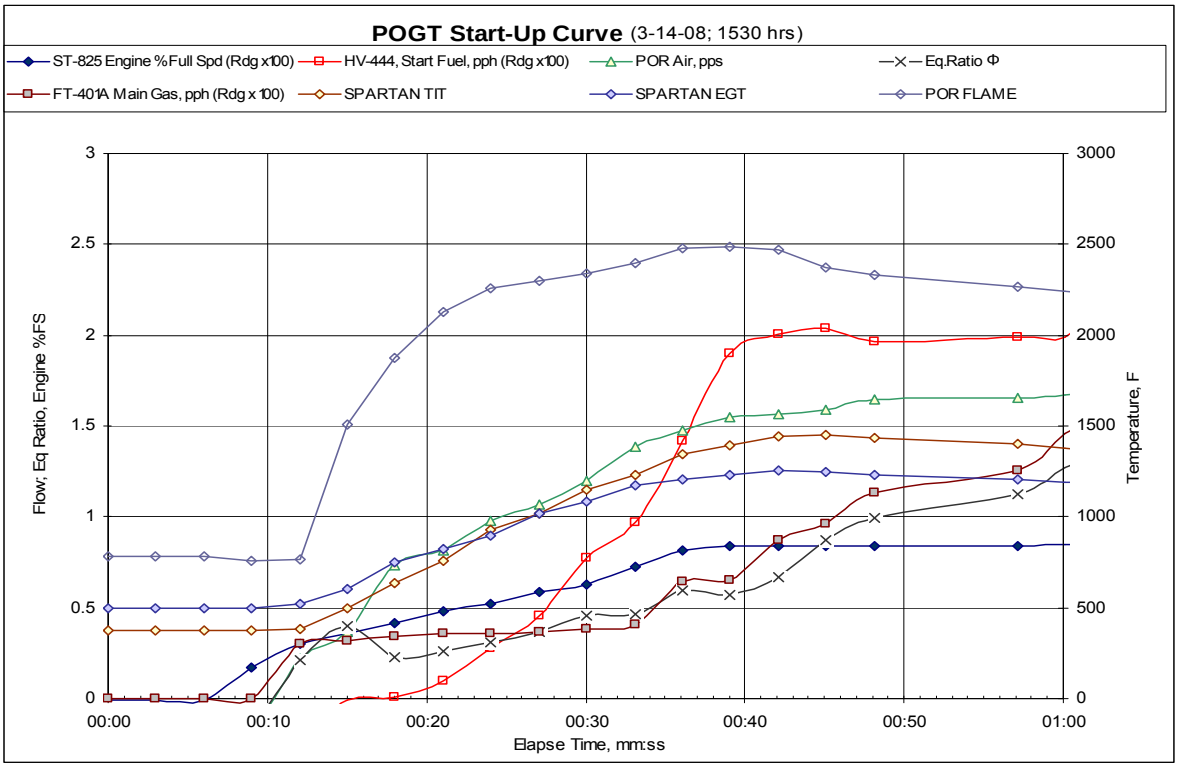

Figure 27. POGT parameters during start-up and conversion from lean to rich operation.

Once the startup procedure was developed, it was implemented in the control system, and successfully tested. In the Figures 28 and 29 below, the POGT parameters during startup are presented in more details from the same recorded data during POGT-Boiler testing on 03-14-08. Transition from lean to rich condition occurred about 25 – 30th seconds after "push-button" where the flame temperature and TIT reached the maximum and gradually went to lower readings. Fuel flow and the calculated equilibrium ratio have a delay due to the long response time (about 1 min) for the natural gas flow meter. According to the low inertia transmitters, the engine speed, air flow and temperature approached stable readings at the 40th second.

The startup procedure and control sequence of operation were used for all POGT performance testing presented later.

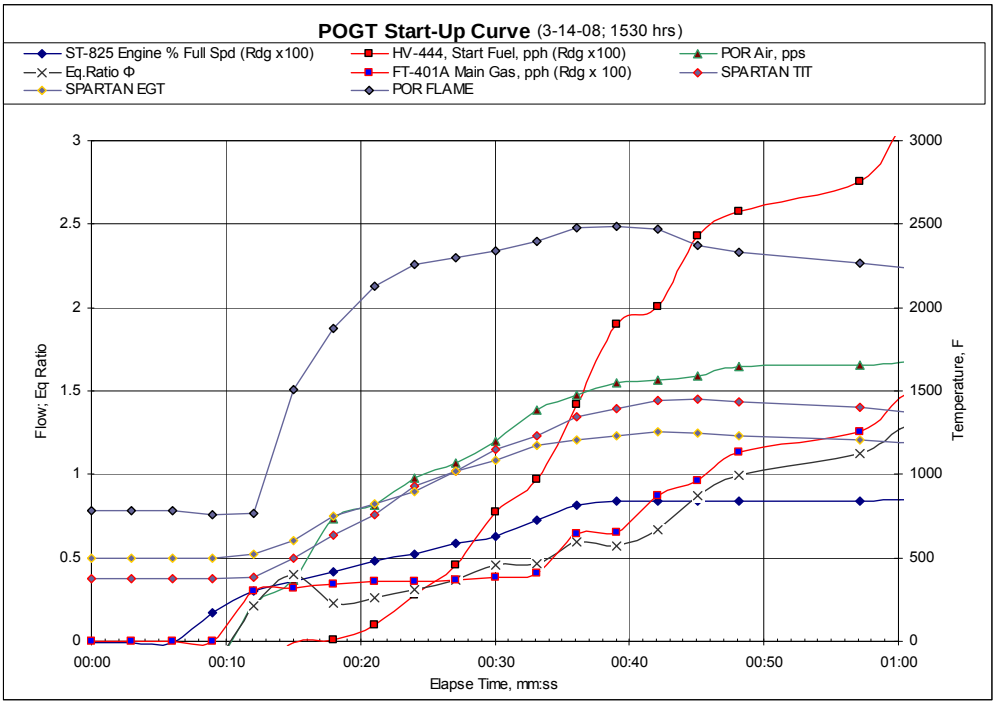

Figure 28. Fuel Flow and Temperature during POGT Start-Up.

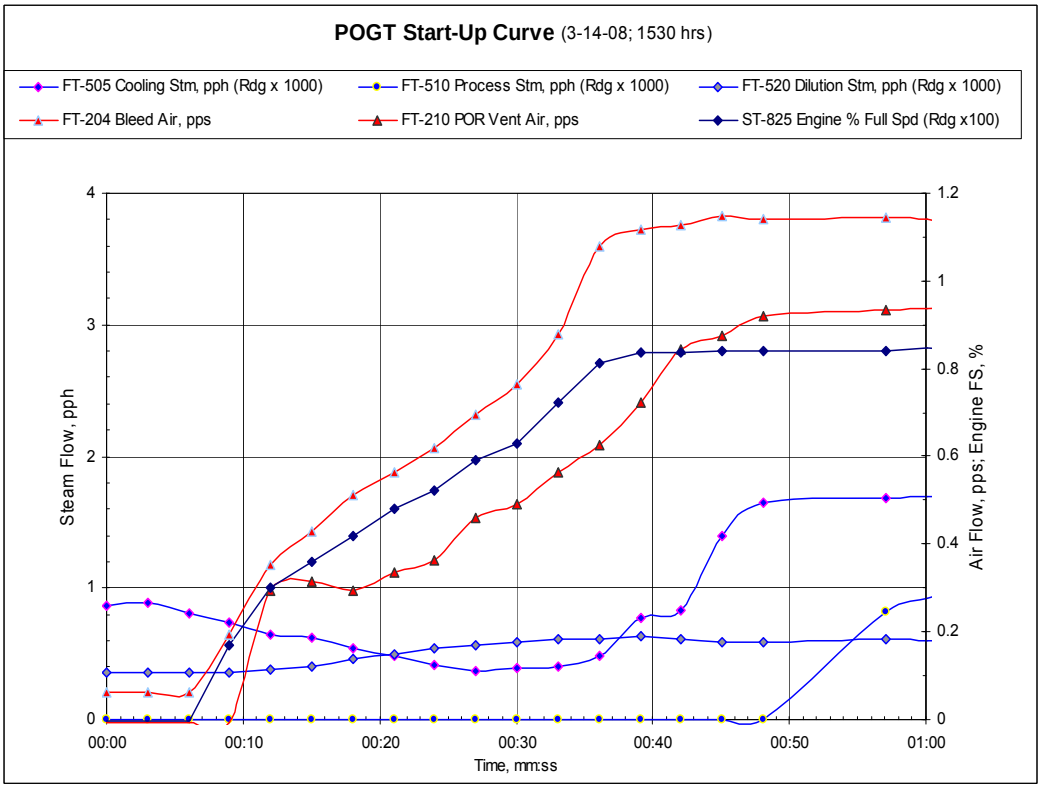

Figure 29. Steam and Air Flow, Engine Speed during POGT Start-Up.

After startup, the POGT was operated at required flows of air, fuel and steam as defined in the plan test matrix. Based upon the recommendations from industrial partners and the "first of a

kind" partial oxidation operation for the unmodified expander of the Spartan turbine, the POGT was operated (in the majority of the tests) at somewhat lower TIT (below 1400◦F) compared to the design TIT of 1600◦F. This general conservatism for research testing of the first POGT prototype was followed to avoid any risk of local overheating or related problems. No TIT related problems arose during any of the testing.

Seventeen POGT tests with up to 130 min duration each were selected for POGT performance analyses. A total of 17 hours of POGT operation were analyzed during the POGT performance testing. About 160 process parameters were recorded by the data acquisition system during each test. A summary of the test variables along with major measured and calculated data is presented in the Table 6 below.

Table 6. Summary of POGT Test Conditions and Key Measurements.

Date	Srart Time	Run Time min	Variables	Speed, %	NG, Total pph	NG, Main pph	Comb. Air pph	Steam Total pph	Expander Total Flow pph	SR	Back Pressure in. WC	PR	Flame Temp. F	TIT F	EGT F	Power, Measured, kW	Power, Actual, kW
11/20/07	4:19 PM	7	SR,TIT	84	560		6200	3900		0.65	0.8		2050	1300			
12/12/07	4:16 PM	19	SR, TIT	84	620		6000	3900		0.6	0.8		2000	1250			
12/12/07	5:19 PM	75	SR, FT, TIT	84	660		6200			0.55	0.9	2.33	2100	1400			
12/13/07	5:58 PM	46	RPM, SR, TIT	84 90	680		6500	3900		0.6	0.8	2.55	2100	1320			
12/14/07	4:52 PM	66	RPM, SR, TIT	75 84	520		5600	2700		0.6	0.8	1.94	2100	1550			
1/14/08	6:00 PM	21	SR, TIT, FT, BP	84	470 630	180 204	5600 6590	3445 3990	9515 11210	0.6 0.8	0.8 30	2.20 2.44	1870 2170	1230 1440	1070 1230	34 115	61 207
1/15/08	2:49 PM	98	SR, TIT, BP	84	460 850	177 207	5610 6520	3450 3980	9520 11350	0.4 0.8	1 27.5	2.17 2.43	1990 2170	1240 1410	1100 1270	53 104	95 187
1/16/08	3:40 PM	94	SR,TIT, FT, BP	84	426 821	158 192	5440 6370	3490 4170	9360 11360	0.4 0.8	1.1 28.2	2.2 2.43	1990 2175	1170 1390	1070 1220	46 107	83 193
1/18/08	5:06 PM	74	RPM, SR, TIT	79 86	365 1010	101 204	5240 6420	2570 4110	8175 11540	0.32 0.8	0.7 1.4	2.14 2.51	1960 2240	1210 1470	1100 1280	52 124	94 223
3/10/08	5:09 PM	12	SR, TIT, FT, BP	84.5	333 670	112 186	5865 7200	2850 4210	9050 12080	0.53 0.8	0.7 8.1	2.34 2.57	2030 2290	1340 1490	1160 1280	78 161	140 290
3/11/08	3:41 PM	14	SR, TIT, FT, BP	83.5 86	319 625	113 186	5760 6580	2690 3930	8770 11130	0.56 0.8	0.7 2.5	2.42 2.58	2030 2280	1320 1490	1160 1250	122 157	220 283
3/11/08	4:20 PM	63	SR, TIT, FT, BP	82.5 86	300 693	97 186	5560 7270	1770 4130	7630 1290	0.5 0.8	0.6 2.9	2.37 2.58	2020 2390	1230 1490	1100 1250	97 157	175 283
3/12/08	12:53 PM	35	SR, TIT, FT, BP	83 86	400 782	139 193	5590 6570	3380 4100	9370 11450	0.45 0.8	0.6 2.5	2.38 2.63	2010 2270	1230 1500	1080 1280	104 158	187 284
3/12/08	2:12 PM	130	SR, TIT, FT, BP	84 86	378 1145	122 254	5870 7350	2470 3920	8720 12410	0.32 0.8	0.8 3.0	2.22 2.61	2040 2350	1230 1510	1150 1300	34 159	61 286
3/13/08	1:32 PM	120	RPM, SR, TIT, FT, BP	78 86	363 1330	150 326	5440 6660	1720 3940	7520 11930	0.25 0.8	0.8 2.9	2.01 2.57	2030 2240	1240 1450	1120 1320	18 147	33 265
3/14/08	3:27 PM	48	SR, TIT, FT, BP	83 85.6	365 1156	138 261	5660 6700	2720 4110	8740 11970	0.32 0.8	0.9 1.5	2.35 258	1990 2290	1250 1480	1100 1280	84 146	151 263
3/14/08	4:30 PM	90	SR, TIT, FT, BP	83 85.3	371 1540	114 394	5680 6850	1990 3710	8040 12100	0.25 0.8	0.8 2.8	2.24 2.52	2010 2330	1250 1480	1140 1240	36 141	65 254
	Total Runs	17															

4.1.7. Data Analysis

The test data were processed and analyzed to evaluate the impact of changes in key POGT parameters included in the test plan. The effect of engine speed (load), TIT, pressure ratio (PR) and back pressure (BP) on POGT power output were determined. Three parameters of power output are considered:

- Measured Generator Power (Gen Power),
- Actual power output (Act Power) calculated as a sum of Gen Power and additional compressor power associated with the bleed and bypass air (As determined by experimental and Aspen calculated data, the Act Power is 1.8 times greater than Gen Power), and
- Specific power output (Spec Power), calculated as power output per pound mass flow through the expander exhaust, kW/(lb/s) or kW/pps.

Effect of Engine Speed on POGT Parameters

Engine speed was varied in several tests at levels measured in RPM (revolution per minute) noted in the column "Variables" of the test summary (Table 6). In those test series, speed was varied from 75 to 90% of full engine speed. Other parameters were kept in a relatively narrow range: TIT = 1330-1390◦F; BP = 0.8-1.1 in.W.C; SR (stoichiometric ratio) = 0.6-0.7.

The effect of engine speed on the measured generator power is shown in Figure 30.

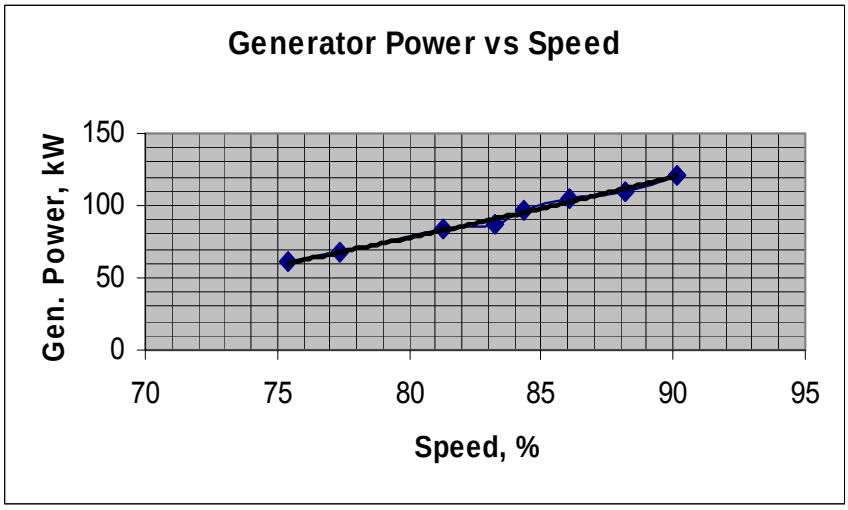

Figure 30. Generator Power measured vs. Engine Speed.

The effect of engine speed on other POGT parameters such as expander mass flow rate, pressure ratio, and actual power output are presented in Figure 31.

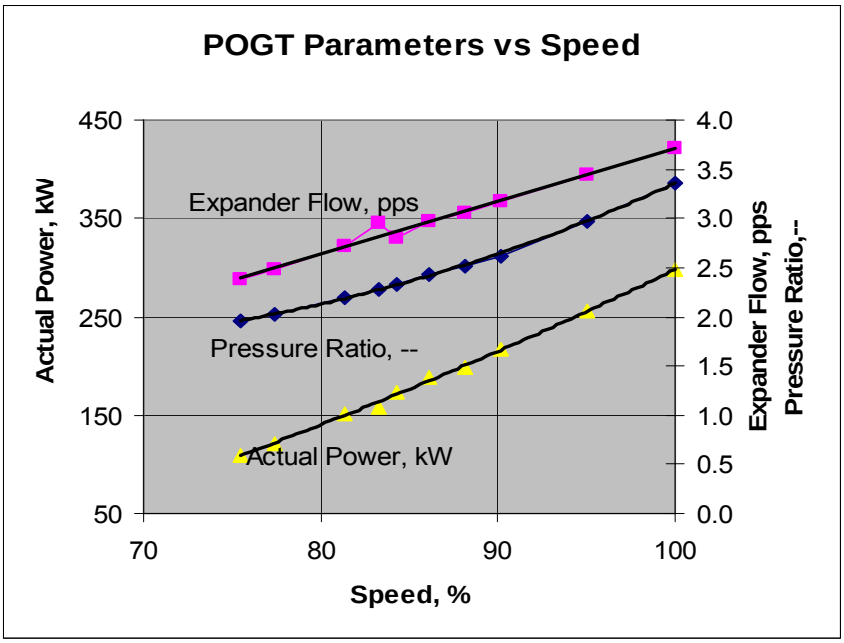

Figure 31. POGT Parameters vs. Engine Speed.

In Figure 30, only experimental data are used and presented. In Figure 31, experimental data are used in the speed range 75 – 90%, and calculated data based on regression functions from the test data are used for the speed 95 – 100%.

Comparison of power output from POGT and conventional Spartan shows that POGT is capable of generating 300 kW at TIT below 1400◦F while the Spartan output was 200 kW at TIT=1600◦F. Specific Power output (kW/pps of expander exhaust flow) is even more favorable for POGT compared to Spartan.

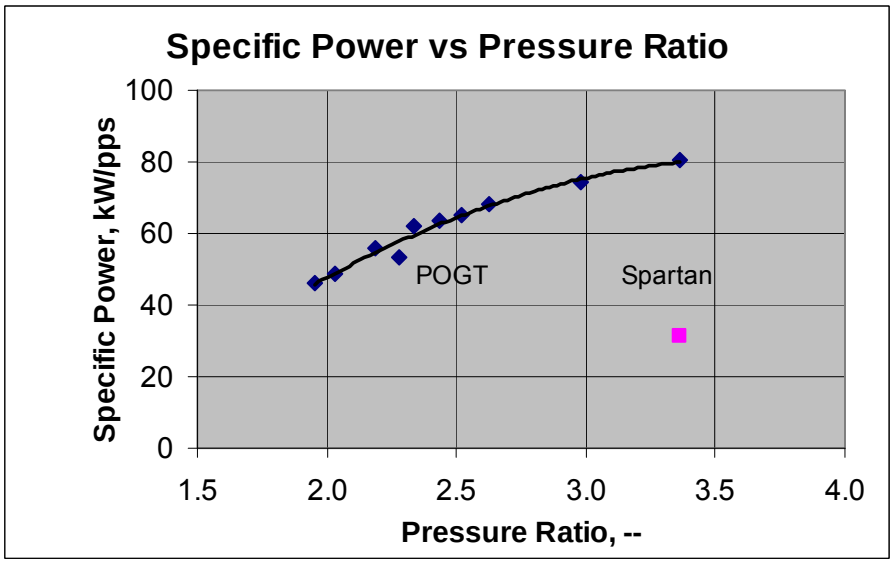

Figure 32. POGT and Spartan Specific Power Output.

Specific power for both POGT and conventional Spartan was calculated based on experimental data obtained during POGT and Spartan testing. The POGT was tested at different speeds, while the Spartan was tested only at full speed with expander pressure ratio of 3.36. In Figure 32, the effect of PR on specific power for POGT and Spartan is shown. An analysis of the data indicates there is about 2.5 times more power output per pound mass flow possible from POGT compared to the conventional Spartan.

Under the DOE sponsored project, ASPEN-based calculations of POGT performance were obtained for several commercially available gas turbines in the range of pressure ratio 3.5 to 20 to evaluate their potential performance if converted to POGT duty. In Figure 33, the results of calculations for both the POGT and conventional turbines are presented. The POGT potential specific power was calculated to be about 2.5 times greater compared to existing gas turbine. For a turbine operated at a pressure ratio of 20, the specific power is projected to approach a remarkable 350 kW/pps.

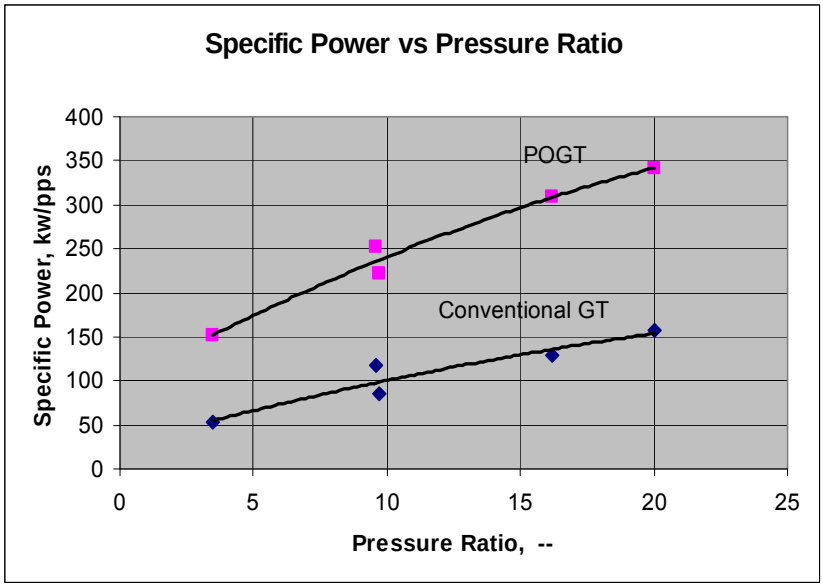

Figure 33. Specific Power Output for POGT and Conventional GT.

Effect of Turbine Inlet Temperature on POGT Parameters

In the majority of the POGT tests, TIT was a variable parameter. The range of the TIT variation is shown in the column "Variables" of the test summary Table 2. To evaluate the effect of TIT on POGT parameters, several tests were selected with TIT varied between 1310 and 1480◦F. In these tests, the other parameters were in the following ranges:

- Speed 84 – 85%
- Back pressure 0.9 – 1.4 in W.C.
- Stoichiometric ratio 0.34 – 0.75

In Figure 34, the experimental data for measured generator power at different TIT are presented.

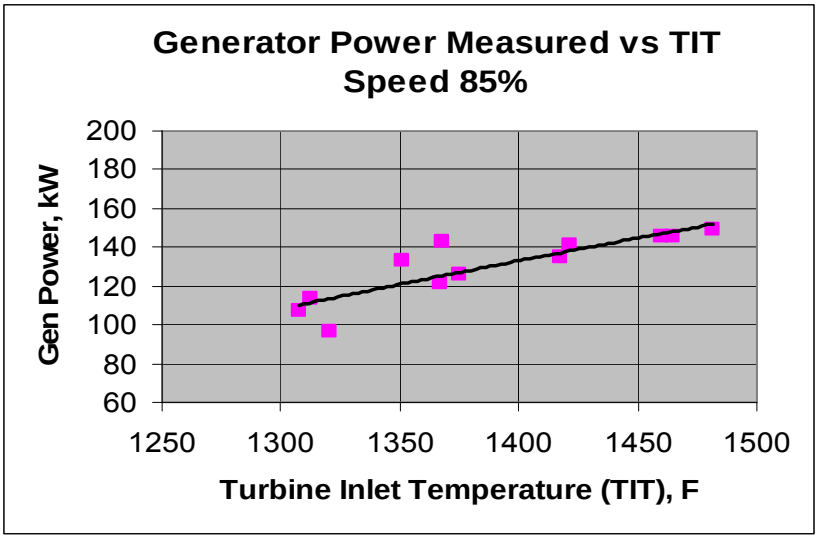

Figure 34. Generator Power Output as a function of TIT.

Based on experimental data for generator power and flow rate through the expander, the specific generator power was calculated as shown in Figure 35.

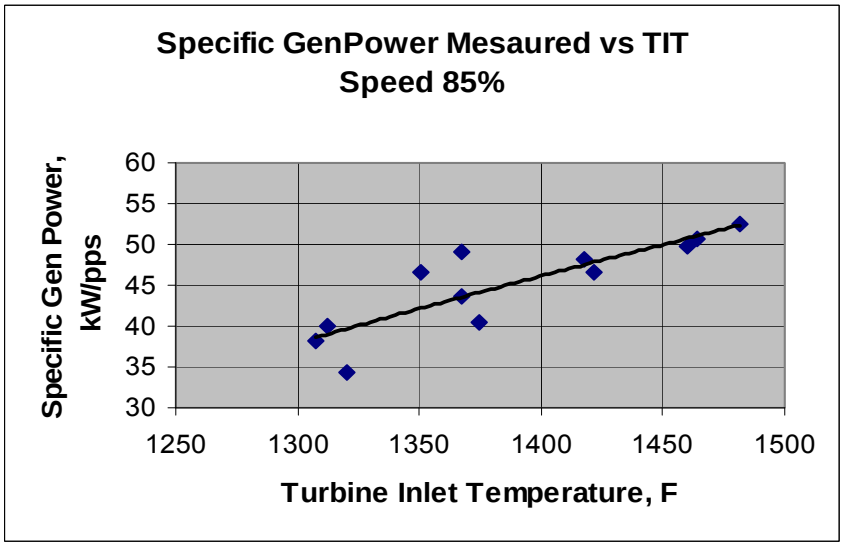

Figure 35. Specific Generator Power as a function of TIT.

Similar to a conventional gas turbine, an increase in the POGT TIT leads to additional power output. When TIT is increased by 100◦F from 1350 to 1450◦F, the Gen Power went up by about 25 kW from 120 kW to 145 kW.

Actual power output calculated from the experimental data for this test series is presented in Figure 36. The parameters were calculated for two speeds, 85 and 100%, and TIT was extended up to 1650◦F, the current TIT for new micro-turbines up to 200 kW capacities.

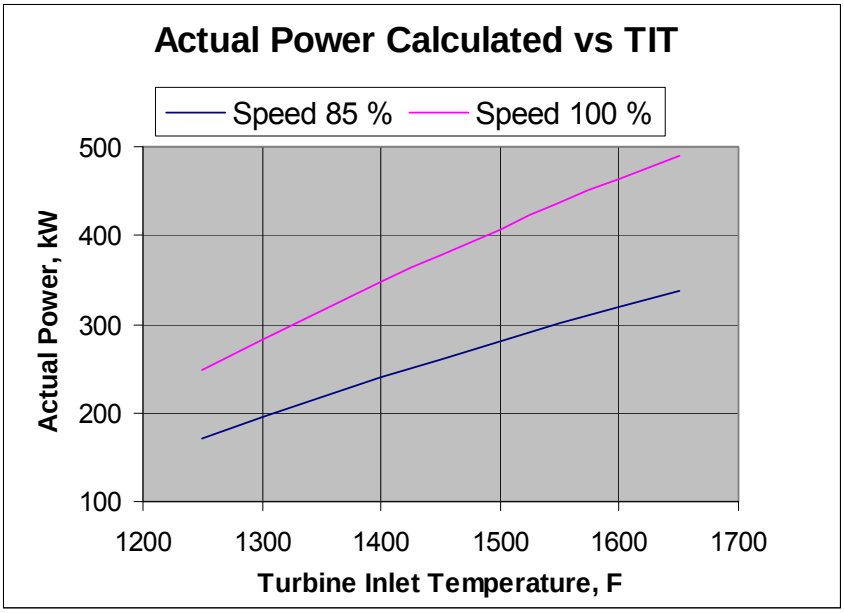

Figure 36. Actual Power Output as a function of TIT.

At full speed and design TIT = 1600◦F, the actual power output from POGT-converted Spartan is calculated to reach 450 kW, and at advanced TIT =1650◦F, the power output is estimated to approach 500 kW.

The specific actual power output was also calculated based on the experimental data from this test series. The results are shown in Figure 37.

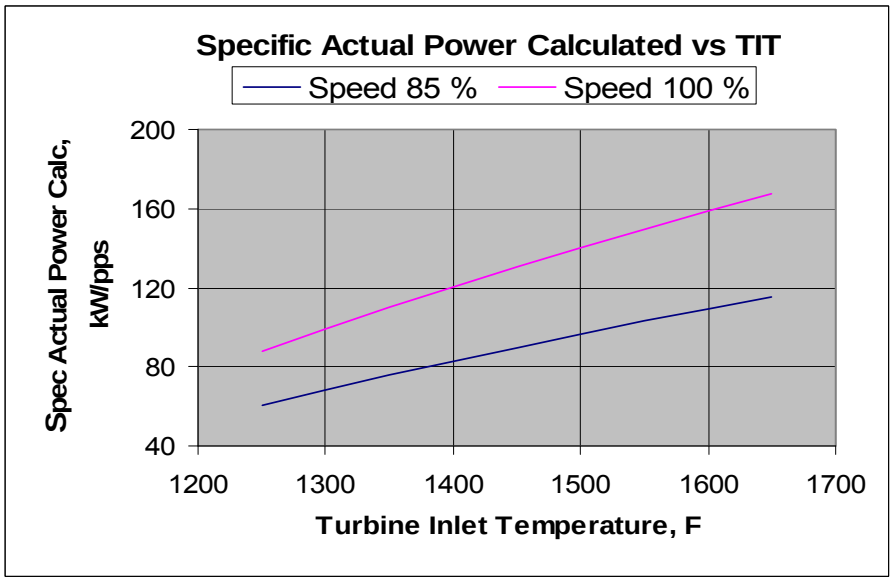

Figure 37. Specific Actual Power Output as a function of TIT.

The POGT-Spartan has a potential to achieve Specific power of 160 kW/pps at TIT=1600◦F and PR=3.36, while a conventional micro-turbine specific power is about 50 kW/pps at similar TIT and PR.

Effect of Back Pressure on POGT Parameters

There was a dedicated series of tests with BP as a variable. In addition, during the POGT-Boiler testing, the BP was also one of the variables. Referring to the test summary Table 12 column "Variables," the tests where BP was varied has a mark "BP." It was varied in the range 0.8 – 28 in W.C., while maintaining other variable parameters (speed, TIT, etc.) within narrow ranges. Experimental data were processed and the results are presented in Figures 38 and 39.

When back pressure is applied, the expander PR is reduced and expander work is lower. As shown in Figure 38, with increasing BP, compressor work is going up, and as a result, the generator power output is decreased. In a properly designed POGT, the reduction of the power output will be much less (about 50%) because the POGT compressor work is a half of the compressor work in the test unit.

Other POGT parameters, e.g., TIT and combustion air flow rate, are almost unchanged when BP is increased. This is shown in Figure 39.

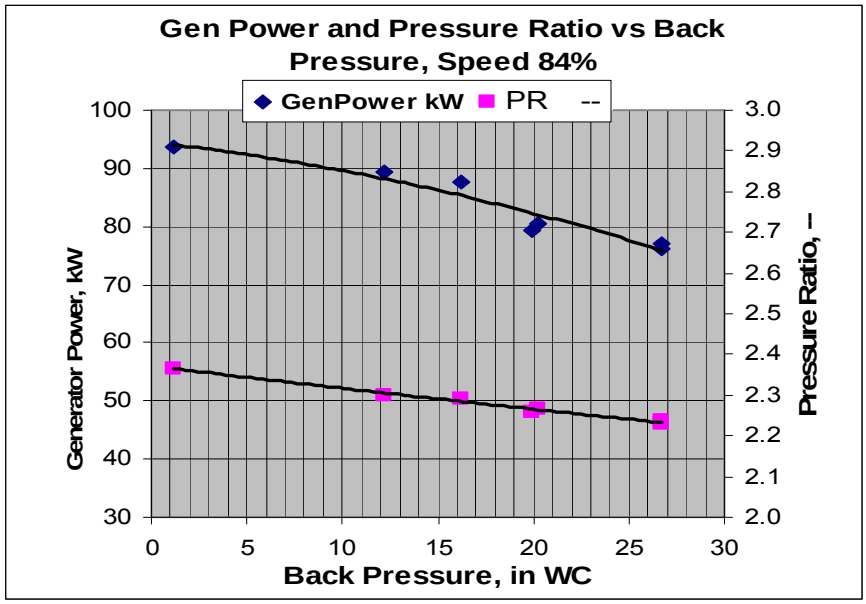

Figure 38. Effect of Back Pressure on Gen Power and Pressure Ratio.

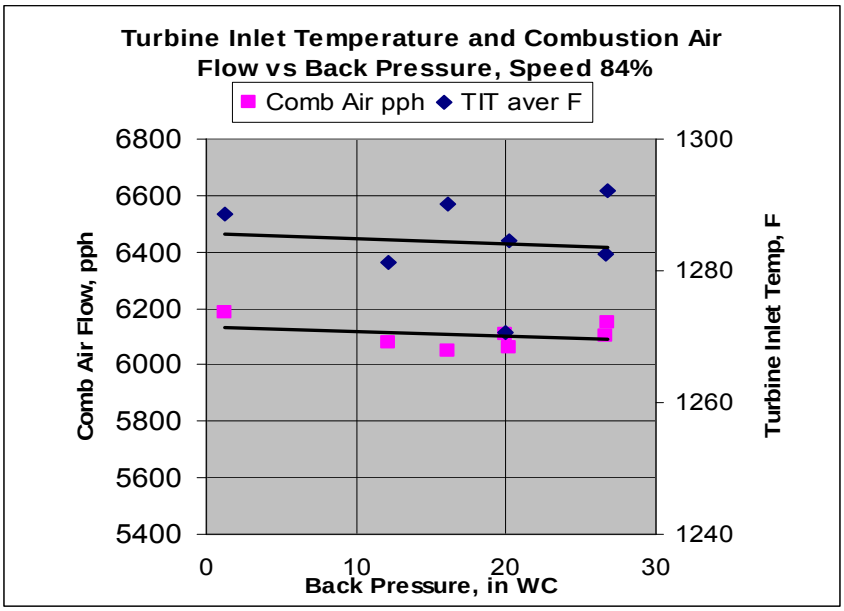

Figure 39. Effect of Back Pressure on TIT and Combustion Air Flow.

In a POGT based system, where the POGT exhaust is used as a secondary fuel in a boiler, furnace or fuel cell, as well as feedstock for hydrogen production, the expected BP would not exceed 20 in WC. The test results show that POGT exhaust parameters, (temperature, flow rate, composition) are practically unchanged when the BP is less than 20 in WC.

Effect of Stoichiometric Ratio on POGT Parameters

SR is defined as a ratio of the actual combustion air (oxidant) flow to the theoretically required air (oxidant) flow for complete combustion of the fuel flow. SR is one of the most important parameters used in evaluating POGT operation and performance. During all POGT performance testing, SR was varied even if there was another major parameter varied for the given test series. The reason for varying SR in all tests is because POGT startup usually ended when SR reached about 0.7 – 0.8. After the POR temperature stabilized, the SR was gradually reduced to about 0.5 - 0.6 for the majority of tests. In the test series for SR as a variable, the SR was varied in the range from 0.8 to 0.25, see Table 6 for POGT testing summary.

SR affects the composition of POGT syngas as well as the power output. The power output is increased with decreasing the SR. When SR is reduced, the specific heat of the turbine working fluid is increased, and the amount of thermal energy converted to mechanical energy in the expander is also increased in the same temperature range. The power output increases proportionally with decreasing SR. Other operating parameters that impact the power output include TIT, PR, and mass flow. These were analyzed earlier in this chapter. In this project, the focus was on evaluating the effect of SR on the syngas parameters such as high heating value (HHV) and fractions of hydrogen and carbon monoxide in the fuel gas.

Syngas compositions were obtained during nine tests using a portable Gas Chromatograph and gas analyzers. In all other tests, the fuel gas composition was recorded from gas analyzers. The HHV of the dry syngas was calculated for each test. The results are presented in Figure 40

where the HHV of the syngas is plotted against SR. As SR is decreased from 0.7 to 0.25, the syngas HHV is increased about 4 times, from 40 to 160 Btu/cf.

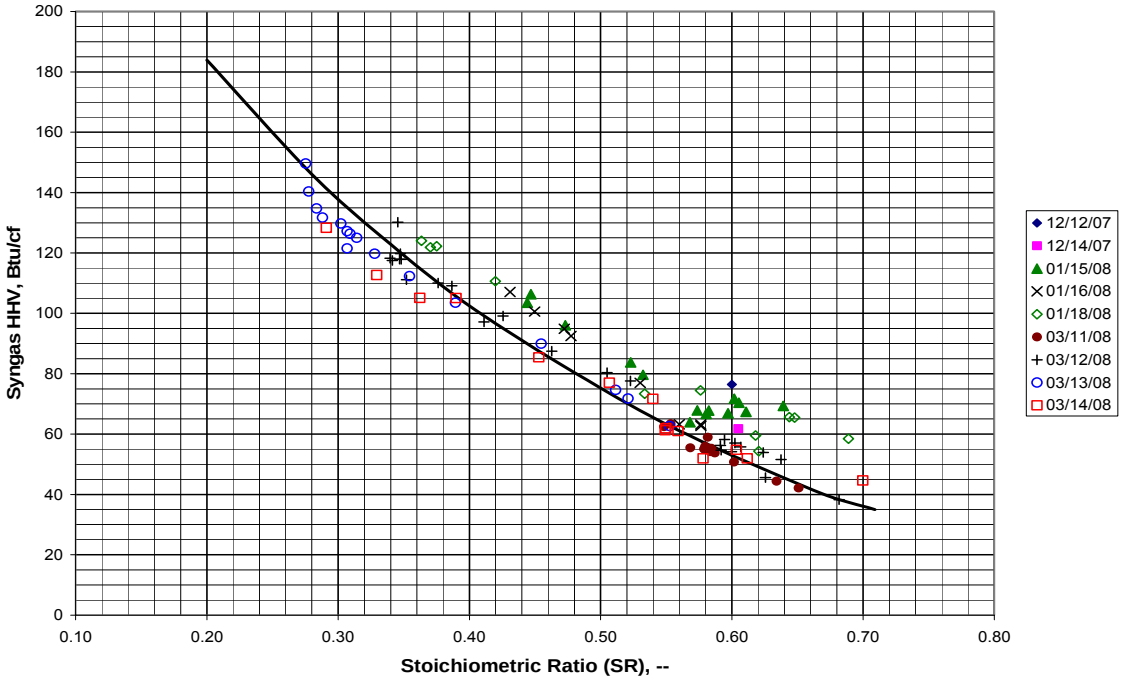

Figure 40. POGT Syngas HHV as a function of Stoichiometric Ratio.

In the partial oxidation process, syngas heating value depends of the SR and the fuel conversion rate. As explained earlier in this report, the operation of the POGT unit was constrained to limits of TIT (<1400◦F) and flame temperature (<2200◦F). Both of these limits impact the fuel to syngas HHV. Syngas HHV was also affected by the dilution from the additional nitrogen injection used to cool the seal plate and for POR exhaust cooling. In a POGT designed for the gas turbines offered today with much higher allowable TIT and flame temperature, the conversion rate can be expected to significantly increase and the syngas HHV should approach at least 250 Btu/cf.

POGT syngas is a valuable product which could be effectively used as a secondary fuel in fuel cells, boilers, furnaces, etc., and as a feedstock for hydrogen and/or gas-to-liquid production. As SR was varied, hydrogen content of the syngas was measured using both portable gas chromatograph and H_2 analyzer. In Figure 41 below, the processed data are shown. The hydrogen content (volume basis) ramps up from about 6 % at SR of 0.7 and syngas HHV about 40 Btu/cf. to 10% at SR of 0.27 and HHV 140 Btu/cf. Aspen-based modeling calculations predict that hydrogen content in POGT syngas could potentially be increased to 20 – 25 % by volume.

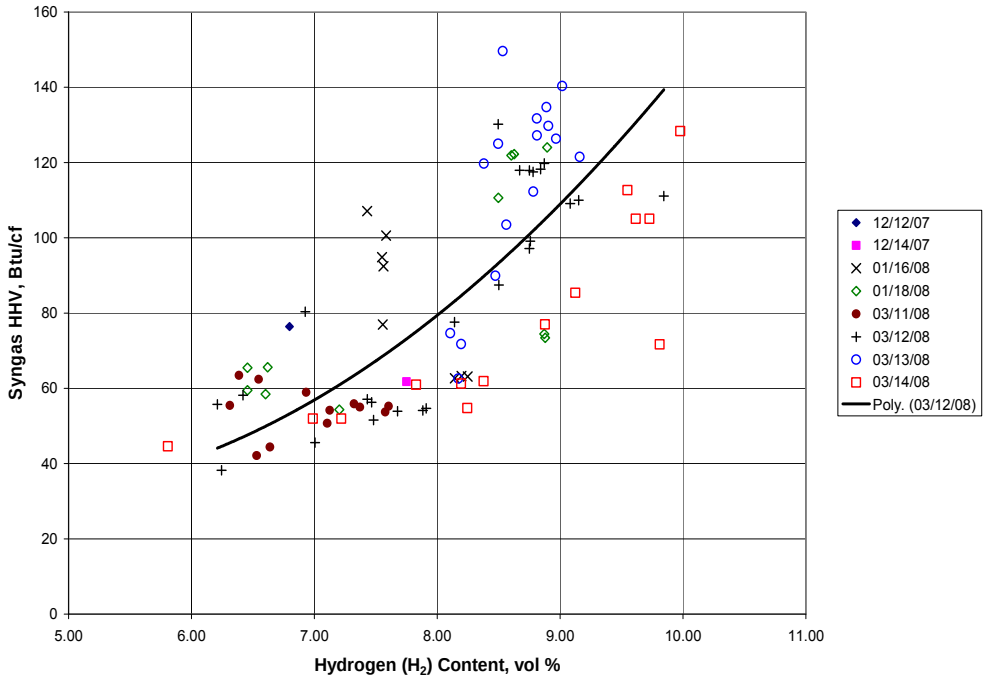

Figure 41. POGT Syngas HHV Correlation with Hydrogen Content.

CO content of the syngas was measured using both portable gas chromatograph and CO analyzers during the POGT tests varying SR. In Figure 42 below, the processed data are shown. CO content ranges from about 3.5% at SR of 0.7 and syngas HHV about 40 Btu/cf to 7% at SR of 0.27 and HHV 140 Btu/cf. Aspen based calculation predict that carbon monoxide content in POGT syngas could reach 10 – 15% by volume.

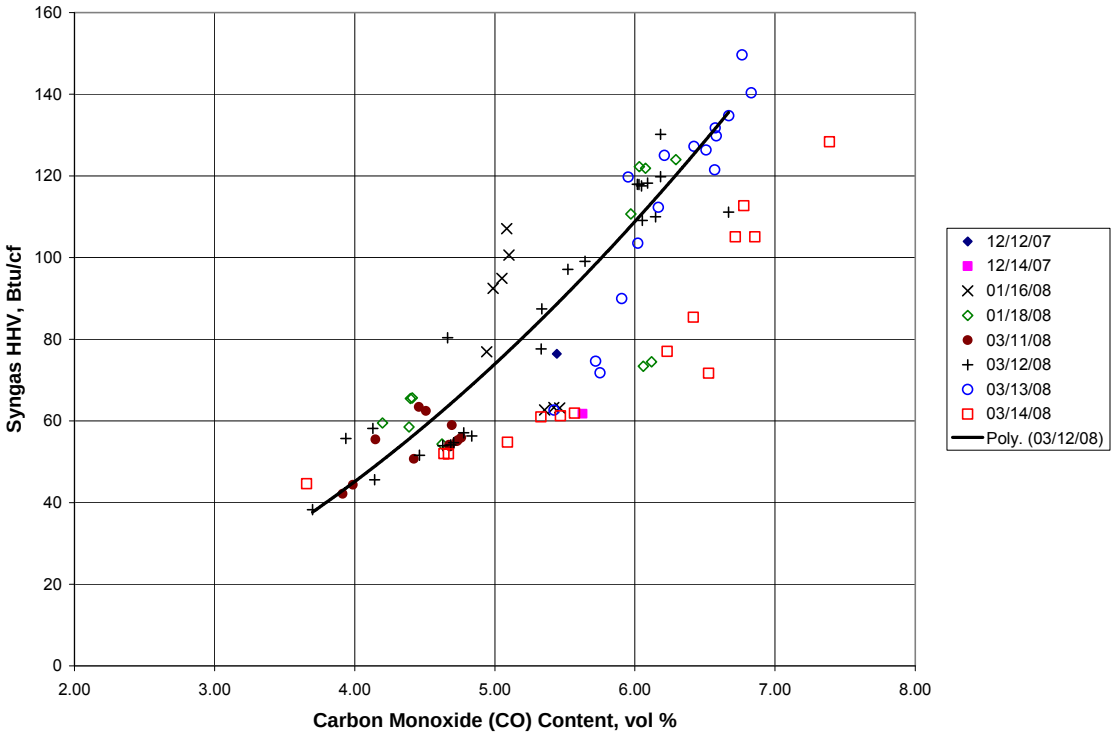

Figure 42. POGT Syngas HHV Correlation with Carbon Monoxide Content.

5.0 POGT Feasibility Design.

5.1. Selection of Candidate Turbines for Retrofit Study.

5.1.1. Identification of Potential Candidate Turbines

Originally, five turbines have been selected as candidates for POGT feasibility design study: SGT-800 and SGT-900 from Siemens, and Mercury 50, Titan 130, and Centaur 40 from Solar. At the time for performing this study, Solar Turbines has reduced their R&D activities and the work for the project was slow down. Siemens agreed to consider two more turbines in the range of 5 to 15 MWe (the same range as for Solar turbines) for the study under the project. Two Siemens turbines SGT-100 and SGT-400 have been selected as candidates for POGT retrofit design study. Finally, three Siemens turbines, SGT-100 (Typhoon), SGT-400 (Cyclone), and SGT-800 in the range 5 to 80 MW when operated in POGT mode, were undergone design study for conversion to POGT duty. As the first step in the study, detailed performance evaluations of the selected turbines were conducted. The performances were defined and compared for turbine operation in both modes, conventional GT and POGT. Later the advanced Siemens turbine, SGT6-6000G, was also studied as a candidate turbine for POGT performance evaluation and following POGT-based system analysis.

5.1.2. Performance Evaluation for the Selected Candidate Turbines

The basic development approach for the POGT is to use existing SGT-engine components as much as possible, making whatever modifications are necessary to meet specified performance

requirements. A heat transfer analysis supported by Aspen-Plus calculation was used to identify the cooling steam flows to provide the required cooling capacity for the turbine expander. The design conditions for the compressor and expander for the POGT are within the capabilities of existing commercial technology, but the equipment is physically different from commercially available equipment. Therefore, a certain amount of development effort would be needed to produce a POGT. Evaluation and comparison of performances for both conventional turbine and POGT modes for four Siemens gas turbines, SGT-100, SGT-400, SGT-800, and SGT6-6000G were accomplished.

Siemens has provided design-point data for these turbines, including mass flows, volumetric flows, pressures, and temperatures for the compressors, burners, and expanders. GTI has produced the Aspen-Plus models for each of the engines for operation in both, conventional and POGT modes. Eight individual models were actually generated. On the first step, GTI has calculated the performance for each of the engines in conventional mode with the goal to match as close as possible the major parameters, such as power output, TIT and pressure ratios for compressor and expander, mass flow rate for compressor and mass and volumetric flow rates for expander, etc. The results of calculation were sent to Siemens, and after approval of the matching parameters for the conventional GT's, GTI has conducted calculations of POGT mode for each of the four SGT's engines. Siemens has reviewed the results of the first Aspen run and sent the comments including required steam flows to provide the needed blade path temperatures and cooling capacities. The results of second iteration (and when necessary third iteration) of Aspen runs for POGT-SGT-100, POGT-SGT-400, POGT-SGT-800, and POGT-SGT6-6000G were sent to Siemens for review, comments, and final approval. The final Aspen-Plus model schematics for POGT-SGT-800 and POGT-SGT6-6000G are presented in Figures 43 and 44below. The POGT-SGT-800 was used in several POGT-based systems in the report.

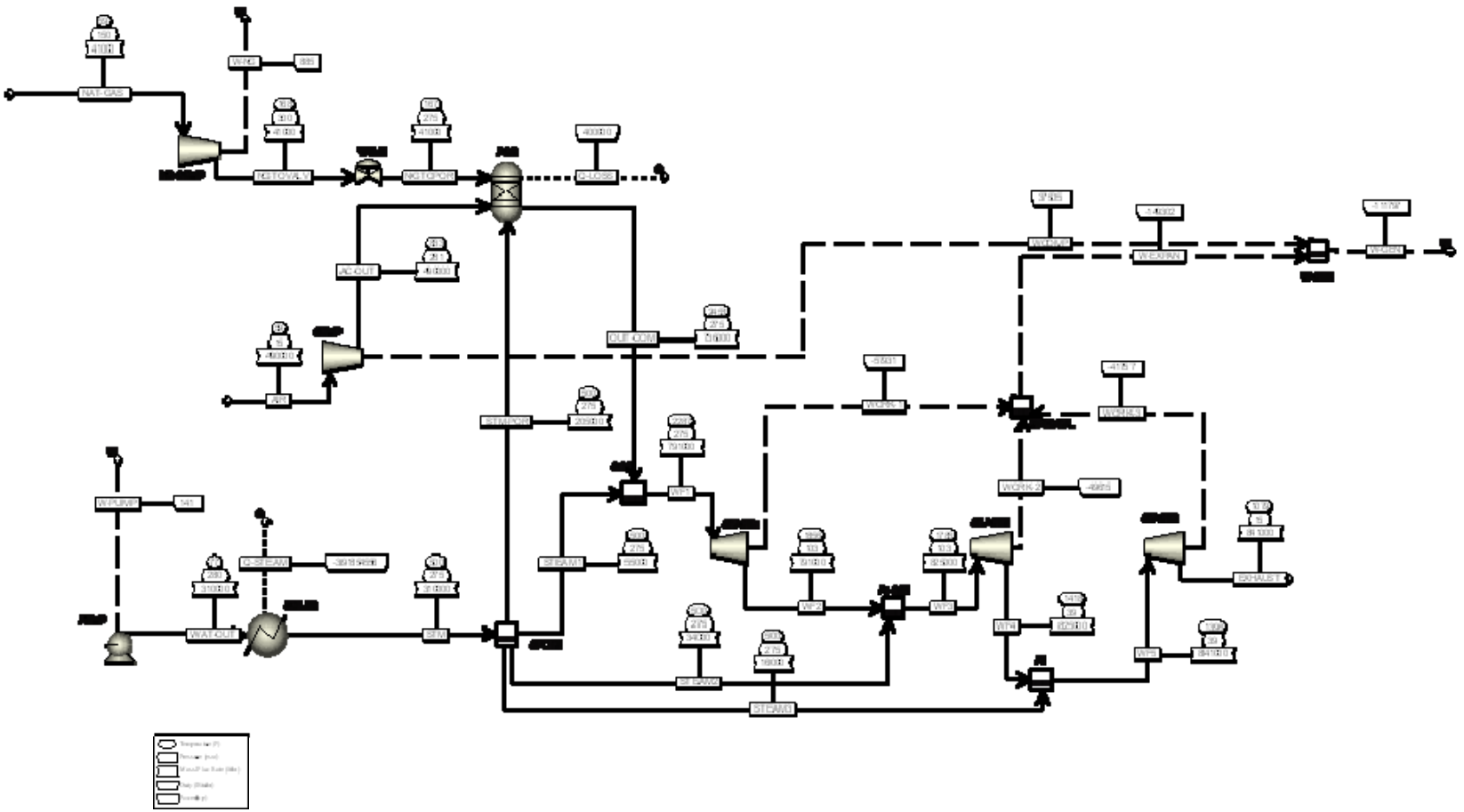

Figure 43. Aspen-Plus Schematics for SGT-800 Converted to POGT.

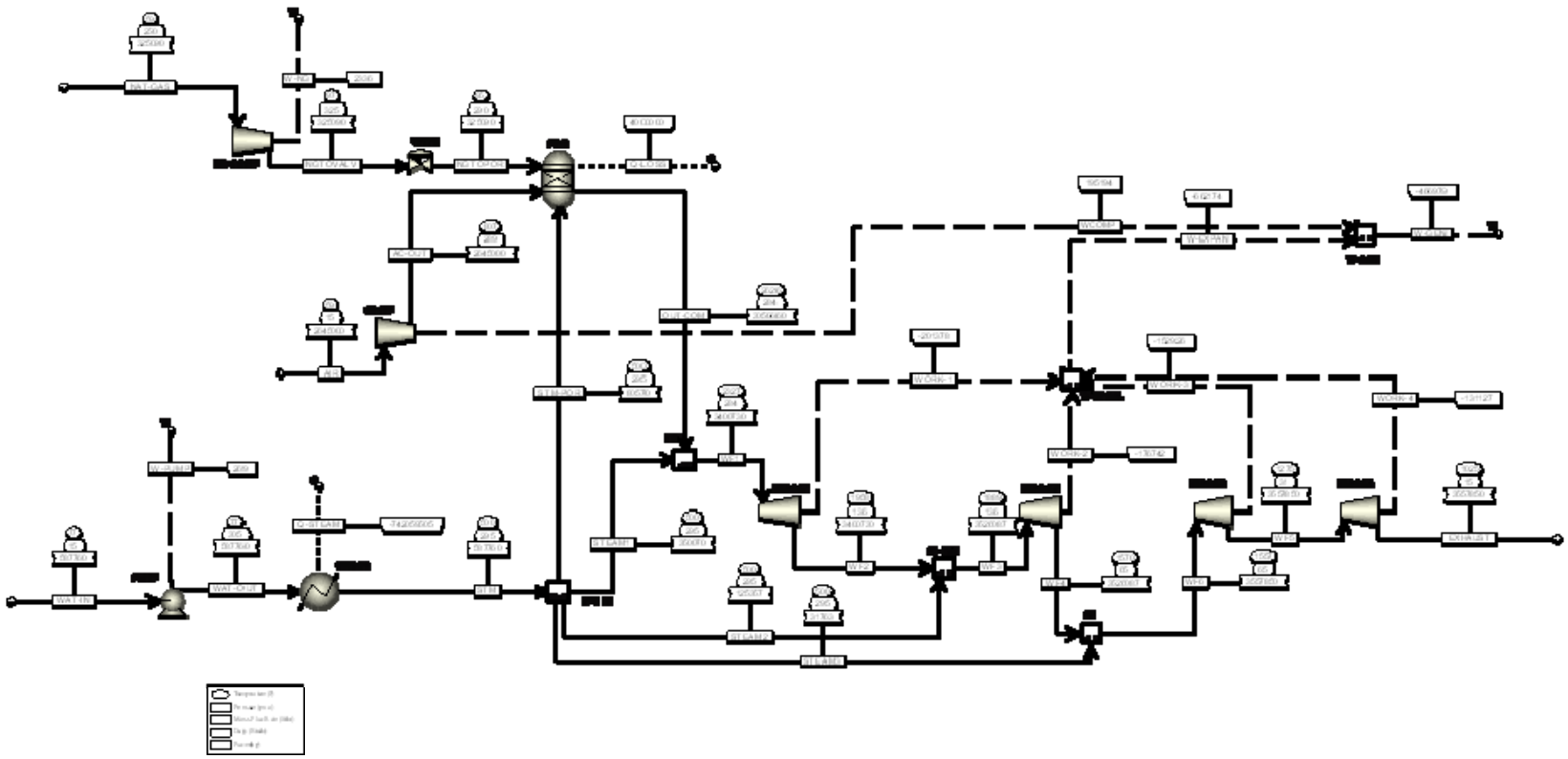

Figure 44. Aspen-Plus Schematics for SGT6-6000G Converted to POGT, version 3.

Table 7. Conventional Turbine and POGT Performances for SGT-100, SGT-400, SGT-800 and SGT6-6000G.

Conventional Turbine and POGT Performances for SGT-100, SGT- 400, SGT-800 and SGT6- 6000G									
		SGT-100	**POGT SGT-100**	**SGT-400**	**POGT SGT-400**	**SGT-800**	**POGT SGT-800**	**SGT6-6000G**	**POGT SGT6-6000G**
Compressor inlet flow rate	lb / h	162,865	95,700	307,310	171,000	1,013,760	490,000	4,513,877	2,645,000
Compressor inlet temperature	° F	59	59	59	59	59	59	59	59
Compressor inlet pressure	psia	14.7	14.7	14.7	14.7	14.7	14.7	14.7	14.7
Compressor exit flow rate	lb / h	128,663	95,700	233,556	171,000	1,013,760	490,000	3,435,407	2,645,000
Compressor exit temperature	° F	759	759	785	785	874.3	833.5	806.9	806.9
Compressor exit pressure	psia	215.3	215.3	245.9	245.9	280.8	280.8	289.5	289.5
Compressor power	MW	8.36	4.91	16.39	9.12	61.1	28	248.4	145.56
Expander inlet flow rate	lb / h	154,074	125920	271,232	217,730	947,030	791,000	4,171,125	3,400,730
Expander inlet temperature	° F	2038	1965	2300	2280	2318	2287	2415	2327.2
Expander inlet pressure	psia	211	211	241	241	275	275	283.71	283.71
Expander exhaust flow rate	lb / h	165,703	130,500	313,345	235,850	1,033,200	841,000	4,613,297	3,557,850
Expander exhaust temperature	° F	980	924	1024	1023	1004	1079	1035	1024.8
Expander exhaust pressure	psia	14.8	14.8	14.8	14.8	14.6	14.6	14.8	14.8
Expander power	MW	13.61	14.88	29.34	30.01	105.4	111.3	493.49	493.78
Turbine net power	MW	5.25	9.96	12.95	20.89	44.4	83.4	245.09	348.23
Turbine specific power	kW / pps	114.1	274.8	148.8	318.9	154.7	357.0	191.3	352.4

The finally calculated turbine performances for four engines SGT-100, SGT-400, SGT-800, and SGT-6000G in both conventional and POGT mode operation are presented in the Table 7above. Comparison of conventional turbine and POGT performances shows that in the POGT mode, the turbine net power output is increased by about 40 to 80% while the expander exhaust mass flow rate is reduced by about 15- 25%. An important turbine parameter, specific power (turbine net power per lb expander exhaust mass flow), for POGT is twice value of conventional turbine, see Figure 45. The two points at pressure ratio about 3.5 are experimental data from GTI's test unit Spartan-POGT; all other points are Aspen calculated data for Siemens and Solar gas turbines.

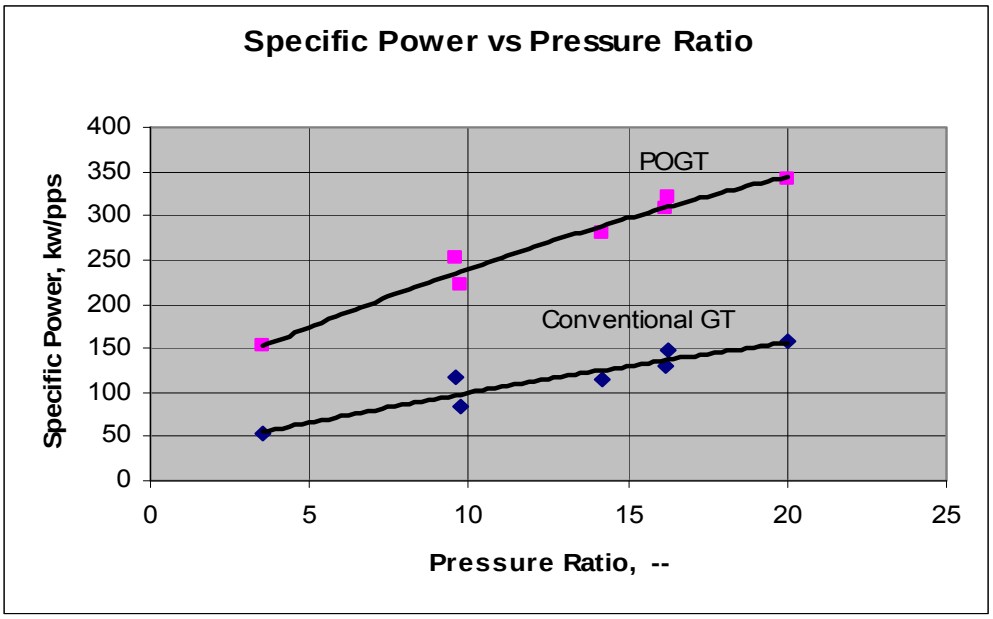

Figure 45. Comparison of Specific Power for Conventional GT and POGT.

5.2. Partial Oxidation Gas Turbine (POGT) Feasibility Study Based on the Siemens SGT-100 and SGT-400 Gas Turbines.

Two Siemens gas turbines in the 5-to-15-MW range were identified as potential candidates for conversion to POGT applications: the 5-MW SGT-100, and the 13-MW SGT-400. The basic development approach for the POGT is to use existing SGT components as much as possible, making modifications as necessary to meet design requirements.

Although some of the modifications needed to convert a gas turbine into a POGT focus on the expander, other changes are also needed for the compressor, reduction gears, and generator.

5.2.1. SGT-100 and SGT-400 Gas Turbines

The selected turbines are the 5-MW SGT-100 and the 13-MW SGT-400 gas turbines. The main operating characteristics of these turbines are listed in Table 8.

Table 8. Siemens Turbine Candidates for POGT Modifications.

Turbine Model	No.	SGT-100	SGT-400
Former Model	Model	Typhoon	Cyclone
Nominal Net Power	MWe	5.2	12.8
Compressor			
Compressor Inlet Air	lb/s	45.2	85.4
Compressor Exit flow	lb/s	35.7	64.9
Compressor Exit Pressure	psia	215.3	245.9
Compressor Exit Temp	°F	759	785
Compressor Pr. Ratio	-	14.8	16.9
Compressor Power	MWe	8.36	16.39
Compressor sections	-	1	1
Compressor stages	-	10	11
Compressor Intercooling	-	No	No
Burner			
Nat. Gas Inlet Flow	lb/s	0.79	1.67
No. of Burners	burners	6	6
Expander			
Exhaust Flow	lb/s	46.0	87.0
Expander Inlet Pressure	psia	211.0	241.0
Turbine Inlet Temp.	°F	2038	2297
Turbine Exhaust Temp.	°F	980	1019
Expander Power	MWe	13.6	29.2
Expander sections	-	1	2
Expander stages	-	2	2 + 2
Cooled expander stages	-	1	2
Power Transmission			
Turbine shaft speed	rpm	17,384	14,10000
Gear Output Speed	rpm	1,500 / 1,800	1,500 / 1,800

The SGT-100 (formerly Typhoon) is a single-shaft gas turbine that produces about 5 MW on natural gas. It has 10 compressor stages, 6 burners, and two expander stages, as depicted in Figure 46. The 17,384-rpm drive shaft at the compressor end is attached to a reduction gear, which is attached to a 1500-rpm or 1800-rpm electric generator.

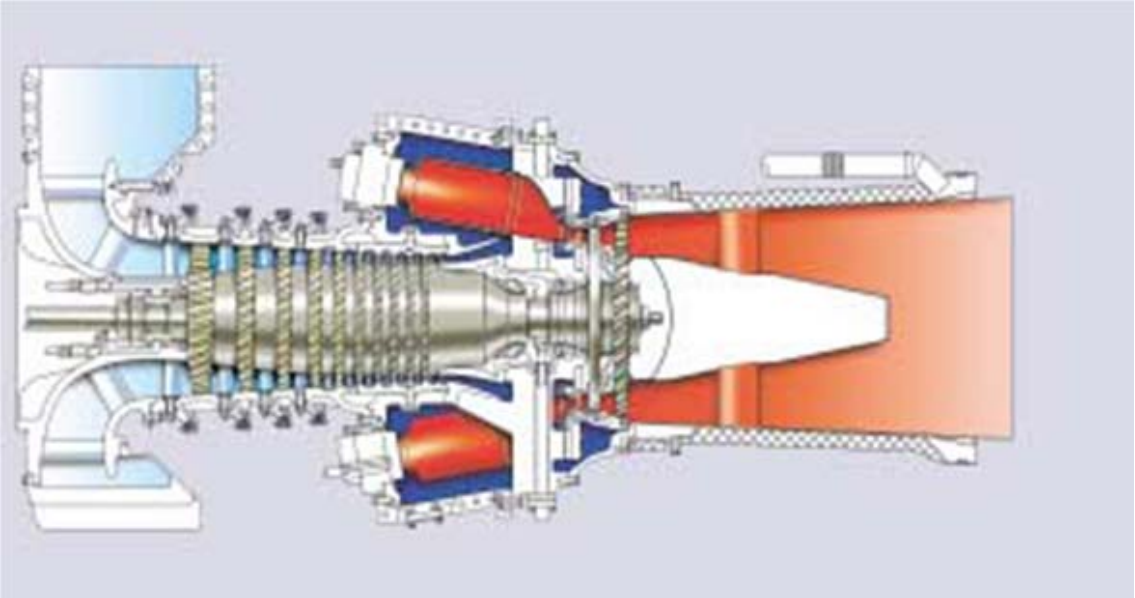

Figure 46. SGT-100 Gas Turbine.

The SGT-400 (formerly Cyclone) is a two-shaft gas turbine that produces about 13 MW on natural gas. It has 11 compressor stages, 6 burners, two expander stages on the same shaft as the compressor, and two expander stages on a separate shaft, as depicted in Figure 47. The HP expander is a "compressor turbine" that provides power only for the compressor with no excess electric power generation. The 14,100-rpm drive shaft at the power turbine end is attached to a reduction gear, which is attached to a 1500-rpm or 1800-rpm electric generator.

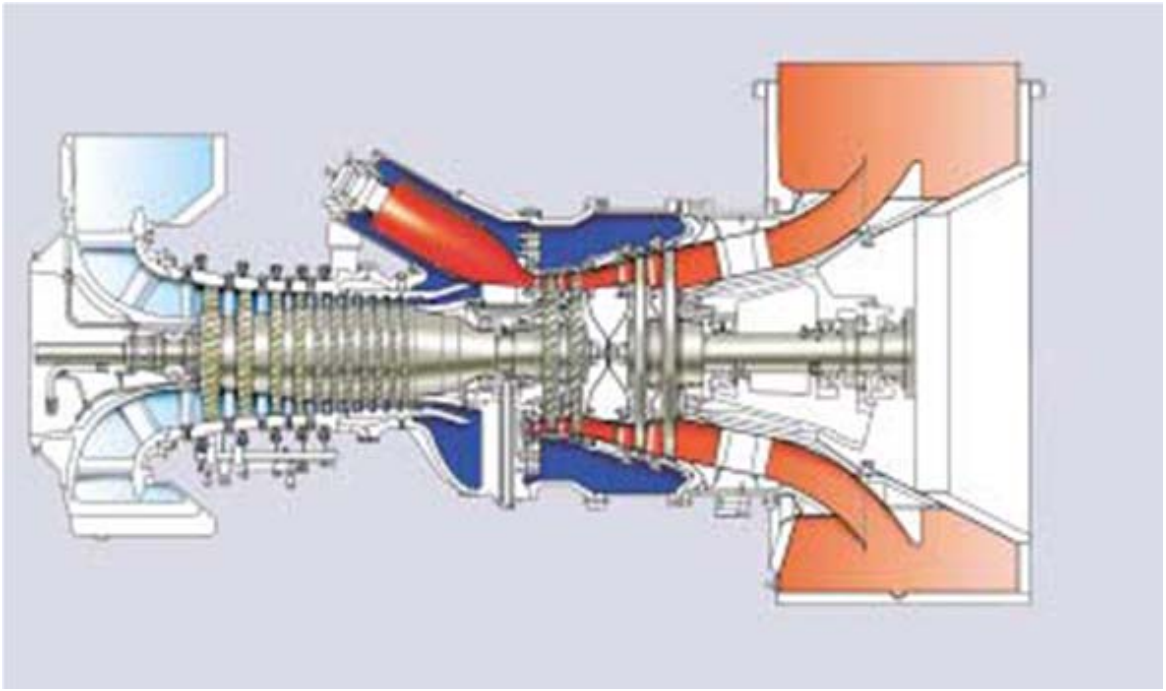

Figure 47. SGT-400 Gas Turbine.

5.2.2. Technical Issues and Feasibility Designs

The basic development approach is to use existing gas turbine components as much as possible, modifying as necessary to the meet design requirements of the POGT.

The design conditions for the compressor and expander for the POGT are within the capabilities of existing commercial technology, but the equipment is physically different from commercially available equipment. Therefore, a certain amount of development effort would be needed to produce POGT components. As with any new product, POGT development would require: (1) sufficiently advanced technology; (2) sufficiently available developmental resources; and (3) the expectation of sufficient market sales to justify the development effort. Discussions of available resources and viable markets are beyond the scope of this study, which focuses only on technology. This section focuses on estimating the magnitude of effort needed to convert subsystems of the SGT-100 and -400 into POGT subsystems.

- Compressor modifications (Section 5.2.3),
- Expander modifications (Section 5.2.5),
- Generator modifications (Section 5.2.6),
- Reduction gear modifications (Section 5.2.7), and
- Rotor and bearing modifications (Section 5.2.8)

The development requirements described in these sections are summarized in Section 6.

5.2.3. Compressor Modifications

The air compressors for POGT are 40 to 45% smaller than those in normal SGT-100 and -400 compressors, as shown in Table 9. The reason for the reduced air requirement is the reduced need for air in the POR and the absence of burners in ion the POGT.

Table 9. and Commercial (SGT) Compressor Comparisons.

		SGT-100	POGT-100	SGT-400	POGT-400
Compressor inlet flow rate	lb/h	162,865	95,700	307,310	171,000
Compressor inlet flow rate	lb/s	45.2	26.6	85.4	47.5
Compressor inlet flow rate	kg/s	20.5	12.1	38.7	21.5
Compressor inlet temperature	° F	59	59	59	59
Compressor inlet pressure	psia	14.7	14.7	14.7	14.7
Compressor exit flow rate	lb/h	128,663	95,700	233,556	171,000
Compressor exit flow rate	lb/s	35.7	26.6	64.9	47.5
Compressor exit flow rate	kg/s	16.2	12.1	29.4	21.5
Compressor exit temperature	° F	759	759	785	785
Compressor exit pressure	psia	215.3	215.3	245.9	245.9
Compressor power	MW	8.36	4.91	16.39	9.12

Four compressor options were identified to satisfy the POGT requirements:

- A. Redesign the compressor blade path to match the reduced air requirement.
- B. Use a compressor from a smaller Siemens gas turbine engine.
- C. Use a separate compressor on the same shaft.
- D. Use a separate compressor on a separate shaft.

Each option is discussed below.

Option A - Redesign Compressor Blade Path

With this option, the blades and vanes of the gas turbine compressor would be redesigned to match the reduce flow requirements of the POGT cycles. The compressor shaft would be checked to verify that it could transmit the increased net power to the generator. If the compressor shaft could not transmit the power, then the generator would be moved from the compressor shaft to the exhaust end of the expander shaft, changing from the normal G=C=E arrangement to a G=E=C arrangement, as shown in Figure 48. With a G=E=C arrangement, the compressor shaft power matches the compressor power.

A new balance piston would need to be added to the shaft to compensate for the loss of axial thrust normally produced by the compressor, which neutralizes the axial thrust produced in the opposite direction by the expander.

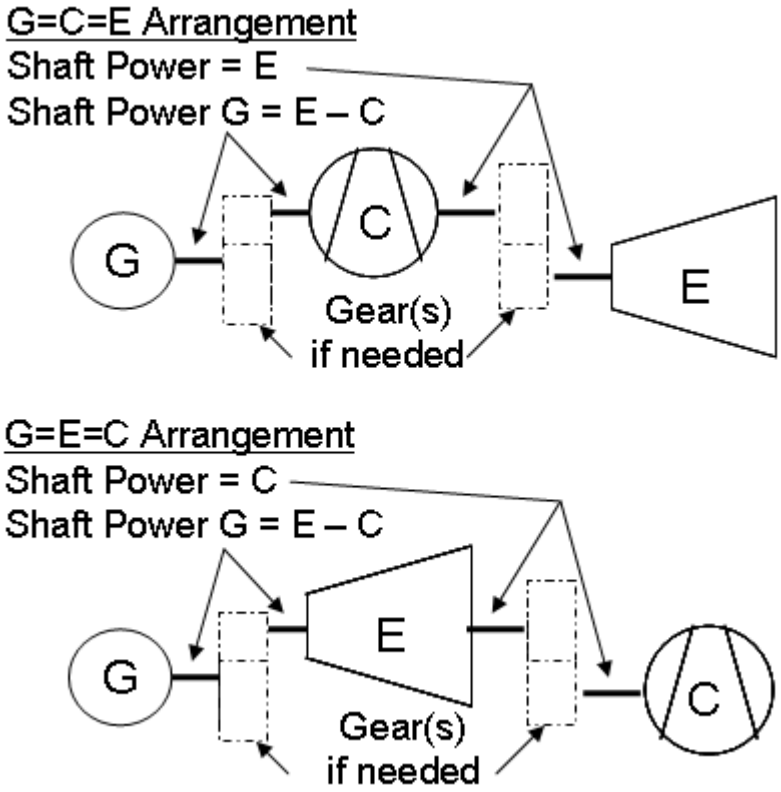

Figure 48. Generator Arrangement Options.

Option B - Smaller Siemens Gas Turbine Compressor

With this option, the normal compressor would be replaced with a compressor from a smaller Siemens gas turbine, selecting from the compressors listed in Table 10. An intermediate gear set could be used to accommodate any shaft speed mismatch between the compressor and the expander. The gear would incur an additional capital cost and a slight reduction in efficiency. A new balance piston would also be needed to compensate for the loss of axial thrust normally produced by the compressor.

Table 10. Siemens Gas Turbine Compressor Data.

Engine Model	Inlet air lb/s	Pressure ratio	Shaft Rev/min	GT Net kW
POGT-100	26.6	14.8	17,384	9,970
SGT-100	45.2	14.8	17,384	5,250
POGT-400	47.5	16.9	9,500	20,890
SGT-200	65.0	12.3	11,053	6,750
SGT-300	66.0	13.8	14,010	7,900
SGT-400	85.4	16.9	9,500	12,950

This option is problematic for the POGT-100 because Siemens does not make any smaller gas turbine compressors. The air flow rate for the POGT-400 turbine compressor is close to that of the SGT-100 compressor, but its required pressure ratio is 14% higher, so that option does not work either.

Option C - Separate Compressor, Same Shaft

With this option, the normal compressor would be replaced with a commercial, a stand-alone compressor, and the generator would be moved from the compressor shaft to the exhaust end of the expander shaft. Table 11 and Figure 49 show commercial compressors that could accommodate POGT-100 and POGT-400 conditions.

Table 11. Separate Commercial Compressor Data.

Make	Model	Max Flow, lb/s	Max psig Comm'l	Max psig POGT	bar(g)	Speed, rpm
Cooper	TA-20000	26.7	508		35	1,800
	POGT-100	26.6		203	14.0	17,384
AG KK&K	RG	33.1	580		40	20,000
Cooper	MSG-8	38.1	725		50	1,800
	POGT-400	47.5		234	16.1	9,500
Cooper	MSG-12	58.5	725		50	1,800
MAN	CP/SKUEL	76.2	725		50	25,000
AG KK&K	KX/KXP	89.6	870		60	45,000
Siemens	STC-GC	89.6	580		40	3,600

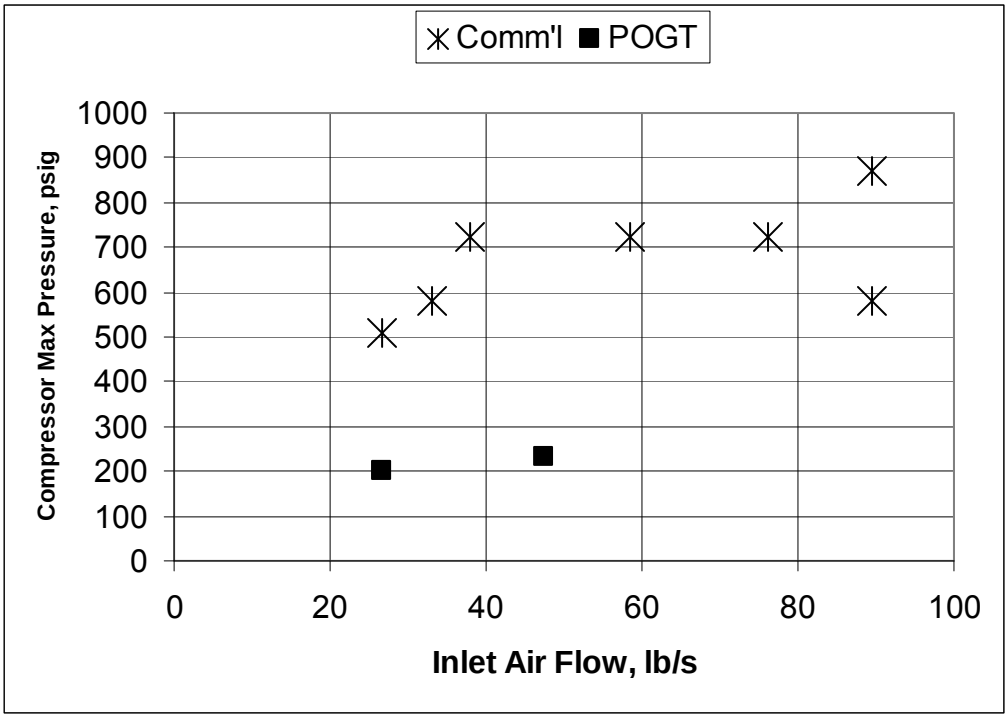

Figure 49. Separate Commercial Compressor Data.

A new balance piston would also be needed to compensate for the loss of axial thrust normally produced by the compressor, which neutralizes the axial thrust produced in the opposite direction by the expander.

This option uses an existing compressor design but would require a new balance piston and an intermediate gear set to accommodate any shaft speed mismatch between the compressor and the expander. The added gear set would increase the capital expense and slightly the efficiency.

Option D - Separate Compressor, Separate Shaft

Option D only applies to the POGT-100 because the 2-shaft POGT-400 needs its compressor attached to the same shaft as its HP expander. With Option D, the normal compressor is removed altogether and a commercial, stand-alone compressor is powered by a separate compressor motor.

A new balance piston would need to be added to the shaft to compensate for the loss of axial thrust normally produced by the compressor, which neutralizes the axial thrust produced in the opposite direction by the expander.

This option uses an existing compressor design but would require a new balance piston and an additional motor, which would increase the capital expense and slightly reduce the efficiency. Since the compressor would not take its power from the expander shaft, a larger generator would also be needed. On the other hand, the use of an independently controlled electric-powered compressor would add operational flexibility to the system, allowing, for example, the POR to be started and pressurized ahead of the POGT.

Best Options

The advantages and disadvantages of these options are listed in Table 12. Options A, C, and D are all feasible, but Option A requires new design work. Options C and D are about equal in efficiency because the losses from gears are about the same as the losses from a motor. For the POGT-100, Option D offers more operational flexibility, and is the selected option. Option C is the best choice for the POGT-400, which must have a compressor attached to its HP expander.

Table 12. Compressor Options.

Option	Advantages	Disadvantages
A. Redesign blade path	Can meet flow and torque requirements	New blade path and balance piston. Possible new rotor design needed.
B. Compressor from another engine (not feasible)	Minimal design work required	Nothing available to match both flow and pressure ratio.
C. Separate compressor, Same Shaft	Commercially available compressor and gear designs	Needs new balance piston and reduction gears. Slightly reduced efficiency.
D. Separate compressor, Separate Shaft	Commercially available compressor designs. Better operational flexibility.	Not feasible for 2-shaft units. Needs new balance piston and additional motor. Slightly reduced efficiency. Larger generator.

5.2.4. POR-POGT Interface

Two options for connecting the POR to the POGT were identified as circumferentially distributed PORs and single POR with volute expander inlet.

Option A: Circumferentially Distributed PORs

A normal SGT-100 and SGT-400 each have six burners aligned radially and distributed circumferentially around the turbine, upstream from the expander inlet. In this POGT configuration, six PORs could replace the six burners. Required modifications include: designing and fabricating six PORs to connect to the POGT.

Option B: Single POR with Volute Expander Inlet

This option connects a single POR to the volute inlet of the expander. Fewer, larger reactors have lower thermal losses and generally lower pressure losses than more, smaller reactors, and controlling a single reactor is simpler than simultaneously controlling several reactors.

The preferred option is Option B, the single POR connected to a volute inlet. Either option requires a new expander inlet casing design. The need for a volute inlet is only an incremental increase in that effort.

5.2.5. Expander Modifications

The POGT expander uses PO syngas instead of combustion products as its working fluid, and is cooled by steam instead of air. For each turbine, the syngas flow rate from the POR was selected

so the PO syngas entering the expander had the same pressure, temperature, and volumetric flow rate as the gases entering the conventional expander, thereby maintaining the same inlet dimensions as the commercial version of the expander. In addition, steam cooling flows were adjusted so metal temperatures, exhaust temperature, and expander power were also about the same as their commercial counterparts. The main differences between the POGT expander and the SGT versions of -800 expander are shown in Table 13.

Table 13. POGT and Commercial (SGT) Expander Comparisons.

		SGT-100	POGT-100	SGT-400	POGT-400
Expander working fluid (inlet)					
Ar	%(vol)	0.89%	0.50%	0.89%	0.54%
CO	%(vol)		11.44%		10.94%
CO2	%(vol)	3.76%	2.76%	3.87%	2.49%
H2	%(vol)		21.41%		17.10%
H2O	%(vol)	8.16%	21.29%	8.38%	23.01%
N2	%(vol)	74.52%	42.60%	74.44%	45.91%
O2	%(vol)	12.67%		12.42%	
Total	%(vol)	100.00%	100.00%	100.00%	100.00%
Molecular weight	lb/mol	28.41	20.82	28.40	21.73
Expander inlet flow rate	lb/h	154,074	125,920	271,232	217,730
Expander inlet flow rate	lb/s	42.8	35.0	75.3	60.5
Expander inlet flow rate	kg/s	19.4	15.9	34.2	27.4
Expander inlet temperature	° F	2038	1965	2300	2280
Expander inlet pressure	Psia	211	211	241	241
Expander exhaust flow rate	lb/h	165,703	130,500	313,345	235,850
Expander exhaust flow rate	lb/s	46.0	36.3	87.0	65.5
Expander exhaust flow rate	kg/s	20.9	16.4	39.5	29.7
Expander exhaust temperature	° F	980	924	1024	1023
Expander exhaust pressure	Psia	14.8	14.8	14.8	14.8
Expander power	MW	13.61	14.88	29.34	30.01
Turbine net power	MW	5.25	9.97	12.95	20.89
Turbine specific power	kW / pps	114.1	275.0	148.8	318.9

These differences can be accommodated by the modifications described below.

POGT-400 Blade Path Re-Design

The HP expander in the SGT-400 is a "compressor turbine" providing power only for the compressor with no excess electric power generation. Since the POGT-400 compressor uses only 56% of the power used by the SGT-400 compressor, the HP expander flow field and blade path would have to be re-designed to produce only 56% power. This significant reduction in power could require shifting the second stage of the HP expander into the LP expander, with corresponding changes in HP and LP shaft lengths.

Expander Inlet and Exhaust

The inlet gases to a normal expander are a combination of hot gas from the burner and excess air from the compressor, while hot PO syngas produced by the POR is the only stream entering the POGT expander. A sealed, high-pressure, high-temperature inlet to the turbine will have to be

designed, replacing the open combustor shells in normal SGT-100 and SGT-400 turbines. The inlet will be configured as a volute to allow a single POR to provide input for the entire circumference of the expander inlet. The connections between the expander, its diffuser, and the HRSG must be tightly sealed to ensure that the syngas does not leak into the ambient air, and the ambient air does not leak into the syngas.

Expander Materials

The flow fields of the POGT expanders are similar to those of their normal SGT counterparts, so only minimal modifications to the airfoil shapes are expected. The gas compositions, however, provide reducing instead of oxidizing environments, so the materials in the flow fields should be checked and possibly changed to ensure they are compatible with PO syngas as a working fluid. The final POGT design should be validated by a blade vibration test, a rig test, a cooling rig test, and a high-temperature rotating rig test.

Expander Cooling

The POGT is intended to produce the purest partially-oxidized syngas possible without overheating the blades, vanes, or other expander parts. Therefore, cooling for the expander rotor, vanes, and blades is provided by steam instead of air, because steam can be condensed out of the exhaust gas stream while nitrogen is more difficult to remove.

Because the cooling properties of steam are different than those of air, separate analyses were performed to determine the appropriate steam flow rates needed to cool the expanders. Steam cooling flow rates that satisfy blade path temperature requirements were determined by iterative calculations for the POGT-100 and POGT-400 expanders. These preliminary cooling analyses indicated steam would provide an adequate substitute for air as a coolant, but further analyses are recommended to validate the preliminary results before the detailed design stage.

5.2.6. Generator Modifications

The generator for the POGT-100, Option D is 183% larger than the generator for the SGT-100 because this POGT compressor is separated from its expander. However, the generator for the POGT-400, Option C is only 61% larger than the SGT-400 generator this reduced-size compressor remains attached to its expander.

Table 14. POGT and SGT Generator Comparisons.

		POGT-100 Option C	Selected POGT-100 Option D	Selected POGT-400 Option C	POGT-400 Option D
POGT Expander Power	MW	14.88	14.88	30.01	30.01
POGT Compressor Power	MW	4.91	4.91	9.12	9.12
Nominal Net Power	MW	9.97	9.97	20.89	20.89
Relative Net Power	-	1.899	1.899	1.613	1.613
Net Power Increase	%	90%	90%	61%	61%
Compressor Motor	MW	0.00	4.91	0.00	9.12
Generator Power	**MW**	**9.97**	**14.88**	**20.89**	**30.01**
Relative Generator Power	-	1.899	2.834	1.613	2.317
Generator Power Increase	%	90%	183%	61%	132%
Grid Frequency	Hz	60	60	60	60
Generator Speed	rev/min	1800	1800	1800	1800
Generator Poles		4	4	4	4
Siemens Generator	**Rating MW**	**Rated Power / Required Power**			
1800-rpm Generators					
SGT-100	**5.25**	0.53	0.35	0.25	0.17
SGT-200	**6.70**	0.67	0.45	0.32	0.22
SGT-300	**7.90**	0.79	0.53	0.38	0.26
SGT-400	**12.90**	1.29	0.87	0.62	0.43
SGT-500	**17.00**	1.71	1.14	0.81	0.57
SGT-600	**24.80**	2.49	1.67	1.19	0.83
SGT-700	**29.10**	2.92	1.96	1.39	0.97
SGT-800	**45.00**	4.51	3.02	2.15	1.50
3600-rpm Generators					
SGT-900	**49.50**	4.96	3.33	2.37	1.65
SGT-1000F	**67.70**	6.79	4.55	3.24	2.26
SGT6-2000E	**109.00**	10.93	7.33	5.22	3.63
SGT6-3000E	**120.50**	12.09	8.10	5.77	4.02

The lower part of

Table 14 compares the rated powers of standard SGT-nnn generators with the requirements of the POGT generators, with rectangles around the selected replacement generators. The 17-MW generator designed for the SGT-500 gas turbine could be used for the 15-MW POGT-100 Option D, while the 25-MW generator designed for the SGT-600 gas turbine could be used for the 21-MW POGT-400 Option C.

5.2.7. Reduction Gear Modifications

The POGT-100 expander shaft rotates at 17,384 rpm and the POGT-400 expander shaft rotates at 9,500 rpm, so reduction gears are needed in both cases to transmit power to electric generators running at 1,800 rpm. The gears normally provided with the SGT-100 and -400 cannot be used because the POGTs generate more power than their SGT counterparts.

Table 8 compares the shaft power and torque requirements for the compressor, expander, and reduction gears in conventional (SGT) and POGT units. In the "Margin" column, a positive (+) percent means that the existing shaft meets POGT requirements, while a negative (-) percent or "New" means that a stronger design is needed. Both the expander and the reduction gears require strengthening, but this would be a design rather than a developmental effort.

Table 15. Shaft Power and Torque Comparisons.

Model		SGT-100	POGT-100(D)	Margin	SGT-400	POGT-400(C)	Margin
Expander Power	kW	13,610	14,880	-9%	29,340	30,010	-2%
Compressor Power	kW	8,360	4,910	70%	16,390	9,120	80%
Expander speed	rev/min	17,384	17,384	0%	9,500	9,500	0%
Compressor speed	rev/min	17,384	17,384	0%	9,500	9,500	0%
Generator speed	rev/min	1,800	1,800	0%	1,800	1,800	0%
HP (Compr) Expander							
Power, LP end	kW	-	-	n/a	-	-	n/a
Power, HP end	kW	-	-	n/a	(16,390)	(9,120)	80%
Expander speed	rev/min	-	-	n/a	9,500	9,500	0%
Torque, LP end	N-m	-	-	n/a	-	-	n/a
Torque, HP end	N-m	-	-	n/a	(16,475)	(9,167)	80%
Main Expander							
Power, LP end	kW	-	9,970	<-New	12,950	20,890	-38%
Power, HP end	kW	13,610	(4,910)	177%	-	-	n/a
Expander speed	rev/min	17,384	17,384	0%	9,500	9,500	0%
Torque, LP end	N-m	-	5,477	<-New	13,017	20,998	-38%
Torque, HP end	N-m	7,476	(2,697)	177%	-	-	n/a
Compressor							
Power, HP end	kW	13,610	(4,910)	177%	(16,390)	(9,120)	80%
Power, LP end	kW	5,250	-	Max	-	-	n/a
Compressor speed	rev/min	17,384	17,384	0%	9,500	9,500	0%
Torque, HP end	N-m	7,476	(2,697)	177%	(16,475)	(9,167)	80%
Torque, LP end	N-m	2,884	-	Max	-	-	n/a
Reduction Gears							
Power, inlet end	kW	5,250	9,970	-47%	12,950	20,890	-38%

Power, exit end	kW	5,250	9,970	-47%	12,950	20,890	-38%
Speed, inlet end	rev/min	17,384	17,384	0%	9,500	9,500	0%
Speed, exit end	rev/min	1,800	1,800	0%	1,800	1,800	0%
Torque, inlet end	N-m	2,884	5,477	-47%	13,017	20,998	-38%
Torque, exit end	N-m	27,851	52,891	-47%	68,700	110,821	-38%

In principle, the gears from larger Siemens gas turbines could be used for POGT applications, , but the gearboxes from those larger turbines are designed for different speeds, so new gear sets are needed.

5.2.8. Rotor and Bearing Modifications

Normally the compressor produces an axial force acting in the direction from its HP end to the LP end, which normally offsets part of the force in the opposite direction produced by the expander (HP end to LP end, but the other way). This unbalanced force must be balanced by (1) adding a rotating balancing "piston" near the HP end of the expander, similar to the kinds used in HP steam turbines; and/or (2) replacing the existing thrust bearing with a thrust bearing able to handle the larger thrust.

5.2.9. Turbine Retrofit Conversion Plan

The modifications that would be needed to convert an SGT-100 or and SGT-400 into a Partial Oxidation Gas Turbine (POGT) system are summarized below.

- The connections between the expander, its diffuser, and the HRSG must be sealed to ensure the containment of the syngas, so that the syngas does not leak into the ambient air, and the ambient air does not leak into the syngas.
- The POGT-400 will need new flow fields and blade paths in both the HP and LP expanders because less HP expander power is needed to balance the smaller POGT compressor.
- The materials in the POGT flow field will have to be checked and possibly changed to ensure that they are compatible with PO syngas as a working fluid. The design will then be validated by a blade vibration test, a rig test, a cooling rig test, and a high-temperature rotating rig test.
- The unbalanced axial force acting in the direction from the HP end to the LP end of the expander must be balanced by either (1) adding a rotating balancing "piston" near the HP end of the expander, and/or (2) replacing the existing thrust bearing with a thrust bearing able to handle the larger thrust.
- A separate, commercially available compressor would be used as the POGT compressor, so no additional development effort would be needed
- In the POGT configuration, a volute expander inlet replaces the 30 burners at the expander inlet. Required modifications include: designing and fabricating the volute inlet.
- Generators designed for use with the SGT-500 and SGT-600 gas turbines would be used for this application, so no additional development effort would be needed.

- The reduction gears are similar to existing designs, although they operate are different rotational speeds. This would be a design rather than a developmental effort.
- Finally, the design of the completed engine would be validated by a mechanical performance test and a thermal paint test.

5.3. Results of feasibility study of Siemens turbines SGT-100 and SGT-400 for POGT applications.

The SGT-100 and SGT-400 gas turbines can be used for POGT application if their compressors are replaced by separate, commercial compressors, their combustors are replaced by volute expander inlets, their generators are replaced by generators from larger SGT engines, and new reduction gears are made. These resulting modifications are of the same magnitude as those that would be required for a turbine upgrade.

5.4. Partial Oxidation Gas Turbine (POGT) Feasibility Study Based on the Siemens SGT-800 Gas Turbine.

5.4.1. Summary.

The Gas Technology Institute (GTI, Des Plaines, Illinois) is developing a Partial Oxidation Reactor (POR) that converts pressurized syngas into partially oxidized (PO) syngas, which is used as the working fluid in a Partial Oxidation Gas Turbine (POGT) expander.

Three Siemens gas turbines in the 30-to-100-MW range were identified as potential candidates for conversion to POGT applications. After review and analysis, the SGT-800 was selected as the basis turbine. The basic development approach for the POGT is to use existing SGT-800 components as much as possible, making whatever modifications are necessary to meet design requirements. Discussions of available resources and viable markets are beyond the scope of this study, which focuses only on technology.

At the beginning of the project, it was assumed that most of the modifications needed to convert a gas turbine into a POGT would focus on the expander. Further analysis, however, has also revealed the need for significant changes to components connected to the expander – the compressor, reduction gears, and generator.

5.4.2. Introduction.

The Gas Technology Institute (GTI, Des Plaines, Illinois) is developing a Partial Oxidation Reactor (POR) that converts pressurized syngas into partially oxidized (PO) syngas. The PO syngas is used without combustion as the working fluid in a Partial Oxidation Gas Turbine (POGT) expander, and the POGT exhaust is finally used as a chemical feedstock. Expander cooling is provided by steam instead of air in order to maintain syngas quality in a reducing environment. Figure 50 is a simplified process flow diagram of the proposed concept, with properties of the numbered streams tabulated in Appendix A.

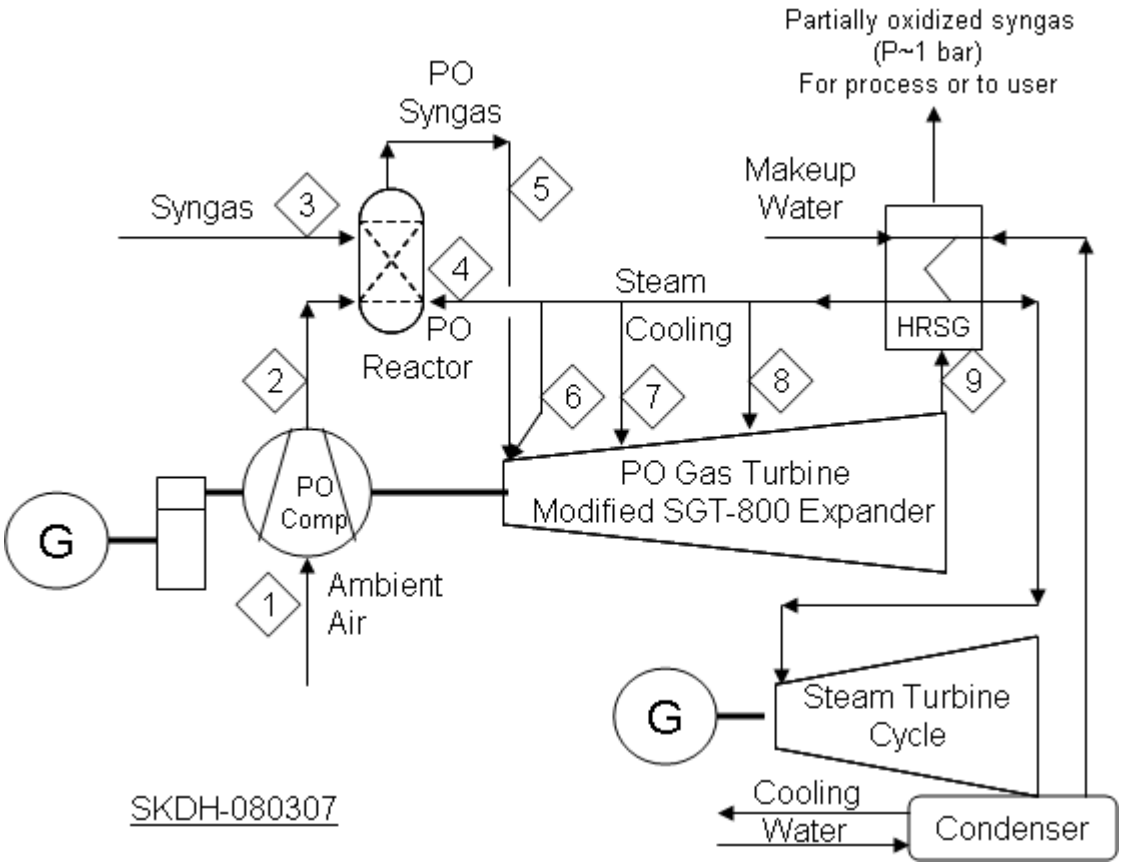

Figure 50. Partial Oxidation Concept.

The air compressor for the POGT is much smaller than the air compressor in a conventional gas turbine because (1) the syngas is only partially oxidized, and (2) air is not allowed to mix with the PO syngas in the expander. With its similar expander and smaller compressor, the POGT requires a larger reduction gear and generator that would be needed for a conventional gas turbine.

This report describes the selection and potential modification of a Siemens gas turbine for POGT application. The selected turbine is a modified SGT-800 (formerly the GTX-100), and its POGT performance is summarized in Table 16.

Table 16. POGT Performance.

Compressor inlet flow rate	402,272 lb/hr	50.7 kg/s
Compressor inlet temperature	59 °F	15 °C
Compressor inlet pressure	14.7 psia	1.01 bar
Compressor exit flow rate	402,272 lb/hr	50.7 kg/s
Compressor exit temperature	874.3 °F	467.8 °C
Compressor exit pressure	280.8 psia	19.4 bar
Compressor power	24.2 MW	
Expander inlet flow rate	793,122 lb/hr	99.9 kg/s
Expander inlet temperature	2283 °F	1250 °C
Expander inlet pressure	275.0 psia	19.0 bar
Exhaust flow rate	837,321 lb/hr	105.5 kg/s
Exhaust temperature	1042.4 °F	561.3 °C
Exhaust pressure	14.6 psia	1.0 bar
Expander power	103.8 MW	
Turbine net power	79.6 MW	

5.4.3. Study Objectives.

The objectives of this POGT conversion study are:

- Identify two Siemens gas turbines in the range 30 to 100 MW for potential conversion to POGT.
- Estimate the performance and capital cost of these converted gas turbines on coal-derived fuel.
- Identify technical issues associated with conversion.
- Select the most promising turbine for following retrofit design.
- Estimate the preliminary performance of the converted gas turbine.
- Prepare a POGT conversion plan and design execution process with required feasibility design details, including budget and schedule estimates.
- Execute the POGT feasibility design for the selected gas turbine including feasibility drawings and narrative.

5.4.4. Candidate Retrofit Turbines.

Three Siemens gas turbines in the 30-to-100-MW range were identified as potential candidates for conversion to POGT applications. The candidate turbines are listed in Table 17, along with their main operating characteristics and probable modification needs for partial oxidation.

Table 17. Siemens Turbine Candidates for POGT Modifications.

Turbine Model	SGT-800	SGT-900	GT-140P
Former Model	GTX-100	W251B	GT-140P
Rated Power, MWe	43	49.5	70
Exhaust flow, kg/s (lb/s)	122 (269)	175 (386)	380 (838)
Exhaust temp, ^{o}C (^{o}F)	546 (1015)	514 (957)	375 (707)
Pressure ratio	20.1	15.3	12.0
Compressor sections	1	1	2
Compressor stages	15	19	8 + 12
Compressor Intercooling	No	No	Yes
Expander sections	1	1	2
Expander stages	3	3	3 + 1
Cooled expander stages	1 and 2	1 and 2	None
Modifications for POGT			
The compressor air flow rate must be reduced because air is needed for the gasifier and POR but not for cooling and dilution of combustion products and cooling the hot parts of the expander.	Required	Required	
The turbine casing between the compressor and the expander must be modified to accommodate air extraction to the gasifier and physical integration with the POR.	Required	Required	
The expander must operate under reducing conditions using partially oxidized syngas with expansion characteristics different from those of conventional gas turbine working fluids.	Required	Required	Required
In order to preserve the chemical properties of the working fluid, hot expander parts cannot be cooled by direct contact with air, as in conventional turbines. Closed-loop or open-loop steam cooling may be required.	Required	Required	
The turbine exit ducting must be durable under reducing conditions, and might be required to accommodate flue gas recirculation.	Required	Required	Required

The GT-140P turbine was removed from consideration because of the complexity associated with modifications to a two-shaft turbine, and the fact that this turbine has not been manufactured for several years.

GTI provided support in the form of a performance model of a Partial Oxidation Reactor (POR) connected to the expander portion of SGT-800 and SGT-900 gas turbines. For each turbine, the POR was sized so that the partially oxidized gas entering the expander had the same pressure, temperature, and volumetric flow rate as the gases entering the conventional expander, and so that the expander power and exhaust temperatures were also about the same as their commercial counterparts.

The first three stages of the POGT expander are to be cooled by steam instead of air, so a separate analysis was started to determine the appropriate cooling steam flow rate needed to cool the turbine.

Conceptual decisions were made regarding the number of PORs to be connected with the SGT-800 and SGT-900 expanders. The commercial SGT-800 gas turbine has 30 burners connected to 30 expander inlet segments, and the commercial SGT-900 gas turbine has 8 burners connected to 8 expander inlet segments. It was decided that the POGT based on the SGT-800 would have 10 PORs, with each POR feeding three expander inlet segments, so that the number of expander inlet segments remains at 30; and that the POGT based on the SGT-900 would have 8 PORs, with each POR feeding one expander inlet segment, so that the number of inlet segments remains at 8.

Upon further review, the SGT-800 was selected as the basis turbine because it is part of the current Siemens product line with more available engineering resources than the SGT-900.

5.4.5. Technical Issues and Feasibility Design.

The basic development approach for the POGT is to use existing SGT-800 components as much as possible, making whatever modifications are necessary to meet design requirements. A first-order heat transfer analysis indicated that steam cooling could provide more than enough cooling capacity for the SGT-800 expander.

The SGT-800 (formerly GTX-100) is a single-shaft gas turbine that produces about 45 MW on natural gas. It has 15 compressor stages, 30 burners, and three expander stages, as depicted in Figure 51. The 6600-rpm drive shaft at the compressor end is attached to a reduction gear, which is attached to an 1800-rpm electric generator.

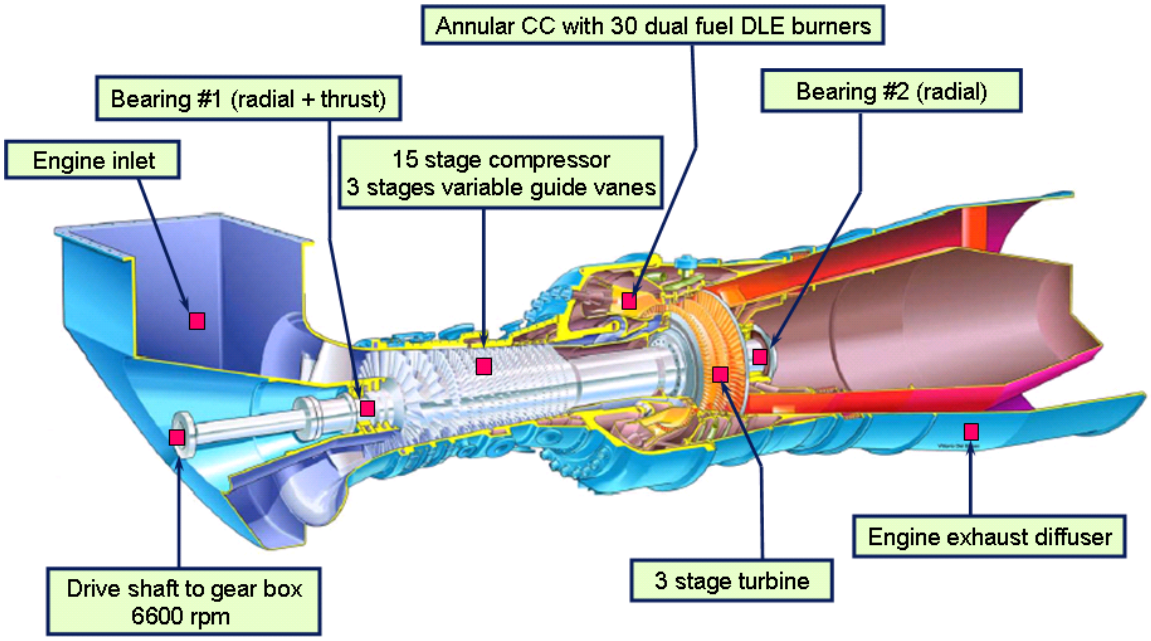

Figure 51. SGT-800 Cross-Section.

Figure 52 shows the plan and elevation views of a complete SGT-800 gas turbine plant.

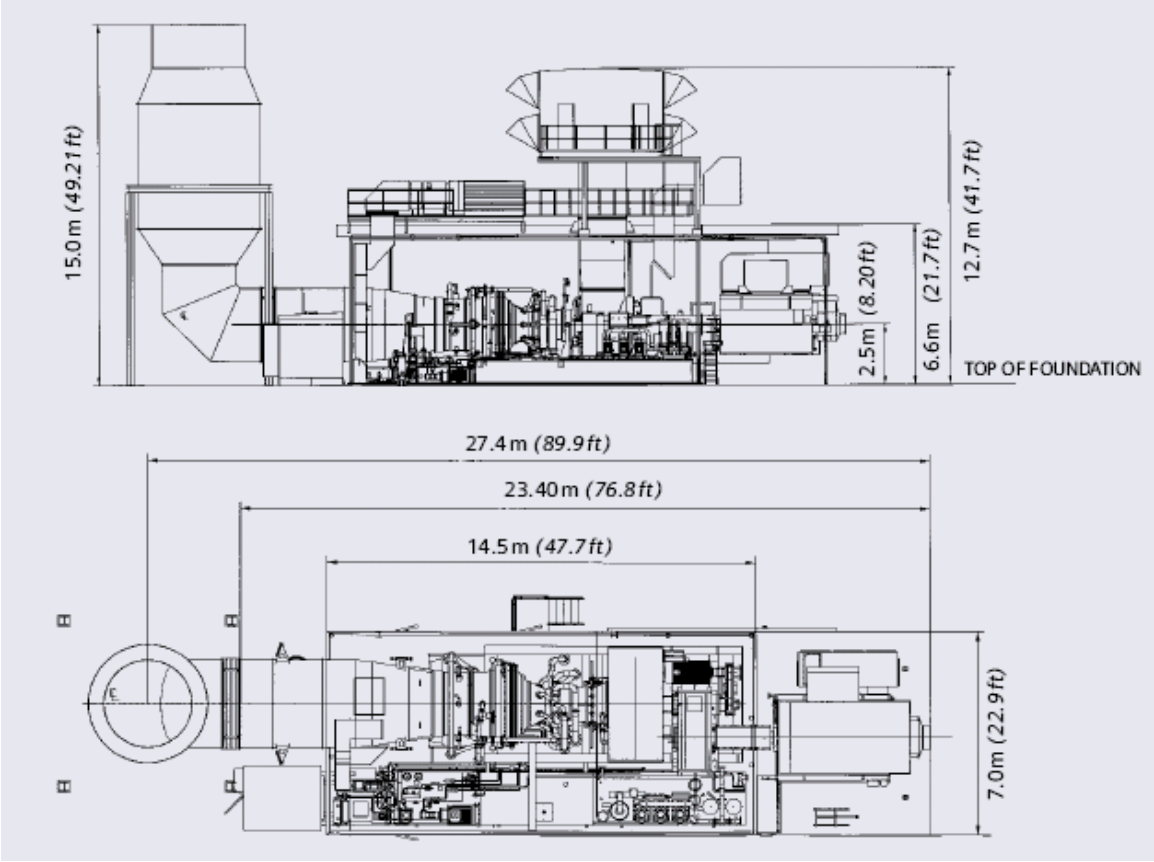

Figure 52. SGT-800 Plan and Elevation.

As with any new product, the development of the POGT would require: (1) sufficiently advanced technology; (2) sufficiently available developmental resources; and (3) the expectation of sufficient market sales to justify the development effort. Discussions of available resources and viable markets are beyond the scope of this study, which focuses only on technology.

The design conditions for the compressor and expander for the POGT are within the capabilities of existing commercial technology, but the equipment is physically different from commercially available equipment. Therefore, a certain amount of development effort would be needed to produce a POGT. This section focuses on estimating the magnitude of effort needed to convert portions of the SGT-800 into a POGT system.

- Expander modifications (Section 5.4.6),
- Compressor modifications (Section 5.4.7),
- Generator modifications (Section 5.4.9),
- Reduction gear modifications (Section 5.4.10), and
- Rotor and bearing modifications (Section 5.4.11)

The development requirements described in these sections are summarized in Section 5.4.12.

5.4.6. Expander Modifications.

The POGT expander has PO syngas instead of combustion products as its working fluid, and is cooled by steam instead of air. The PO syngas temperature and volumetric flow rate are approximately equal to the design conditions of the SGT-800. The main differences between the POGT expander and the SGT-800 expander are listed in Table 18.

Table 18. POGT and SGT-800 Expander Comparison.

Design Parameter	POGT	SGT-800
Source(s) of Expander Flows	Burners (PORs) only	Compressor + Burners
Nominal Working Fluid, %vol		
Ar	0.36%	0.90%
CO	17.20%	- 0 -
CO_2	9.57%	3.40%
H_2	10.91%	- 0 -
H_2O	30.80%	7.60%
N_2	31.15%	74.70%
O_2	- 0 -	13.40%
Expander Inlet Temperature	~1250 ^oC (~2321 ^oF)	~1270 ^oC (~2318 ^oF)
Nominal Exhaust Flow	105.0 kg/s (232.6 lb/s)	130.4 kg/s (287.4 lb/s)
Nominal Exhaust Temperature	561 ^oC (1042 ^oF)	538 ^oC (1001 ^oF)
No. of turbine stages	3	3
Cooling fluid and type		
Cooling fluid	Steam	Air
Stage 1 cooling type:	Film	Film
Stage 2: cooling type	Convection	Convection
Stage 3: cooling type	None	None
Expander Materials	Suitable for hot, reducing syngas	Normal materials
Expander Exhaust Connection to HRSG	Sealed connection	Normal connection
Expander Power	103,800 kW	105,400 kW

These differences can be accommodated by the modifications described below.

Expander Inlet and Exhaust

Hot PO syngas produced by the POR is the only stream entering the POGT expander. Since nothing is coming from the compressor, a sealed, high-pressure, high-temperature inlet to the turbine will have to be designed, replacing the open combustor shell of the SGT-800.

The connections between the expander, its diffuser, and the HRSG must be sealed to ensure the containment of the syngas, so that the syngas does not leak into the ambient air, and the ambient air does not leak into the syngas.

Expander Materials.

The flow field of the POGT expander is similar to that of an SGT-800, so only minimal modifications are expected. The materials in the flow field, however, will have to be checked and possibly changed to ensure that they are compatible with PO syngas as a working fluid.

The POGT design will be validated by a blade vibration test, a rig test, a cooling rig test, and a high-temperature rotating rig test.

Expander Cooling

Cooling air for the expander rotor, vanes, and blades will be provided by steam instead of air.

From a POGT perspective, the expander should produce the purest (least steam) partially-oxidized syngas without overheating the blades, vanes, or other expander parts. From a gas turbine perspective, the blade path temperatures should be about the same as in natural-gas-fueled versions of the same turbines, to minimize the need for design changes to the expander. The objective, therefore, was to determine the steam cooling flow needed to cool the blades and vanes to the same temperatures as in the natural gas design, given that the heat transfer characteristics and cooler temperature of steam are better than those of air.

Because steam has different cooling properties than air, a separate analysis was performed to determine the appropriate cooling steam flow rate needed to cool the turbine. After several iterations, steam cooling flow rates were established that satisfy blade path temperature requirements for the SGT-800 (GTX-100) POGT expander with oxygen-blown syngas.

This preliminary analysis has indicated that steam would provide an adequate substitute for air as a coolant, but further analysis to validate the preliminary results is recommended before the detailed design stage.

5.4.7. Compressor Modifications.

The air compressor for the POGT is 60 percent smaller than the compressor for an SGT-800 because of the reduced need for air in the Partial Oxidation Reactor. All of the compressed air is extracted from the compressor exit and directed to the PORs. None of the air is allowed to mix with the Partially Oxidized syngas in the expander.

The main differences between the POGT compressor and the SGT-800 compressor are listed in Table 19.

Table 19. POGT and SGT-800 Compressor Comparison.

Design Parameter	POGT	SGT-800

Design Parameter	POGT	SGT-800
Compressor Inlet Air Flow	112 lb/s 51 kg/s 402,272 lb/hr 182,466 kg/hr 88,040 cu.ft/min 2,363 m^3/min 141,801 m^3/hr	282 lb/s 128 kg/s 1,013,915 lb/hr 459,902 kg/hr 221,904 cu.ft/min 5,957 m^3/min 357,407 m^3/hr
Compressor Power	24,200 kW	61,100 kW
Expander Power Entering Rotor	103,800 kW	105,400 kW
Generator Power Leaving Rotor	79,600 kW	44,300 kW
Compressor Exit Flow	Extracted to POR	To combustor shell

The five compressor options in Table 20 were identified for POGT application. Each option is described below.

Table 20. Compressor Options.

Option	Advantages	Disadvantages
1. Re-designed Compressor	Meets flow and torque requirements	New design cost
2. Compressor from another engine	Minimal design work required	Nothing available
3. Compr-Gen-Exp	Reasonable compressor	Need 104-MW reduction gear, but max commercial size is ~90 MW
4. Separate compressor branch	Reasonable compressor and gear sizes	Increased gear complexity and gear losses; new design
5. Compr-Exp-Gen	Reasonable compressor and gear	Generator connected to turbine exhaust end (manageable)

Option 1: New Compressor

The blades and vanes of the SGT-800 compressor could be shortened to accommodate the smaller air flow, and the compressor rotor could be strengthened to transmit additional torque from the expander to the generator. Figure 53 depicts this option, as well as Option 2.

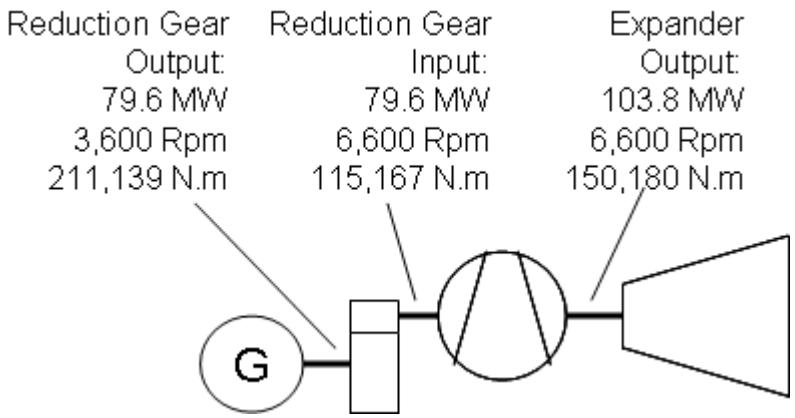

Figure 53. Compressor on Turbine Shaft.

Option 2: Compressor from Another Engine

A smaller compressor from a different gas turbine engine could be used in place of the SGT-800 compressor. This compressor would also need to transmit the additional torque from the expander through to the generator, requiring a strengthened rotor.

Siemens has no compressors that can simultaneously meet both POGT requirements – less flow and more torque. Compressors from SGT-500 and above are too large, and compressors from SGT-400 and below are too small. Table 21 and Figure 54 compare the inlet air flows and exit pressures of standard SGT-xxx compressors with the requirements of the POGT compressor.

Table 21. POGT and SGT-xxx Compressor Comparison.

Former Model	Current Model	Inlet Air Flow, lb/s	Approx Shaft Power, MW	Speed, rev/min
Typhoon	SGT-100	45.1	2.1	17,384
Tornado	SGT-200	63.7	2.7	11,053
Tempest	SGT-300	64.6	3.2	14,010
Cyclone	SGT-400	85.2	5.2	9,500
>>>>>>	POGT	111.7	24.2	6,608
GT10B	SGT-600	174.1	9.9	7,700
GT10C	SGT-700	197.4	11.6	6,500
GTX100	SGT-800	281.6	18.0	6,608
W251B	SGT-900	379.3	19.8	5,425
V64.3A	SGT-1000F	413.5	27.1	5,400

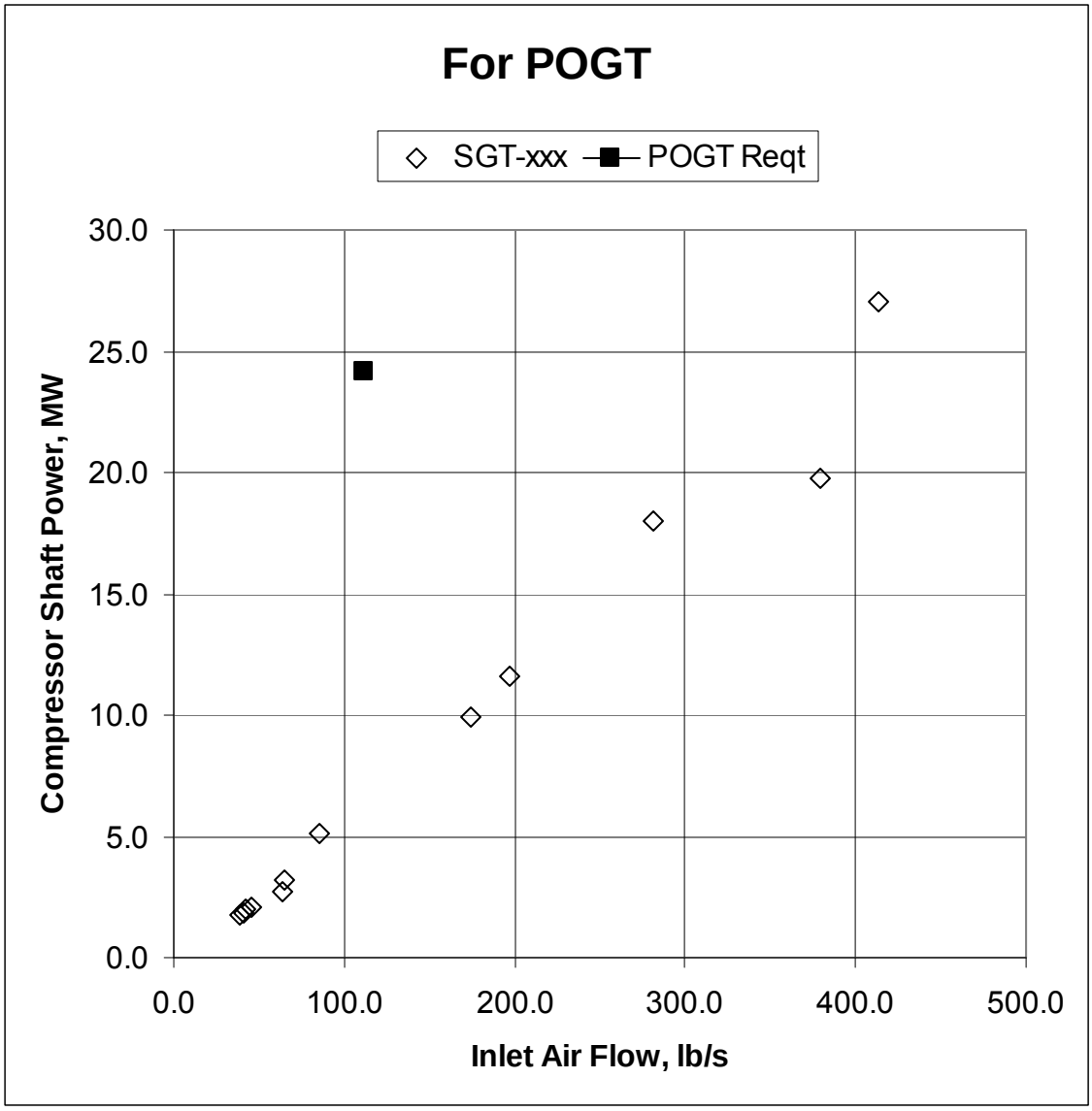

Figure 54. POGT and SGT-xxx Compressor Comparison.

The attachment of a third-party compressor to a Siemens engine would have the same mismatch of flow and torque requirements, and would likely also be problematic from a commercial viewpoint. Therefore, using a substitute compressor on the same shaft does not seem to be a viable option.

Option 3: Connect Separate Compressor to Generator

Connecting a separate compressor to the other end of the generator from the expander reduces its shaft power requirements, since the compressor shaft is not required to transmit the net power through to the generator. This option, depicted in Figure 55, would use a commercially available compressor such as those listed in Appendix B, from the *2006 GTW Handbook*.

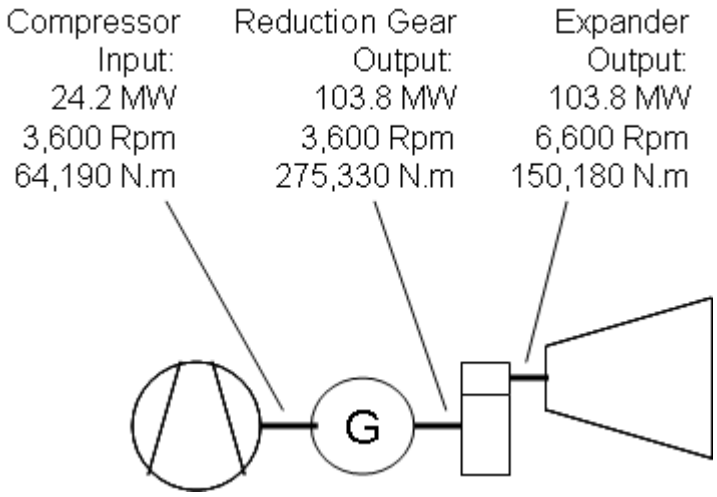

Figure 55. Compressor on Generator Shaft.

However, this option shifts the problem from the compressor to the gear box, which would then have to handle all 104 MW of expander power. Since the largest reduction gears can only transmit about 90 MW, this option does not seem viable either.

Option 4: Separate Compressor Branch from Drive Train

Another variation of the separate-compressor option is to drive the compressor with gears at right angles to the main drive train, as shown in Figure 56. This option would reduce the power requirements of both the compressor rotor and the reduction gear, but would require the addition of a 25-MW right-angle gear set, incurring increased complexity and more gear losses. Torque requirements for the compressor shaft depend on the speed of the compressor.

This option would also use a commercially available compressor such as those listed in Appendix B, from the *2006 GTW Handbook*.

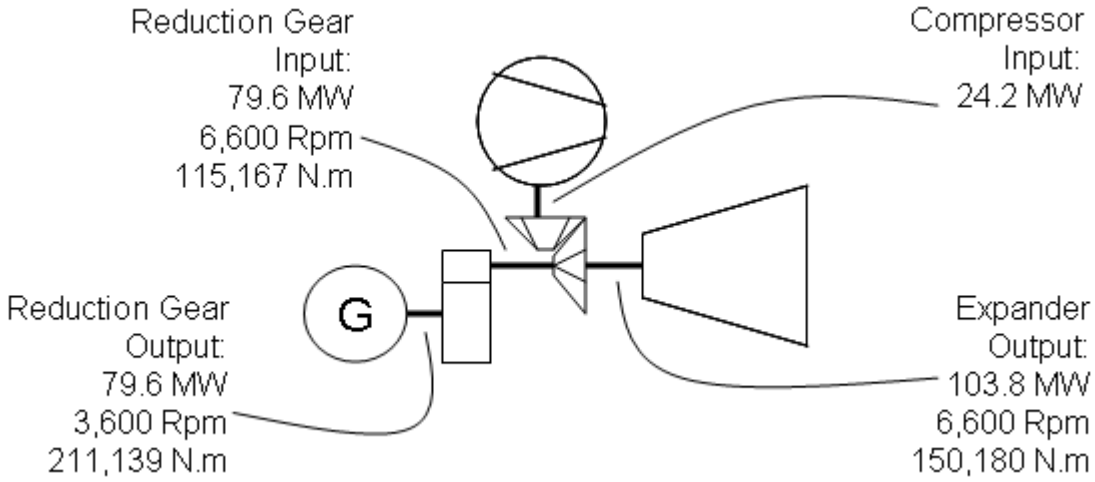

Figure 56. Compressor Branched from Drive Train.

Option 5: Compressor-Expander Generator Arrangement

Figure 57 shows this arrangement, in which the expander is located between the compressor and the reduction gear for the generator. The compressor in this option is the same re-designed compressor described in Option 1. This option features reasonable flow and torque requirement for the compressor and reduction gear. The generator is connected to the exhaust (hot) end of the expander, so the expander would have a side exhaust instead of the more conventional axial exhaust.

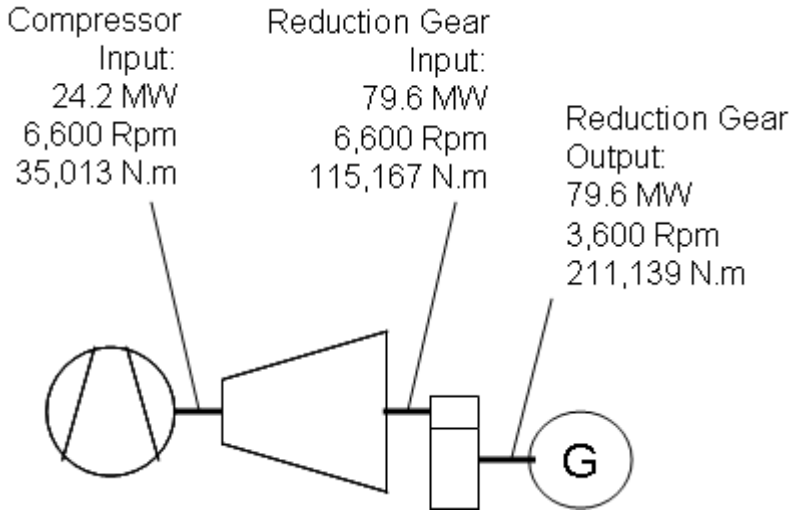

Figure 57. Compressor-Expander-Generator.

Best Option

Since there does not seem to be any commercial compressor that can meet the flow, pressure, torque, and speed requirements of the POGT compressor, the only feasible option seems to be the re-designed compressor in Option 5. After the compressor flow field and rotor are designed, the compressor would go through blade vibration testing and rig testing.

5.4.8. POR-POGT Interface.

A normal SGT-800 has 30 burners aligned radially and distributed circumferentially around the turbine, upstream from the expander inlet. The main differences between the POGT "burners" and the SGT-800 burners are listed in Table 22.

Table 22. POGT and SGT-800 Burner Comparison.

Design Parameter	POGT	SGT-800
Burner type	POR (by GTI)	Single, annular chamber, low-emission variant, dry
Number of burners	10	30

Two arrangements are available to connect the POR to the POGT: multiple PORs distributed circumferentially around the expander inlet; and a single POR connected to a volute inlet.

Option 1: Circumferentially Distributed PORs

In this POGT configuration, ten Partial Oxidation Reactors (PORs) replace the 30 burners and the exit stream from each POR is evenly distributed to three adjacent locations formerly occupied by burners. Required modifications include: designing and fabricating 10 PORs, and designing and fabricating 10 manifolds to connect the PORs to the POGT.

The advantage of this arrangement is minimal turbine modification, since existing burner ports would be used. The disadvantages include the need to design ten burner manifolds and increased heat losses from multiple PORs compared to the reduced losses from a single POR.

The conventional burner arrangement for an SGT-800 is shown in Figure 58, for reference. The compressor inlet and compressor blades shown in the left-hand portion of the figure would each be smaller than shown in the figure, but the burner connections and expander in the right-hand portion would stay the same sizes.

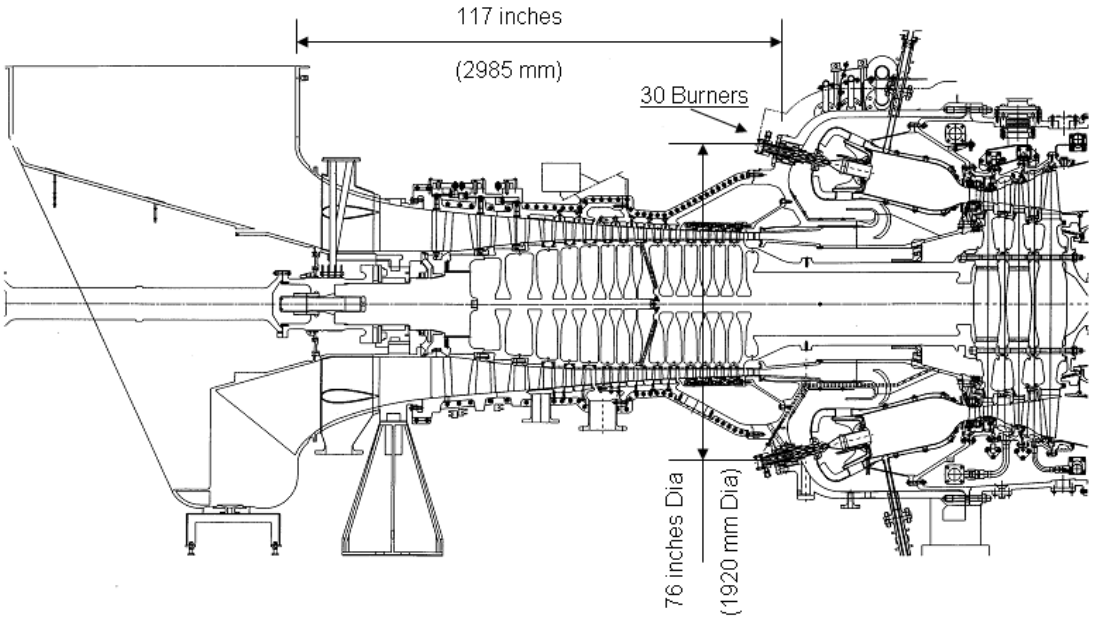

Figure 58. SGT-800 Burner Arrangement.

The POR-POGT interface (burner-turbine interface) is further defined in Figure 59. The interface consists of 30 ports located on a circle that is approximately 67 inches (1920 mm) in diameter. The ports are arranged circumferentially around the turbine centerline in 12-degree increments, and their centerlines are canted approximately 13.5 degrees from the turbine centerline. The inside of each port is approximately 5 inches (140 mm) in diameter and the outside diameter is approximately 8 inches (210 mm) in diameter. All dimensions are approximate and should not be used for detailed design or manufacture.

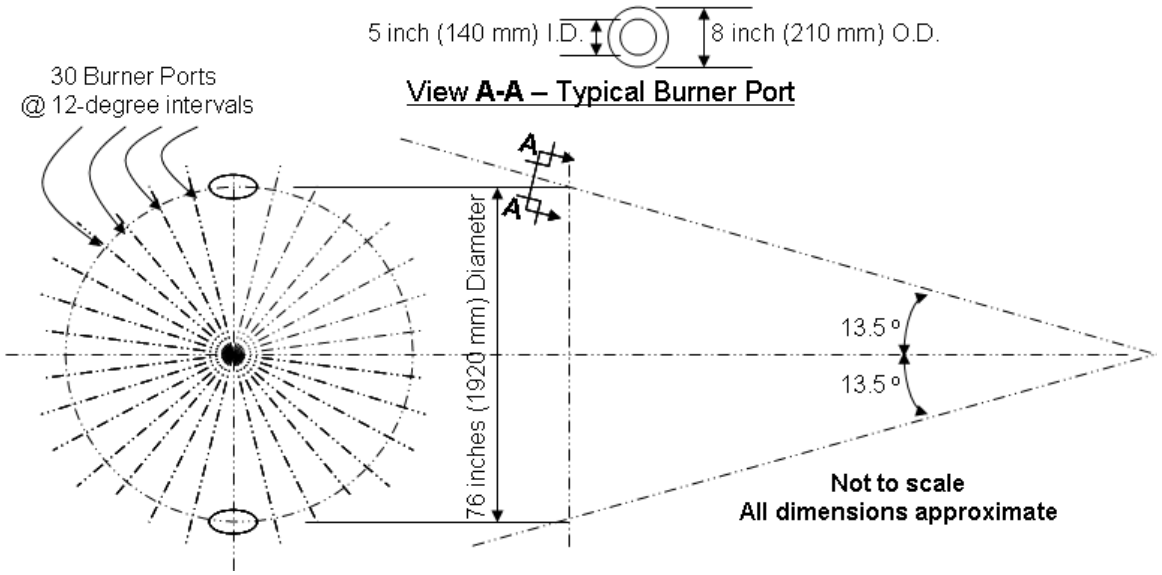

Figure 59. POR-POGT Interface.

Option 2: Single POR with Volute Expander Inlet

For this option, a new volute expander inlet is design to connect a single POR with the inlet annulus of the POGT. Advantages of this option include lower thermal losses and easier control with one POR than with multiple PORs. The disadvantage is the need to design a new volute inlet.

Better Option

Option 2 with its single POR and volute expander inlet was selected because of its reduced thermal losses, and the fact that a some design work would be required with either option – either new manifolds or a new volute.

5.4.9. Generator Modifications.

The generator for the POGT is 78 percent larger than the generator for an SGT-800 because of the reduced size of the POGT compressor. The main differences between the POGT generator and the SGT-800 generator are listed in Table 23.

Table 23. POGT and SGT-800 Generator Comparison.

Design Parameter	POGT	SGT-800
Nominal Net Power	79,600 kW	44,400 kW
Grid Frequency	60 Hz	60 Hz
Generator Poles	2	4

Design Parameter	POGT	SGT-800
Generator Speed	3600 rev/min	1800 rev/min

As a reference, Table 24 and Figure 60 compare the rated powers of standard SGT-xxx generators with the requirements of the POGT generator. It is noteworthy that smaller generators (such as the SGT-800) rotate at 1800 rev/min while larger generators rotate at 3600 rev/min. At 79.6 MW, the POGT generator would fall into the larger, 3600-rpm category.

The 109-MW generator designed for the SGT6-2000E gas turbine would be used for this application.

Table 24. POGT and SGT-xxx Generator Comparison.

Former Model	Current Model	Rated Power, MW	Speed, rev/min
			1800
Typhoon	SGT-100	4.3	1800
Typhoon	SGT-100	4.7	1800
Typhoon	SGT-100	5.0	1800
Typhoon	SGT-100	5.2	1800
Tornado	SGT-200	6.7	1800
Tempest	SGT-300	7.9	1800
Cyclone	SGT-400	12.9	1800
GT35	SGT-500	17.0	1800
GT10B	SGT-600	24.8	1800
GT10C	SGT-700	29.1	1800
GTX100	SGT-800	45.0	1800
W251B	SGT-900	49.5	3600
V64.3	V64.3	61.1	3600
V64.3A	SGT-1000F	67.7	3600
	POGT	79.6	3600
V84.2	SGT6-2000E	109.0	3600
W501D5A	SGT6-3000E	120.5	3600

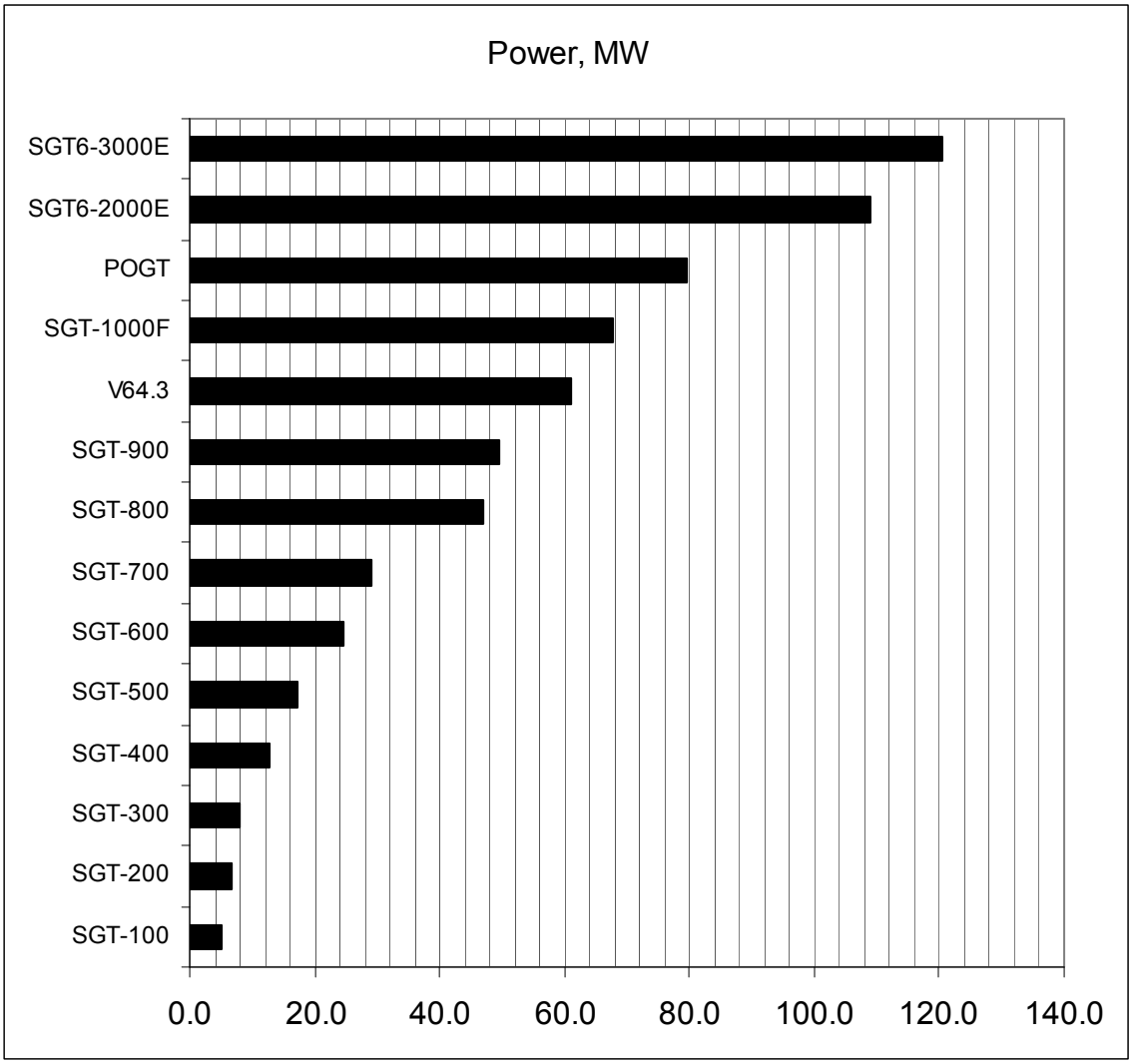

Figure 60. POGT and SGT-xxx Generator Comparison.

5.4.10. Reduction Gear Modifications.

As shown in Figures 61 and 62, the design requirements for the reduction gear are identical for either the Expander-Compressor-Gear arrangement or the Compressor-Expander-Gear arrangement. The turbomachinery shaft rotates at 6,600 rpm, so a reduction gear is needed to transmit the power to an electric generator running at synchronous speed. Reducing the compressor size reduces the parasitic power normally consumed by the compressor, which could be as much as half of the power produced by the expander. With more net power being produced, the existing generator, coupling, and compressor shaft must be strengthened.

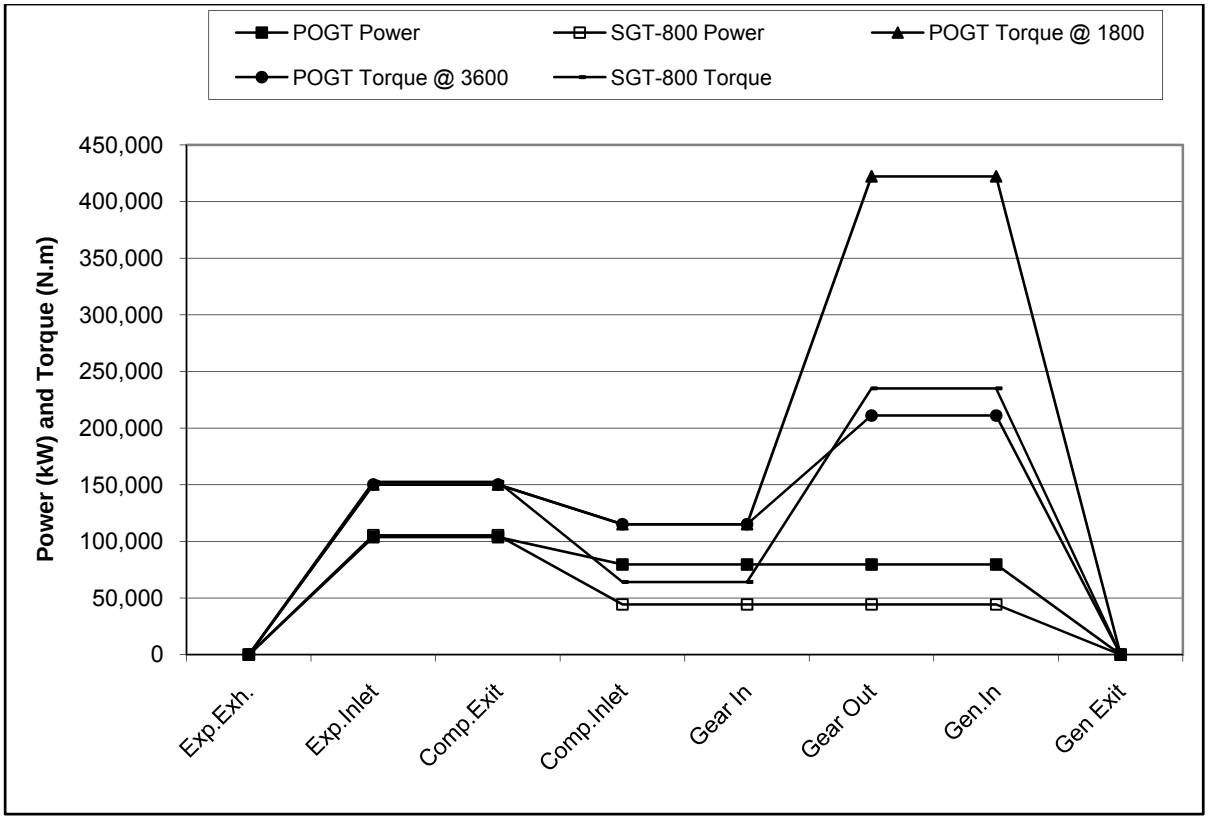

Figure 61. Shaft Power and Torque for Exp-Comp-Gen Arrangement.

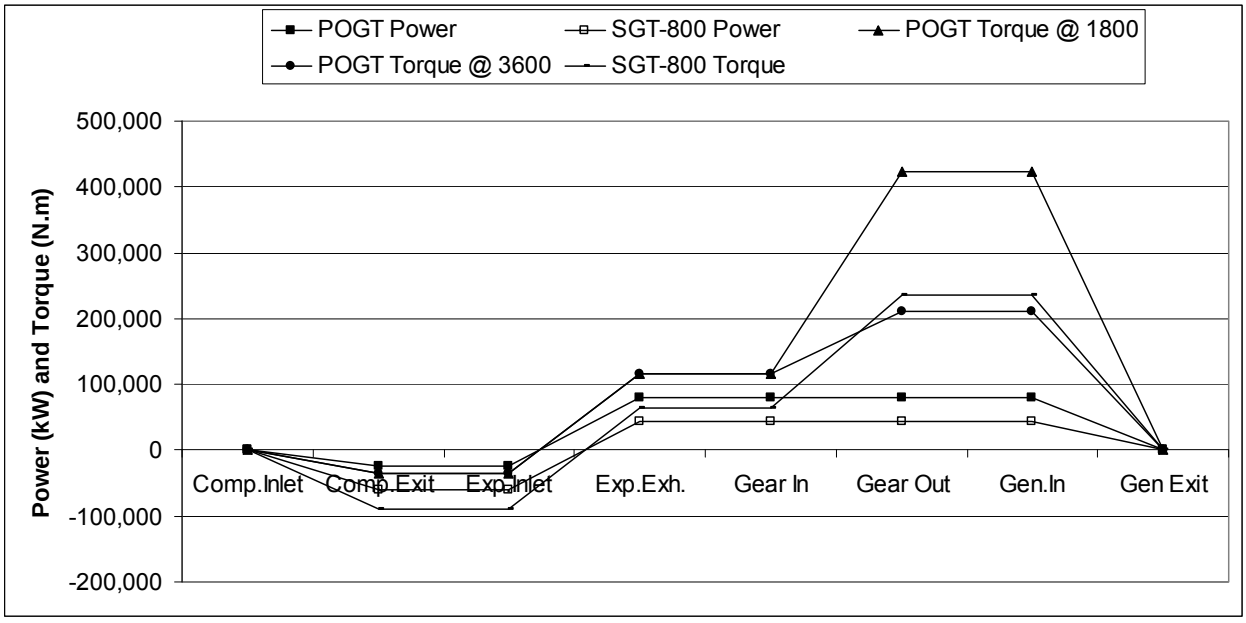

Figure 62. Shaft Power and Torque for Comp-Exp-Gen Arrangement.

The generator and coupling could be exchanged for the generator and coupling from a larger gas turbine, but the compressor end of the shaft would have to be strengthened to handle the larger torque requirement.

Increasing the power rating of the reduction gear from 55 MW to over 80 MW appears to be within the envelope of current technology. Hitachi (2007) offers a gas turbine reduction gearbox "capable of transmitting 90 MW, one of the biggest capacity [units] in domestic [production]." The website description of the *Reduction Gear for Gas-Turbine Generator* shows a "reduction gearbox for gas-turbine generator capable of transmitting 90 MW, one of the biggest capacity [units] in domestic [production]. In the gas-turbine generating units made by Hitachi, the gearboxes exclusively developed by our technology are utilized. They have been supplied all over the world and enjoying the best reputation. Other than this, we are manufacturing vertical offset type in which the pinion shaft is located just on the gear wheel shaft. The gears are carburized, case-hardened and ground with high reliability, and all the bearings are of sleeve type. The thrust load due to meshing of the gears can be supported by the tapered-land type bearing provided on the side of the sleeve bearings. Accordingly, it has high reliability." (http://www.hitachi-nico.jp/en/product/industrial/reduction_gear_dynamo/gas_turbine/index.html, 28 October 2007.)

The main differences between the POGT reduction gear, the Hitachi gear, and the SGT-800 gear are listed in Table 25.

Table 25. POGT and SGT-800 Reduction Gear Comparison.

Design Parameter	POGT	Hitachi	SGT-800
Reduction gear continuous rated power	80,000 kW	90,000 kW	55,000 kW
Gear input speed	6,600 rpm	5,235 rpm	6,600 rpm
Gear output speed	3,600 rpm	3,000 rpm	1,800 rpm

The 90-MW Hitachi gear reduces shaft speed from 5,235 rpm to 3,000 rpm (1.745:1) for 50-Hz power generation, while the POGT gear should reduce shaft speed from 6,600 rpm to 3,600 rpm (1.833:1) for 60-Hz power generation. The POGT gears transmit less power than the Hitachi gears, and the POGT input and output shafts and gears rotate faster than the Hitachi shafts and gears, so the POGT shafts and gears have lower torque requirements than the Hitachi shaft and gears.

5.4.11. Rotor and Bearing Modifications.

Using a smaller compressor increases the amount or torque that is transmitted from the expander to the reduction gear and generator, so the compressor rotor for the POGT will be larger and stronger than its SGT-800 counterpart. Using a smaller compressor also reduces the axial force acting in the direction from the HP end to the LP end, which normally offsets part of the force in the opposite direction produced by the expander (HP end to LP end, but the other way). This unbalanced force must be balanced by some method, such as (1) adding a rotating balancing "piston" near the HP end of the expander, similar to the kinds used in HP steam

turbines; and/or (2) replacing the existing thrust bearing with a thrust bearing able to handle the larger thrust.

5.4.12. Turbine Retrofit Conversion Plan.

The modifications that would be needed to convert an SGT-800 into this Partial Oxidation Gas Turbine (POGT) system are summarized below.

- The connections between the expander, its diffuser, and the HRSG must be sealed to ensure the containment of the syngas, so that the syngas does not leak into the ambient air, and the ambient air does not leak into the syngas.
- The materials in the POGT flow field will have to be checked and possibly changed to ensure that they are compatible with PO syngas as a working fluid. The design will then be validated by a blade vibration test, a rig test, a cooling rig test, and a high-temperature rotating rig test.
- For the POGT compressor, the best option is a re-designed compressor. After the compressor flow field and rotor are designed, the compressor would go through blade vibration testing and rig testing.
- In the POGT configuration, a volute expander inlet replaces the 30 burners at the expander inlet. Required modifications include: designing and fabricating the volute inlet.
- The 109-MW generator designed for the SGT6-2000E gas turbine would be used for this application, so no additional development effort would be needed.
- A reduction gear similar to the 90-MW Hitachi gear will be developed to reduce shaft speed from 6,600 rpm to 3,600 rpm (1.833:1) for 60-Hz power generation.
- The compressor rotor for the POGT will be larger and stronger than its SGT-800 counterpart, as will the axial force acting in the direction from the HP end to the LP end. The unbalanced force must be balanced by either (1) adding a rotating balancing "piston" near the HP end of the expander, and/or (2) replacing the existing thrust bearing with a thrust bearing able to handle the larger thrust.
- In addition, the design of the completed engine would be validated by a mechanical performance test and a thermal paint test.

5.5. Results of feasibility study of Siemens turbine SGT-800 for POGT applications.

The SGT-800 gas turbine can be used for POGT application if the compressor is re-designed for a smaller air flow, the combustors are replaced by a volute expander inlet, the generator is

replaced by a larger generator that is attached to the exhaust end of the expander, connected by a new set of reduction gears.

At the beginning of the project, it was assumed that most of the modifications needed to convert a gas turbine into a POGT would focus on the expander. Further analysis, however, revealed the need for significant changes to components connected to the expander – the compressor, reduction gears, and generator. The resulting modifications are of the same magnitude as those required for a significant turbine upgrade.

6.0 POGT-Natural Gas firing System Study.

6.1. Partial Oxidation Gas Turbine Cycles for Power and Syngas/Hydrogen Production from Natural Gas.

6.1.1. Natural gas as a fuel.

Natural gas is, in many ways, an ideal fossil fuel. It is clean, easy to transport, and convenient for efficient and environmentally friendly utilization. Industrial customers use almost half of the gas produced in the US. A large portion is also used in residential area for heating, lighting, and cooking. According to DOE forecasts, planned number of new generators to be added in 2010 – 2013 is 450 of that 222 (49%) will use natural gas. Total nameplate capacity of added natural gas - fired generators is expected to be 34.1 GW (56% of total new generators to be added in 2010 – 2013's)[20]. Planned capacity additions in Electric Power Sector in 2009 – 2012 will be 33.79 GW of which 13.02 GW (38%) are assigned to combined cycle plants. Total capacity of combined cycle plants in Electric Power Sector is expected to increase from 196.2 GW (2009) to 200.8 GW (2012).[21] In view of this, the increasing efficiency of natural gas use can contribute significantly into global target of a more energy efficient world.

6.1.2. Modeling study of advanced natural gas – fired POGT cycles for power production.

Advanced Natural Gas – fired POGT concepts.

POGT technology allows converting natural gas chemical energy into both electricity and chemical energy of lower-grade fuel (syngas). Also, hydrogen could be produced by using hydrogen separation techniques. Some of these approaches have been described in IGCC-POGT section. Development of POGT-based systems for electric power production using natural gas – includes the following main concepts:

- Application of POGT in parallel with conventional gas turbine (recuperated) fueled either by natural gas or syngas produced in the POR. Fuel (syngas) from POGT exhaust is fired in HRSG to provide high temperature flue gases required to produce (i) high temperature superheated steam for bottoming steam turbine, and (ii) preheated combustion oxidant; ('Parallel' scheme).
- POGT is fueled by hydrogen which is extracted from a two-stage combustor in a conventional gas turbine. POGT is operated in parallel to a conventional gas turbine in

an advanced combined cycle similar to previous version; ('Parallel' scheme with hydrogen fueled POGT).

- Using of prospective high – pressure (≅1120 psig) POGT as a fuel source for regular combined cycle combustion turbine ('Series' scheme).
- Utilization of oxygen depleted air (O_2<21 %) in the POGT as well as in GT. In POGT, this will allow significantly reduced steam usage for temperature control and cooling, and in GT operation, this will be at low oxygen content to reduce emissions from GT exhaust.

Several advanced GT-POGT cycles have been developed and detailed ASPEN calculations have been performed. Cycles descriptions, schematics and full results of calculations are presented in the confidential part of the report.

Major results from ASPEN modeling are shown in Tables 26 – 30.

Table 26. Modeling results of POGT-GT in parallel with natural gas.

SGT-6000	NG input	lb/hr	83,552
		Btu/hr(HHV)	1,994,151,778
		Btu/hr(LHV)	1,797,122,416
		MW (LHV)	527
	Air input	lb/hr	4,529,718
	TIT	F	2415
	Pressure ratio	--	19.1
	GT flowrate	lb/hr	4,171,097
	Exhaust temperature	F	1,031
	Expander work	MW	492
	Compressor work	MW	249
	Net power	MW	243
SGT-400 POGT	NG input	lb/hr	20,890
		Btu/hr(HHV)	498,587,799
		Btu/hr(LHV)	449,325,533
		MW (LHV)	132
	Air input	lb/hr	178,118
	Total steam flow	lb/hr	54,181
	TIT	F	2278
	Pressure ratio	--	16.2
	POGT flowrate	lb/hr	233,738
	Exhaust temperature	F	1,036
	Expander work	MW	32
	Compressor work	MW	9
	Net power	MW	23
Total simple cycle electricity		MW	266
Total simple cycle thermal efficiency		--	40.3%
Bottom cycle	Total heat from topping cycle	MW	366
	Heat available for superheat (above 1000 F)	MW	51
	Maximum temperature available	F	1,717
	Assumed thermal efficiency	--	42%
	Electricity produced	MW	154
Total electricity produced		MW	419
Total combined cycle thermal efficiency (LHV)		--	63.7%

Table 27. Modeling results of POGT-GT in parallel with hydrogen.

POR-6000	NG input	lb/hr	110,491
		Btu/hr(HHV)	2,637,112,355
		Btu/hr(LHV)	2,376,556,178
		MW (LHV)	696.3
	Steam input	lb/hr	77,344
	Air input	lb/hr	643,021
SGT-6000	SG input	lb/hr	821,549
		Btu/hr(HHV)	1,671,395,008
		Btu/hr(LHV)	1,512,196,750
		MW (LHV)	443.1
	Air input	lb/hr	4,435,273
	TIT	F	2,415
	Pressure ratio	--	19.1
	GT flowrate	lb/hr	4,171,629
	Exhaust temperature	F	1,042
	Expander work	MW	495.1
	Compressor work	MW	244.0
	Net power	MW	251.1
SGT-400 POGT	Hydrogen input	lb/hr	9,306
		Btu/hr(HHV)	566,855,822
		Btu/hr(LHV)	479,610,151
		MW (LHV)	140.5
	Air input	lb/hr	62,358
	Steam input	lb/hr	19,386
	TIT	F	2,280
	Pressure ratio	--	16.2
	POGT flowrate	lb/hr	84,055
	Exhaust temperature	F	1,019
	Expander work	MW	20.5
	Air compressor work	MW	3.3
	Hydrogen compressor work	MW	4.6
	Net power	MW	12.6
Total simple cycle electricity		MW	263.7
Total simple cycle thermal efficiency		--	37.9%
Bottom cycle	Total heat from topping cycle	MW	390.9
	Heat available for superheat (above 1000 F)	MW	90.2
	Maximum temperature available	F	2,031
	Assumed thermal efficiency	--	42.0%
	Electricity produced	MW	164.2
Total electricity produced		MW	427.9
Total combined cycle thermal efficiency (LHV)		--	61.4%

Table 28. Modeling results of POGT-GT in parallel with natural gas. POGT is cooled by nitrogen.

SGT-6000	NG input	lb/hr	83,552
		Btu/hr(HHV)	1,994,151,778
		Btu/hr(LHV)	1,797,122,416
		MW (LHV)	526.6
	Air input	lb/hr	4,529,718
	TIT	F	2,415
	Pressure ratio	--	19.1
	GT flowrate	lb/hr	4,171,097
	Exhaust temperature	F	1,031
	Expander work	MW	492.0
	Compressor work	MW	249.2
	Net power	MW	242.8
SGT-400 POGT	NG input	lb/hr	20,890
		Btu/hr(HHV)	498,587,799
		Btu/hr(LHV)	449,325,533
		MW (LHV)	131.7
	Oxidant input	lb/hr	276,981
	Oxygen content	vol %	15%
	Total steam flow	lb/hr	10,445
	Cooling nitrogen flow	lb/hr	100,579
	TIT	F	2,278
	Pressure ratio	--	16.2
	Exhaust temperature	F	998
	POGT flowrate	lb/hr	353,939
	Expander work	MW	43.6
	Compressor work	MW	20.4
	Net power	MW	23.2
Total simple cycle electricity		MW	266.0
Total simple cycle thermal efficiency		--	40.4%
Bottom cycle	Total heat from topping cycle	MW	378.9
	Heat available for superheat (above 1000 F)	MW	39.2
	Maximum temperature available	F	1,583
	Assumed thermal efficiency	--	42%
	Electricity produced	MW	159.1
Total electricity produced		MW	425.2
Total combined cycle thermal efficiency (LHV)		--	64.6%

Table 29. Modeling results of POGT-GT in series with oxygen-deficient air as an oxidant – combined cycle.

HP POGT	NG input	lb/hr	112,529
		Btu/hr(HHV)	2,568,940,773
		Btu/hr(LHV)	2,319,253,011
		MW (LHV)	679.7
	O_2-deficient air input	lb/hr	963,047
	Oxygen concentration	vol %	15%
	Total steam/water flow	lb/hr	56,265
	TIT	F	1,900
	Pressure ratio	--	4.0
	POGT flowrate	lb/hr	1,131,841
	Exhaust temperature	F	1,296
	Expander work	MW	75.6
	Compressors+pump work	MW	36.5
	Net power	MW	39.1
SGT-6000	SG input	lb/hr	1,131,841
		Btu/hr(HHV)	2,031,353,993
		Btu/hr(LHV)	1,820,967,643
		MW (LHV)	533.7
	Air input	lb/hr	3,481,457
	TIT	F	2,415
	Pressure ratio	--	19.1
	GT flowrate	lb/hr	4,171,125
	Exhaust temperature	F	1,046
	Expander work	MW	501
	Compressor work	MW	245
	Net power	MW	256
Total simple cycle electricity		MW	295
Total simple cycle thermal efficiency		--	43.4%
Bottom cycle	Total heat from topping cycle	MW	356.5
	Maximum temperature available	F	1,046
	Assumed thermal efficiency	--	35.0%
	Electricity produced	MW	124.8
Total electricity produced		MW	419.7
Total combined cycle thermal efficiency (LHV)		--	61.8%

Table 30. Modeling results of POGT-GT in series with oxygen-deficient air as an oxidant – simple cycle.

HP POGT	NG input	lb/hr	103,678
		Btu/hr(HHV)	2,366,869,762
		Btu/hr(LHV)	2,136,822,258
		MW (LHV)	626.2
	O_2-deficient air input	lb/hr	876,633
	Oxygen concentration	vol %	15.0%
	Total steam/water flow	lb/hr	82,942
	TIT	F	1,900
	Pressure ratio	--	4.0
	POGT flowrate	lb/hr	1,063,253
	Exhaust temperature	F	1,300
	Expander work	MW	71.9
	Compressors+pump work	MW	28.8
	Net power	MW	43.1
SGT-6000	SG input	lb/hr	1,063,253
		Btu/hr(HHV)	1,889,077,324
		Btu/hr(LHV)	1,688,159,118
		MW (LHV)	494.8
	Air input	lb/hr	3,550,045
	TIT	F	2,415
	Pressure ratio	--	19.1
	Exhaust temperature	F	867
	GT flowrate	lb/hr	4,171,125
	Expander work	MW	501.8
	Compressor work	MW	244.0
	Net power	MW	257.7
Total simple cycle electricity		MW	300.8
Total simple cycle thermal efficiency		--	48.0%

Findings

- Advanced natural gas–fired POGT cycles based on existing and prospective gas turbines demonstrate significant efficiency increase of natural gas usage for electricity production.
- Siemens gas turbines SGT6–6000G (conventional mode) and SGT–400 (POGT mode) integrated in a GT–POGT unit can provide 61.4 – 63.7% LHV efficiency for fuel to electricity in combined cycle. Such a high efficiency arise from using of syngas from POGT exhaust as a fuel can provide the required temperature level for superheated steam generation in HRSG, and for combustion air preheating. Further efficiency increase, up to 64.6%, can be achieved by using nitrogen for cooling in POGT.
- The selected turbines (SGT6–6000G and SGT–400) can be used to make similar cycles fueled by syngas produced from natural gas in a separate POR. In this case, total cycle efficiency will be at least at the level 61.4%, but this cycle has a possibility to extract hydrogen from POR and supply the compressed hydrogen as required.
- If high–pressure gas turbine will become available; it can be combined with existing turbines to produce a unit with at least 61.8% LHV efficiency in a combined cycle and 48% in a simple cycle. Using of oxygen deficient air as an oxidant in the high – pressure

turbine running in POGT mode, can benefit significantly due to decreasing of in–cycle steam demand and provide additional increase in efficiency by 2-3 percentage points.

- Patent application #12/748,908 has been filed with the U.S. Patent and Trademark Office for Combined Fuel and Air Staged Power Generation System. Details can be requested from authors.

6.1.3. Advanced natural gas – fired POGT cycles for power and syngas/hydrogen production.

POGT concept can be used for co-production of electric power and syngas/hydrogen which then can be used in various chemical syntheses or as a fuel for electricity production in steam Rankine cycle. Hydrogen can be extracted both from POR (before expanding) and from POGT exhaust (after expanding) through hydrogen selective membranes. The latter way usually requires following pressurizing of the extracted hydrogen.

Modeling results are shown in Tables 31 – 36.

Table 31. Hydrogen/electricity co-production. Hydrogen membrane at the POR exhaust.

Chemical energy input	Btu/hr	1.45E+09	100%
Net electricity produced in POGT	Btu/hr	3.01E+08	21%
Hydrogen energy produced	Btu/hr	6.32E+08	44%
Total heat produced	Btu/hr	1.53E+08	11%
Hydrogen sensible heat	Btu/hr	2.48E+06	0.2%
FFB exhaust heat	Btu/hr	3.50E+08	24%
Heat losses	Btu/hr	2.18E+06	0.2%
Electricity production through bottoming steam cycle	Btu/hr	6.44E+07	4%
Total energy production	Btu/hr	9.97E+08	69%

Table 32. Hydrogen/electricity co-production. Hydrogen membrane at the POR exhaust, no bottoming cycle.

Chemical energy input	Btu/hr	1.25E+09	100%
Net electricity produced in POGT	Btu/hr	3.19E+08	25%
Hydrogen energy produced	Btu/hr	5.48E+08	44%
Total heat produced	Btu/hr	2.28E+06	0%
Hydrogen sensible heat	Btu/hr	2.15E+06	0.2%
FFB exhaust heat	Btu/hr	3.77E+08	30%
Heat losses	Btu/hr	1.86E+06	0.1%
Electricity production through bottoming steam cycle	Btu/hr	0.00E+00	0%
Total energy production	Btu/hr	8.69E+08	69%

Table 33. Hydrogen/electricity co-production. Hydrogen membrane at the POGT exhaust.

Chemical energy input	Btu/hr	1.14E+09	100%
Net electricity produced in POGT	Btu/hr	3.40E+08	30%
Hydrogen energy produced	Btu/hr	2.72E+08	24%
Total heat produced	Btu/hr	1.10E+08	10%
Hydrogen sensible heat	Btu/hr	1.07E+06	0.1%
FFB exhaust heat	Btu/hr	4.13E+08	36%
Heat losses	Btu/hr	2.43E+06	0.2%
Electricity production through bottoming steam cycle	Btu/hr	4.61E+07	4%
Total energy production	Btu/hr	6.59E+08	58%

Table 34. Hydrogen/electricity co-production. Hydrogen membrane at the POGT exhaust. No bottoming cycle.

Chemical energy input	Btu/hr	1.00E+09	100%
Net electricity produced in POGT	Btu/hr	3.56E+08	35%
Hydrogen energy produced	Btu/hr	2.03E+08	20%
Total heat produced	Btu/hr	4.39E+05	0%
Hydrogen sensible heat	Btu/hr	7.96E+05	0.1%
FFB exhaust heat	Btu/hr	4.36E+08	43%
Heat losses	Btu/hr	2.16E+06	0.2%
Electricity production through bottoming steam cycle	Btu/hr	0.00E+00	0%
Total energy production	Btu/hr	5.59E+08	56%

Table 35. Hydrogen/electricity co-production. Hydrogen membrane at the POR and POGT exhaust.

Chemical energy input	Btu/hr	1.45E+09	100%
Net electricity produced in POGT	Btu/hr	2.97E+08	21%
Hydrogen energy produced	Btu/hr	6.81E+08	47%
Total heat produced	Btu/hr	1.20E+08	8%
Hydrogen sensible heat	Btu/hr	2.67E+06	0.2%
FFB exhaust heat	Btu/hr	3.40E+08	23%
Heat losses	Btu/hr	2.17E+06	0.1%
Electricity production through bottoming steam cycle	Btu/hr	5.06E+07	3%
Total energy production	Btu/hr	1.03E+09	71%

Table 36. Hydrogen/electricity co-production. Hydrogen membrane at the POR and POGT exhaust. No bottoming cycle.

Chemical energy input	Btu/hr	1.30E+09	100%
Net electricity produced in POGT	Btu/hr	3.12E+08	24%
Hydrogen energy produced	Btu/hr	6.07E+08	47%
Total heat produced	Btu/hr	9.56E+06	1%
Hydrogen sensible heat	Btu/hr	2.38E+06	0.2%
FFB exhaust heat	Btu/hr	3.63E+08	28%
Heat losses	Btu/hr	1.69E+06	0.1%
Electricity production through bottoming steam cycle	Btu/hr	0.00E+00	0%
Total energy production	Btu/hr	9.23E+08	71%

Complete ASPEN Plus modeling results for cases listed are presented in the confidential part of the report.

Findings

- A conventional gas turbine (Siemens SGT–800) converted to POGT technology is capable to produce electricity and hydrogen from natural gas with thermal efficiency up to 71% of fuel LHV. A hydrogen selective membrane could be used for hydrogen separation from POR as well as from POGT exhaust.

- Modeling results of advanced POGT cycles for hydrogen/power production can be used for optimization of cycle performance with desired hydrogen and power production rates.

6.2. Advanced natural gas – fired POGT cycles for Co-production of Liquid Fuels, Chemicals and Electric Power.

Another prospective POGT application is for the co-production of specific syngas and electric power from natural gas, and subsequent conversion of the syngas to various liquid fuels (e.g., diesel, gasoline, ethanol or LPG) and/or chemicals (e.g., ammonia and methanol). Various types of oxidants and oxygen carriers can be used including oxygen-enriched air, near-pure oxygen, air, CO_2, and their mixtures. A few key chemical reactions for the production of syngas from natural gas are:

- $CH_4 + 0.5\ O_2 \rightarrow CO + 2H_2$
- $CH_4 + CO_2 \rightarrow 2CO + 2H_2$
- $CH_4 + H_2O \rightarrow CO + 3H_2$
- $CO + H_2O \rightarrow CO_2 + H_2$

These processes include the following major steps:

- Desulfurization of natural gas fuel. Although gas turbines (including POGT) can consume typical natural gas without sulfur removal, the further syngas processing requires very low sulfur content due to the use of catalysts.
- Partial oxidation of gaseous natural gas with oxidant and oxygen carrier mixture in a partial oxidation reactor (POR-1 in Figures 63 and 64) under sub-stoichiometric combustion conditions.
    - For typical operations, the exit temperature at the outlet of POR-1 would be maintained at 2,200-2,500 F. However, in the future, with improvements in metallurgy of the turbine blades in the expander section, this temperature could be increased accordingly.
    - The POR-1 design may involve two separate sections: (i) where the initial section can be filled with suitable catalysts to enhance reaction kinetics for conversions of the hydrocarbons to CO and H_2 via reactions with oxygen and (ii) final section can be non-catalytic.
    - Depending on the desired compositions of product liquid fuels and chemicals, the levels of various oxidants and oxygen carriers (O_2, air, steam, CO_2) would be controlled to achieve required levels of H_2/CO ratios and nitrogen in the effluent syngas.
- Expansion of the hot syngas from the POR-1 unit through a POGT to produce electric power and relatively cool syngas (typically, at 900-1,200 F).
    - Typically, for conventional gas turbines, the inlet pressure of hot gas at the inlet of the expander is about 200-300 psia with an outlet pressure of about 15 psia.

Depending on the stream pressure of available natural gas feed, the required pressure for the syngas feed to the downstream liquid fuels production unit (e.g., for Fischer Tropsch liquids), the required syngas feed pressure is about 350-450 psig. With the availability of high-pressure gas turbines, the expander can be operated with a higher inlet and outlet pressures to reduce the cost of the syngas compressor unit.

- Syngas Conditioning: according to the downstream process requirements, this step may include (i) gas cooling using conventional heat exchangers or a HRSG step, or a TCR for the production of extra syngas from a part of the feed natural gas for recycle to the POR-1 unit); the TCR step would also increase the overall system efficiency by converting a part of the heat energy into chemical energy, (ii) the use of a water-gas shift reactor to increase the ratio of H_2/CO ratio, (iii) removal of water vapor and CO_2 ,and (iv) syngas compression.
- A suitable syngas-to-liquids (e.g., Velocys FT diesel, or ExxonMobil MTG or Haldor-Topsoe TIGAS gasoline) or Chemical (e.g., ammonia, methanol) processing step.
- Finally, the tail fuel gases would be used for steam and power generation in a bottoming steam turbine cycle.

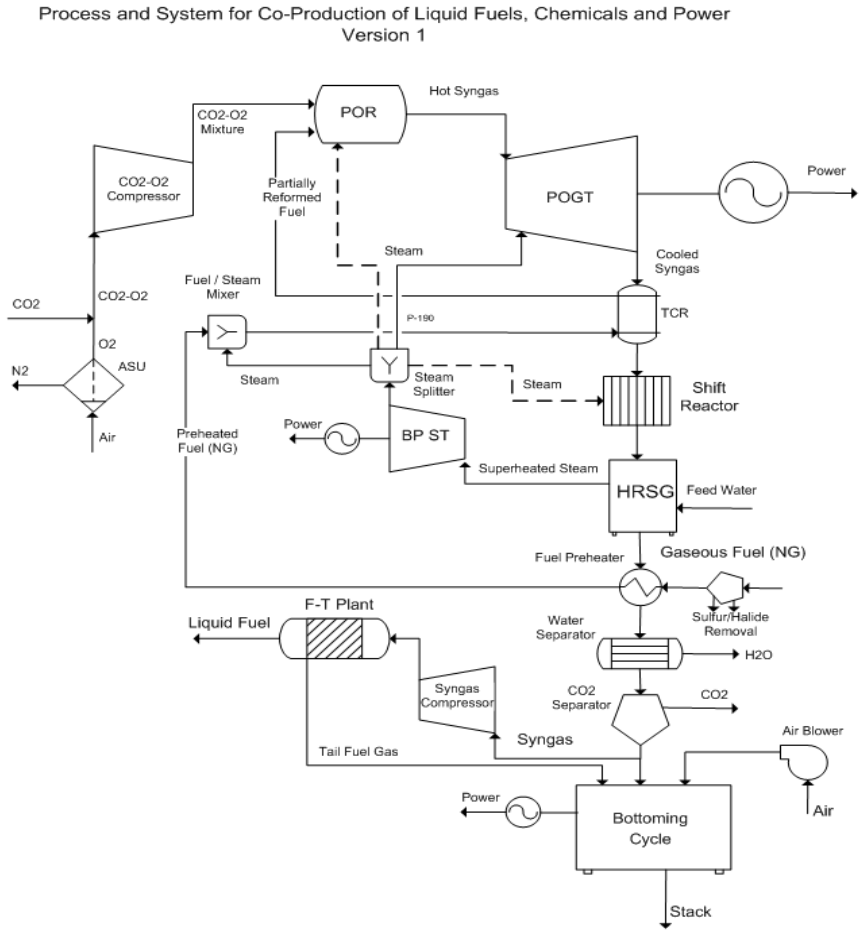

Figure 63. POGT-based Process for co-production of liquid fuels and electric power from natural gas.

A general concept schematic for the coproduction of liquid fuels (in this example: FT diesel as the primary product) is shown in Figure 63, here, a mixture of CO_2 and enriched air (e.g., from a, Vacuum Pressure Swing Adsorption (VPSA) unit) is used as the oxidant. In other applications, one can use near-pure oxygen from a cryogenic ASU. The FT Block would include other processing steps such as hydrocracking of wax made in the FT reactor.

In a FT process, some methane/ethane type hydrocarbons are produced in the FT reactor. Another POR (POR2) can be added to convert a large fraction of these hydrocarbons (with enriched oxygen and steam) to generate additional syngas that can be recycled to the FT reactor.

Specific details of such a POGT-based FT process and example calculations are shown in Table 37. For this design case, the H_2/CO molar ratio in the syngas from the expander is about 0.69 (typical of those achieved in coal gasification[22]). Thus, for this specific case (Design Case #2), a downstream Water-Gas Shift reactor is not required.

Table 37. Comparative Data: Co-production of FT-type liquid fuels and electric power.

Case	Case 1: Power Generation only	Case-2: Co-production of FT Liquids + Power Using the proposed POGT system	Case 3: Co-production of FT Liquids + Power Using Conventional Technology[23]
Gas Turbine Unit	Siemens SGT -400	Siemens SGT-400	--------
Natural gas flow rate, lb/hr	6,035	37,622	37,622
Air to Combustor/POR, lb/hr	307,310	None	Not Applicable (NA)
Enriched O_2 (@90% O2) flow to POR, lb/hr	None	63,818	NA
Extra CO_2 flow to POR, lb/hr	None	84,800	None
Total gas or Syngas at the Expander Inlet (P:241 psia and T: 2280 F), Million Cuft/hr	1.18	1.20	-----
Conc. of O_2 at Combustor or POR Inlet, mol%	20.7	47.4	NA
Syngas composition after the Expander, mol% H_2 CO CO_2 N_2	---------	 32.9 47.5 16.0 3.5	Not available in this specific Reference
H_2/CO molar ratio of syngas to the FT Complex		0.69	2.0
Pressure of syngas to the Fischer Tropsch Complex, psig		345	490
Net power produced, MW	13.0	18.8	17.0
Total liquids produced, bbl/day	----	2,060[23]	1,785

Similarly, Figure 65 provides specific details of a process schematic for a MTG-based (Methanol-to-Gasoline) type syngas-to-liquid production process where the H_2/CO ratio should be about 2.0. Table 38 shows typical examples of operating conditions for the POGT concept where the syngas (with a total H_2+CO mol% level at ~55.3%) from the expander would contain a H_2/CO

ratio of about 1.66; this can be increased to about 2.0 by using a shift reactor (as shown in this Figure 65). The syngas pressure to the MTG section would be about 800-1500 psig. There are other technologies (such as the Haldor-Topsoe TIGAS technology) for the production of gasoline from syngas where the H_2/CO ratio requirements could be less than 2.0.

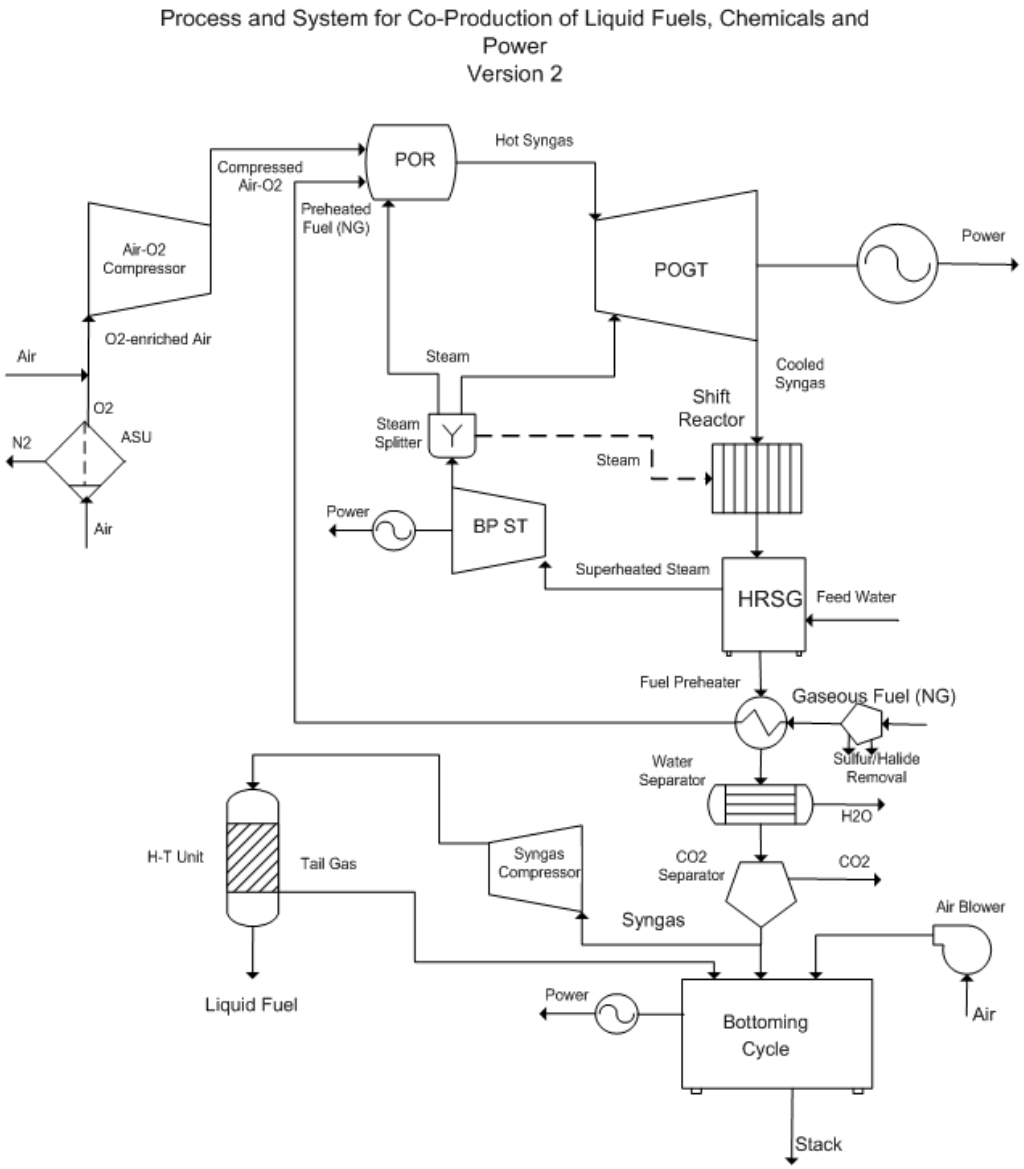

Figure 64. Specific Schematic for a POGT-based Process to Co-produce gasoline type liquid fuels (e.g., using the ExxonMobil MTG Technology) plus electric power from Natural gas (Example Calculations shown in Table 38).

Table 38. Comparative Data: Co-production of FT-type liquid fuels and electric power. Basis: Gas Turbine Siemens SGT-400.

Case	Case-2: Co-production of FT **diesel** Liquids + Power Using the proposed POGT system	Case 4: Co-production of MTG-based **gasoline** type Liquids + Power Using the proposed POGT system	Case 4: Co-production of **Ammonia** + Power Using the proposed POGT system
natural gas flow rate, lb/hr	37,622	31,883	38,878
Air to Combustor/POR, lb/hr	None	122,778	61,693
Enriched O_2 (@90% O2) flow to POR, lb/hr	63,818	22,992	44,601
Extra CO_2 flow to POR, lb/hr	84,800	none	none
Total gas or Syngas at the Expander Inlet (P:241 psia and T: 2280 F), Million Cuft/hr	1.20	1.29	1.24
Total syngas (on a CO_2 and water free basis; before the Shift Reactor) produced, lb/hr	146,083	160,436	129,207
Conc. of O_2 at Combustor or POR Inlet, mol%	47.4	30.9	48.3
Syngas composition after the Expander, mol%			
H_2	32.9	34.5	46.7
CO	47.5	20.8	27.2
CO_2	16.0	2.9	2.8
N_2	3.5	41.4	23.1
H_2/CO molar ratio of syngas to the liquid production Complex	**0.69**	**1.66**	**1.72**
Pressure of syngas to the liquid production Complex, psig	345	345	345
Net power produced, MW	18.8	16.4	17.7
H_2/CO molar ratio after the Water-Gas Shift Reactor	No Shift Reactor is used	2.0	3.0

Figure 66 provides a schematic for a system to co-produce a chemical like ammonia and electric power. The key chemical reaction is: $3H_2 + N_2 \rightarrow 2\,NH_3$. For this system, required syngas pressure is about 200 atm before the ammonia reactor.

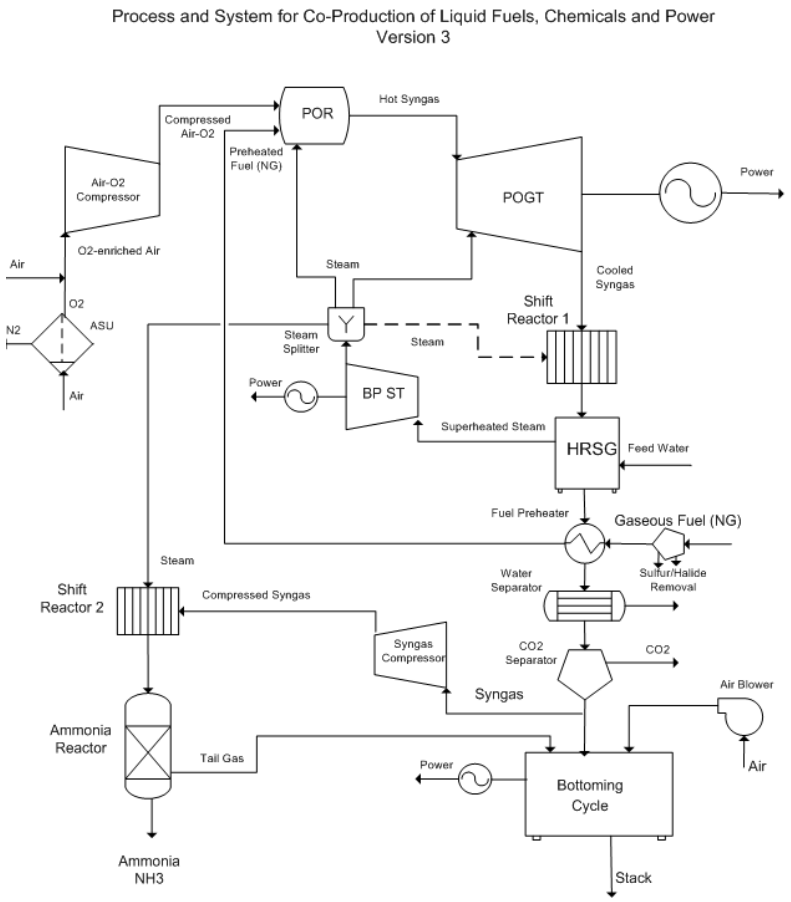

Figure 65. Schematic Diagram for the coproduction of ammonia and electric power.

6.3. Advantages of natural gas – fired POGT cycles for Co-production of Liquid Fuels, Chemicals and Electric Power.

The conventional syngas generation processes (e.g., a Steam Methane Reformer or SMR), is shown in Figure 67. The Autothermal Reformer or ATR is in Figure 68 and involve reactions of natural gas with oxygen + steam using a catalytic reactor or a non-catalytic POR with each process involving reactions of natural gas with oxygen + steam. The outlet temperature of the syngas is rather limited, typically, to about 1600-1700ºF at 20-40 atm pressure. Limitations include the (i) metallurgy for the equipment used in the syngas cooling step (e.g., for the use of a waste heat boiler for production of steam) and (ii) the catalyst used for reforming reactions.

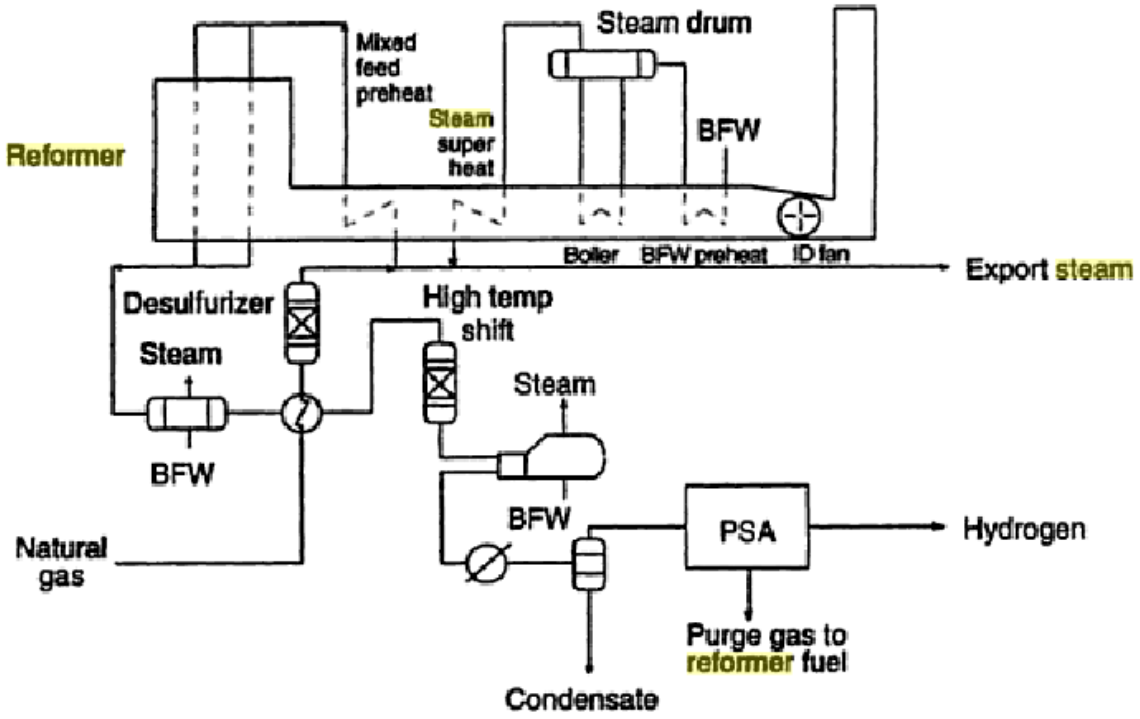

Figure 66. Schematic of a SMR Process for the Production of syngas (and hydrogen) from natural gas and Steam.

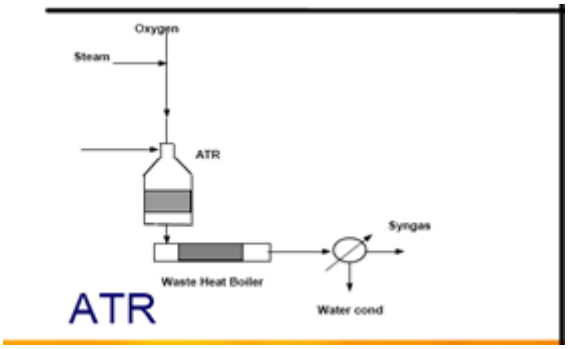

Figure 67. Schematic of an ATR (Autothermal) Process for the Production of syngas from natural gas and oxygen/steam.

For the POGT-based process, the syngas is cooled through near isoentropic expansion in the gas turbine expander and direct production of electric power. With continued improvements in expander designs, the inlet temperature can be significantly higher (currently at about 2,300-2,400ºF, for pressures of about 200-250 psig) than those achieved in SMR or ATR/PO_x designs. For higher pressure operations, e.g., at inlet pressure of 600 psig and effluent pressure of about 350 psig for a given gas turbine, the upper limit on the inlet gas temperatures has to be determined experimentally.

Another key advantage for the process is a concentrated CO_2 stream for sequestration is produced; this is similar to the ATR or PO_x designs. In case of a SMR, though, the endothermic heat of reaction for reforming reactions is supplied to tubes (filled with catalysts) indirectly in a

furnace type design (Figure 67). In this case, the CO_2 level in the flue gas is significantly low which makes CO_2 recovery rather difficult and expensive.

The key advantage of the process, for the co-production of Fischer-Tropsch type diesel fuels and electric power, are summarized in Table 37.

As shown, under the POGT operating conditions (Case 2) with this Siemens SGT-400 -POGT, the flow rate of natural gas can be increased from 6,035 lb/hr for the conventional power generation mode (Case 1) to about 37,622 lb/hr. The inlet temperature and gas flow rates at the GT expander are the same for both cases. For Case 1, the power generation is about 13.0 MW vs. 18.8 MW power plus 2,060 BSD of liquids in Case 2. In contrast, for a conventional technology (with an ATR type reformer), one can only produce about 17 MW of power plus 1785 BSD of FT liquids. Thus, the overall thermal efficiency for the POGT Case is significantly higher than Case-3.

For specific applications, for example for the utilization of Associated Natural Gas in a Floating Production Storage and Offloading scenario, the smaller foot print for the proposed POGT system (vs. a conventional SMR) and co-production of electric power (using the same gas turbine) may be quite advantageous.

In Table 38, specific data are shown to indicate that the POGT process can be tailored to produce syngas with a range of H_2/CO required ratios that may be needed for a specific syngas-to-liquids technology. For example, in the ExxonMobil MTG process, the syngas feed to a MTG unit should preferably have a H_2/CO ratio of about 2.0. As shown for the Design Case-4 (referring to Figure 65), the amounts of air and enriched-oxygen can be varied to modify the composition of the syngas produced and then use a Water-Gas Shift Reactor to produce a syngas with the desired H_2/CO ratio.

7.0 POGT MATERIAL STUDY.

Evaluation of the materials for hot sections of POGT has been performed by Oak Ridge National Laboratories (ORNL). In the beginning of the project, GTI and ORNL have held a technical meeting to discuss the material specifics for POGT application. ORNL has reviewed the previous and ongoing high temperature material studies and evaluated how the available results could be applied for the POGT study. It was decided to conduct an experimental study of material samples for POGT application. Siemens and GTI participated in a conference call with ORNL regarding turbine alloys and coatings designed to operate in the hot, reducing atmospheres of the POGT. Siemens agreed to identify candidate materials, prepare samples, and send them to ORNL for testing. Similarly, Solar and GTI have held a conference call with ORNL regarding the same subject, turbine alloys and coatings designed to operate in the hot, reducing atmospheres of the POGT. Solar has identified candidate materials and prepared a detailed report titled “Solar’s Hot Gas Component Materials” which was sent to ORNL and GTI. Team has agreed on the list of materials as well as their shape and design to be tested at ORNL, and Siemens and Solar have also sent the samples (two of each material) to ORNL for testing.

A test plan was prepared by GTI and ORNL, and agreed with Siemens and Solar. The test plan includes the following major items:

- All materials suggested by Siemens and Solar were included in the list of samples for testing; total of 25 materials were tested.
- Material coupons were prepared by Siemens and Solar and sent to ORNL for testing. Coupon size, shape, and dimensions were agreed.
- Testing was planned to be conducted at two different gas compositions: 1.POR exhaust from O_2-blown syngas and air firing at selected fuel-air ratio; and 2. POR exhaust at similar to substoichiometric combustion of natural gas at given fuel-air ratio.
- Temperature and pressure in the test unit were selected, and set at 1700ºF (927ºC) and 350 psia (~24 atm)
- Test duration for one gas composition: 1000 hrs
- Test data processing and analyses were conducted under the procedure used by ORNL for similar tests.

The first series of tests was run at gas composition selected to represent the turbine inlet composition of a fuel gas produced by the partial oxidation of natural gas firing with air as an oxidant. The reducing atmosphere was containing hydrogen, carbon monoxide, carbon dioxide, water vapor and nitrogen. A picture of the POGT material test unit is shown in Figure 69.

Figure 68. POGT material test unit at ORNL experimental facility.

The array of samples was exposed by suspending them on an alumina sample holders as shown in Figure 70.

Figure 69. Sample holders with samples that were being exposed at 1700 F and 350 psia in a gas that simulates the products of substoichiometric combustion of natural gas at given fuel-air ratio.

Samples provided by Siemens and Solar were cleaned and weighed before being installed in the test apparatus and then weighed again after completion of the 1000 hours testing. Following weighing, one sample of each material was selected for metallographic examination. These samples were mounted in epoxy to retain any surface layers or deposits, then polished and photographed to document the amount of surface material and subsurface reactions. As one example of the results, a micrograph of the cross-sectioned surface of a sample of IN738 is shown in

Figure 71, where it can be seen that a reaction product formed on the surface and subsurface attack also occurred.

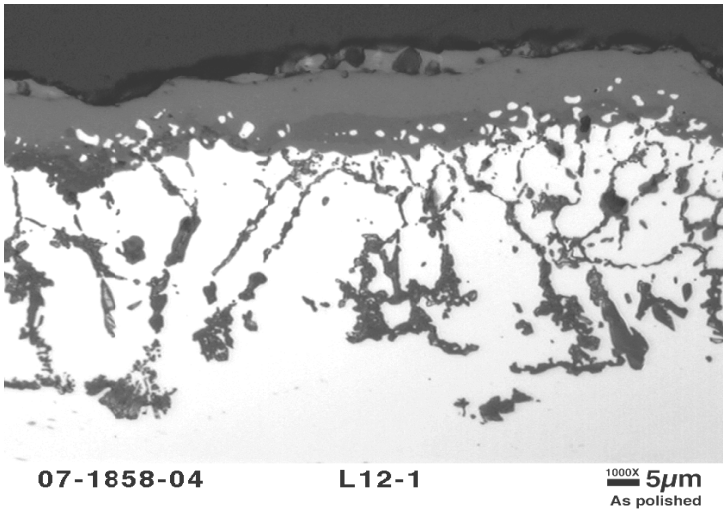

Figure 70, Cross section of IN738 sample after being exposed at 1700°F and 350 psia in a gas that simulates the product of partial oxidation of natural gas in air.

After completion of the 1000 hours exposure, the samples were cooled, removed from the test apparatus and then cleaned and weighed. It should be noted that most of the coated samples were only coated on one side of the coupon, so the weight change measurements for those samples are of questionable significance. In many cases, the coated samples showed a much greater weight gain than did the uncoated sample. This result was somehow expected taking into account that the composition of coating materials was selected for operation in an oxidizing atmosphere but not for the reducing atmosphere. Since spalling of an oxide layer and/or the coating is not addressed, as noted, these weight change comparisons have to be viewed cautiously, particularly until the results of the micro structural examinations can be considered.

For example, the uncoated Haynes 230 shows subsurface attack; the coated sample has some porosity and reaction of the significant surface area of the coating may account for the significant weight gain of this sample, more the three times compared to uncoated sample, see Figures 78 and 79 below.

One sample of every material exposed was mounted in epoxy, cut transversely, then ground and polished. Each mounted sample was examined metallographically to get a better indication of the extent of the reaction with the reducing environment. Micrographs of eight of the samples are shown in Figures 72-79. Except for the micrograph of the IN 738, the micrographs were taken at a magnification of 1000X; the IN 738 is at 200X. The APMT sample shows very little evidence of reaction with the environment which agrees with the weight change measurements. In contrast, the IN 738, IN617, and the IN 939 all show a thick surface reaction layer and subsurface attack. The other four micrographs compare the coated and uncoated surfaces of MAR-M-247 and Haynes 230. The uncoated M-247 shows more surface reaction product which is consistent with the weight change measurements. The uncoated Haynes 230 shows subsurface attack; the coated sample has some porosity and reaction of the significant surface area of the coating may account for the significant weight gain of this sample.

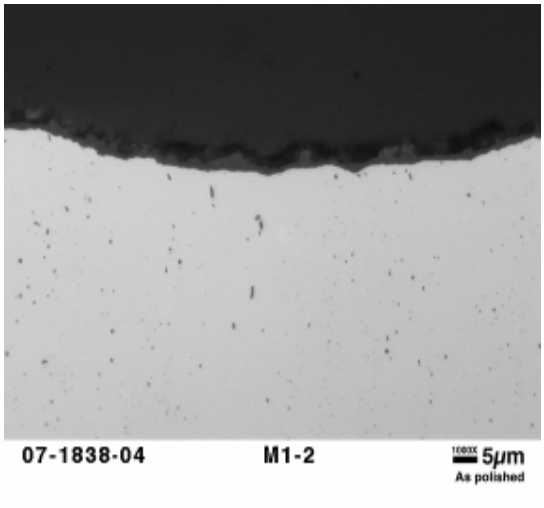

Figure 71. APMT

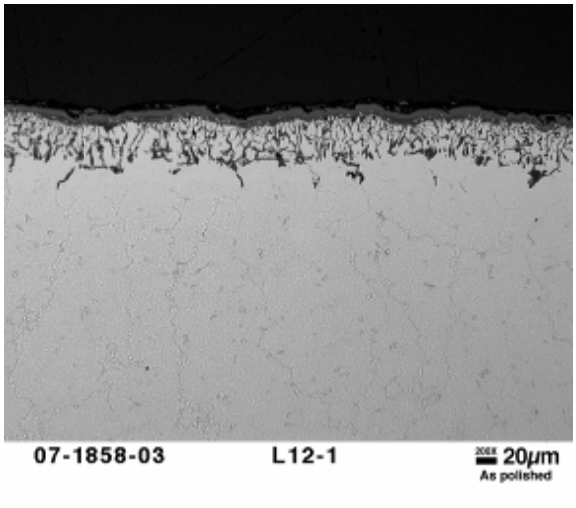

Figure 72. IN 738

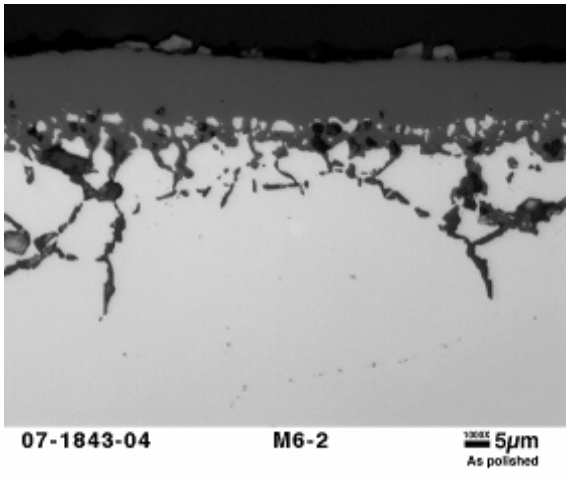

Figure 73. IN 617

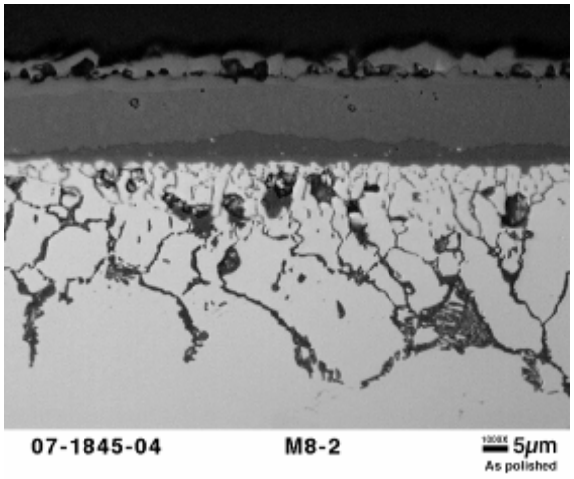

Figure 74. IN 939

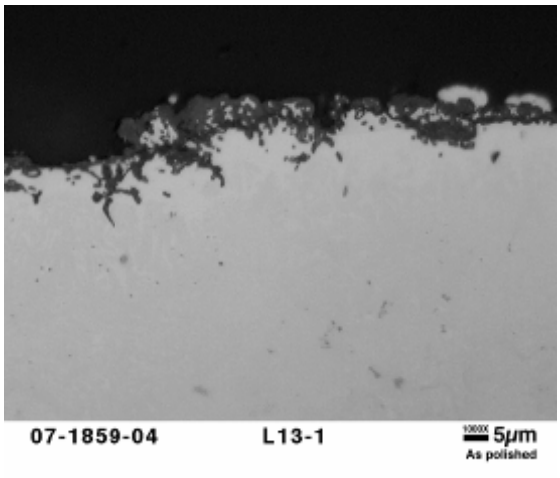

Figure 75. MAR-M-247

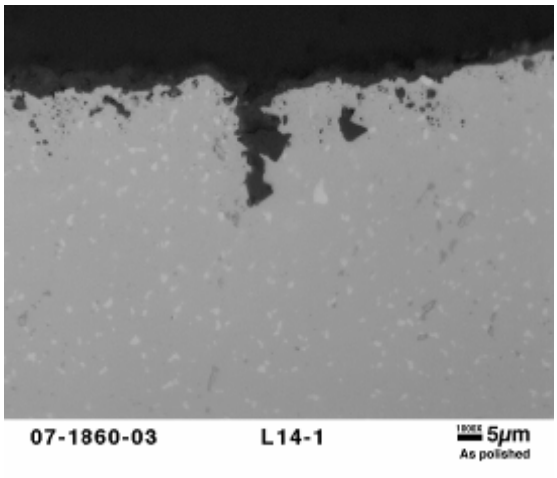

Figure 76. MAR-M-247 Coated

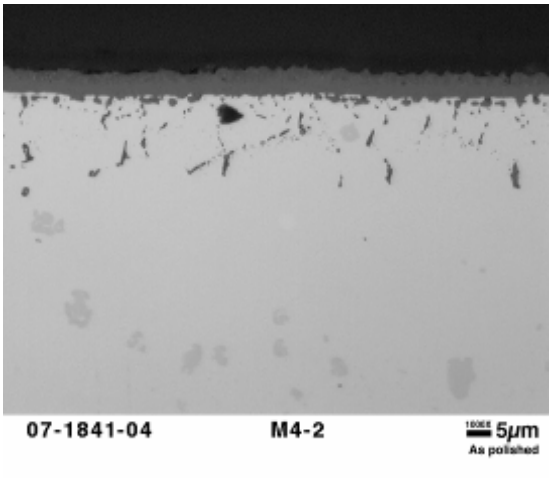

Figure 77. Haynes 230

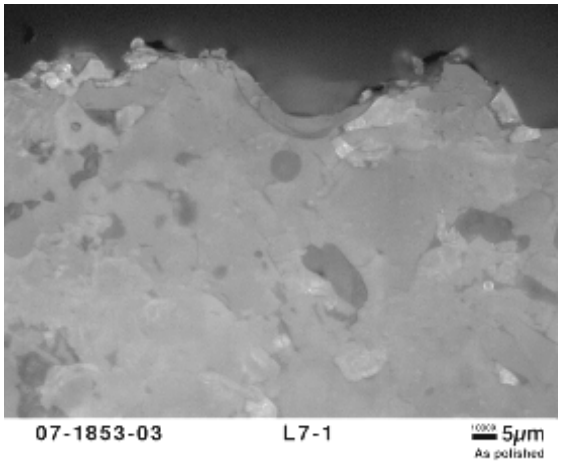

Figure 78. Haynes 230 Coated

Figures 72 - 79. Micrographs Showing the Cross Section of the Sample Surfaces Exposed 1000 hr in an Environment Simulating Partial Oxidation of Natural Gas

A second series of tests, also of 1000 hours, was planned for operation at similar temperature and pressure but with a gas containing the same components but with higher concentrations of hydrogen and carbon monoxide that result from the partial oxidation of syngas from an oxygen-blown gasifier. Samples for the second test are available from Siemens and Solar. The second series of testing was not performed due the lack of available funds.

A brief **s**ummary of the major results from testing of POGT hot sections materials operated in reducing atmosphere conducted at ORNL are presented below.

- Samples of 25 different base material/coating combinations were exposed to a simulated POGT reducing environment produced by the partial oxidation of natural gas with air. The samples were selected and supplied by Siemens and Solar;
- Most coatings did not provide an improvement on the corrosion resistance;
- The alumina forming alloys generally showed smaller weight gains than the majority of chromia forming alloys.

8.0 Combustion Instability Study in POGT.

Study of combustion instabilities in a POGT has been conducted by Georgia Tech.

Final report titled "Assessment of Combustion Instability of Partial Oxidation Gas Turbine Combustion Chambers" is attached. The work at Georgia Tech evaluated the response of rich, premixed combustion systems to acoustic oscillations.

There are two key mechanisms which must be considered in rich systems: these are the response of the flame to velocity oscillations (such as due to vortex shedding) and fuel/air ratio oscillations. The first section of this report describes a theory for predicting these response characteristics for rich, premixed flames, such as would be encountered in a POGT. The second section of the report describes the possible implications of these analyses on systems for

combustor designers. The entire report will be attached to the project final report. In this quarterly report, the major findings from the second section are presented.

The implications of the study of combustion instabilities in POGT are divided into two subsequent subsections, which consider the implications of each of the two mechanisms: velocity oscillations and fuel/air ratio oscillations.

8.1. Velocity Oscillations.

Georgia Tech analysis indicates the response of rich and lean premixed flames to velocity oscillations is comparable, indicating a similar proclivity of rich systems to instabilities than lean ones. This indicates that the knowledge base built up by original equipment manufacturers on the behavior of their lean, premixed systems directly carries over to the POGT. Assuming that the flame temperature and combustor geometry remains fixed (thereby fixing the natural acoustic frequencies), then t*he key parameter influencing the flame response is convective time from the point of formation of the vortex to the "center of mass" of the flame*. The effect on the convective time can be better understood from the following equation which expresses the convective time as the sum of the convective time in the premixer (τ_{pm}) and the convective time in the combustor (τ_{comb}):

$$\tau_{conv} = \tau_{pm} + \tau_{comb} \quad (1)$$

$$\tau_{conv} = [L_{pm} / u_{pm}] + [L_f / u_{comb}] \quad (2)$$

where L_{pm} refers to the distance from the point of origin of the disturbance to the entrance to the combustor, u_{pm} refers to the mean convective velocity in the premixer, L_f refers to the distance the perturbation travels from the combustor entrance to the "center of mass" of the flame, and u_{comb} refers to the mean convective velocity in the combustor.

The effect of variations in stoichiometry on the convective time is primarily exercised through its influence upon the location of the flame "center of mass." A rule of thumb for predicting the behavior of the POGT stability off of a known database of stability for the lean premixed system is the following: estimate the value of τ_{conv} for the POGT operating point. Then, determine what corresponding operating condition for the lean, premixed system gives an equivalent convective time.

Stoichiometry and fuel composition will exercise an important influence on this center of mass. For example, for rich flames, a higher equivalence ratio results in lower flame speeds and, presumably therefore, a longer flame. This increases the convective delay, shifting the instability to a higher velocity operating point. Similarly, altering the fuel composition at a fixed flame temperature also alters the flame position.

8.2. Fuel/Air Ratio Oscillations.

The flame response of rich systems is quite different than lean ones, indicating that the experience from lean, premixed systems *will not directly carry over* from DLN (Dry Low NO_x) systems to POGT systems. This is in contrast to the vortex shedding mechanism discussed above.

Combustion instabilities occur when the rate of energy release by the flame exceeds the damping processes. Two processes influence this rate of energy release: the gain of the flame response, and its phase with respect to the pressure. B*oth the gain and phase of a rich flame response differ substantially from DLN systems and so are discussed separately.*

Fundamentally, the fuel/air ratio oscillations lead to oscillations in the flame speed and heat of the reaction of the reactant mixture about their respective quiescent values. The slopes of the flame speed vs. equivalence ratio curve and the heat of reaction vs. equivalence ratio curve are referred to as the flame speed sensitivity and the heat of reaction sensitivity respectively.

As such, the heat release response of a premixed flame is caused due to three mechanisms – (i) Heat of reaction oscillations due to fuel/air ratio oscillations, (ii) Mass burning rate oscillations due to flame speed oscillations, and (iii) Flame surface area oscillations due to kinematic flame surface wrinkles arising from flame speed oscillations. These will be referred to as the heat of reaction contribution, flame speed contribution and area contribution respectively.

To characterize the flame response at different frequencies, it is instructive to define a non-dimensional frequency, called the Strouhal number, as $St = (2\pi f) L_f / U_o$, where f, L_f, U_o respectively denote the excitation frequency, length of the quiescent flame and the mean flow velocity. Further, a reduced Strouhal number, St_2, may be defined in terms of the flame angle θ, as $St_2 = St / \cos^2(\theta/2)$.

The qualitative differences between the response of lean flames and rich flames can be more easily understood from Figure 80 below, which is a plot of the variation of the gain and phase of the response of lean and rich flames at various mean equivalence ratios for a CH_4-air flame with reduced Strouhal number.

The disparities in variation of gain and phase are discussed separately and can be interpreted in terms of the three 'contributions' mentioned earlier.

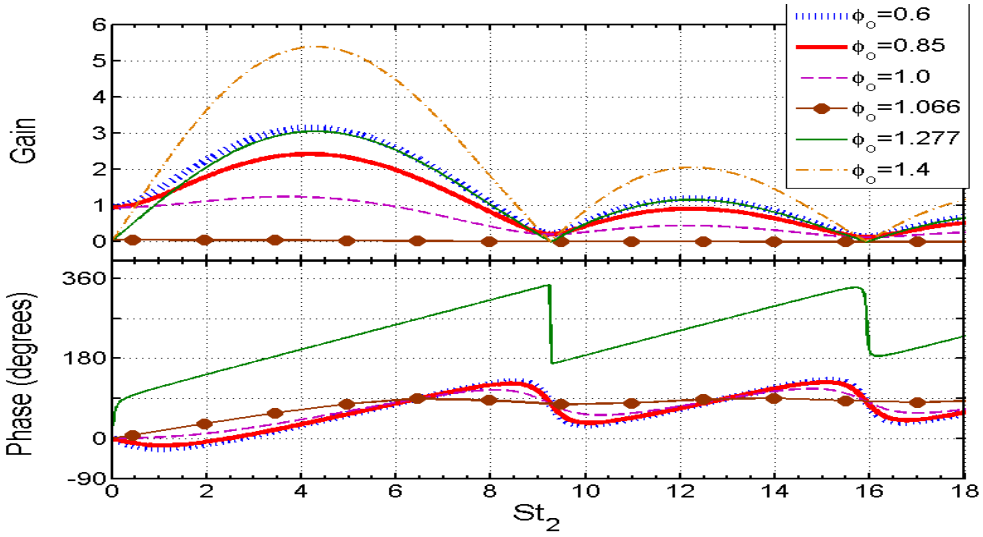

Figure 79. Variation of the heat release response with non-dimensional excitation frequency, for different values of equivalence ratio, for a CH_4-Air flame with β=4 for equivalence ratio excitation amplitude of 0.05.

8.3. Gain of Flame Response.

The gain of the flame response is equal to the amplitude of heat release fluctuations excited by a fuel/air ratio disturbance of a given magnitude. A high gain implies a flame that is very sensitive to such disturbances; a low gain is a system that does not respond appreciably to such fluctuations. From a stability point of view, the lower the gain, the less likely is the system to have instabilities. Moreover, the instability "islands" are smaller than a flame with a higher gain.

In the Figure 80, the upper graph overlays the gain of the flame response for a CH_4-air reactant mixture over a range of fuel/air ratios. By comparing the lean and the rich gains, two significant observations may be made. Firstly, in the limit of low Strouhal numbers, the gain for the lean response tends approximately to unity, while that for the rich response tends almost to zero. Secondly, for equivalence ratios such that the mean flame speeds are equal, the maximum gain of the rich response is greater than the maximum gain of the lean response.

The first observation may be explained that in the limit of low Strouhal numbers, the flame response is entirely controlled by the heat of reaction sensitivity in the quasi-steady case. For the case of a fuel-lean reactant mixture, the heat of reaction increases approximately linearly with equivalence ratio, while for a fuel-rich reactant mixture, the heat of reaction is nearly constant, i.e., it has a very small, but non-zero slope.

The gain for all the mean equivalence ratios then initially grows with increasing Strouhal number, because the burning area and the fluctuating flame speed contributions progressively come into phase with each other. As the mean equivalence ratio is increased from an initial lean value, e.g. ϕ=0.6, the flame speed and heat of reaction sensitivities progressively decrease and stay nearly constant, respectively, until ϕ~1.06 where the flame speed and heat of reaction sensitivities vanish. Hence the magnitude of the flame response drops from a finite value at ϕ=0.6 to a nearly zero response at ϕ~1.06. This is due to the occurrence of the flame speed

maximum at this equivalence ratio for a CH_4-air flame. The heat of reaction is a very weak function of equivalence ratio for ϕ_b>1.0. Hence,the magnitude now increases from a nearly zero value with increasing St_2 for rich mean equivalence ratios.

The second observation may be attributed for the same amount of change in equivalence ratio, about a mean value with the same quiescent flame speeds (as chosen here), the change in flame speed for the lean mixture is much lesser than the change in flame speed for the rich mixture. The flame speed is more sensitive to changes in equivalence ratio for a rich reactant mixture than for a lean.

The key takeaway point from this plot is the gain of POGT systems is much less than DLN systems at low Strouhal numbers. It is higher than the DLN systems at intermediate Strouhal numbers, and the two systems have comparable sensitivities at higher Strouhal numbers. This suggests that one should attempt to have flames with low Strouhal numbers. This implies short flames, with high flow velocities. Short flames implies high turbulence intensities and operating closer to stoichiometric, where the flame speed is higher. For example, in order to achieve a Strouhal number less than 0.5, where the gain response is low, see Figure 80. The Table 39 below summarizes the required flame length, assuming a flow velocity at the leading edge of the flame of 40 and 80 m/s. Results are shown for combustors with instability frequencies ranging from 80 to 400 Hz, which encompasses the range of frequencies encountered in Siemens heavy duty scale engines, to the smaller engines of Solar.

Table 39. Required flame length for various flow velocities and instability frequencies.

Instability Frequency	Velocity	Flame Length
80	40 m/s	4 cm
200	40 m/s	1.6 cm
400	40 m/s	0.8 cm
80	80 m/s	8 cm
200	80 m/s	3.2 cm
400	80 m/s	1.6 cm

This table shows that the required flame lengths range from 0.8 to 8 cm. Such flame lengths are likely much shorter than what can be achieved in an engine, particularly for the lower velocity case and 200 and 400 Hz cases. However, 8 cm may be somewhat practical, indicating that minimizing flame length may be a reasonable design goal for lower frequency instabilities, such as encountered in large, frame type engines. However, it also indicates that control of flame response gain is probably less useful as a means for dealing with instabilities at the higher frequencies. In these cases, one must target phase control, which is discussed next.

8.4. Phase of Flame Response.

In Figure 80, the lower graphs plot the phase (in degrees) of the response of a CH_4-air flame for various equivalence ratios, at different excitation frequencies.

Figure 80 shows the heat release response lags the excitation in the lean case and leads it in the rich case. This is from the linear flame speed sensitivity changes sign from the positive to the

negative when ϕ_b>1.07 for CH_4-air. This may be understood physically from the burning area response due to flame speed fluctuations that, in turn, are induced by equivalence ratio oscillations. The change in sign of the flame speed sensitivity implies that an instantaneous increase in equivalence ratio results in an increase and decrease in the instantaneous value of the flame speed on the lean and rich side, respectively. Therefore, given the same instantaneous equivalence ratio perturbation, the corresponding instantaneous burning area can decrease and increase for the lean and the rich case, respectively.

For values of lean and rich mean equivalence ratios, such that the mean flame speed is the same, for example, 0.85 (solid red line) and 1.28 (solid green line), the flame responses are nearly 180 degrees out of phase. Their relative phase disparity is not exactly 180 degrees and is attributed to the existence of the contribution of heat of reaction to the flame response, which, however small, is non-zero.

This indicates the phase response of a POGT system is nearly 180 degrees different than that of a DLN system, when they operate at fuel/air ratios that render the same mean flame speed. This is a very useful result as it basically implies that regions prone to fuel/air ratio driven instabilities in DLN systems will be stable in a POGT configuration. Conversely, it also implies that stable regions in DLN systems may be unstable in POGT configurations. This insight provides a very useful design criterion for fuel nozzle design of a POGT system. To illustrate, assume for now that the flame lengths and shapes are identical for the two systems, that the fuel nozzle can be identical. However, the optimized POGT and optimized DLN fuel peg axial locations must be spaced half of a convective wavelength, λ_c, apart, where λ_c=U/F. This ensures the flame response is 180 degrees different for the POGT system – as such, a good starting design is to take the optimized nozzle design from the DLN system and move the fuel pegs either forward or backward one convective wavelength, ΔX. In mathematical form:

Location of POGT fuel pegs relative to DLN system: $\Delta X = U_{nozzle}/2f_{instability}$

Table 40. Convective wavelength at various flow velocities and instability frequencies.

Instability Frequency	Velocity	ΔX
80	40 m/s	25 cm
200	40 m/s	10 cm
400	40 m/s	5 cm
80	80 m/s	50 cm
200	80 m/s	20 cm
400	80 m/s	10 cm

Note that these numbers are quite large and probably impractical for lower frequencies and higher nozzle velocities, but reasonable for the higher frequencies. In contrast to the gain control discussed above (which seemed a doable strategy for low frequencies), this suggests that phase control is the best option for the higher frequencies.

However, the values in the Table 40 above will be altered by the accompanying change in location in flame length and flame standoff distance for the POGT vs. DLN systems. However,

the corrected ΔX can be easily determined once one has a prediction for flame "center of mass" location. The key idea is to adjust the fuel peg/flame center of mass location for the POGT system such that comparable values are achieved for the convective time delay, as for the DLN system. In this way, knowledge gained from the DLN system of instability free regions can be translated over to the POGT system.

The main conclusion is "POGT systems are stable wherever DLN systems are unstable.

9.0 Market Study for POGT Applications.

In a 1997 paper[24] by R.A. Newby and others at Westinghouse, there is stated "Compared to conventional turbine power cycles, the Partial Oxidation (PO) power cycle shows potential for significant plant heat rate and cost of electricity improvements. However, significant development remains to verify and commercialize PO for combustion turbine power systems". They later state "The development requirements for the PO Power Plant to reach a state of commercial readiness are:

- Sub-scale experimental verification of the partial oxidation reactor (POR)performance,
- Detailed cycle optimization evaluations in parallel with PO reactor design optimization,
- Sub-scale combustor performance verification testing with the very low- heating- value fuel gas and low excess oxygen,
- Detailed cycle optimization and plant integration evaluations,
- Demonstration plant operations."

A 7 MW (thermal) pressurized, non-catalytic Partial Oxidation Reactor was built and tested at GTI laboratories and results have been used to calibrate models used for evaluations of various POGT cycles. A 20 MM Btu/hr boiler burner was designed and tested with low-heating value fuel gas and low excess oxygen. Detailed cycle simulations have been performed using Aspen for several potential poly-generation schemes involving POGT systems with coal or natural gas as the fuel input. These schemes include:

- IGCC Plant Scheme using POGT for Co-Production of Power and Hydrogen,
- Partial Oxidation Gas Turbine Cycles for Power and Syngas/Hydrogen Production from Natural Gas, and
- POGT cycles for Co-production of Liquid Fuels, Chemicals and Electric Power from Natural Gas.

In a paper presented in 2003 by R. M. Jones and N. Z. Schilling of GE Power Systems, they state that "Today's challenge for IGCC systems is to meet market requirements (which demand lower capital costs, improved operating reliability, and increased fuel flexibility) in combination with increasing efficiency and environmental performance standards". At the time the paper was presented, they go on to point out that "Current market drivers are favorable for refinery-based IGCC projects driven in part by high investment costs for environmental compliance". The paper included a Cost of Electricity (COE) breakeven curve for IGCC plants using various

opportunity fuels feed stock versus natural gas combined cycle (NGCC). This comparison is provided below in Figure 81 and shows that at natural gas prices of $2.50 per MMBtu higher than IGCC fuel prices, IGCC provided a cost of electricity equivalent to NGCC. When based upon COE, the Henry Hub natural gas spot price on 4/14/10 of $4.15 suggests that the economics for IGCC are more favorable than NGCC.

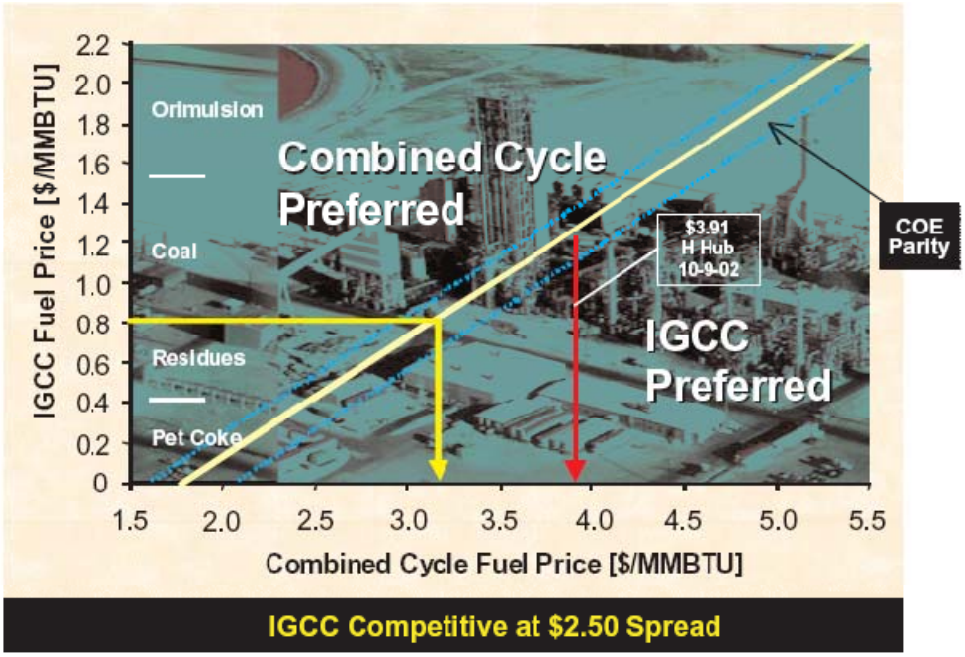

Figure 80. Breakeven fuel price comparison (Source GE Power Systems).

GE pointed out in its paper that it had to invest and make modifications to its turbines for the IGCC applications. Provided that the technical advantages of using a POGT rather than a conventional combustion turbine are supportable, then it becomes a question of whether there is sufficient market opportunity to warrant the required investment of multi-millions of development $. In general, the POGT should have a lower specific cost expressed as $ per kWe than conventional gas turbines because of the smaller compressor size required for a comparable power rating and the simpler combustion system. In addition to producing shaft power, the POGT system functions as a fuel reformer converting hydrocarbons (in the partial oxidation reactor) into syngas.

9.1. Developing POGT from Siemens Gas Turbines.

A portion of the project was devoted to developing a study of what modifications would be required to convert certain of the Siemens commercial gas turbines to POGT. The SGT 100, 400 and 800 models were selected for this assessment. The overarching goal in the technical approach for POGT development was to use as much of the existing commercial gas turbine design and hardware as possible.

The expander modifications were identified by Siemens and included re-design of the high pressure and low pressure flow fields (SGT 400 only), modifications to the inlet and exhaust,

design of air foils and blade cooling modifications. Once developed, the modified expander would need to be rig tested.

Modifications to the compressor and generator would also be required for conversion to POGT-duty. Figure 82 depicts conceptually what the required modifications would include.

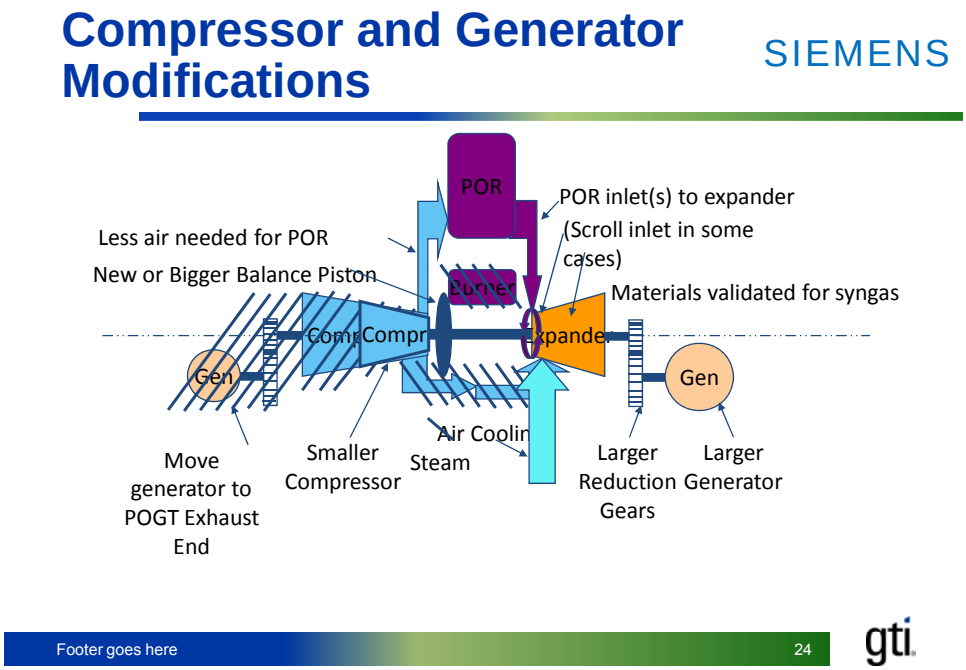

Figure 81. Conceptual depiction of required POGT modifications to compressor and generator.

To have some idea how much development time would be needed to convert the SGT 100, 400 and 800 to POGT, Siemens provided its estimates at the task levels and added items up for a cumulative value. These projections are included in Table 41 which suggests that it would take Siemens between 6 to7 years to develop and test a POGT before it would be ready for a commercial demonstration.

Table 41. Projected development time for POGT (Source: Siemens).

		POGT-100	POGT-400	POGT-800
Expander	Re-design HP & LP flow fields	-	7%	-
	Modify inlet and exhaust, Design airfoils, modify cooling	7%	7%	7%
	Blade vibration test, Rig test (Aero/Ht.Tr.), Film cooling rig test, Heat Transfer Test, High-Temp Rotating Rig Test	28%	37%	28%
Compressor	Use separate commercially available compressor	Purchase	Purchase	-
	Shorten blades and vanes, Blade vibration test	-	-	3%
	Design (scaled for rig test) Rig test	-	-	7%
Generator	Use larger model	Purch	Purch	Purch
Reduction Gears	Design new reduction gears	Purch	Purch	13%
Rotor & Bearings	Larger rotor, different bearings	10%	10%	10%
Tooling	Tooling Development	3%	3%	3%
	Tooling Manufacture	8%	8%	8%
Engine Testing	Engine initial test, Thermal paint test	21%	21%	21%
	Totals	**77%**	**92%**	**100%**
	Development Time (Years)	6	7	6

The POGT is projected to have a lower specific cost ($/kW) than the conventional combustion turbine. This is mostly because POGT specific power (power output per lb mass at expander exhaust) is up to twice compared to a conventional turbine. Therefore, the projected price of say a 10 MW conventional turbine should be about the same as the price of a POGT producing 15 - 18 MW power output.

9.2. Preliminary Market Assessment for Utilization of the Developing Partial Oxidation Gas Turbine for Oil Refinery Hydrogen and Power Applications.

According to GTI subcontractor SFA Pacific, "Hydrogen is the life blood of a modern oil refinery. Hydrogen requirements of the U.S. oil refineries are high and increasing. This is due to a combination of increasingly heavier higher sulfur crude oil supply, limited heavy fuel oil markets and cleaner specifications for gasoline and diesel. For example typical oil refineries in California require about 1,000 standard cubic feet (scf) of hydrogen per barrel of crude oil processed with only 30% of that required hydrogen from internal byproduct sources (mainly from naphtha reforming).The POGT is an innovative and unique process. It transforms a slightly modified natural gas-fired gas turbine into a compact and likely low cost, natural gas based syngas generator. The POGT also eliminates the expensive high temperature raw syngas cooling via turbo expansion syngas cooling to cogeneration shaft power electricity".

GTI subcontracted with SFA to provide the project with a preliminary market assessment report with the following scope of work: "Analyze the market potential for oil refinery hydrogen and

cogeneration power via the developing POGT process. This will include market overview of the growth in oil refinery hydrogen along with typical U.S. oil refinery net ("on-purpose") hydrogen and electricity requirements. This preliminary market analysis will also address potential market changes and enabling technologies what could enhance the POGT process market potential".

The deliverable from the study was provided in PowerPoint presentation and is included in the Appendix D. This format was selected to keep the project costs and time requirements within allowable budget.

9.2.1. Major Findings

Oil refineries that require additional hydrogen capacity would typically add a steam methane reformer (SMR) or consider purchasing hydrogen in an "over the fence" arrangement with one of the industrial gas suppliers. Some of the refineries are installing cogeneration systems that recover some of the exhaust gas from the SMR in a HRSG. An SMR with a topping cycle is illustrated in Figure 83.

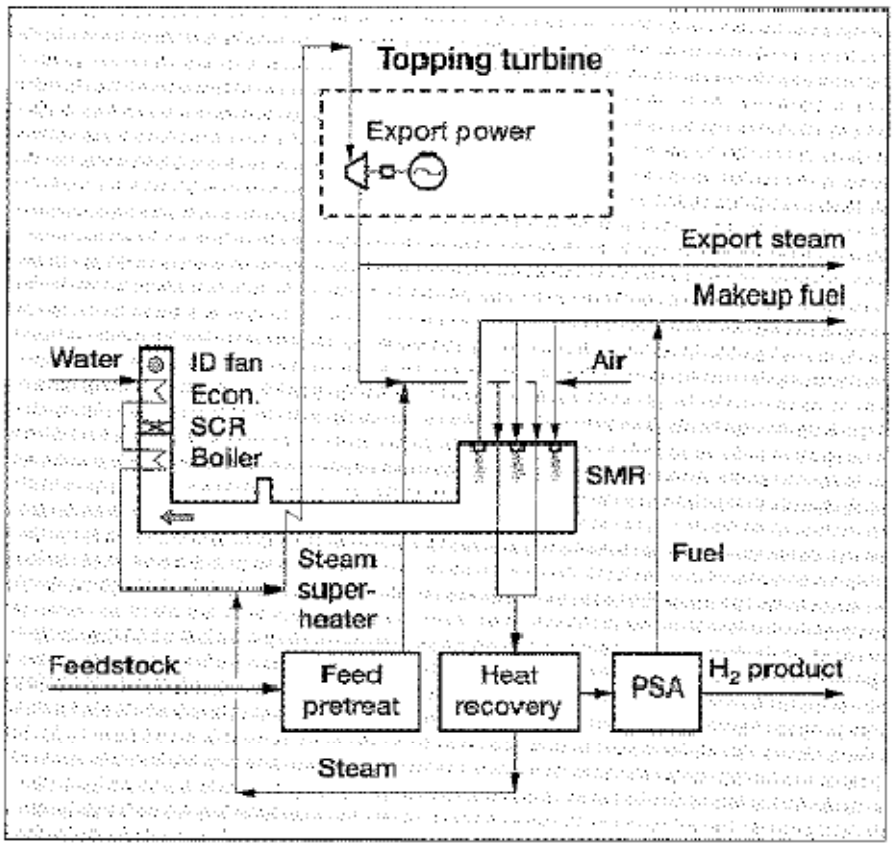

Figure 82. Process Flow Diagram of Hydrogen plant with a topping cycle. (Source: Hydrogen Processing- December 1999).

Using the POGT to supply both electricity and H2 from syngas instead of the SMR with topping cycle should provide some advantages including:

- Indirect heat transfer to the highly exothermic SMR reaction requires expensive reactor tubes & large heat transfer surface area while the POGT is direct reaction heating to even higher temperatures.
- SMR are relatively expensive (traditional unit cost as $ per scf/d H2 of $1-2 per scf/d at 100 MM scf/d scale) & much high unit capital costs and lower efficiency at small scale.

The potential "target" for POGT in the oil industry for hydrogen production was for requirements of between 10 and 100 MMSCFD. It was estimated that this demand could be covered by POGT systems based upon Siemens engines SGT-100, SGT-400, and SGT-800. These engines, when converted to POGT, would generate power output ranging from 9 to 80 MWe and be capable of supplying syngas covering the range of hydrogen supply.

The market study points out that using O_2 instead of air would greatly simplify the H_2 purification and pressure challenges facing the POGT-based system for poly-generation of electricity and hydrogen. However, using oxygen instead of air would reduce the mass flow of turbo-expander and result in a higher cost for the gas turbine per MW of electricity produced.

It was the opinion of SFA Pacific that even using oxygen with the POGT-based poly generation system, the technology would be very challenged trying to compete with the industry-standard SMR with PSA for high H_2 purity. Poly-generation of both hydrogen and electricity would have additional barriers when trying to compete with relatively low-priced electricity supplied by coal and nuclear power plants. The ultra-conservative nature of the refiners with regard to new technology would present an additional barrier for consideration of POGT-based systems.

It was pointed out that refinery H_2 is increasingly served by industrial gas companies via "over-the-fence" plants or pipelines. While there may be some technically feasible way to integrate the POGT concept with industrial gas company operations, it was pointed out that this would involve a major change from their current practices based upon SMR technology.

9.2.2. Co-production of Liquid Fuels, Chemicals and Electric Power from Natural Gas Using POGT

POGT technology could be a cost-effective means for the co-production of liquid fuels such as gasoline plus electric power from what the industry refers to as "stranded" or Associated Natural Gas at a Floating Production Storage and Offloading (FPSO)type offshore production facility for crude oil.

In this application, a POGT concept would likely include the use of enriched oxygen (at 90% oxygen purity). GTI has run its Aspen Plus simulation models to estimate the amount of Fischer Tropsch-type liquid fuels and electric power that could be generated using the Siemens SGT-400 (rated at 13-MW nominal net electric power output in the simple cycle power production mode only). Preliminary results are presented in Table 42 comparing poly-generation using POGT to simple cycle electricity production and conventional F-T co-production of liquid fuels and power. For the same natural gas feed, the POGT concept offers higher potential net power and total liquids. Table 43 provides estimates of the number of stranded gas fields for various sizes

and the projected number of SGT-400 machines that could be converted to POGT at an estimated market penetration rate of 20%.

Table 42. Poly-Generation of FT Liquids+ Electric Power.

	Case-1: Siemens SGT-400 Gas Turbine : Power Gen Mode Only	Case-2: Gas turbine Siemens SGT-400 in the POGT Mode: FT liquids + Power (i)	Case 3: Conventional FT Technology: FT Liquids + Power (Bechtel Data)[23]
Natural Gas Feed, lb/hr	6,035	37,622	37,622
Extra CO_2 lb/hr	None	84,800	None
Net Electric Power, MW	13.0	18.8	17.0
Total Liquids, Bbl/day	---	2,060	1,785

(i) Assume that syngas form the GT outlet is processed to remove water and CO_2 before compression to 360 psia; the estimates for liquid yields are based on DOE NETL Report 2007/1260, April 9, 2007. The flow rate to the expander is the same for Design Cases 1 and 2.

Table 43. Market Potential for POGT from Stranded Natural Gas Fields[25].

		Field Size: 0.5-1 TCF	0.25-0.5 TCF	0.1-0.25 TCF
# of Stranded NG fields		347	719	1043
Number of SGT-400 POGT machines, if 20% of these can be Monetized		356	370	250

9.2.3. Summary.

Several potential POGT configurations have been identified and examined in the report including:

- IGCC Plant Scheme using POGT for Co-Production of Power and Hydrogen,

- Partial Oxidation Gas Turbine Cycles for Power and Syngas/Hydrogen Production from Natural Gas, and
- POGT cycles for Co-production of Liquid Fuels, Chemicals and Electric Power from Natural Gas.

A very preliminary qualitative and quantitative assessment of the potential market opportunities and barriers for POGT-based poly generation systems has been provided. Based upon this preliminary study, a very promising POGT application appears to be stranded natural gas wells. The POR will be the only substantially new technology component in POGT systems and all other components are currently either in production today or could be based on that technology, albeit with different matching of compressors and turbines than currently is used. GTI believes that this is one of a major feature of POGT favoring its prompt commercialization once an integrated POGT system has been demonstrated with a participating manufacturer committed to product development and commercialization. It is believed that the first generation operating POR should be quite similar to a gas turbine combustor and this should result in a rapid, not expensive, low-risk development effort. All components can be made in existing facilities with currently commercial materials.

10.0 CONCLUSION.

POGT feasibility study was performed in two major directions: (i) feasibility design for conversion a conventional gas turbine to POGT duty; and (ii) system analyses of POGT-based units for production of power solely, and combined production of power and syngas/hydrogen for different applications. Below are the main findings from these studies.

- Three conventional turbines have been selected as candidate turbines for design study of retrofit conversion to POGT: SGT-800, SGT-400, and SGT-100 from Siemens with power output in the range from 5 to 100 MW. Also, POGT performance evaluation was performed for SGT6-6000G from Siemens with power output 350 MW in POGT mode;
- Retrofit design study was completed and detailed plans including schedule and budget have been developed for the SGT-800, SGT-400, and SGT-100: replacing the combustor with the POR, compressor downsizing for about 50% design flow rate, generator replacement with 60-90% power output increase, and overall unit integration, and extensive testing;
- POGT performances for three selected turbines have been calculated. The more detailed calculations were performed for the SGT-800. Comprehensive calculations of the SGT-400 and SGT-100 in POGT mode were also completed. In addition, GT and POGT performances were calculated for SGT6-6000G. With a POGT as the topping cycle for power generation systems, the power output from the POGT could be increased up to 90% compared to conventional engine keeping hot section temperatures, pressures, and volumetric flows practically identical. In POGT mode, the turbine specific power

(turbine net power per lb mass flow from expander exhaust) is twice the value of the conventional turbine;

- A 200 kW POGT unit has been designed, built, and successfully tested. The unit is consisted of a non-catalytic POR integrated with the retrofitted 200 kW gas turbine. The experimental studies were completed for the 200 kW POGT solely, and for a CHP unit consisting of the POGT and a boiler with modified burner. The results are positive and demonstrated expected POGT performances;
- An advanced POGT-based IGCC plant conceptual design has been developed and major components have been identified. Fuel-flexible fluid bed gasifier with moderate product gas temperature, ~1800 °F, (~980 °C) and novel POGT unit are the key components of the 100 MW IGCC plant for co-producing electricity, hydrogen and/or syngas;
- Gasifier performance has been calculated for bituminous coal in both air-blown and oxygen-blown versions. The oxygen-blown gasifier and a cryogenic ASU have been selected for the study. Two versions of gas cooling and cleaning systems have been considered, and the more advanced warm system has been selected;
- Performance calculations were conducted for several IGCC-POGT systems with different power/hydrogen or power/syngas ratios. Results for four versions are presented in the report;
- Several POGT-based, natural gas fueled systems for production of electricity only, co-production of electricity and hydrogen, and co-production of electricity and syngas for gas-to-liquid and chemical processes were developed and evaluated. Performance calculations for several versions of these systems were conducted and results are presented in the report;
- The gas turbines SGT6 – 6000G (conventional mode) and SGT – 400 (POGT mode) integrated in a GT – POGT unit can provide 61.4 – 64.6 % LHV efficiency for fuel to electricity in combined cycle. Such a high efficiency arise from using of syngas from POGT exhaust as a fuel that can provide required temperature level for superheated steam generation in HRSG, and combustion air preheating;
- SGT-800 (POGT mode) based systems for co-production of electricity and hydrogen have been detailed evaluated and total efficiency of 71% was achieved;
- Preliminary market assessment was performed, and recommendations for POGT systems applications in oil industry were defined;
- ORNL has completed one series testing for POGT hot section materials in a reducing atmosphere. Total of 25 samples from Siemens and Solar have been tested. Processing and analyses of the test data have been performed and reported;
- Study of combustion instabilities in POR has been completed by Georgia Tech, and final report has been submitted. The main conclusion is “POGT systems are stable wherever DLN systems are unstable”.

11.0 References.

[1] Tampa Electric Integrated Gasification Combined-Cycle Project. An Update. TOPICAL REPORT NUMBER 19. JULY 2000. http://www.netl.doe.gov/technologies/coalpower/cctc/topicalreports/pdfs/topical19.pdf

[2] The Wabash River Coal Gasification Repowering Project. An Update. TOPICAL REPORT NUMBER 20. SEPTEMBER 2000. http://www.netl.doe.gov/technologies/coalpower/cctc/topicalreports/pdfs/topical20.pdf

[3] J.K. Rabovitser, M. J. Khinkis, R. L. Bannister, and F. Q. Miao, "Evaluation of Thermochemical Recuperation and Partial Oxidation Concepts for Natural Gas-Fired Advanced Turbine Systems," presented at International Gas Turbine and Aeroengine Congress & Exhibition, Birmingham UK, June 1996.

[4] S.A. Christianovich, V. M. Maslennikov, and V. L. Sterenberg, "Steam-Gas Power Stations with Multi-Stage Residual Oil Combustion," Applied Energy, Great Britain, 2 (1995):175-187.

[5] J. Ribesse, "Gas Turbine with Catalytic Reactor for the Partial Oxidation of Natural Gas and Its Application in Power Stations," Gas Wärme International,July-August, 1971.

[6] J.J. Ribesse, "Isothermal Gas Turbine Using Catalytic Partial Oxidation," International Patent WO 91/05946, May 2, 1991.

[7] J.J. Ribesse, "The Isotherm Partial Oxidation Gas Turbine," Eur. J. Mech. Eng. 36 no. 1 (1991): 27-32.

[8] V.M. Maslennikov and V. J. Sterenberg, "Steam-Gas Units for the Modifi cation of Existing Steam Power Plants," IVTAN, Moscow, 1992.

[9] R.C. Hodrien and G.W. Fairbairn, "Power Into the 21st Century," Gas Engineering & Management (March, 1994).

[10] B. Kalitventzeff, M. N. Dumont, and F. Marechal, "Process Integration Techniques in the Development of New Energy Technologies: Application to the Isothermal Gas Turbine," Univ. Liege, Belgium; M.A. Korobitsyn, P.W. Kers, and G.G. Hirs, "Analysis of a Gas Turbine Cycle with Partial Oxidation," American Society of Mechanical Engineers (Paper), 98-GT-33 (1998): 7;G. Heyen and B. Kalitventzeff, "A Comparison of Advanced Thermal Cycles Suitable for Upgrading Existing Power Plants," Applied Thermal Engineering 19 (1998): 227-237; F. Desmaré and G. Heyen, "High-Temperature Heat and Power Generation using a partial Oxidation Gas Turbine : Application to an annealing Furnace," IcheaP-5 Symposium, Florence, May 20-23, 2001; M. Korobitsyn, "Enhancing Direct-Fired Power Plants Performance by Use of Gas Turbine Technology," Journal of Propulsion and Power 16 no. 4 (2000): 568-571; B. Kalitventzeff, M.N. Dumont, and F. Maréchal, "Process Integration Techniques in the Development of New Energy Technologies : Application to the Isothermal Gas Turbine, proceedings of Chisa 1998, August 24-28, Prague; B. Albrecht, "Reactor Modeling and Process Analysis for Partial Oxidation of Natural Gas," (PhD diss. University of Twente, Oct. 14, 2004).

[11] Newby et. al, "An Evaluation of a Partial Oxidation Concept for Combustion Turbine Power Systems," ASME paper 97- AA-24, 1997

[12] G.Q. Lu, J.C. Diniz da Costa, M. Duke, S. Giessler, R. Socolow, R.H. Williams, T. Kreutz. J. Coll. Int. Sci. 314 (2007) 589–603

[13] R.W. Spillman, Chem. Eng. Prog. 85 (1989) 41

[14] M. Oertel, J. Schmitz, W. Weirich, D. Jendryssek-Neumann, R. Schulten, Chem. Eng. Technol. 10 (1987) 248.

[15] J. Shu, B.P.A. Grandjean, S. Kaliaguine, Appl. Catal. A 119 (1994) 305–325.

[16] W.J. Koros, Y.H. Ma, T. Shimidzu, J. Membr. Sci. 120 (1996) 149–159.

[17] R.G. Gardner, R.A. Crane, J.F. Hannan, Chem. Eng. Prog. 73 (1977) 76.

[18] M. Bracht, P.T. Alderliesten, R. Kloster, R. Pruschek, G. Haupt, E. Xue, J.R.H. Ross, M.K. Koukou, N. Papayannakos, Energy Convers. Manage. 38 (1997) S159–S164

[19] Schora F. C., Palat P., Patel J. G. Proceedings: Conference on Coal Gasisfication Systems and Synthetic Fuels for Power Generation. Vol. I, p. 16-1. Electric Power Research Institute, 1985.

[20] Electric Power Annual 2008. Released: January 21, 2010.

[21] Energy Information Administration / Annual Energy Outlook 2010.

[22] DOE NETL Report 2007/1260, April 9, 2007

[23] G. N. Choi et al (Bechtel Corp) & N. L. Carr et al (Syncrude Technology Inc)

[24] Newby, R.A., Yang, W.C. and Bannister, R.L., "An Evaluation of a Partial Oxidation Concept (i.e., the POGT) for Combustion Turbine Power Systems", Presented at ASME ASIA '97 Congress and Exhibition, Singapore, September 30-Oct.2 , 1997

[25] Gasification Plant Cost and Performance Optimization. Final report to DOE NETL under contract DE-AC26-99FT40342. 2003

APPENDICES.

TABLE OF CONTENT.

Appendix A - POGT Stream Properties

Table A- 1. Conceptual Stream Properties.

Stream Number		1	2	3	4	5
Component		Compr	Compr	POR	POR	POR
Location		Inlet	Exit	Inlet	Inlet	Exit
Fluid		Moist Air	Air	Oxy-Syngas	Steam	Oxy-PORgas
Phase		Gas Mix	Gas Mix	Gas Mix	Vapor	Gas Mix
Mass Flow	kg/s	50.7	50.7	39.4	5.1	95.2
Pressure	Bar	1.0	19.4	19.6	19.0	19.0
Temperature	C	15.0	467.8	315.6	315.6	1,317.8
Mass Flow	lb/hr	402,272	402,272	313,023	40,227	755,522
Mass Flow	lb/s	111.7	111.7	87.0	11.2	209.9
Pressure	psia	14.7	280.7	284.9	275.1	275.1
Temperature	F	59.0	874.1	600.0	600.0	2,404.1
Mol %						
Ar	%(mol)	0.94%	0.94%	0.00%	0.00%	0.42%
CH4	%(mol)	0.00%	0.00%	12.46%	0.00%	0.00%
C2H6	%(mol)	0.00%	0.00%	0.00%	0.00%	0.00%
C3H8	%(mol)	0.00%	0.00%	0.00%	0.00%	0.00%
C4H10	%(mol)	0.00%	0.00%	0.00%	0.00%	0.00%
CO	%(mol)	0.00%	0.00%	41.40%	0.00%	19.74%
CO2	%(mol)	0.03%	0.03%	13.53%	0.00%	10.98%
H2	%(mol)	0.00%	0.00%	20.72%	0.00%	12.52%
H2O	%(mol)	0.99%	0.99%	10.17%	100.00%	20.61%
H2S	%(mol)	0.00%	0.00%	0.00%	0.00%	0.00%
HCN	%(mol)	0.00%	0.00%	0.00%	0.00%	0.00%
N2	%(mol)	77.26%	77.26%	1.72%	0.00%	35.74%
NH3	%(mol)	0.00%	0.00%	0.00%	0.00%	0.00%
O2	%(mol)	20.78%	20.78%	0.00%	0.00%	0.00%
SO2	%(mol)	0.00%	0.00%	0.00%	0.00%	0.00%
Mol %	%(mol)	100.00%	100.00%	100.00%	100.00%	100.01%

Table A- 1. Conceptual Stream Properties. (Concluded)

Component		6 POGT	7 POGT	8 POGT	9 POGT
Location		Cooling#1	Cooling#2	Cooling#3	Exhaust
Fluid		Steam	Steam	Steam	Syngas
Phase		Vapor	Vapor	Vapor	Gas Mix
Mass Flow	kg/s	4.7	3.1	2.5	105.5
Pressure	Bar	19.0	19.0	19.0	1.0
Temperature	C	315.6	315.6	315.6	561.3
Mass Flow	lb/hr	37,600	24,700	19,499	837,321
Mass Flow	lb/s	10.4	6.9	5.4	232.6
Pressure	psia	275.1	275.1	275.1	14.6
Temperature	F	600.0	600.0	600.0	1,042.4
Mol %					
Ar	%(mol)	0.00%	0.00%	0.00%	0.37%
CH4	%(mol)	0.00%	0.00%	0.00%	0.00%
C2H6	%(mol)	0.00%	0.00%	0.00%	0.00%
C3H8	%(mol)	0.00%	0.00%	0.00%	0.00%
C4H10	%(mol)	0.00%	0.00%	0.00%	0.00%
CO	%(mol)	0.00%	0.00%	0.00%	17.20%
CO2	%(mol)	0.00%	0.00%	0.00%	9.57%
H2	%(mol)	0.00%	0.00%	0.00%	10.91%
H2O	%(mol)	100.00%	100.00%	100.00%	30.80%
H2S	%(mol)	0.00%	0.00%	0.00%	0.00%
HCN	%(mol)	0.00%	0.00%	0.00%	0.00%
N2	%(mol)	0.00%	0.00%	0.00%	31.15%
NH3	%(mol)	0.00%	0.00%	0.00%	0.00%
O2	%(mol)	0.00%	0.00%	0.00%	0.00%
SO2	%(mol)	0.00%	0.00%	0.00%	0.00%
Mol %	%(mol)	100.00%	100.00%	100.00%	100.00%

Appendix B - Commercial Air Compressors

Centrifugal air compressors with exit pressures less than 1,000 psig are listed in Table A- 2. Compressors with flow capacities similar to that of the POGT compressor are listed in ***bold italics*** in the table and plotted in Figure A- 1. Data were extracted from the *2006 GTW Handbook*.

Table A- 2. Commercial Air Compressors.

Make	Model	Inlet Air Flow, lb/s	Exit Pressure, psig
Cooper Compression	TA-2000	2	145
Sundyne Compressors	Blowers	2	51
Cooper Compression	TA-3000	5	145
Cooper Compression	TA-6000	10	145
Cooper Compression	TA-11000	14	247
AG Kuhnle Kopp & Kausch	VRZ	15	170
Cooper Compression	MSG-4	18	754
Cooper Compression	TA-20000	27	508
AG Kuhnle Kopp & Kausch	RG	33	580
Cooper Compression	MSG-8	38	725
Cooper Compression	MSG-12	59	725
MAN Turbo AG	***CP/SKUEL***	***76***	***725***
AG Kuhnle Kopp & Kausch	***KX/KXP***	***90***	***870***
Siemens	***STC-GC***	***90***	***580***
GE Energy AC Compressor	***V***	***95***	***696***
GE Energy AC Compressor	***VS***	***95***	***696***
	POGT	***112***	***266***
Cooper Compression	***MSG-25***	***114***	***135***
MAN Turbo AG	***TURBAIR***	***126***	***0***
AG Kuhnle Kopp & Kausch	***GX/GXP***	***148***	***870***
AG Kuhnle Kopp & Kausch	***SFOG***	***222***	***36***
Hitachi	MCH	260	653
Hitachi	2MCH	260	653
GE Oil & Gas Nuovo Pignone	MCL	261	725
AG Kuhnle Kopp & Kausch	RK	267	580
Mitsubishi	Integrally Geared	314	725
GE Energy AC Compressor	D Overhung	317	145
GE Oil & Gas Nuovo Pignone	DMCL	373	725
AG Kuhnle Kopp & Kausch	SFO	412	36
GE Oil & Gas Nuovo Pignone	ANR	448	363
Siemens	STC-GT	448	290
Siemens	STC-GVT	448	290
MAN Turbo AG	RIK, RIKT, RIO	493	290
Mitsubishi	H Type	538	870
MAN Turbo AG	ARI	744	261
MAN Turbo AG	AG, AR	986	276
MAN Turbo AG	AK, AKF	986	276
Siemens	STC-SR	1,031	218
Siemens	STC-SX	1,031	116
MAN Turbo AG	A, AV	1,141	363

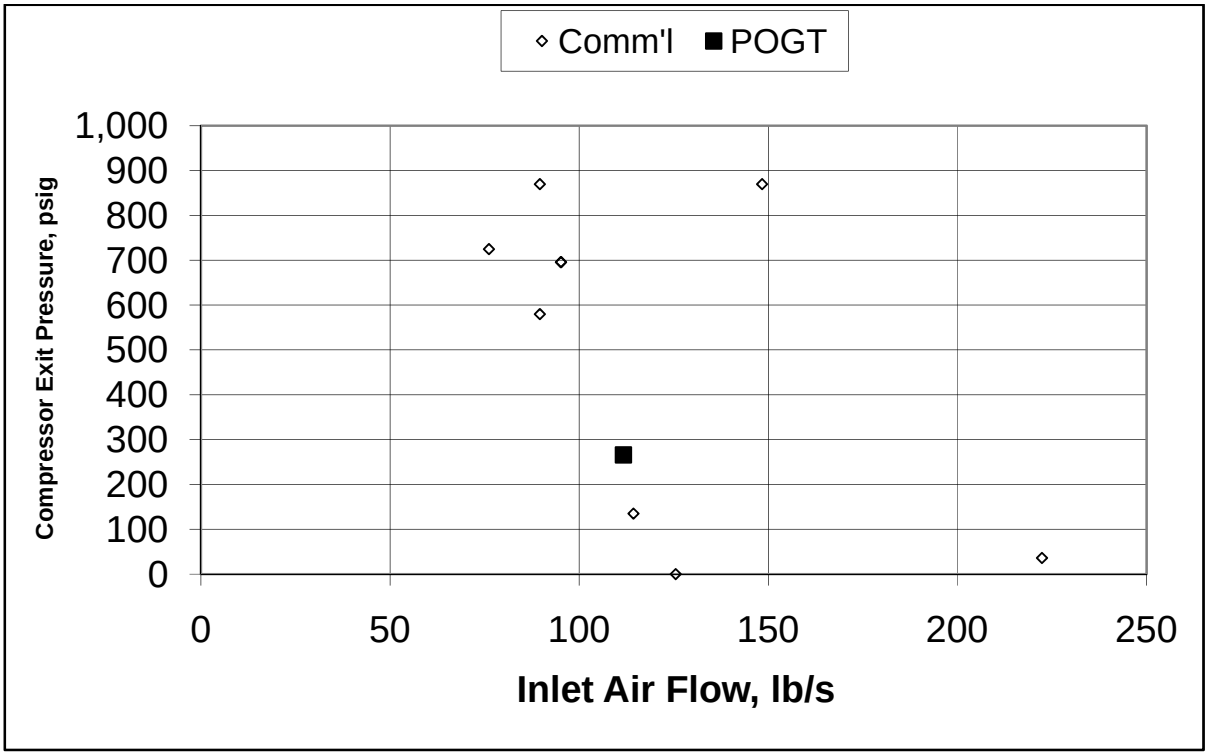

Figure A- 1. Commercial Air Compressors.

Appendix C – Assessment of Combustion Instability of Partial Oxidation Gas Turbine Combustion Chambers

Report by Georgia Institute of Technology.

Assessment of Combustion Instability of Partial Oxidation Gas Turbine Combustion Chambers

FINAL REPORT

Tim Lieuwen, Shreekrishna, Santosh Hemchandra
Georgia Institute of Technology

I. Abstract

This program evaluated the response of rich, premixed combustion systems to acoustic oscillations. There are two key mechanisms which must be considered in rich systems: these are the response of the flame to velocity oscillations (such as due to vortex shedding) and fuel/air ratio oscillations. The first section of this report describes a theory for predicting these response characteristics for rich, premixed flames, such as would be encountered in a POGT. The second section of this report fleshes out the implications of these analyses on systems for designers.

II. Analysis of Premixed Flame Response to Equivalence Ratio Perturbations

Nomenclature

G	=	*Level-set function*
ξ	=	*Axial co-ordinate flame surface*
L_f, R	=	*Length of flame and burner radius respectively*
β	=	*Flame aspect ratio* $= L_f / R$.
α	=	*Constant* $= \beta^2 / \left(1+\beta^2\right)$
ω	=	*Excitation frequency in* rad s^{-1}.
St	=	*Strouhal number* $= \omega L_f / U_o$
St_2	=	*Reduced Strouhal number* $= St\left(\beta^2+1\right)/\beta^2$
s_L	=	*Laminar flame speed*
h_R	=	*Heat of reaction*
ϕ	=	*Instantaneous equivalence ratio*
ϕ_o	=	*Mean equivalence ratio*
$\phi_{s_L \max}$	=	*Equivalence ratio value at which* s_L *is a maximum.*
ε	=	*Excitation amplitude* $= \phi'/\phi_o$.
F	=	*Transfer function.*

Introduction

THIS report describes the response of laminar premixed flames to perturbations in reactant mixture equivalence ratio. This work is motivated by combustion instability, which causes significant problems in the operations of premixed combustion systems. Unsteady heat release processes in a combustor can result in a two-way coupling with one or more of its acoustic modes, potentially causing high amplitude pressure and velocity oscillations. These oscillations can result in poor system performance and hardware damage.

Modeling these phenomena in order to develop rational design techniques for combustors requires an understanding of the various mechanisms that cause heat release oscillations in lean premixed combustors. Significant among these are flame burning area fluctuations driven by acoustic velocity oscillations[1,2], large scale convected coherent structures[3,4], flame extinction and re-ignition, flame-wall interactions[5] and reactant mixture composition, i.e. equivalence ratio fluctuations[6-10]. Equivalence ratio fluctuations driven by pressure and velocity fluctuations in lean premixed combustors have been shown to be a significant cause of combustion instability. Several studies have shown strong evidence for the significance of this mechanism to cause heat release oscillations either by direct measurement of equivalence ratio oscillations during instabilities[11,12] or by comparing the dependence of instability characteristics on geometry and operating conditions with correlations developed from theoretical analyses[7,8].

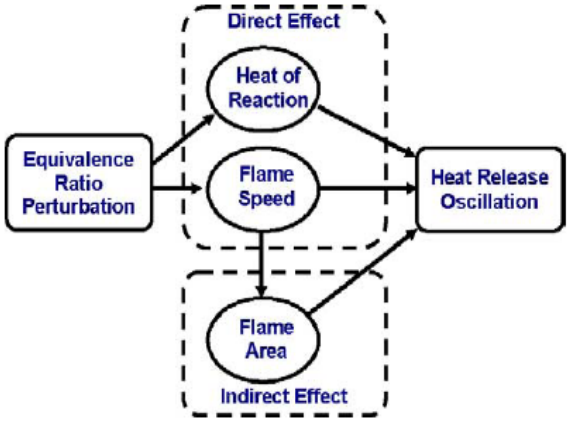

Figure 1: Fundamental processes controlling the heat release response of premixed flames to equivalence ratio oscillations. (Ref: Cho and Lieuwen[20]).

Much insight into the phase response of the flame to such perturbations can be obtained from a simple time delay analysis that treats the flame as a concentrated source of heat release[13]. In general, however, flames are distributed axially over a length scale where the mixture equivalence ratio can significantly vary. The flame Strouhal number, St ($=\omega L_f/U_o$), which equals the length of the flame to the length scale of the imposed excitation determines whether the flame can be regarded as being a compact ($St << 1$) or distributed source ($St \sim O(1)$). Models that take this fact into account with varying degrees of fidelity have been put forth by, e.g., Putnam[14], Lieuwen et al.[8], Krebs et al[15], Hubbard and Dowling[16], Dowling and Hubbard[17], Prashant et al.[18], Stow and Dowling[19] and Cho and Lieuwen[20].

Following the latter study[20], it is known that the basic phenomenology of the flame response is controlled by a superposition of three processes, shown schematically in Figure 1. Equivalence ratio perturbations cause fluctuations in local flame speed and heat of reaction along the flame surface. This directly causes the heat release rate to oscillate. Flame speed variations also cause the flame surface to wrinkle and change shape. This leads to an oscillation in the net burning area of the flame, also causing the net heat release rate to oscillate. This is an indirect effect.

This work generalizes the above analyses by considering two effects. First, although the analysis in Refs. 8,14-20 are valid for any stoichiometry, results and discussion were only presented for lean flames. We also consider rich flames in this study because of the interest in operating premixed systems in partial oxidation mode that can, for example, be used for co-production of synthesis gas[21]. The flame response dynamics here are quite different from that of lean flames for two reasons that can be inferred from Figure 2, which plots the typical ϕ dependence of the flame speed and heat of reaction.. First, the sensitivity of the flame speed to fuel/air ratio fluctuations of lean and rich flames is inverted; i.e., an increase in fuel/air ratio causes a flame speed increase and decrease on the lean and rich side, respectively. Second, the heat release per unit mass of reactant varies with fuel/air ratio on the lean side, but is nearly constant on the rich side. As such, there is no influence of the heat of reaction (h_R) term on the rich flame response – this term plays an important role in the lean flame response, particularly under low Strouhal number conditions.

Because these s_L and h_R transition regions do not occur at the same ϕ value, the flame response has qualitatively different characteristics in three stoichiometry regions, illustrated schematically in the figure. Region I is the lean regime which has been explicitly considered in the prior studies, Region II, associated with the same s_L sensitivity as a lean flame, but no h_R sensitivity, and Region III, associated with the opposite s_L sensitivity but no h_R sensitivity. Depending upon the specific flame chemistry and reactant composition, the size of Region II in ϕ space can vary; e.g., for fuels like methane, the nature of both flame speed and heat of reaction change at $\phi \sim 1.0$ leading

to a very narrow Region II width of ϕ~0.07. On the other hand, the flame speed for 80%H_2/ 20%CO- air synthesis gas mixture peaks at values close to $\phi \sim 1.8$. This leads to a much larger Region II width of ~0.8.

The second focus of this study that is the consideration of finite amplitude effects; i.e., the modification of the linear results as nonlinear effects become significant. This has been addressed by performing a third order perturbation analysis to understand the factors that influence the initial onset of nonlinearity, and complementary computations of the fully non-linear G-equation, so as to capture the flame front dynamics and heat release saturation at high excitation amplitudes. This nonlinear analysis is needed because prediction of instability amplitudes requires consideration of non-linear processes that control the response of the flame to equivalence ratio perturbations at large amplitudes of excitation[19] - a linear analysis is not applicable in this regime.

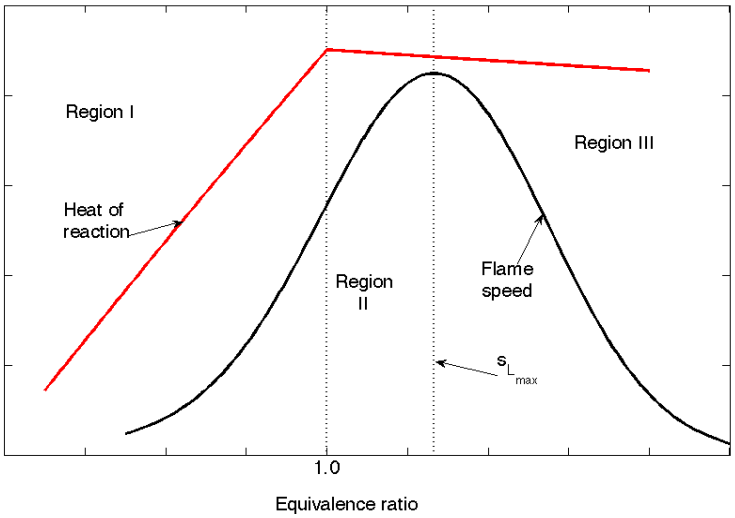

Figure 2: Qualitative plot showing dependence of flame speed, s_L, and heat of reaction, h_R, dependence on fuel/air ratio, ϕ.

The remainder of this report is presented as follows. The analytical development of higher order corrections to the transfer function and details of the numerical method are presented in section titled "Formulation and Analysis". Details of the numerical method are provided in this section. The section titled "Results and conclusions" presents and discusses the results and conclusions of this study. The final section titled 'conclusions' concludes the report with a summary of the results and comments on issues that must be addressed in future work.

Formulation and Analysis

The analytical framework adopted to model the flame response closely follows that of Preetham and Lieuwen[22]. The flame is assumed to consist of a thin sheet whose surface can be represented implicitly by the zero contour of a two dimensional function $G(r,z)$. The evolution of this contour can then be tracked using the G-equation[23].

$$\frac{\partial G}{\partial t} + \vec{U}.\nabla G = s_L \left|\nabla G\right| \tag{1}$$

where, $\vec{U}$ is the local flow velocity. This equation can be solved numerically to capture complex flame front motions, such as cusp and pocket formation, or multi-valued flame fronts. This will be discussed later in the section on the numerical approach to follow.

For the analytical development, the axial location of the flame is given by a function $\xi(r,t)$. Thus, we may express G in an explicit form as $G = z - \xi(r,t)$. Using this in Eq. (1), we obtain the following flame front tracking equation.

$$\frac{\partial \xi}{\partial t} + s_L \sqrt{1 + \left(\frac{\partial \xi}{\partial r}\right)^2} = U_o \tag{2}$$

where the radial mean velocity component has been neglected in comparison with the axial component. Introducing the non-dimensionalization scheme - $r^* = r/R$, $z^* = z/L_f$ and $t^* = tU_o/L_f$ with R being chosen to be an appropriate flameholder length scale- in the above yields,

$$\frac{\partial \xi}{\partial t} + \frac{s_{L_o}}{U_o} f(\phi) \sqrt{1 + \beta^2 \left({}^{\partial \xi}\!/_{\partial r} \right)^2} = 1 \tag{3}$$

where the asterisks have been dropped for the sake of convenience of notation. The subscript '*o*' denotes the value of the respective quantity evaluated at the mean equivalence ratio, ϕ_o, or the mean value as in the case of flow velocity. The function $f(\phi) = s_L(\phi) / s_{L_o}$, is the ratio of the instantaneous burning velocity magnitude to the value at the mean equivalence ratio. The flame aspect ratio, $\beta \left(= L_f / R \right)$ is given by the following relation

$$\frac{U_o}{s_{L_o}} = \sqrt{1 + \beta^2} \tag{4}$$

Finally, Eq. (3) may be written as,

$$\frac{\partial \xi}{\partial t} + f(\phi) \sqrt{\frac{1 + \beta^2 \left({}^{\partial \xi}\!/_{\partial r} \right)^2}{1 + \beta^2}} = 1 \tag{5}$$

In addition, the following boundary condition for ξ is utilized, which states that the flame remains attached at the burner lip.

$$\xi(t)\big|_{flame-holder} = 0 \tag{6}$$

The upstream equivalence ratio perturbations are assumed to harmonically oscillate in time and are advected by the mean flow. Thus, the following form can be assumed for the spatio-temporal variation of equivalence ratio.

$$\phi = \phi_o \left[1 + \varepsilon \cos\left\{ St\left(z - t \right) \right\} \right] \tag{7}$$

where ε is the perturbation amplitude at the center the tube exit plane normalized by the mean equivalence ratio. The effects of diffusion due to spatial equivalence ratio inhomogeneities are neglected. The Strouhal number in the RHS of the above is given by $St = \omega L_f / U_o$.

In comparing the finite amplitude response of lean and rich flames, it is important to note the influence of the above definition of perturbation amplitude. The definition of fuel/air ratio is intrinsically non-symmetric, i.e., the lean side ranges from 0 to 1 while the rich ranges from 1 to infinity. The opposite behavior occurs for the inverse of ϕ, λ=1/ϕ. Thus, for a given ϕ, a perturbation of ε results in a significantly larger absolute perturbation in ϕ on the rich side than on the lean. As such, response graphs plotted in the next section show the rich flames exhibiting nonlinear behavior at lower ε values than lean flames – this is due to the definition of ε used here. The opposite behavior would be observed if ε were used to measure perturbation amplitude in terms of air/fuel ratio, λ.

The instantaneous heat release of the flame is given by,

$$q(t) = \int_{flame} \rho s_L h_R \, dA \tag{8}$$

We assume here that the fuel/air ratio perturbation occurs at constant density. Then, Eq. (8) can be rewritten in terms of burning velocity magnitude and heat of reaction perturbations as,

$$\frac{q(t)}{q_o} = \frac{A(t)}{A_o} + \int_{flame} \frac{s_L'}{s_{L_o}} \frac{dA}{A_o} + \int_{flame} \frac{h_R'}{h_{R_o}} \frac{dA}{A_o} + \int_{flame} \frac{s_L' h_R'}{s_{L_o} h_{R_o}} \frac{dA}{A_o} \tag{9}$$

The first term on the RHS denotes the contribution to heat release fluctuation due to oscillations in the net burning area of the flame. The second term combines the contributions due to burning velocity fluctuations. The third and fourth terms represent the nonlinear contributions due to heat of reaction oscillations and nonlinear coupling between flame speed and heat of reaction respectively. These terms can be evaluated in terms of the flame surface geometry, e.g., the first term may be evaluated as[22],

$$\frac{A(t)}{A_o} = 2\int_0^1 r\sqrt{\frac{1+\beta^2\left(\frac{\partial\xi}{\partial r}\right)^2}{1+\beta^2}}\,dr \tag{10}$$

The heat-release transfer function of the flame due to equivalence ratio fluctuations is defined as

$$F = \frac{\bar{q}'(\omega)/q_o}{\hat{\phi}'/\phi_o} \tag{11}$$

where the numerator and denominator are the heat release and equivalence ratio perturbations, evaluated at the excitation frequency.

In the quasi-steady case, the flame speed and heat of reaction term are functions of fuel/air ratio, fuel type, and operating condition. In the general unsteady case, however, these quantities, particularly the flame speed, introduce additional dynamics related to the flame structure so that the instantaneous flame speed is also a function of frequency (Lauvergne and Egolfopoulos[24], Sankaran and Im[25]).

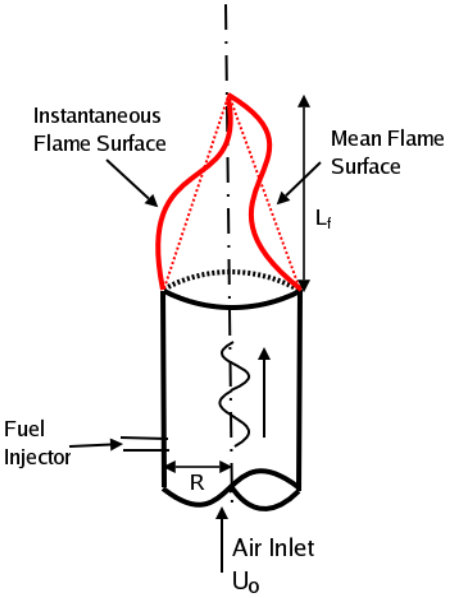

Figure 3: Schematic of investigated geometry.

Perturbation Analysis

The above equations were analytically solved using a third order perturbation analysis. For the sake of illustration, we consider an axi-symmetric conical flame stabilized on a burner tube as shown schematically in Figure 3. The origin of co-ordinates is chosen to be the center of the tube exit plane. As such, Eq. (6) (in non-dimensional form) becomes

$$\xi(1,t)=0 \tag{12}$$

where the flame holder length scale parameter, *R*, is chosen to be the burner tube radius. We expand the flame front position function $\xi(r,t)$ in terms of the parameter ε as,

$$\xi(r,t)=\xi_0(r)+\varepsilon\xi_1(r,t)+\varepsilon^2\xi_2(r,t)+\varepsilon^3\xi_3(r,t) \tag{13}$$

Using the above in eqs. (5) and (12), and collecting terms of the same order in ε yields the following.

$$\xi_o(r)=1-r \tag{14}$$

$$\frac{\partial\xi_1}{\partial t}-\alpha\frac{\partial\xi_1}{\partial r}+S_{L1}\cos(St(1-r-t))=0 \tag{15}$$

$$\frac{\partial\xi_2}{\partial t}-\alpha\frac{\partial\xi_2}{\partial r}-\alpha S_{L1}\cos(St(1-r-t))\left(\frac{\partial\xi_1}{\partial r}\right)+\frac{1}{2}\left(\alpha-\alpha^2\right)\left(\frac{\partial\xi_1}{\partial r}\right)^2+S_{L2}\cos^2(St(1-r-t))=0 \tag{16}$$

$$\begin{aligned}\frac{\partial\xi_3}{\partial t}-\alpha\frac{\partial\xi_3}{\partial r}-\alpha\left(S_{L2}\cos^2\left(St\left(1-r-t\right)\right)\frac{\partial\xi_1}{\partial r}+S_{L1}\cos\left(St\left(1-r-t\right)\right)\frac{\partial\xi_2}{\partial r}\right)+\frac{1}{2}\alpha\left(\alpha-\alpha^2\right)\left(\frac{\partial\xi_1}{\partial r}\right)^3+\\ \left(\alpha-\alpha^2\right)\frac{\partial\xi_1}{\partial r}\frac{\partial\xi_2}{\partial r}+\frac{1}{2}S_{L1}\cos\left(St\left(1-r-t\right)\right)\left(\alpha-\alpha^2\right)\left(\frac{\partial\xi_1}{\partial r}\right)^2+S_{L3}\cos^3\left(St\left(1-r-t\right)\right)=0\end{aligned} \tag{17}$$

The parameter α is given by the expression, $\alpha=\beta^2/\left(1+\beta^2\right)$ and,

$$s_{Lj}=\frac{1}{j!}\frac{\partial^j f(\phi)}{\partial\left(\phi'/\phi_0\right)^j}\bigg|_{(\phi'/\phi_0)=0};\qquad h_{Rj}=\frac{1}{j!}\frac{\partial^j\left(h_R/h_{R0}\right)}{\partial\left(\phi'/\phi_0\right)^j}\bigg|_{(\phi'/\phi_0)=0} \tag{18}$$

are the j^{th} order sensitivities of the burning velocity magnitude and heat of reaction of the reactant mixture respectively, to fluctuations in equivalence ratio. For cases where the flame does not respond in a quasi-steady manner, these sensitivity derivatives are also functions of frequency. Within the linear approximation, the character of the solution does not change as the s_{L1} and h_{R1} terms are now functions of mean fuel/air ratio and frequency. In the non-linear case, things are much more complex and new terms arise which are not present in the above expressions. As such, the nonlinear corrections implicitly assume quasi-steady sensitivities of flame speed and heat of reaction.

Equations (15)-(18) can be solved to yield expressions for $\xi_i(r,t)$. We present below the solution obtained for $\xi_1(r,t)$.

$$\xi_1(r,t) = \frac{s_{L1}}{(1-\alpha)St}\left[\sin\left\{St(1-r-t)\right\} - \sin\left\{(St/\alpha)(1-r-\alpha t)\right\}\right] \tag{19}$$

This solution explicitly contains two contributions to the linear dynamics of the flame surface evolution. The first term within the brackets on the RHS represents the effect of local non-uniformities in the burning velocity due to the spatial and temporal oscillations in equivalence ratio. The second term arises because of the boundary condition, i.e., Eq. (12), that the flame does not move at the burner lip, even though its flame speed is oscillating. In physical terms, Eq. (19) shows that the flame front position is controlled by two sets of flame wrinkling waves that travel along the front – 1) waves generated at each point along the flame due to spatial variations in flame speed and 2) waves generated at the flame attachment point due to the boundary condition, Eq. (12). Notice that the propagation velocities of these two waves along the flame surface are different. The former travels with the mean flow velocity (unity in the nondimensional case) and the latter with a velocity $1/\alpha$ respectively, along the axis of the flame. Thus these two waves interfere constructively at some flame surface locations and destructively at others. This has a great influence on the characteristics of the heat release transfer function of the flame. This is similar to the result obtained by Preetham and Lieuwen[22] who emphasized these superposition effects upon the dynamics of flames subjected to excitation in flow velocity. The corresponding expressions for the nonlinear corrections to the flame position, ξ_2 and ξ_3, are presented in the appendix. The transfer function in Eq. (11)can be decomposed in a manner similar to that of heat release in Eq. (9). In the linear limit, i.e., for very small excitation amplitudes, the transfer function F_o , can be written as a sum of three contributions, due to flame area oscillation, burning velocity oscillations and heat of reaction oscillations, the expressions for which may be written as follows.

$$F_{o,s_L} = s_{L_1}\left\{\frac{2}{St^2}\left(1+iSt-\exp(iSt)\right)\right\} \tag{20}$$

$$F_{o,h_R} = h_{R_1}\left\{\frac{2}{St^2}\left(1+iSt-\exp(iSt)\right)\right\} \tag{21}$$

$$F_{o,A} = s_{L_1}\left\{\frac{2\alpha}{1-\alpha}\left(\frac{1-\alpha-\exp(iSt)+\alpha\exp\left(iSt/\alpha\right)}{St^2}\right)\right\} \tag{22}$$

(23)

The same decomposition however, cannot be strictly performed in the non-linear regime. Thus, following Eq. (9), we decompose the net transfer function in the nonlinear regime as,

$$F = F_A + F_{s_L-A} + F_{h_R-A} + F_{s_L-h_R-A} \tag{24}$$

The detailed expressions for the terms on the RHS are presented in the appendix.

Numerical Approach

Formally, Eq. (1) is a Hamilton-Jacobi equation. This equation is non-conservative and has the property that the non-linear term, due to flame propagation normal to itself, results in cusps, or discontinuities in derivative, and possible topological changes (i.e. pocket formation) in the solution. Hence robust numerical schemes that can capture these effects without excessive smearing are required.

The solution domain is discretized using a uniform grid. The initial value for the *G*-field was constructed from the assumed quiescent flame shape. This was done by defining the value of *G* at each grid location to be the signed distance of that location from the quiescent flame surface. The solution at later times was obtained using a low

diffusion Courant-Isaacson-Rees scheme with back and forth error compensation and correction (BFECC)[26]. The *G*-field was reset to a distance function after each time step using the re-initialization procedure described by Peng *et al.* [27].

A considerable reduction in computation time can be obtained by solving Eq. (1) in only a narrow band around the actual flame location, rather than in the entire two-dimensional domain. This was achieved by adopting the localization procedure introduced by Peng *et al.* [27]. This band evolves in time as the flame moves or as pockets form and burnout. These computations were performed using the general purpose level-set program LSGEN2D developed by the authors.

As noted in the assumptions introduced at the beginning of the previous section, the flame remains attached at the burner lip. This is achieved by setting G=0 after every time step of the BFECC scheme at the points corresponding to the burner tube. The velocity of these points is maintained to be identically zero throughout the simulation to provide additional robustness in capturing the flame surface evolution.

The instantaneous heat release of the flame is given by Eq. (8). Following Smereka[28], Eq. (8) can be written using G as,

$$q(t) = \int_{\Omega} 2\pi r \rho s_L h_R \delta(G) |\nabla G| d\Omega \tag{25}$$

where the integration is performed over the whole narrow band computational domain described earlier and $\delta(G)$ is the Dirac-delta function. This integral is then evaluated at every sampling time step, using the numerical technique described by Smereka[28]. The grid size (Δr^*) for all the above computations was fixed at 0.001 non-dimensional units in both directions. The time-step was fixed at $0.1\Delta r^*$. These were chosen by successive refinement of the grid until the temporal heat release variation obtained did not visibly change between two successive refinements. Sufficient numbers of grid points were taken along the z-direction to ensure that all pockets shed from the tip of the flame would burn out before being convected out of the grid. The first three contributions to the total heat release on the RHS of Eq. (8) were obtained independently using the same techniques described above.

These exact results were used to determine the accuracy of the third order perturbation approach. The domain in $St_2 - \varepsilon$ space where the magnitude and phase of the transfer function can be determined within specified accuracies E_m and E_ϕ respectively is defined by,

$$St_2(E_m, E_\phi, \varepsilon_0) = \min\left\{ St_2 : \left(\left| \frac{|F_{comp}(St_2)| - |F_{asymp}(St_2)|}{|F_{comp}(St_2)|} \right| \le E_m \right), \left(\left| \angle F_{comp}(St_2) \right| - \left| \angle F_{asymp}(St_2) \right| \le E_\phi \right) \right\} \Big|_{\varepsilon=\varepsilon_0} \tag{26}$$

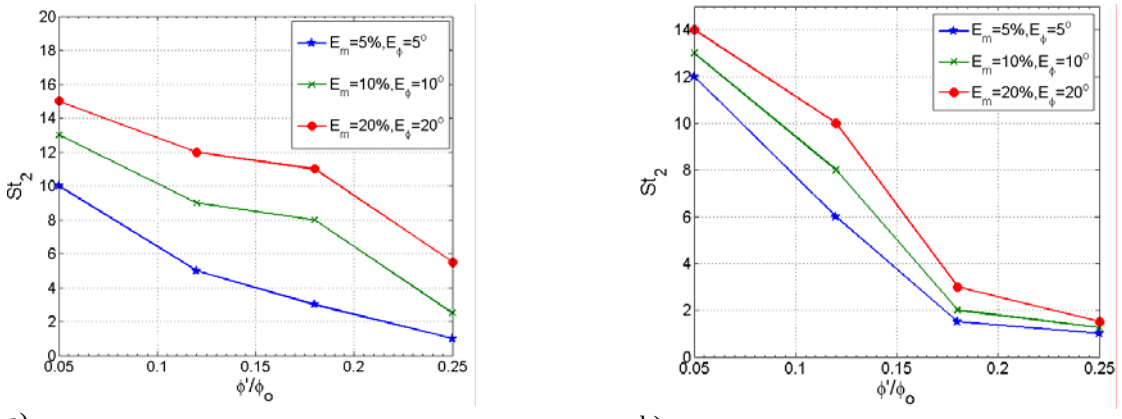

Figure 4 : Domain of applicability of asymptotic analysis (a) $\phi_o = 0.85$ **(lean) (b)** $\phi_o = 1.277$ **(rich),** $\beta = 4$ **.**

The first term within the braces on the RHS gives the value of St_2 for which the error in magnitude prediction from the approximate solution obtained using asymptotics is bounded by E_m. The second term gives the value of St_2 for which the error in phase prediction in the asymptotics solution is bounded by E_ϕ. The size of these regions depend on the assumed burning velocity and heat of reaction dependencies on equivalence ratio (eg. Eq. (27) and Eq. (28)).

As will be shown later, two mechanisms contribute to non-linearity in the flame response. The first is due to flame sheet dynamics, as described by the G-equation, see Eq. (1). The second is the nonlinearity of the quasi-steady flame speed and heat of reaction dependence upon fuel/air ratio, as plotted qualitatively in Figure 2 and described in the sensitivity derivatives in Eq. (18). Figure 4 shows the regions of specified accuracy of the asymptotic solutions for various values of E_m and E_ϕ for two flames viz., ϕ_o=0.85 (lean) and ϕ_o=1.277 (rich). It can be seen that there is an opposing influence of perturbation magnitude and Strouhal number – i.e., the analysis is valid at larger fuel/air perturbation amplitudes at lower Strouhal numbers. This is due to the effects of nonlinearity in the G-equation which grow with amplitude and frequency, see Preetham and Lieuwen[22]. At low Strouhal numbers, the analysis validity is limited by nonlinearities in the quasi-steady flame speed and heat of reaction dependencies upon fuel/air ratio. The characteristics of the transfer function are discussed next.

Results and Discussion

This section presents explicit results for a conical flame with aspect ratio, β=4.0. The investigated geometry is shown schematically in

Figure 3. The following experimentally determined correlations for the burning velocity magnitude and heat of reaction respectively with equivalence ratio for a methane-air flame were assumed (Abu-Orf and Cant[29])

$$s_L(\phi) = A\phi^B e^{-C(\phi-D)^2}; \quad A = 0.6079,\ B = -2.554,\ C = 7.31,\ D = 1.230 \tag{27}$$

$$h_R(\phi) = \frac{2.9125\times10^6 \min(1,\phi)}{1+0.05825\phi} \tag{28}$$

Linear Dynamics

We begin with a brief discussion of the characteristics of the linear transfer function. We refer the reader to Cho and Lieuwen[20] for a more complete discussion of these linear dynamics and focus the discussion here primarily on the manner in which the rich flame results are different from those of lean flames. In order to make this comparison, results are presented for two mean equivalence ratios, ϕ_o=0.85 and ϕ_o=1.28, which correspond to conditions where the flame speeds are identical.

Figure 5 shows the variation of the phase and magnitude of the linear transfer function for the two equivalence ratios. Also shown are the phase and magnitude of the individual contributions to the total transfer function. Firstly, note that the variation of both the phase and the magnitude do not monotonically vary with St_2. This is due to the fact that the linear flame response is determined by the net superposition of a boundary generated "wave" and a local disturbance, as discussed in the previous section. Therefore the net flame response depends on exactly how these waves superpose at different Strouhal numbers. It must also be noted from eqs (20) and (21) that the phase of the flame speed and the heat of reaction contributions will be identical in the linear limit. The linear transfer function for the rich case is shown in Figure 5(b). Notice that the transfer function goes to a near zero value, given by the heat of reaction sensitivity, at low values of St_2 (see Eq. (33)). This is in striking contrast to the corresponding lean case and is due to the fact that the heat of reaction is a nearly constant function of equivalence ratio in the rich regime. This means that in the linear regime, the heat release of a rich flame is relatively insensitive to perturbations in equivalence ratio when compared to the lean flame at low values of St_2.

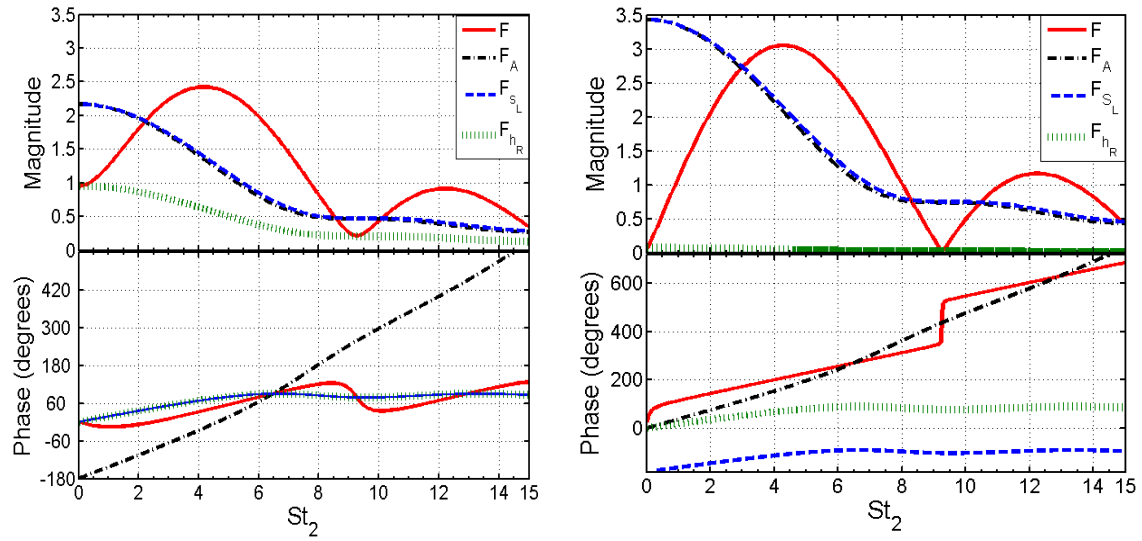

a) b)

Figure 5: Linear transfer function of a) $\phi_o = 0.85$ **(lean) b)** $\phi_o = 1.277$ **(rich).** $\beta = 4$ **.**

Another interesting difference between the two transfer functions is the presence of a zero response in the rich case at $St_2 \sim 8.7$. At this point, the oscillating flame speed and area oscillation response exactly cancel each other. In the lean case, however, the node is not present. This is due to the fact that the lean case has an additional contribution to the total transfer function, *viz.*, the heat of reaction oscillations. Therefore, in general, a zero response will not occur in the lean flame response. However, it must be noted that these characteristics are strong functions of the sensitivities of flame speed and heat of reaction to equivalence ratio.

Figure 6 overlays the flame response over a range of fuel/air ratios. Note, first, that the lean cases all start with a gain of nearly unity and the rich cases with a gain of nearly zero at low Strouhal numbers. This is due to the fact that the flame response is entirely controlled by the heat of reaction sensitivity in the quasi-steady case. All transfer functions then initially grow with increasing Strouhal number, because the burning area and the fluctuating flame speed terms progressively come into phase with each other. As the mean equivalence ratio is increased from an initial lean value, e.g. ϕ=0.6, the s_L and h_R sensitivities progressively decrease and stay nearly constant, respectively, until ϕ~1.06 where the s_L and h_R sensitivities vanish. Hence the magnitude of the flame response drops from a finite value at ϕ=0.6 to a nearly zero response at ϕ~1.06. This is due to the occurrence of the flame speed maximum at this equivalence ratio. The heat of reaction is a very weak function of equivalence ratio for ϕ_o>1.0. Hence, we see, as before, that the magnitude now increases from a nearly zero value with increasing St_2 for rich mean equivalence ratios.

Even though the flame speeds at ϕ_o=0.85 and ϕ_o=1.277 are identical, the magnitude of the maximum gain is higher in the rich case due to the higher value of s_L sensitivity at ϕ_o=1.277. The other interesting feature is that the heat release response lags the excitation in the lean case, and leads it in the rich case. This again is due to the fact that the linear s_L sensitivity, $s_{L1,}$ changes sign from positive to negative when ϕ_o>1.066. This may be understood physically from the fact that the burning area response is due to s_L fluctuations that, in turn, are induced by equivalence ratio oscillations. The change in sign of s_{L1} implies that an instantaneous increase in equivalence ratio results in an increase and decrease in the instantaneous value of s_L on the lean and rich side, respectively. Therefore, given the same instantaneous equivalence ratio perturbation, the corresponding instantaneous burning area decreases and increases for the lean and the rich case, respectively.

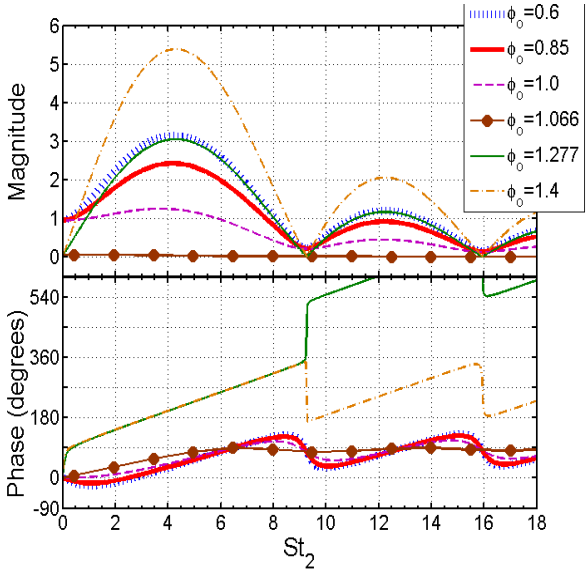

Figure 6: Variation of the linear transfer function with St_2 for different values of equivalence ratio. β=4.

Nonlinear Dynamics

As the excitation amplitude/frequency is increased, the higher order contributions to the transfer function become significant. Figure 7 shows typical boundaries for the regions in the parametric space of the current study where the various non-linearity mechanisms are operative. These regions are shown for the lean flame corresponding to ϕ_o=0.85 and are nearly the same for the rich case (not shown). Note that the heat release response in the region labeled '1' in Figure 7 is essentially linear and has the characteristics described in the previous subsection.

There are two basic processes causing nonlinearity in the flame response

(1) non-linearities in burning area oscillation, due to the nonlinearities in flame kinematics (term 1 in Eq. 9) and

(2) quasi-steady nonlinearities in the s_L-ϕ and h_R-ϕ relationships, as plotted qualitatively in Figure 2 (terms 2-4 in equation 9).

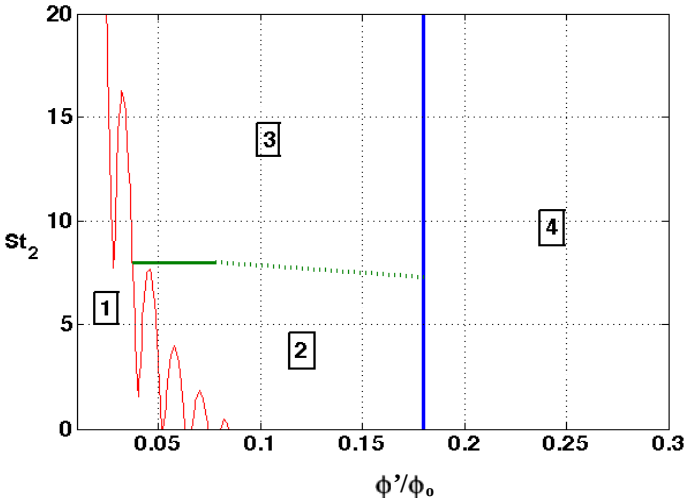

Figure 7: Qualitative map illustrating regimes of dominance of various nonlinearity mechanisms at ϕ_o=0.85. (1) Linear, (2) s_L-ϕ non-linearity, (3) kinematic restoration and (4) "cross-over".

There is an additional complication, however, in the fact that the s_L-ϕ nonlinearity has both a direct and indirect influence on the heat release response through term 2 and term 1 in Eq. 9, respectively. It is this latter, indirect mechanism which dominates the heat release nonlinearities in Region '2' in Figure 7. Physically the source of these mechanisms may be explained as follows. The flame surface kinematics is controlled by the flame speed fluctuations. Therefore, the propagation speed of the flame surface is controlled by the local flame speed and, hence, depends on the location of the flame surface itself in general. At a given St_2, for low excitation amplitudes, the deviations of the flame from its quiescent location are not large and this is not a significant effect. Hence, the dynamics are approximately linear. As the amplitude is increased, however, the

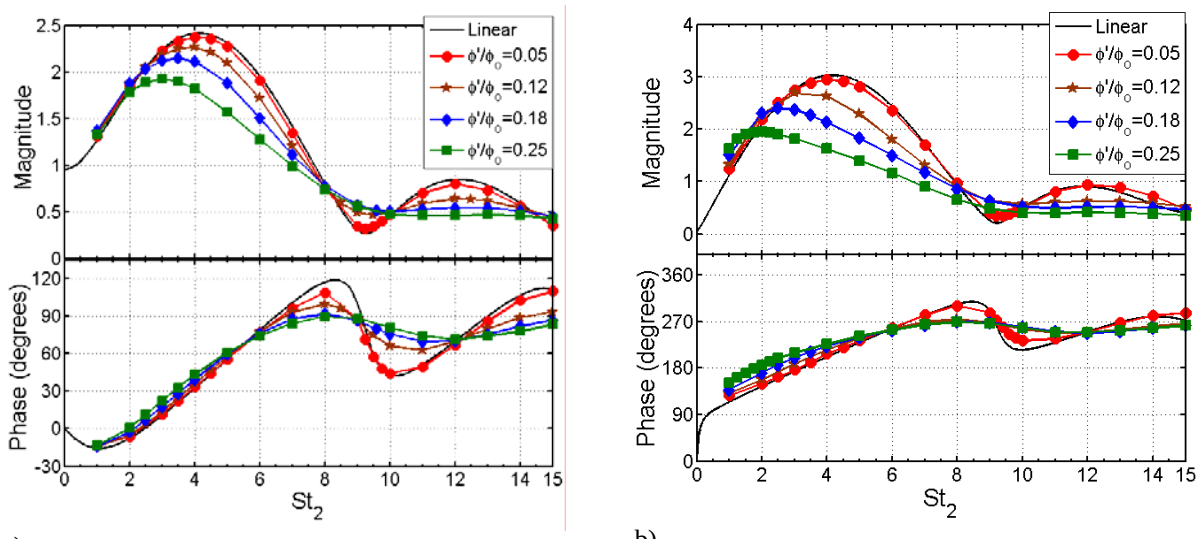

a) b)

Figure 8 Variation of the magnitude and phase of the non-linear transfer function with reduced Strouhal number, (a) $\phi_o = 0.85$ **and (b)** $\phi_o = 1.277$ **,** $\beta = 4$ **.**

nonlinear dependence of the local propagation velocity at various flame surface locations on the actual location of the flame surface itself becomes important. This induces nonlinearities in the burning area response and is the key mechanism of nonlinearity in Region 2.

The flame kinematic nonlinearities dominate the heat release nonlinearities in Region '3' in Figure 7. Larger amplitude fluctuations in flame position slope cause kinematic nonlinearities to correspondingly grow in significance. As *St* is increased, Eq. (19) shows that the wavelength of the induced wrinkles on the flame surface are both $O(1/St)$. Thus, at high frequencies, propagation of the flame surface normal to itself results in the rapid destruction of these wrinkles (Lieuwen[30]) causing the net flame burning area to saturate. This phenomenon, known as kinematic restoration[31,32], is an additional source of flame kinematic nonlinearity and dominates the flame response at St_2>8.0 in Region 3 in Figure 7[*].

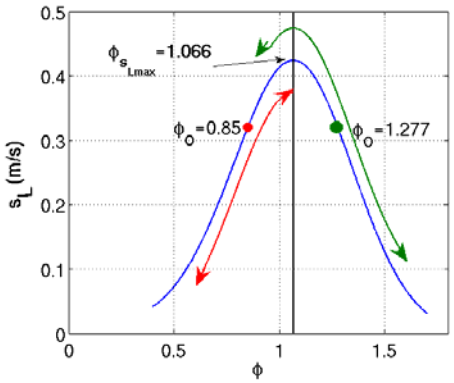

Figure 9: Variation of flame speed with equivalence ratio. The vertical line marks the equiv. ratio for maximum s_L**. The arrows show the extent of variation of** s_L **over one excitation cycle at** $\phi'/\phi_o = 0.25$ **in each case.**

We finally consider Regime 4, labeled the "crossover" mechanism. This nonlinearity is related to that of Region 2 in that, it is completely due to the second source of nonlinearity noted above, i.e. the s_L-ϕ and h_R-ϕ nonlinearities. However, in this region, this mechanism dominates for all Strouhal numbers and is due to the drastic change in s_L and h_R characteristics on the lean and rich side of stoichiometric. As was described earlier in the introduction section, the equivalence ratio space can be divided into three distinct regions (see Figure 2). For large excitation amplitudes, the local equivalence ratio can

[*] The boundary between Regions 2 and 3 was determined as follows. In the perturbation analysis, the higher order flame speed sensitivities, s_{L2} and greater are artificially set to be zero. The only source of kinematic non-linearity is then due to kinematic restoration. Although not shown here, comparison of the nonlinear flame contributions in the cases with and without the higher order s_L sensitivity showed that the two contributions become of nearly equal magnitude beyond an St_2 of approximately 8.0. The reader must keep in mind that this approach is limited by the validity of asymptotics at high amplitudes. Hence the part of the boundary between regions '2' and '3' in Figure 7 that may be determined from asymptotics alone is shown with a solid line. The remaining part of the boundary was extrapolated for the sake of illustration and is shown by the broken line.

instantaneously cross over from region I to region II or region I to region III and vice versa. The trend in the variation of s_L and h_R qualitatively changes when this cross over occurs. For the sake of illustration, consider an instantaneous variation of ϕ over an excitation cycle shown in Figure 9. The instantaneous value of s_L falls with decreasing ϕ over a portion of the excitation cycle in the rich case, as opposed to rising further. Hence, if for some instantaneous oscillation amplitude ϕ around some mean equivalence ratio ϕ_o, if $|\phi-\phi_o|>|\phi_{s_L,\max}-\phi_o|$, the trend of s_L variation over one excitation cycle changes and causes a very abrupt saturation of the mass burning rate contribution to the total heat release, i.e the second term in Eq. (9). Similarly, a sufficiently high excitation amplitude can result in significant nonlinearities in the heat of reaction contributions in Eq. (9) if $|\phi-\phi_o|>|1-\phi_o|$. The fact that differentiates this mechanism from the kinematic mechanisms is that even if the net burning area oscillation has not saturated, these alone can cause the net heat release to saturate; i.e., even if the first term in Eq. (9) does not saturate, the contributions of the 2^{nd} – 4^{th} terms to nonlinearity are dominant and can cause net heat release saturation. Fortunately, determining the excitation amplitude, ε, when this mechanism becomes significant is very straightforward, as it is simply the minimum of the absolute difference in value between the mean equivalence ratio and the stoichiometric or the value corresponding to the maximum s_L; i.e.,

$$\varepsilon=\frac{1}{\phi_o}\min\left\{|1-\phi_o|,|\phi_{s_L\max}-\phi_o|\right\} \tag{29}$$

Henceforth this second non-linearity mechanism will be referred to as the "cross-over" mechanism. Note that with the assumption of quasi-steadiness for s_L and h_R, this mechanism is controlled purely by the oscillation amplitude. Hence the boundary of the region 4 in Figure 7, where this mechanism is operative has no dependence on St_2. However, the fact that the flame speed sensitivity to fuel/air ratio oscillations at high frequencies will progressively diminish (Lauvergne and Egolfopoulos[24]), implies that, in reality, there will be an upper boundary to region 4 determined by both St_2 and excitation amplitude beyond which the nonlinearities will be purely flame kinematic in nature.

Consider further the behavior of the transfer function in the low St_2 limit for the cases where the asymptotic analyses detailed in the previous sections are valid. We have the following results for the terms on the RHS of Eq. (24),

$$\lim_{St_2\to 0}F_A=-\lim_{St_2\to 0}F_{s_L-A}=-s_{L1}-\frac{3}{4}\varepsilon^2\left({s_{L1}}^3-2s_{L1}s_{L2}+s_{L3}\right) \tag{30}$$

$$\lim_{St_2\to 0}F_{s_L-h_R-A}=\frac{3}{4}\varepsilon^2\left(h_{R2}s_{L1}-h_{R1}{s_{L1}}^2+h_{R1}s_{L2}\right) \tag{31}$$

$$\lim_{St_2\to 0}F_{h_R-A}=h_{R1}+\frac{3}{4}\varepsilon^2\left(h_{R3}-h_{R2}s_{L1}+h_{R1}{s_{L1}}^2-h_{R1}s_{L2}\right) \tag{32}$$

From Eq. (30), it can be seen that in the low St_2 limit, the contributions due to the burning area fluctuations and those due to the burning rate oscillations have the same absolute magnitude, but opposite signs. This means that the contributions in this limit are exactly out of phase and cancel each other. Physically, this may be reasoned as follows. Two lean flames with the same fuel flow rate but different air-flow rates will have the same steady heat release rate. In the same way, local variations in mass burning rate due to slow time scale perturbations in s_L must be balanced by the oscillations in the net burning area. As such, the low frequency limit for the transfer function is given by:

$$\lim_{St_2\to 0}F=h_{R1}+\frac{3}{4}\varepsilon^2h_{R3} \tag{33}$$

From this, it follows that in the limit of $St_2\to 0$, the net flame response is purely dependent on the sensitivities of the heat of reaction, h_{Rj} (see Eq. (18)). As such, the discussion of this point above for the linear case applies equally

well here - rich flames are insensitive to equivalence ratio fluctuations even at significantly large amplitudes in the low St_2 limit.

With the preceding material as background, we next proceed to actual results, obtained from numerical computations. Figure 8a and 9b plot the variation of the magnitude and phase of the total heat release transfer function with increasing excitation amplitudes for the lean and the rich flames respectively. Notice first that the transfer function response for all excitation amplitudes tends toward the linear value in both the lean and the rich flame cases as $St_2 \rightarrow 0$. This is due to the low frequency behavior of the transfer function as explained in the previous paragraph. With increasing St_2, the transfer function begins to deviate significantly from the linear value. For $St_2 < 8.0$ in either case, kinematic restoration effects are not important, as explained earlier. As such the slight deviation from the linear value at low amplitudes with increasing St_2 can be ascribed to the manifestation of s_L-ϕ non-linearities in both cases. Beyond St_2=8.0, kinematic restoration effects contribute to slight deviation from the linear response observed at low excitation amplitudes. As the excitation amplitude is increased beyond $\phi'/\phi_o = 0.18$ in the lean case and $\phi'/\phi_o = 0.15$ in the rich case, the crossover mechanism becomes dominant.

The above plots illustrate the behavior of the transfer function with variations in St_2 at various excitation amplitudes. We now examine the converse scenario, i.e. the variation of heat release response with excitation amplitude at a fixed value of St_2. Figure 10a and 10b plot the variation of the magnitude of the heat release response with increasing excitation amplitude for the lean and rich cases respectively. The solid vertical lines on both show the amplitude where the cross-over mechanism is initiated. Overlaid are the magnitudes of the individual constituent components (see Eq. (9)) of the heat release response in each case. These data have been obtained at $St_2 \sim 2\pi$. From Figure 7, this corresponds to regions where kinematic restoration is not significant. Notice, therefore, that in either case, the amplitude of the burning area oscillation varies non-linearly with excitation. The burning rate term, labeled 's_L-A', increases up to the crossover boundary in both cases. Figure 10b shows that the magnitude of this term saturates beyond the crossover boundary along with the net heat release amplitude. Notice that the area oscillation term, labeled 'A'/A_o', has not saturated in either case. The trends in the magnitude of area fluctuation in either case may be explained as follows. As the excitation amplitude increases, the local value of the flame speed at the flame surface attains higher and higher values until the cross over amplitude is reached, causing the flame area oscillation amplitude to fall due to increasing efficiency in burning area destruction. Beyond this amplitude, as the flame speed variation trends change over a part of the cycle, the efficiency of burning area destruction reduces and the burning area oscillation amplitude begins to rise again as can be seen from Figure 10b. This nonlinear variation of the burning area oscillation amplitude with excitation amplitude shows that heat-release saturation is controlled completely by the cross-over mechanism at this value of $St_2(\sim 2\pi)$ and not by the kinematic restoration mechanism. This is in contrast with the results for flames perturbed by velocity oscillations[22], which show kinematic restoration to be the dominant mechanism leading to heat release saturation.

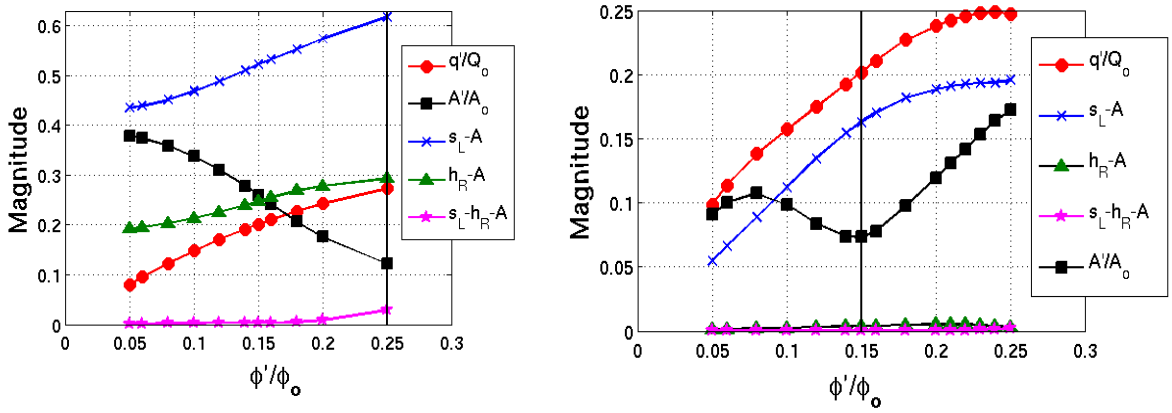

a) b)

Figure 10: Magnitude of individual contributions on the total heat release (a) $\phi_o = 0.85$ and (b) $\phi_o = 1.277$, for an oscillation amplitude of $\phi'/\phi_o = 0.25$, St_2=6.68 (St=2π), β=4.0. The vertical black line marks the amplitude at which the instantaneous equivalence ratio begins to cross over into the rich/lean region over a part of the excitation cycle.

Finally, to see that kinematic restoration does indeed cause heat release saturation to occur at higher frequencies, consider Figure 11b. These figures plot the variation of the magnitude of the heat release response with increasing excitation amplitude for the lean and rich cases, respectively, at a higher excitation frequency, $St_2 \sim 4\pi$. Overlaid are the variations of the magnitudes of the individual contributions to the total heat release. The net burning area oscillation is seen to be a weak function of excitation amplitude in either case-kinematic restoration processes cause burning area saturation. The total heat release in the rich case therefore shows saturation (see Figure 11b).

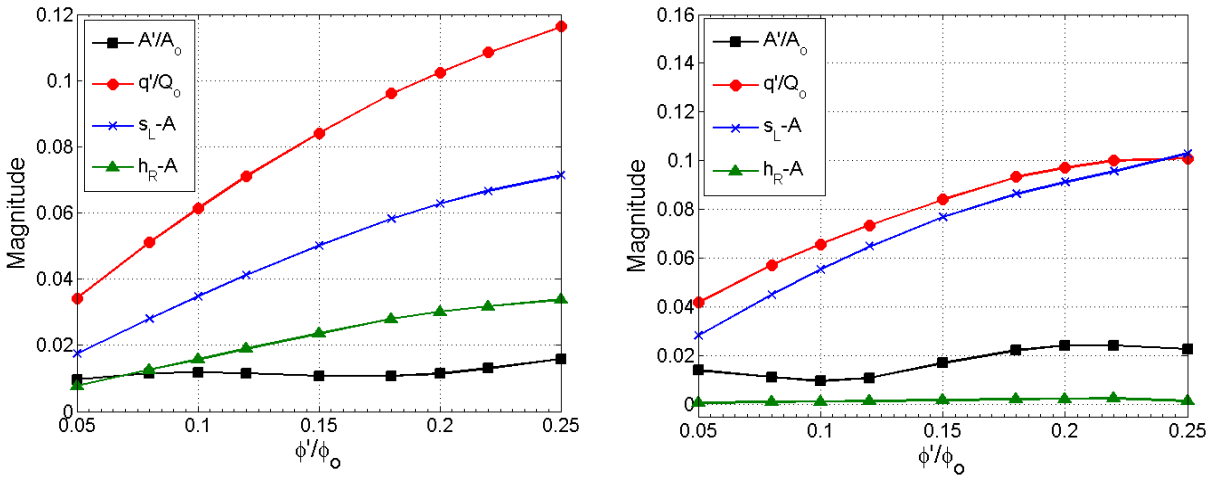

Figure 11: Magnitude of individual contributions to the total heat release (a) $\phi_o = 0.85$ **and (b)** $\phi_o = 1.277$ **, for an oscillation amplitude of** $\phi'/\phi_o = 0.25$ **, St_2=13.36 (St=4π), β=4.0.**

III. Assessment of POGT Stability

There are two key mechanisms which must be considered in rich systems: these are the response of the flame to velocity oscillations (such as due to vortex shedding) and fuel/air ratio oscillations. This section is divided into two parts, which consider the implications of this work on each of these two mechanisms:

IV. Velocity Oscillations:

Our analysis indicates that the response of rich and lean premixed flames to velocity oscillations is comparable, indicating a similar proclivity of rich systems to instabilities than lean ones. This indicates that the knowledge base built up by OEM's on the behavior of their lean, premixed systems directly carries over to the POGT. Assuming that the flame temperature and combustor geometry remains fixed (thereby fixing the natural acoustic frequencies), then *the key parameter influencing flame response is convective time from the point of formation of the vortex to the "center of mass" of the flame.* The effect on the convective time can be better understood from the following equation which expresses the convective time as the sum of the convective time in the premixer (τ_{pm}) and the convective time in the combustor (τ_{comb}):

$$\tau_{conv} = \tau_{pm} + \tau_{comb} \qquad (34)$$

$$\tau_{conv} = [L_{pm} / u_{pm}] + [L_f / u_{comb}] \qquad (35)$$

where L_{pm} refers to the distance from the point of origin of the disturbance to the entrance to the combustor, u_{pm} refers to the mean convective velocity in the premixer, L_f refers to the distance the perturbation travels from the combustor entrance to the "center of mass" of the flame, and u_{comb} refers to the mean convective velocity in the combustor.

The effect of variations in stoichiometry on the convective time is primarily exercised through its influence upon the location of the flame "center of mass". A rule of thumb for predicting the behavior of the POGT stability off of a known database of stability for the lean premixed system is the following: estimate the value of τ_{conv} for the POGT operating point. Then, determine what corresponding operating condition for the lean, premixed system gives an equivalent convective time.

Stoichiometry and fuel composition will exercise an important influence on this center of mass. For example, for rich flames, a higher equivalence ratio will result in lower flame speeds and, presumably therefore, a longer flame. This will increase the convective delay, shifting the instability to a higher velocity operating point. Similarly, altering the fuel composition at a fixed flame temperature will also alter the flame position. For example, the figures below were obtained by Prof. Santavicca at Penn state, showing Abel-inverted images of a natural gas and hydrogen enriched lean flame, showing the shift in location of the flame location with fuel composition. This causes a corresponding shift in instability region.

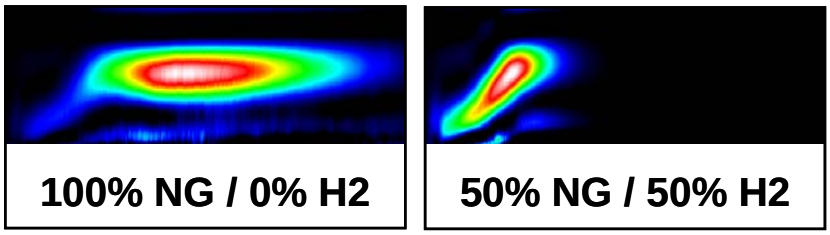

Figure 12 Two-dimensional chemiluminescence images of flame structure (flow is from left to right) illustrating the effect of fuel composition on flame shape and location due to changes in the flame speed[33].

To illustrate this graphically, we present in Figure 13 a set of data obtained by Santavicca and co-workers[33] that plots the effect of hydrogen addition (0%, 15%, 25%), inlet temperature (200°C, 300°C) and inlet velocity (75, 90, 105 m/s) on the location of a flame's "center of mass". Figure 4 shows that the location of the flame "center of mass" varies with operating conditions and fuel composition. Note that the axial flame location varies substantially, depending upon these parameters.

According to Eqs. (3) and (4), for a fixed combustor geometry and combustor velocity one would expect that there would be a relatively well-defined range of flame locations (L_f) for which the combustor would be unstable. The color coding in Figure 5 indicates whether or not unstable combustion was observed at that operating condition and fuel composition. These measurements were made in a variable length combustor where the combustor length was varied from 45 inches to 60 inches, which corresponded to a range of acoustic frequencies from approximately 300 Hz to 400 Hz. As shown in Fig. 5, when the flame is closest to the combustor inlet, no instabilities (triangle symbols) are observed over this range of combustor lengths, however, as the distance to the flame's "center of mass" increases, there is a transition to unstable operation (square symbols) at approximately X=2.0" and then a transition back to stable operation (triangle symbols) at approximately X=2.5". The instability frequencies observed in the unstable regime were between 345 Hz and 390 Hz. This clearly illustrates that instabilities are only observed when the convective time falls within a certain range of values.

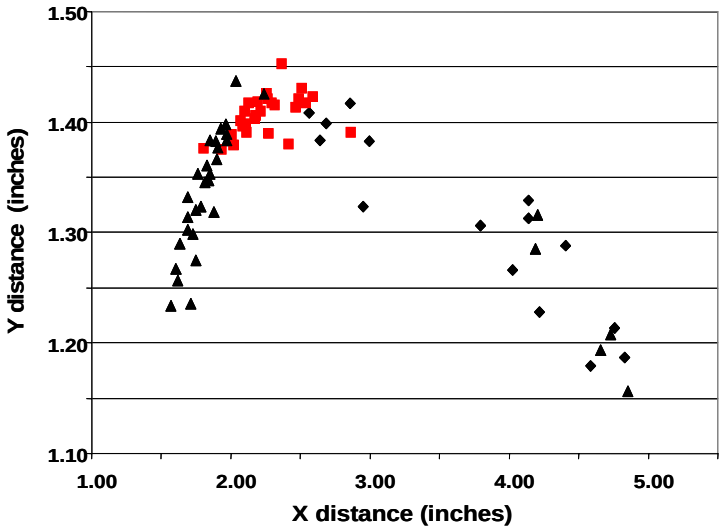

Figure 13 Location of the flame "center of mass" over a range of hydrogen addition (0%, 15%, 25%), inlet temperature (200°C, 300°C) and inlet velocity (75, 90, 105 m/s). X=0 and Y=0 corresponds to the combustor inlet. Triangular symbols indicate stable operation, Square symbols unstable operation, indicating well defined band of flame locations giving stable and unstable operation[33]

V. Fuel/Air Ratio Oscillations

As detailed above, the flame response of rich systems is quite different than lean ones, indicating that the experience from lean, premixed systems *will not directly carry over* from DLN systems to POGT systems – this is in contrast to the vortex shedding mechanism discussed above. Combustion instabilities occur when the rate of energy release by the flame exceeds the damping processes. Two processes influence this rate of energy release: the gain of the flame response, and its phase with respect to the pressure. B*oth the gain and phase of a rich flame response differ substantially from DLN systems and so are discussed separately.*

Fundamentally, the fuel/air ratio oscillations lead to oscillations in the flame speed and heat of reaction of the reactant mixture about their respective quiescent values. The slopes of the flame speed vs. equivalence ratio curve and the heat of reaction vs. equivalence ratio curve are referred to as the flame speed sensitivity and the heat of reaction sensitivity respectively. As such, the heat release response of a premixed flame is caused due to three mechanisms – (i) Heat of reaction oscillations due to fuel/air ratio oscillations (ii) Mass burning rate oscillations due to flame speed oscillations (iii) Flame surface area oscillations due to kinematic flame surface wrinkles arising from flame speed oscillations. These will be referred to as the heat of reaction contribution, flame speed contribution and area contribution respectively.

To characterize the flame response at different frequencies, it is instructive to define a non-dimensional frequency, called the Strouhal number, as $St = (2\pi f) L_f / U_o$, where f, L_f, U_o respectively denote the excitation frequency, length of the quiescent flame and the mean flow velocity. Further, a reduced Strouhal number, St_2, may be defined in terms of the flame angle θ, as $St_2 = St / \cos^2(\theta/2)$.

The qualitative differences between the response of lean flames and rich flames can be more easily understood from **Error! Reference source not found.**, which is a plot of the variation of the gain and phase of the response of lean and rich flames at various mean equivalence ratios for a CH_4-air flame with reduced Strouhal number. The disparities in variation of gain and phase are discussed separately and can be interpreted in terms of the three 'contributions' mentioned earlier.

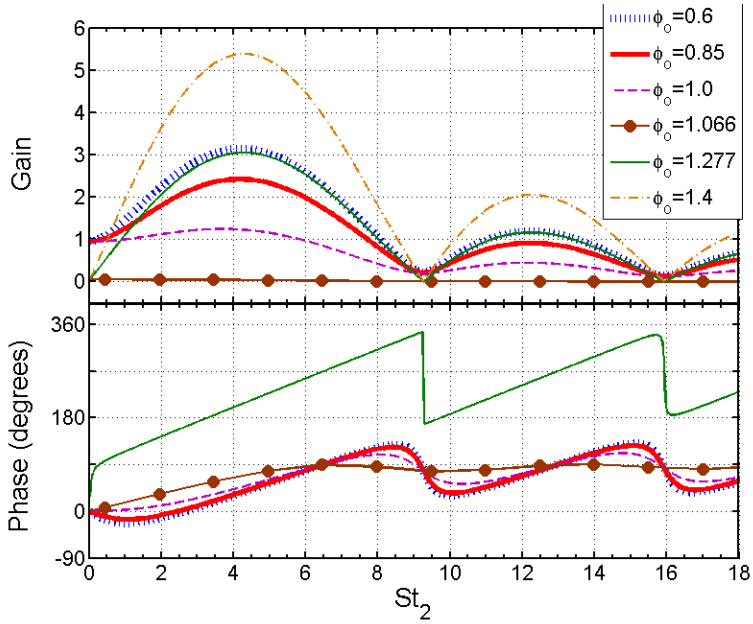

Figure 14 Variation of the heat release response with non-dimensional excitation frequency, for different values of equivalence ratio, for a CH_4-Air flame with β=4 for equivalence ratio excitation amplitude of 0.05.

Gain of Flame Response

The gain of the flame response is equal to the amplitude of heat release fluctuations excited by a fuel/air ratio disturbance of a given magnitude. Clearly, a high gain implies a flame that is very sensitive to such disturbances; a low gain is a system that does not respond appreciably to such fluctuations. From a stability point of view, the lower the gain, the less likely is the system to have instabilities. Moreover, the instability "islands" are smaller than a flame with a higher gain.

The upper graph in **Error! Reference source not found.** overlays the gain of the flame response for a CH_4-air reactant mixture over a range of fuel/air ratios. By comparing the lean and the rich gains, two significant observations may be made. (i) Firstly, in the limit of low Strouhal numbers, the gain for the lean response tends approximately to unity, while that for the rich response tends almost to zero. (ii) Secondly, for equivalence ratios such that the mean flame speeds are equal, the maximum gain of the rich response is greater than the maximum gain of the lean response.

The first observation may be explained due to the fact that, in the limit of low Strouhal numbers, the flame response is entirely controlled by the heat of reaction sensitivity in the quasi-steady case. For the case of a fuel-lean reactant mixture, the heat of reaction increases approximately linearly with equivalence ratio, while for a fuel-rich reactant mixture, the heat of reaction is nearly constant, i.e., it has a very small, but non-zero slope.

The gain for all the mean equivalence ratios then initially grow with increasing Strouhal number, because the burning area and the fluctuating flame speed contributions progressively come into phase with each other. As the mean equivalence ratio is increased from an initial lean value, e.g. ϕ=0.6, the flame speed and heat of reaction sensitivities progressively decrease and stay nearly constant, respectively, until ϕ~1.06 where the flame speed and heat of reaction sensitivities vanish. Hence the magnitude of the flame response drops from a finite value at ϕ=0.6 to a nearly zero response at ϕ~1.06. This is due to the occurrence of the flame speed maximum at this equivalence ratio for a CH_4-air flame. The heat of reaction is a very weak function of equivalence ratio for ϕ_o>1.0. Hence, it may be seen, that the magnitude now increases from a nearly zero value with increasing St_2 for rich mean equivalence ratios.

The second observation may be attributed to the fact that for the same amount of change in equivalence ratio, about a mean value with the same quiescent flame speeds (as chosen here), the change in flame speed for the lean mixture is much lesser than the change in flame speed for the rich mixture. In other words, the flame speed is more sensitive to changes in equivalence ratio for a rich reactant mixture than for a lean.

The key takeaway point from this plot is that the gain of POGT systems is much less than DLN systems at low Strouhal numbers. It is higher than that of DLN systems at intermediate Strouhal numbers, and the two systems have comparable sensitivities at higher Strouhal numbers. This suggests that one should attempt to have flames with low Strouhal numbers. This implies short flames, with high flow velocities. Short flames implies high turbulence intensities and operating closer to stoichiometric (where the flame speed is higher) For example, in order to achieve a Strouhal number less than 0.5 (where the gain response is low, see Figure **14**) the table below summarizes the required flame length, assuming a flow velocity at the leading edge of the flame of 40 and 80 m/s. Results are shown for combustors with instability frequencies ranging from 80 to 400 Hz, which encompasses the range of frequencies encountered in Siemens heavy duty scale engines, to the smaller engines of Solar.

Instability Frequency	**Velocity**	**Flame Length**
80	40 m/s	4 cm
200	40 m/s	1.6 cm
400	40 m/s	0.8 cm
80	80 m/s	8 cm
200	80 m/s	3.2 cm
400	80 m/s	1.6 cm

This table shows that the required flame lengths range from 0.8 to 8 cm. Such flame lengths are likely much shorter than what can be achieved in an engine, particularly for the lower velocity case and 200 and 400 Hz cases. However, 8 cm may be somewhat practical, indicating that minimizing flame length may be a reasonable design goal for lower frequency instabilities, such as encountered in large, frame type engines. However, it also indicates that control of flame response gain is probably less useful as a means for dealing with instabilities at the higher frequencies. In these cases, one must target phase control, which is dealt with next.

Phase of Flame Response

The lower graphs in **Error! Reference source not found.** plots the phase (in degrees) of the response of a CH_4-air flame for various equivalence ratios, at different excitation frequencies. It is evident from **Error! Reference source not found.** that the heat release response lags the excitation in the lean case, and leads it in the rich case. This is due to the fact that the linear flame speed sensitivity changes sign from positive to negative when ϕ_o>1.07 for CH_4-air. This may be understood physically from the fact that the burning area response is due to flame speed fluctuations that, in turn, are induced by equivalence ratio oscillations. The change in sign of the flame speed sensitivity implies that an instantaneous increase in equivalence ratio results in an increase and decrease in the instantaneous value of the flame speed on the lean and rich side, respectively. Therefore, given the same instantaneous equivalence ratio perturbation, the corresponding instantaneous burning area decreases and increases for the lean and the rich case, respectively.

For values of lean and rich mean equivalence ratios, such that the mean flame speed is the same, for eg., 0.85 (solid red line) and 1.28 (solid green line), the flame responses are nearly 180 degrees out of phase. The fact that their relative phase disparity is not exactly 180 degrees is attributed to the existence of the contribution of heat of reaction to the flame response, which, however small, is non-zero.

The key takeaway point from this is that the phase response of a POGT system is nearly 180 degrees different than that of a DLN system, when they operate at fuel/air ratios that render the same mean flame speed. This is a very useful result as it basically implies that regions prone to fuel/air ratio driven instabilities in DLN systems will be stable in a POGT configuration. Conversely, it also implies that stable regions in DLN systems may be unstable in POGT configurations. This insight provides a very useful design criterion for fuel nozzle design of a POGT system. To illustrate, assume for now that the flame lengths and shapes are identical for the two

systems. Basically, it says that the fuel nozzle can be identical, but that the optimized POGT and optimized DLN fuel peg axial locations must be spaced half of a convective wavelength, λ_c, apart, where $\lambda_c=U/F$. This will ensure that the flame response is 180 degrees different for the POGT system – as such, a good starting design is to take the optimized nozzle design from the DLN system and move the fuel pegs either forward or backward one convective wavelength, ΔX. In mathematical form:

Location of POGT fuel pegs relative to DLN system: $\Delta X=U_{nozzle}/2f_{instability}$

Instability Frequency	**Velocity**	**ΔX**
80	40 m/s	25 cm
200	40 m/s	10 cm
400	40 m/s	5 cm
80	80 m/s	50 cm
200	80 m/s	20 cm
400	80 m/s	10 cm

Note that these numbers are quite large and probably impractical for lower frequencies and higher nozzle velocities, but reasonable for the higher frequencies. In contrast to the gain control discussed above (which seemed a doable strategy for low frequencies), this suggests that phase control is the best option for the higher frequencies.

However, the values in the above table will be altered by the accompanying change in location in flame length and flame standoff distance for the POGT vs DLN systems. However, the corrected ΔX can be easily determined once one has a prediction for flame "center of mass" location. The key idea is to adjust the fuel peg/flame center of mass location for the POGT system such that comparable values are achieved for the convective time delay, as for the DLN system. In this way, knowledge gained from the DLN system of instability free regions can be translated over to the POGT system.

Appendix

The expressions for the higher order contributions to the flame surface response are presented below.

$$\xi_2(r,t)=\frac{1}{8(1-\alpha)^2\alpha^2 St}\left\{\begin{array}{l}2(1-\alpha)rSt\left(1+3\alpha^2\right)s_{L1}{}^2+2a(1-\alpha)s_{L2}+s_{L1}{}^2\cos\left(2St_2\left(\alpha t-1+r\right)\right)\\+\alpha^2\left(\begin{array}{l}8s_{L1}{}^2\sin\left(St_2(1-r)(1-\alpha)\right)+\left(3\alpha s_{L1}{}^2+2(1-\alpha)s_{L2}\right)\sin\left(2St(1-r-t)\right)\\-\left((3\alpha-8)s_{L1}{}^2+2(1-\alpha)s_{L2}\right)\sin\left(2St_2(1-r-\alpha t)\right)-8s_{L1}{}^2\sin\left(St_2\left((1+\alpha)(1-r)-2\alpha t\right)\right)\end{array}\right)\end{array}\right\} \quad (36)$$

and,

$$\xi_3(r,t)=\frac{1}{24(1-\alpha)^3 St_2}\sum_{j=1}^{12}\zeta_j(r,t) \quad (37)$$

where,

$$\begin{aligned}
\zeta_1&=12(1-\alpha)(1-r)St_2s_{L1}{}^3\cos\left(St_2\left((2-\alpha)(1-r)-\alpha t\right)\right)\\
\zeta_2&=3\alpha^{-1}s_{L1}St_2(1-\alpha)(1-r)\left\{\left(12\alpha^3-5\alpha^2+8\alpha-3\right)s_{L1}{}^3-2\alpha(1-\alpha)(3-4\alpha)s_{L2}\right\}\cos\left(St_2(1-r-\alpha t)\right)\\
\zeta_3&=3\alpha^{-1}s_{L1}St_2(1-\alpha)(1-r)\left\{\left(3\alpha^2-8\alpha+1\right)s_{L1}{}^2+2\alpha(1-\alpha)s_{L2}\right\}\cos\left(3St_2(1-r-\alpha t)\right)\\
\zeta_4&=-12s_{L1}{}^3St_2(1-\alpha)(1-r)\cos\left(St_2\left((a+2)(1-r)-3\alpha t\right)\right)\\
\zeta_5&=-3\sin\left(St(1-r-t)\right)\left\{\left(2-4\alpha+9\alpha^2-12a^3\right)s_{L1}{}^3+2\alpha(4-9\alpha)(1-\alpha)s_{L1}s_{L2}-6\alpha(1-\alpha)^2s_{L3}\right\}\\
\zeta_6&=\alpha\sin\left(3St(1-r-t)\right)\left\{\alpha s_{L1}{}^3(1+4\alpha)-6\alpha(1-\alpha)s_{L1}s_{L2}+2(1-\alpha)^2s_{L3}\right\}\\
\zeta_7&=3\sin\left(St_2\left((2-\alpha)(1-r)-\alpha t\right)\right)\left\{\left(6\alpha^2-18\alpha+1\right)s_{L1}{}^3+4\alpha(1-\alpha)s_{L1}s_{L2}\right\}\\
\zeta_8&=-3\sin\left(St_2(1-r-t)\right)\left\{\begin{array}{l}\left(12\alpha^3-6\alpha^2-11\alpha-1\right)s_{L1}{}^3+6\alpha(1-\alpha)(1-3\alpha)s_{L1}s_{L2}-\\6\alpha(1-\alpha)^2s_{L3}+(1-\alpha)^2(1-r)^2St_2{}^2s_{L1}{}^3\alpha^{-1}\end{array}\right\}\\
\zeta_9&=-\sin\left(3St_2(1-r-\alpha t)\right)\left\{\begin{array}{l}\left(4\alpha^3-26\alpha^2+39\alpha-3\right)s_{L1}{}^3-6\alpha(1-\alpha)(3-\alpha)s_{L1}s_{L2}+\\2\alpha(1-\alpha)^2s_{L3}-3\alpha^{-1}(1-\alpha)^2(1-r)^2St_2{}^2s_{L1}{}^3\end{array}\right\}\\
\zeta_{10}&=-3s_{L1}\sin\left(St_2\left((2+\alpha)(1-r)-3\alpha t\right)\right)\left\{\left(6\alpha^2-18\alpha+1\right)s_{L1}{}^2+4\alpha(1-\alpha)s_{L2}\right\}\\
\zeta_{11}&=3\alpha(1-\alpha)\left\{s_{L1}\left(3s_{L1}{}^2-2s_{L2}\right)\right\}\sin\left(St_2\left((2\alpha-1)(1-r)-\alpha t\right)\right)\\
\zeta_{12}&=-3\alpha s_{L1}\left((5+3\alpha)s_{L1}{}^2+2(1-\alpha)s_{L2}\right)\sin\left(St_2\left((1+2\alpha)(1-r)-3\alpha t\right)\right)
\end{aligned} \quad (38)$$

The expressions for the constituents of the non-linear transfer function up to second order in perturbation amplitude are presented below.

1. Burning area contribution

$$F_A = F_{o,A} + \varepsilon^2 F_{2,A} \tag{39}$$

Where ,

$$F_{o,A} = s_{L_1}\left\{\frac{2\alpha}{1-\alpha}\left(\frac{1-\alpha-\exp(iSt)+\alpha\exp\left(iSt/\alpha\right)}{St^2}\right)\right\} \tag{40}$$

and,

$$F_{2,A} = \frac{1}{4\alpha^4(2\alpha-1)^2(1-\alpha)^3(2-\alpha)^3 St_2^2}\sum_{j=1}^{27} A_j \tag{41}$$

where the A_j s are defined on the following page.

$$
\begin{aligned}
A_1 &= -\alpha(1-\alpha)^3\left(32\alpha^7-216\alpha^6+594\alpha^5-839\alpha^4+591\alpha^3-214\alpha^2+72\alpha-16\right)\\
A_2 &= -8\alpha\left(3\alpha^9+2\right)s_{L1}{}^3\exp\left(i\alpha St_2\right)\\
A_3 &= 336\alpha^{10}s_{L1}{}^3\exp\left(iSt_2\right)\\
A_4 &= \alpha^4(1-\alpha)(1+2\alpha)(2-\alpha)^3\,s_{L1}{}^3\exp\left(i(2\alpha-1)St_2\right)\\
A_5 &= \alpha^3(2\alpha-1)^2\left(3\alpha^4-23\alpha^3+56\alpha^2-37\alpha-10\right)s_{L1}{}^3\exp\left(i(2-\alpha)St_2\right)\\
A_6 &= -\alpha^3\left(32\alpha^8+1508\alpha^6-3748\alpha^5+5567\alpha^4-4963\alpha^3+2538\alpha^2-676\alpha+72\right)s_{L1}{}^3\exp\left(iSt_2\right)\\
A_7 &= \alpha^2\left(156\alpha^7-330\alpha^6+113\alpha^5+552\alpha^4-948\alpha^3+778\alpha^2-396\alpha+120\right)s_{L1}{}^3\exp\left(i\alpha St_2\right)\\
A_8 &= 2\alpha^2(2-\alpha)(1-\alpha)^3\left(12\alpha^5-24\alpha^4-44\alpha^3+103\alpha^2-52\alpha+8\right)s_{L1}s_{L2}\\
A_9 &= 48\alpha^{10}s_{L1}s_{L2}\exp\left(i\alpha St_2\right)\\
A_{10} &= 120\alpha^{10}s_{L1}s_{L2}\exp\left(iSt_2\right)\\
A_{11} &= -2\alpha^5(1-\alpha)(2-\alpha)^3\,s_{L1}s_{L2}\exp\left(i(2\alpha-1)St_2\right)\\
A_{12} &= 2\alpha^4(1-\alpha)(2-\alpha)(3-\alpha)(2\alpha-1)^2\,s_{L1}s_{L2}\exp\left(i(2-\alpha)St_2\right)\\
A_{13} &= -6\alpha^3\left(4\alpha^8-3\alpha^6+208\alpha^5-549\alpha^4+656\alpha^3-408\alpha^2+128\alpha-16\right)s_{L1}s_{L2}\exp\left(iSt_2\right)\\
A_{14} &= -2\alpha^2\left(188\alpha^7-566\alpha^6+789\alpha^5-419\alpha^4-136\alpha^3+264\alpha^2-112\alpha+16\right)s_{L1}s_{L2}\exp\left(i\alpha St_2\right)\\
A_{15} &= -6\alpha^3(2\alpha-1)^2(1-\alpha)^3(2-\alpha)^3\,s_{L3}\\
A_{16} &= -24\alpha^{10}s_{L3}\exp\left(i\alpha St_2\right)\\
A_{17} &= -216\alpha^{10}s_{L3}\exp\left(iSt_2\right)\\
A_{18} &= 6\alpha^4\left(4\alpha^7+133\alpha^5-260\alpha^4+289\alpha^3-182\alpha^2+60\alpha-8\right)s_{L3}\exp\left(iSt_2\right)\\
A_{19} &= 6\alpha^3\left(4\alpha^2-5\alpha+2\right)\left(9\alpha^4-22\alpha^3+33\alpha^2-20\alpha+4\right)s_{L3}\exp\left(i\alpha St_2\right)\\
A_{20} &= -2i\alpha^2(2-\alpha)(2\alpha-1)(1-\alpha)^4\left(2\alpha^3-7\alpha^2+8\alpha+2\right)s_{L1}{}^3St_2\\
A_{21} &= 48i\alpha^{11}s_{L1}{}^3St_2\exp\left(iSt_2\right)\\
A_{22} &= 2i\alpha^3(1-\alpha)(2-\alpha)(3-\alpha)(2\alpha-1)^2\,s_{L1}{}^3St_2\exp\left(i(2-\alpha)St_2\right)\\
A_{23} &= -i\alpha^2\left(404\alpha^8-1388\alpha^7+2537\alpha^6-2727\alpha^5+1809\alpha^4-717\alpha^3+118\alpha^2+20\alpha-8\right)s_{L1}{}^3St_2\exp\left(iSt_2\right)\\
A_{24} &= 4i\alpha^3(1+\alpha)(2\alpha-1)(2-\alpha)^2(1-\alpha)^4\,s_{L1}s_{L2}St_2\\
A_{25} &= -32i\alpha^{11}s_{L1}s_{L2}St_2\exp\left(iSt_2\right)\\
A_{26} &= 2i\alpha^3\left(156\alpha^7-640\alpha^6+1439\alpha^5-1936\alpha^4+1595\alpha^3-786\alpha^2+212\alpha-24\right)s_{L1}s_{L2}St_2\exp\left(iSt_2\right)\\
A_{27} &= \alpha^2(1-\alpha)^2(2\alpha-1)^2(2-\alpha)^3\,s_{L1}{}^3St_2^2\exp\left(iSt_2\right)
\end{aligned}
\tag{42}
$$

2. Mass Burning Rate contribution

$$F_{s_L-A} = F_{o,s_L-A} + \varepsilon^2 F_{2,s_L-A} \tag{43}$$

Where,

$$F_{o,s_L-A} = F_{o,s_L-A} = s_{L1}\left\{\frac{2}{St^2}\left(1+iSt-\exp\left(iSt\right)\right)\right\} \tag{44}$$

and,

$$F_{2,s_L-A} = -\frac{1}{4\alpha^2(1-2\alpha)^2(1-\alpha)^2(2-\alpha)^3 St_2^2}\sum_{j=1}^{16} S_j \tag{45}$$

where,

$$\begin{aligned}
S_1 &= -2\alpha(1-\alpha)^2\left(8\alpha^5-44\alpha^4+91\alpha^3-102\alpha^2+60\alpha-10\right){s_{L1}}^3\\
S_2 &= 2\alpha^2(1-\alpha)(2-\alpha)^3{s_{L1}}^3\exp\left(iSt_2(2\alpha-1)\right)\\
S_3 &= \alpha(2\alpha-1)^2\left(3\alpha^3-14\alpha^2+12\alpha+4\right){s_{L1}}^3\exp\left(i(2-\alpha)St_2\right)\\
S_4 &= 4\alpha^2\left(4\alpha^6-24\alpha^5+45\alpha^4-13\alpha^3-42\alpha^2+36\alpha+8\right){s_{L1}}^3\exp\left(iSt_2\right)\\
S_5 &= 3\alpha(2-\alpha)^3(2\alpha-1)^3{s_{L1}}^3\exp\left(i\alpha St_2\right)\\
S_6 &= 2(2-\alpha)(1-\alpha)^3\left(8\alpha^4-48\alpha^3+95\alpha^2-48\alpha+8\right)s_{L1}s_{L2}\\
S_7 &= -2\alpha^2(1-\alpha)(2-\alpha)^3 s_{L1}s_{L2}\exp\left(i(2\alpha-1)St_2\right)\\
S_8 &= -2\alpha^2(1-\alpha)(2-\alpha)(2\alpha-1)^2 s_{L1}s_{L2}\exp\left(i(2-\alpha)St_2\right)\\
S_9 &= 4\alpha^2(1-\alpha)(2\alpha-1)^3(2-\alpha)^3 s_{L1}s_{L2}\exp\left(iSt_2\right)\\
S_{10} &= 4(1-\alpha)(3\alpha-1)(2\alpha-1)^2(2-\alpha)^3 s_{L1}s_{L2}\exp\left(i\alpha St_2\right)\\
S_{11} &= -6(1-\alpha)^2(2\alpha-1)^2(2-\alpha)^3 s_{L3}\\
S_{12} &= 6(1-\alpha)^2(2\alpha-1)^2(2-\alpha)^3 s_{L3}\exp\left(i\alpha St_2\right)\\
S_{13} &= -2i\alpha(2-\alpha)(2\alpha-1)(1-\alpha)^2\left(2\alpha^3-10\alpha^2+11\alpha-1\right){s_{L1}}^3 St_2\\
S_{14} &= -2i\alpha(1-\alpha)(2-\alpha)(2\alpha-1)^2{s_{L1}}^3 St_2\exp\left(i(2-\alpha)St_2\right)\\
S_{15} &= -2i\alpha(2\alpha-1)(1-\alpha)^2(2-\alpha)^2 s_{L1}s_{L2}St_2\\
S_{16} &= -6i\alpha(1-\alpha)^2(2\alpha-1)^2(2-\alpha)^3 s_{L3}St_2
\end{aligned} \tag{46}$$

3. Heat of reaction contribution

$$F_{h_R-A} = F_{o,h_R-A} + \varepsilon^2 F_{2,h_R-A} \tag{47}$$

where,

$$F_{o,h_R-A} = h_{R1}\left\{\frac{2}{St^2}\left(1+iSt-\exp\left(iSt\right)\right)\right\} \tag{48}$$

and,

$$F_{2,h_R-A} = -\frac{1}{4\alpha^2(1-2\alpha)^2(1-\alpha)^2(2-\alpha)^3 St_2^2}\sum_{j=1}^{19} H_j \tag{49}$$

where,

$$
\begin{aligned}
H_1 &= -6(1-\alpha)^2(2\alpha-1)^2(2-\alpha)^3 h_{R3} \\
H_2 &= 6(1-\alpha)^2(2\alpha-1)^2(2-\alpha)^3 h_{R3}\exp(i\alpha St_2) \\
H_3 &= -2\alpha(1-\alpha)^2(8\alpha^2-12\alpha+3)(2-\alpha)^3 h_{R2}s_{L1} \\
H_4 &= -4\alpha^2(1-\alpha)(1-2\alpha)^2(2-\alpha)^3 h_{R2}s_{L1}\exp(iSt_2) \\
H_5 &= 6\alpha(1-\alpha)(1-2\alpha)^2(2-\alpha)^3 h_{R2}s_{L1}\exp(i\alpha St_2) \\
H_6 &= -2\alpha^2(1-\alpha)(2-\alpha)^3 h_{R2}s_{L1}\exp(i(2\alpha-1)St_2) \\
H_7 &= -2\alpha(1-\alpha)^2(8\alpha^5-44\alpha^4+91\alpha^3-102\alpha^2+60\alpha-10)h_{R1}{s_{L1}}^2 \\
H_8 &= \alpha(1-2\alpha)^2(3\alpha^3-14\alpha^2+12\alpha+4)h_{R1}{s_{L1}}^2\exp(i(2-\alpha)St_2) \\
H_9 &= -4\alpha^2(1+\alpha)(1-2\alpha)^2(2-\alpha)^3 h_{R1}{s_{L1}}^2\exp(iSt_2) \\
H_{10} &= 3\alpha(2-\alpha)^3(2\alpha-1)^3 h_{R1}{s_{L1}}^2\exp(i\alpha St_2) \\
H_{11} &= 2\alpha^2(1-\alpha)(2-\alpha)^3 h_{R1}{s_{L1}}^2\exp(iSt_2(2\alpha-1)) \\
H_{12} &= 2(2-\alpha)(1-\alpha)^2(2\alpha-1)^2(3\alpha^2-12\alpha+8)h_{R1}s_{L2} \\
H_{13} &= -2\alpha^2(1-\alpha)(2-\alpha)(2\alpha-1)^2 h_{R1}s_{L2}\exp(i(2-\alpha)St_2) \\
H_{14} &= 2(1-\alpha)(3\alpha-2)(2\alpha-1)^2(2-\alpha)^3 h_{R1}s_{L2}\exp(i\alpha St_2) \\
H_{15} &= -6i\alpha(1-\alpha)^2(2-\alpha)^3(2\alpha-1)^2 h_{R3}St_2 \\
H_{16} &= 4i\alpha^2(2\alpha-1)(1-\alpha)^2(2-\alpha)^3 h_{R2}s_{L1}St_2 \\
H_{17} &= -2i\alpha(2\alpha-1)(2-\alpha)(1-\alpha)^2(2\alpha^3-10\alpha^2+11\alpha-1)h_{R1}{s_{L1}}^2St_2 \\
H_{18} &= -2i\alpha(1-\alpha)(2-\alpha)(2\alpha-1)^2 h_{R1}{s_{L1}}^2St_2\exp(i(2-\alpha)St_2) \\
H_{19} &= -2i\alpha(3\alpha-4)(1-\alpha)^2(2-\alpha)^2(2\alpha-1)^2 h_{R1}s_{L2}St_2
\end{aligned}
\tag{50}
$$

4. Nonlinear s_L-h_R interaction contribution

$$
F_{s_L-h_R-A} = \varepsilon^2 F_{2,s_L-h_R-A} \tag{51}
$$

where,

$$
F_{2,s_L-h_R-A} = -\frac{1}{2\alpha^2(1-\alpha)(2\alpha-1)^2 St_2^2}\sum_{j=1}^{11} T_j \tag{52}
$$

and,

$$
\begin{aligned}
T_1 &= 3\left(4\alpha^3 - 8\alpha^2 + 5\alpha + 1\right) h_{R2} s_{L1} \\
T_2 &= 3(1-\alpha)(2\alpha-1)^2 h_{R2} s_{L1} \exp(i\alpha St_2) \\
T_3 &= -\alpha(1-\alpha)\left(8\alpha^2 - 12\alpha + 3\right) h_{R1} {s_{L1}}^2 \\
T_4 &= -2\alpha^2 (2\alpha-1)^2 h_{R1} {s_{L1}}^2 \exp(iSt_2) \\
T_5 &= -\alpha^2 h_{R1} {s_{L1}}^2 \exp\left(i(2\alpha-1)St_2\right) \\
T_6 &= 3\alpha(2\alpha-1)^2 h_{R1} {s_{L1}}^2 \exp(iSt_2) \\
T_7 &= -3(1-\alpha)(2\alpha-1)^2 h_{R1} s_{L2} \\
T_8 &= 3(1-\alpha)(2\alpha-1)^2 h_{R1} s_{L2} \exp(i\alpha St_2) \\
T_9 &= -3i\alpha(1-\alpha)(2\alpha-1)^2 h_{R2} s_{L1} St_2 \\
T_{10} &= 2i\alpha^2 (1-\alpha)(2\alpha-1) h_{R1} {s_{L1}}^2 St_2 \\
T_{11} &= -3i\alpha(1-\alpha)(2\alpha-1)^2 h_{R1} s_{L2} St_2
\end{aligned}
\tag{53}
$$

References

[1] M. Fleifil, A. M. Annaswamy, Z. A. Ghoneim, and A. F. Ghoneim, "Response of a laminar premixed flame to flow oscillations: A kinematic model and thermoacoustic instability results", *Combustion and Flame*, Vol. 106, 1996, pp. 487, 510.

[2] S. Ducruix, D. Durox, S. Candel, "Theoretical and experimental determination of the transfer function of a laminar premixed flame", *Proceedings of the Combustion Institute*, Vol. 28, 2000, pp. 765-773.

[3] E. J. Gutmark, T. P. Parr, D. M. Parr, J. E. Crump and K.C. Schadow, "On the role of large and small scale structures in combustion control", *Combustion Science and Technology* , Vol. 66, 1989, pp. 167-186.

[4] J. C. Broda, S. Seo, R. J. Santoro, G. Shirhattikar, V. Yang, "Experimental study of combustion dynamics of a premixed swirl injector", *Proceedings of the Combustion Institute*, Vol. 27, 1998, pp. 1849-1856.

[5] T. Schuller, D. Durox and S. Candel, "Dynamics of noise radiated by a perturbed impinging premixed jet flame", *Combustion and Flame*, Vol. 128, 2002, pp. 88-110.

[6] T. Lieuwen, B. T. Zinn, "The role of equivalence ratio oscillations in driving combustion instabilities in low NOX gas turbines", *Proceedings of the Combustion Institute*, Vol. 27, 1998, p. 1809-1816.

[7] D. L. Straub, G. A. Richards, "Effect of fuel nozzle configuration on premix combustion dynamics", *ASME* paper 98-GT-492, 1998.

[8] T. Lieuwen, H. Torres, C. Johnson, B. T. Zinn, "A mechanism of combustion instability in lean premixed gas turbine combustor", *Journal of Engineering in Gas Turbines and power*, Vol. 120, 1998, pp. 294-302.

[9] G. A. Richards, M. C. Janus, "Characterization of oscillations during premix gas turbine combustion", *Journal of Engineering for Gas Turbines and Power*, Vol. 120, 1998, pp. 294-302.

[10] D. W. Kendrick, T. J. Anderson, W. A. Sowa, T. S. Snyder, "Acoustic sensitivities of lean-premixed fuel injector in a single nozzle rig", *Journal of Engineering for Gas Turbines and Power*, Vol. 121, 1999, pp. 429-436.

[11] R. Mongia, R. Dibble, J. Lovett, "Measurement of air-fuel ratio fluctuations caused by combustor driven oscillations", *ASME* paper 98-GT-304, 1998.

[12] D. S. Lee, T. J. Anderson, "Measurements of Fuel/Air-Acoustic coupling in lean premixed combustion system", *AIAA* paper # 99-0450, 1999

[13] A. P. Dowling, "Thermoacoustic Instability", 6th International Congress on Sound and Vibration, July 1999, pp. 3277-3292.

[14] A. Putnam, Combustion Driven, Oscillations in Industry, Elsevier, New York, 1971.

[15] W. Krebs, P. Flohr, B. Prade and S. Hoffman, "Thermoacoustic instability chart for high-intensity gast turbine combustion systems", *Combustion Science and Technology*, Vol 174, No. 7, 2002,
pp. 99-128.

[16] S. Hubbard, A. P. Dowling, "Acoustic instabilities in premix burners", *AIAA* paper # 98-2272, 1998.

[17] A. P. Dowling and S. Hubbard, "Instability in lean premix combustors", *Proceeding of the Institute of Mechanical Engineers*, Vol. 214(A), 2000, 317-332.

[18] R. K. Prashant, A. M. Annaswamy, J. P. Hathout and A. F. Ghoniem, "When do Open-loop Strategies for Combustion Control Work?", *Journal of Propulsion and Power*, Vol. 18, No. 3, 2002, pp. 658-668.

[19] Simon. R. Stow and A. P. Dowling, "Low order modeling of thermoacoustic limit cycles", *ASME* paper # GT2004-54245.

[20] J. H. Cho and Tim Lieuwen, "Laminar premixed flame response to equivalence ratio oscillations", *Combustion and Flame*, Vol. 140, 2005, pp. 116-129.

[21] J.K. Rabovitser, M.J. Khinkis, R.L. Bannister and F.Q. Miao, "Evaluation of thermochemical recuperation and partial oxidation concepts for natural gas-fired advanced turbine systems", ASME paper #96-GT-290.

[22] Preetham and Tim Lieuwen, "Nonlinear Flame-flow transfer function calculations: Flow disturbance celerity effects, Part II", 2005. *AIAA paper* #2005-0543.

[23] G.H. Markstein, "Non-steady flame Propagation", Pergamon, New York, 1964.

[24] R. Lauvergne and F. N. Egolfopoulos, "Unsteady response of C_3H_8/Air laminar premixed flames submitted to mixture composition oscillations", Proceedings of the Combustion Institute, volume 28, 2000, pp. 1841-1850.

[25] R. Sankaran and H. G. Im, "Dynamic Flammability Limits of Methane/Air Premixed Flames with Mixture Composition Fluctuations", Proceedings of the Combustion Institute, v. 29, n. 1, 2002, pp. 77-84.

[26]Todd F. Dupont and Yingjie Liu, "Back and Forth Error Compensation and Correction Methods for Semi-Lagrangian Schemes with Application to Level Set Interface Computations", *Mathematics of Computation*, 76 (2007), pp 647--668.

[27] Peng, D., Merriman, B., Osher, S., Zhao, H., Kang, M., "The local level-set Method", 1996, *J. Comput. Phys*., 155, pp. 410-438.

[28] Smereka, P., 2006, "Numerical approximations of a delta function", *Journal of Computational Physics*, 211, 77-90

[29] G.M. Abu-Orff, R. S. Cant, in: Proceedings of the Joint Spanish, Portuguese, Swedish and British sections of the Combustion Institute, Maderia, 1996.

[30] Lieuwen, T. "Nonlinear Kinematic Response of Premixed Flames to Harmonic Velocity Disturbances",Proceedings of the Combustion Institute, Volume 30, 2004

[31] N. Peters, "Turbulent Combustion", Cambridge University Press, Cambridge, UK, 2000.

[32] C. J. Sung, C. J. Sun and C. K. Law, "Analytic Description of the Evolution of Two-Dimensional Flame Surfaces", Combustion and Flame, 107, 1996, pp. 114-124.

[33] Figura, L., Lee, J.G., Quay, B.D. and D.A. Santavicca, "The Effects of Fuel Composition on Flame Structure and Combustion Dynamics in a Lean Premixed Combustor," ASME Paper #. GT2007-27298.

Appendix D – Preliminary Market Assessment of the Partial Oxidation Gas Turbine (POGT) for Oil Refinery Hydrogen and Power Applications

Presentation by SFA Pacific, Inc.

Preliminary Market Assessment of the Partial Oxidation Gas Turbine (POGT) for Oil Refinery Hydrogen and Power Applications

For:

Gas Technology Institute (GTI)

March 20, 2009

By

Dale Simbeck

SFA Pacific, Inc.

444 Castro Street, Suite 720

Mountain View, California 94041

E-mail: simbeck@sfapacific.com

Phone: 650-969-8876

Outline

Objective

Background

- **POGT concept**
- **Refinery hydrogen and power requirements**
- **Existing refinery competition**
  - **Hydrogen – steam methane reforming (SMR)**
  - **Steam and Power**

Integration challenges

Best applications

Conclusions

Objective

Preliminary analysis of market potential for oil refinery hydrogen and cogeneration power via POGT system

Minimal time and budget of only about a 15 days effort

Market overview of “on-purpose” refinery hydrogen and electricity requirements

Address potential market changes and enabling technologies that could enhance the POGT process potential

The POGT Concept Is Interesting

Use existing gas turbine to: (1) compress the oxidant (air) in the GT air compressor, (2) convert NG, H2O & oxidant to syngas (H2 & CO) in a now partial oxidation modified combustor and (3) cool the resulting hot raw syngas via direct GT turbo expander to generate net shaft power

Benefit:

- **Should be much smaller & hopefully more effective than traditional alternative of separate steam methane reforming (SMR) for H2 & steam boiler/ST or GT for power generation**
- **Indirect heat transfer to the highly exothermic SMR reaction requires expensive reactor tubes & large heat transfers, the POGT is direct reaction heating to even higher temperatures**
- **SMR are relatively expensive (traditional unit cost as $ per scf/d H2 of $1-2 per scf/d at 100 MM scf/d scale) & much high unit capital costs and lower efficiency at small scale**

The Basic POGT Concept Is Not New

- **Another GT vendors did some analysis & development of this concept in the 1980s - unclear what is public, thus nameless**
- **From non-confidential discussions with retiree involved in that work, was oxygen-blown, catalyst autothermal reforming (ATR) type PO in the modified GT combustion**
  - **Thus, likely for large H2 applications (due to needed economics of scale for O2) but also more radical existing GT modifications**
  - **Oxygen operating reduce the total power for oxidant compression (only 5 atm air to ASU cold box + just small mass O2 compressor to 20-40 atm), but also reduces the mass flow of turbo-expander**
  - **As this GT vendor also has aero-derivative GT, may have investigated GTs for higher pressure aero PO, variable speed multi shaft flexibility & final syngas to a moderate pressure after just the high pressure aero type turbo-expander**
- **The O2 option greatly simplify the H2 purification and pressure challenges facing of POGT concept applications**

Oil Refinery Overview

Oil refining is ultra conservative & generally resist change

- Should not be confused with oil E&P which makes the money + appreciate & support risks vs. big rewards of new technologies
- Generally oil refinery managers get few rewards for successful tech risks but sever punishment for failures or lost availability
- Volatile oil prices makes oil refiners even more conservative

Every oil refinery is slightly different relative to design, size, products & feedstock – nevertheless, clear trends:

- Crude oil supplies continues to get heavier (lower API gravity) & higher in: sulfur, acids, metals & Conradson carbon residue-CCR
- Increasing light-to-heavy crude oil price differential & long-term higher oil prices due to developing nations ever increasing use
- Cleaner transportation fuels, lower: sulfur, nitrogen & aromatics
- Increasing jet & especially diesel fuel use in Europe
- Decreasing residue oil markets, especially for power generation

Oil Refinery Overview - continued

Oil refiners are slowly but surely moving into more electric power generation, including sales to the grid

- **Traditionally very fearful of power gen due to it being the most regulated energy industry sector**
- **However, oil industry is a lot of things and move slowly, but are very smart and understands long-term trends toward power gen**
  - **Electricity is the future as its use steadily grows faster than oil**
  - **Increasing % of remaining world oil is government owned where big oil has limited options for good profit margins in its utilization**
- **Change started with electric deregulation & generally in the oil company NG marketing (not oil refining) to expand NG sales**
- **Some oil refineries have moved into cogen with excess power sales due to cogen incentives – like PURPA in 1980s in U.S.**
- **Now most major oil and NG companies have power gen groups plus strategic appreciation of increasing importance of electricity to their long-term energy business**

Oil Refinery – Utilities

Assume unit capacity 100,000 bbl/d refinery feed reference

- Internal electric power needs (assuming no ST drivers) is about 6-12 kWh/bbl or 25-50 MWe for 100,000 bbl/d feed depending on refinery complexity & crude quality (higher for heavy crude oil)
- Extreme case is Canadian oil sands steam assisted gravity drain (SAGD) production with field upgrading to just light bottomless syncrude at about 100 MWe per 100,000 bbl/d feed plus an additional 20-30 MWe for simple refining to final products (pipelines can be short or long if to US refineries & sometimes GT or ST pipeline pump drives)

The general trend is away from “on-purpose” steam boilers

- Big energy use is NG & refinery gas fired heaters for radiant heat transfer & steam gen as waste heat recovery convection section
- Note: the main crude oil fired heater can be half of the entire internal oil refinery energy followed by many increasingly smaller fired heaters

Oil Refinery – Utilities

Relative to overall oil refinery energy flow, utilities are small even for a complex relatively "white" CA oil refinery

- **100,000 bbl/d crude oil in = 7,100 MWt**
- **NG in of 47 MM scf/d for fuel & H2 = 575 MWt**
- **Electricity in if none make onsite = 35 MWe**
- **Net products out (including petcoke) 6,600 MWt or 86% effic.**

Above assumes:

- **Vacuum distillation residue of 58,000 bbl**
- **Coker feed 26,000 bbl of vacuum residue making 1,160 t/d of coke**
- **Heavy oil markets limited to just bunker C fuel oils for ocean ships**
- **Consume 70 MM scf/d of "made" hydrogen + all the byproduct H_2**
  - **Total H_2 about 1,000 scf/bbl with "on-purpose" H_2 of 700 scf/bbl**
- **Consume 47 MM scf/d natural gas + all the byproduct refinery gas**

Energy Balance of an Almost "White" California Oil Refinery based on 100,000 bbl/d in COE units

Refiners flows in bbl/d & energy in crude oil equivalent or COE units

Inputs in crude oil equivalents (COE) of 5.8 MM Btu per bbl

- **100,000 bbl/d heavy low quality crude oil at >$40/bbl (currently)**
- **8,000 bbl/d COE NG at >$30/bbl COE or 47 MM scf/d >$5.00 MM Btu**
  - **5,000 bbl/d COE NG or 29 MM scf/d NG (feed & fuel) for 70 MM scf/d H_2**
  - **3,000 bbl/d COE NG or 18 MM scf/d NG as refinery fuel with refinery gas**
- **500 bbl/d COE electric power or 35 MWe at 8 cents/kWh or $135/bbl COE**

Outputs from a total of 108,500 bbl/d COE fuel inputs

- **51,000 bbl/d COE gasoline or 56,000 bbl/d actual**
- **25,000 bbl/d COE jet & diesel or 27,000 bbl/d actual**
- **11,000 bbl/d COE others - olefins, LPG, asphalt & bunker C fuel oil**
- **6,000 bbl/d COE petcoke or 1,160 t/d fuel grade at 30 MM Btu/t & the only low value product at normally 70% of high sulfur coal Btu prices**

Internal energy used NG & electricity + in-refinery recovered heat & fuel gas of 4,000 bbl/d + heat loses for total energy of 15,500 bbl/d COE

Oil Refinery – Utilities Continued

Large cogen potential in oil refineries due to the mostly indirect heat transfer to heat & distill liquids

- **Moderate to large low pressure steam demand for distillation**
- **Many fired heaters for liquids to maximum temperatures of 900°F**

However effective refinery cogen requires baseload power sales to the grid at fair prices (the traditional electric utility's worst nightmare) & innovation refinery changes (the oil refinery manager's worst nightmare) – examples:

- **Flue gas to feed air heat exchangers on major fired heaters to reduced steam make & create need for GT cogen LP steam make**
- **NG fired GT cogen power with hot raw GT exhaust gas (still 12% O2) directly used as oxidant with NG fired crude oil heaters**
  - **Shell Oil has this in their Pernis refineries likely the "whitest", most complex & most innovative oil refinery in Europe**
  - **More conservative variations of this used is at least 2 other European oil refineries where effective cogen power sales to the grid is acceptable**

Oil Refinery – Hydrogen

Increasingly the life-blood of a modern oil refinery

- Increasing demand for more & cleaner transportation “white” products while declining demand for heavy fuel oil “black” products (less fuel oil based power gen, only bunker C fuels)
- Crude oil supplies to get heavier and higher in sulfur
- Cleaner transportation fuel also mean lower aromatics & sulfur thus less by-product H2 from naphtha reforming to more aromatics

Assume unit capacity 100,000 bbl/d refinery feed

- On-purpose H2 from 250-1,000 scf H2/ bbl or 25 to 100 MM scf/d H2 depending on refinery complexity, use of coking & crude oil
- Heavy oil sands 50% residue to coking) at about 1,000 scf/bbl to just a light bottomless syncrude or 1,500 to final refinery products
- Extreme case very heavy crude oil or oil sands with sever residue hydrocracking (like new Eni slurry phase) at about 2,000 scf H2/bbl residue feed or about 1,500 - 2,000 scf overall to final refinery products depending on percent of crude oil that is residues

Oil Refinery – Hydrogen continued

High oil prices & high light-to-heavy oil price differential could drive refinery H2 demand to extremely high levels

- **Sever residue hydrocracking compared to coking can significantly increase the liquid product yield per barrel oil feed**
  - **Example, Valero (world's biggest oil refiner) in 2008 proposed the biggest oil refinery H2 project in the world – 450 MM scf/d via pet coke gasification for increased hydrocracking to clean diesel**
  - **However, recent oil price drop and increasing recession could delay or force cancellation of this type very capital intensive hydrocracking and big H2 gasification project**

On the other hand, continuing oil price and light-to-heavy oil price volatility could promote the <u>opposite</u>

- **Small "as needed" H2 production additions to minimize risk with "just in time" small modular H2 units based on NG could become a major advantage and excellent market potential for POGT**

Oil Refinery – Hydrogen Specification

Typically 99.9% H2 purity and 300-400 psig pressure

- **NG-SMR with PSA sets the H2 market specification standard with the view it is hopeless to try to sell at lower purity or pressure**

High purity H2 via use of a PSA is a win-win

- **Reduces the H2 loses and purge H2 recovery costs in most oil refiner H2 utilization processes**
  - **This is because many hydrotreating processes of liquids rely on relatively constant high H2 partial pressure with large H2 recycle**
  - **Some light end gases (C1-C3) are formed in the hydrotreating processes, forcing some purge from the recycle H2**
  - **High purity make-up H2 reduces the purge H2 losses/recovery**
- **Reduces the SMR costs and complexity**
  - **The PSA enables elimination of the CO2 amine scrubber/stripper & a second stage of CO shifting of the raw H2 leaving the SMR**
  - **The PSA's low pressure purge gas (containing all the C1, CO & CO2 + 10% of the gross H2) is effectively used as part of the fuel gas to fire the big SMR fired heater (can 2 stage PSA for higher net H2 yield)**

Refinery H2 Cost Comparison Simple Screening Estimates for Large Units

- **Coke & pitch gasification vs SMR only practical as large sizes**
- **At small scale only NG option but also higher H2 costs for any assumed NG price than for this large H2 unit estimate**
- **Capital—$2006 & various location factor vs. U.S. Gulf Coast**
- **Capital charge rate—20% of total capital per year (5 year simple capital payback) and a 90% annual load factor**
- **7% per year of capital for non-fuel O&M**
- **High sulfur coke price set at $1/million (MM) Btu for baseline then**:
  - **Natural gas price varied to "breakeven" price where cost of SMR H_2 is the same as coke H_2 (including capital charges)**
  - **Pitch price varied to "breakeven" price where cost of pitch H_2 is the same as coke and SMR H_2 (including capital charges)**

Results from SFA Pacific Baseline Case

Feedstock Options:	Natural Gas	Pitch	Coke
Capital cost	base of $1.40/scf/d H2	x 2.2	x 2.7

Feedstock "breakeven" price for same H_2 cost ($1.52/kg or $3.70/1,000 scf) @ 125% of U.S. Gulf Coast location factor & 2006 dollars

Price $/MM Btu	$6.60	$2.40	$1.00 baseline
Feed rate mt/hr	60.2	98.1	117.0 (dry)
Hydrogen in feed mt/hr	12.1	8.1	4.1

- Pitch contains twice as much hydrogen as coke to make the same amount of H_2
- Pitch could be feed to cokers for increased distillates

For small 6 MM scf/d NG-SMR designs we estimate about $6/1,000 scf H2 for same economics basis

- Increase mainly due to 2.5 time higher unit capital costs of 6 MM scf/d vs 2x100 MM scf/d size SMR

"Breakeven" Natural Gas and Pitch Prices vs. Same H_2 Costs as from $1/MM Btu Coke

Feedstock

$/MM Btu (HHV)

Note – for large 200 MM scf/d H2 plant where gasification become an alternative to NG - SMR

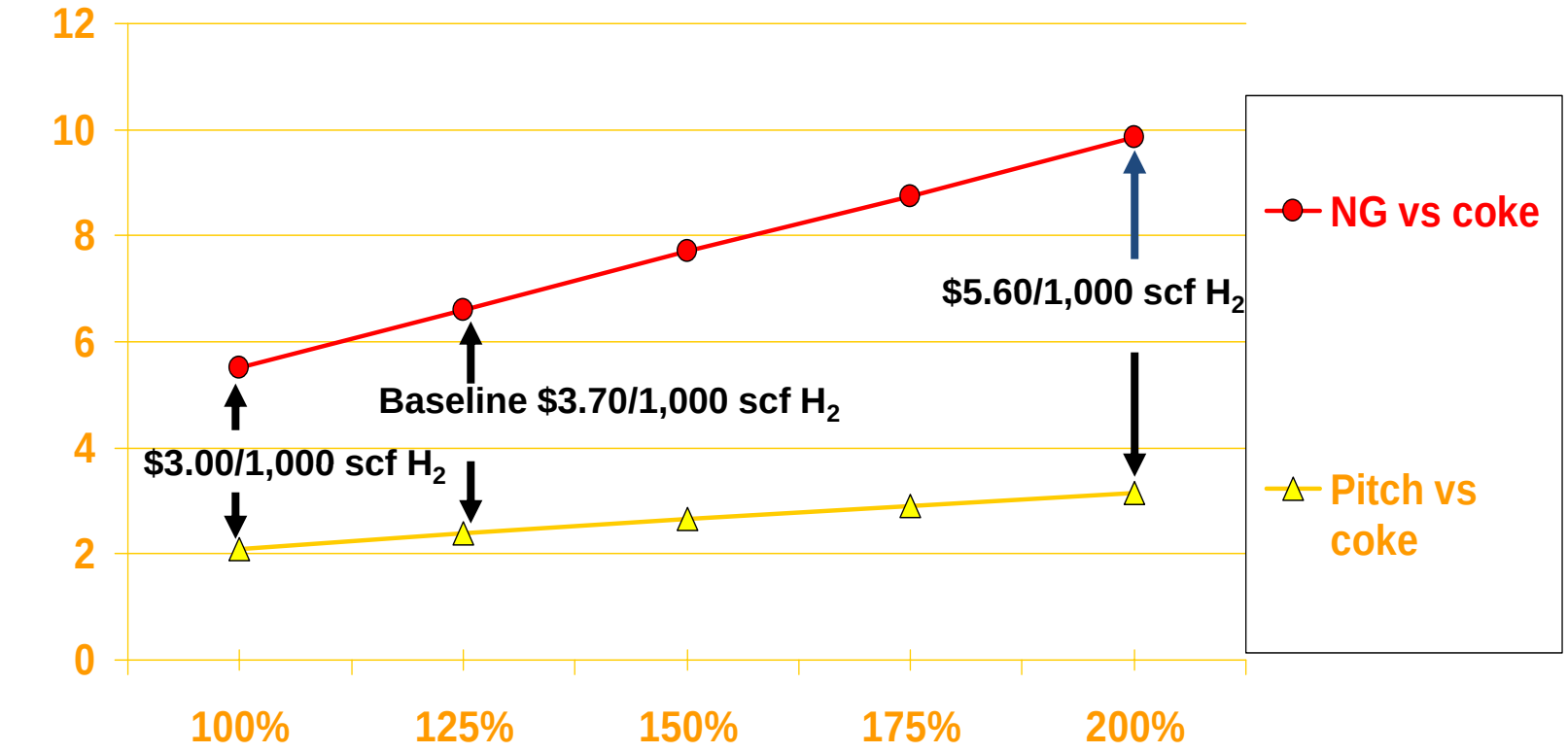

Site Specific Location Factor – % of U.S. Gulf Coast Construction Costs

Source: SFA Pacific derived from *2007 Gasification Multisponsored Analysis*

Air-Blown POGT Challenges

Meeting the industry SMR with PSA high H2 purity and moderate pressure standards

- Highly questionable market unless meeting this standard
- Likely require big re-compression of the N2 & H2 mixture for big PSA plus finding an effective use of the ultra-low energy content (H2 loses with mostly N2) in the PSA low pressure fuel gas
  - Unclear if this could be competitive with traditional SMR or even the O2-blown POGT alternatvie

Competing with the relatively low U.S. electric power prices

- Baseload power costs in most area of the U.S. are very low due to 70% of total electricity from mostly paid-off coal and nuclear power plants with low operating (mostly fuel) costs
  - Effectively blocking de-regulation and new high cleaner, more efficiency power options that have added costs of capital charges as well as the higher NG fuel costs

CO2 capture favors big O2-blown & maybe CO2 recycle

Suggested POGT Oil Refinery Applications Market Strategy

- **Consider integrating POGT with advanced metallic ionic membranes to more effective generate high-purity H2**
  - **Perhaps with the high temperature PO combustor so the high purity H2 is also produced at pressure**
    - **Perhaps fired heater applications for the low pressure and lower energy content fuel gas after the membrane & turbo-expander**
    - **May even consider a second stage to totally combustion of the remaining low energy content fuel gas after the membrane**
- **Consider standard small modular unit Size set by the specific GT to be modified to POGT**
- **Focus on areas without cheap old baseload coal power**
- **Perhaps look at air-blown POGT for applications where there is demand for both H2 & N2**
  - **However PSA or cryogenic separation favors feed at pressure**

Suggested POGT Oil Refinery Applications Market Strategy

Consider areas where baseload cogen power can be sold into the grid at a fair price (at least the power costs from a new NGCC with capital charges & same NG price)

- **Like the European GT hot 12% O2 flue gas to fire the big crude oil unit, except with POGT even better**
- **POGT with advanced metallic H2 membrane can feed NG with some of NG converted and recovered as H2 plus the remaining fuel gas expanded then used to fire the big crude oil heater**
  - **Could vary the size and H2/power/fuel gas amounts plus always use just NG to blend or totally fire the all important crude oil heater**

Use POGT effectively switch between NG to H2 & electricity based on time of day electric rates

- **This would help industrial gas companies with H2 pipelines where there is back-up and pipeline packing potential**

Suggested Companies and Contacts

Shell Oil

- Shell Hydrogen is looking for small NG to H2 ventures, have already done JVs for small H2 generators like HydrogenSource
- Shell Oil appears to have done work on an advanced small NG to H2 generator utilizing metallic membranes to separate the H2
- Shell and Statoil did pilot plant JV on integrated NG SOFC and SOFC as ionic transport membrane (ITM) for O2 – perhaps integrate GT with ITM for small oxygen-fired POGT

Hydro-Chem

- U.S. Linde owned company that specialized in small, pre-fab, skid-mounted NG based H2 units for chemical & metal industries
- Many units sold to other industrial gas companies

CB&I

- Owns Howe-Baker with good experience in both H2 refinery unit design/construction and small modular NG based SMR units

Suggested Companies and Contacts

Air Products & Chemicals

- Now making it own small H2 units via recent purchase of Harvest Energy Technology (x-KTI people)
- World's leading developer of the ironic transport membrane (ITM) for O2 & syngas from NG – perhaps integrate GT with ITM for small oxygen-fired POGT or better ITM to O2 design

Any of the other start-ups (still alive) promoting small H2 generators – generally for PEM fuel cells

- Companies such as: HyRadix (UOP & Sud Chemie JV), ZTEK, H2 Gen, HydrogenSource, Membrane Reactor Technologies, ect.
- However most of these companies are looking for a sugar daddy as small H2 & PEM fuel cells has become "bleeding edge" tech.
- Also, as trace CO poisons PEM fuel cells - will require a very pure H2 but can still contain N2

Summary

If POGT development want to stay with air-blown, may limit it to integration with advanced metallic ionic membranes to effectively recovery pure H2 at pressure which is generally considered essential for oil refinery H2 uses

Refinery H2 demand continues to increase at around 4-6% per year but could go higher if oil prices go back up

- **Continuing oil price volatility could create a market for smaller modular units (say 5-10 MM scf/d H2) for “just in time” additions**

Refinery power gen limited by low power prices in many areas with mostly paid-off coal & nuclear power

- **Key exceptions in the U.S is California and Texas where NGCC or GT is the marginal baseload power source**
- **European acceptance of cogen power sales to the grid at a fair price and limited coal based power could favor POGT integration such are for H2 with fuel gas for fired heaters**

Summary - continued

Refinery H2 is increasingly by industrial gas companies owned supplies via over-the-fence or pipelines

- Expect there could be some cleaver ways to integrate the POGT concept with industrial gas company operations
  - However, would be a major change from traditional SMR to POGT
- Air Products is likely a good first choice due to their own small H2 unit design & especially their leading ITM development position for even more integration & application options
- Hydro-Chem (Linde) is a good second choice due to their specialization in small, pre-fab, skid-mounted H2 units

Oil refineries are very conservative and resist change

- But oil industry facing long-term changes to power markets
- Forward thinking integrated oil companies might consider POGT
  - Shell Oil is a good first choice due to Shell Hydrogen and work on advanced metallic ionic H2 membranes one step NG to H2 system